Heterogeneous electrochemical reactions taking place on metallic iron in ammoniacal-carbonate solutions containing dissolved nickel, cobalt, copper and thiosulfate ions

Anna d'Aloya de Pinilla

MSci (Chemistry), King's College, University of London

This thesis is presented for the degree of

Doctor of Philosophy in Extractive Metallurgy

Murdoch University

2015

DECLARATION

I declare that this thesis is my own account of my research and contains as its main content work which has not previously been submitted for a degree at any tertiary education institution.

Anna d'Aloya de Pinilla

September 2015

ABSTRACT

In the Caron process, nickeliferous laterite ores undergo a pyrometallurgical pre-treatment step, in which their nickel and cobalt content is reduced to the metallic state. This is followed by leaching in ammoniacal-carbonate solutions, where metallic nickel and cobalt dissolve by forming complexes with ammonia. Since the reductive pre-treatment step also results in some metallic iron being formed, nickel and cobalt are present in the pre-reduced ore mainly as ferro-alloys. As a result, the dissolution behaviour of metallic nickel and cobalt is strongly influenced by the behaviour of metallic iron. In particular, the passivation of iron has been identified as a potential factor contributing to the relatively low metal value recoveries suffered by the process (80-82% nickel and 50-60% cobalt).

The present study consists of an investigation into various heterogeneous reactions involving metallic iron and ions commonly found in Caron leach liquors, namely nickel(II), cobalt(II), copper(II) and thiosulfate, in order to identify interactions which may adversely affect the extraction efficiency. The study was carried out using a combination of electrochemical and surface characterisation techniques, as well as thermodynamic calculations.

Metallic iron was found to generally dissolve in ammoniacal-carbonate solutions by forming ferrous ammine complexes, but a few specific conditions were found to promote its spontaneous passivation: the presence of copper(II) ions and the presence of both cobalt(II) and thiosulfate ions.

In the presence of copper(II) ions, the passivation process was promoted by the cementation and subsequent redissolution of metallic copper, as confirmed by surface characterisation studies. However, when thiosulfate ions were also present,

passivation was not observed and the formation of a partially adherent layer containing metallic copper dendrites and cuprous sulfide took place on the iron surface.

In the presence of both cobalt(II) and thiosulfate ions, the passivation process, which was not observed when either species was present on its own, was promoted by the formation of an amorphous cobalt sulfide or polysulfide species. The loss of cobalt from the leach solution into this layer was identified as another potential factor contributing to the poor cobalt extractions suffered by the process.

ACKNOWLEDGEMENTS

I wish to thank my supervisors Dr Aleks Nikoloski, Dr David Ralph and Associate Professor Gamini Senanayake for their valuable guidance in completing this thesis. I am also very grateful to Murdoch University and the Parker Cooperative Research Centre for Integrated Hydrometallurgy Solutions for their financial support. I thank Ken Seymour, Chanika Lekamalage, Justin McGinnity, Dmitry Pugaev and all my peers and close friends for their support and friendship throughout my studies. Finally, I would like to thank all my family, in particular my precious daughters Leila and Sofia, who lived most their lives being mothered by a PhD student, and my late father, who encouraged me to take up this journey but did not live to see me complete it.

RESEARCH PUBLICATIONS

D'Aloya, A. and Nikoloski, A.N., 2014. The anodic dissolution of iron in ammoniacal-carbonate-thiosulfate-copper solutions with formation of Cu_2S and dendritic copper. Hydrometallurgy, 144-145: 163-169

D'Aloya, A. and Nikoloski, A.N., 2013. An electrochemical investigation of the formation of CoS_x and its effect on the anodic dissolution of iron in ammoniacal-carbonate solutions. Hydrometallurgy, 131-132: 99-106

D'Aloya, A. and Nikoloski, A.N., 2012. The passivation of iron in ammoniacal solutions containing copper(II) ions. Hydrometallurgy, 111-112: 58-64

ABBREVIATIONS

at%	Atomic percentage
a_x	Activity of species X
α	Transfer coefficient
c_e	Species concentration at the electrode
c_0	Species concentration in the bulk of the solution
D	Diffusion coefficient
δ	Diffusion layer thickness
ΔG°	Standard Gibbs free energy change (298 K and unit species' activities)
E°	Standard electrode reduction potential (298 K and unit species' activities)
Eh	Electrode reduction potential difference from the hydrogen reduction potential
E_{mix}	Mixed potential of an electrode
E_p	Peak potential
$E_{p/2}$	Half-peak potential
E_{pa}	Anodic peak potential
E_{pc}	Cathodic peak potential
η	Overpotential
F	Faraday constant (96485 C mol^{-1})
GIXRD	Grazing Incidence X-Ray Diffraction
I	Current
i	Current density (current per unit area)
I_0	Exchange current
I_a	Anodic current
I_c	Cathodic current
ICP-OES	Inductively Coupled Plasma - Optical Emission Spectroscopy

i_L	Limiting current density
I_p	Peak current
i_{pa}	Anodic peak current density
i_{pc}	Cathodic peak current density
'iR drop'	Voltage drop due to solution resistance
n	Number of electrons
ν	Kinematic viscosity of the solution
OCP	Open Circuit Potential
QN	Queensland Nickel
R	universal gas constant (8.3145 J K^{-1} mol^{-1})
RDE	Rotating Disk Electrode
RRDE	Rotating Ring Disk Electrode
SCE	Saturated Calomel Electrode
SEM/EDX	Scanning Electron Microscopy/Energy Dispersive X-ray Spectroscopy
SHE	Standard Hydrogen Electrode
T	Absolute temperature
UV-VIS	Ultra-Violet-Visible Spectrophotometry
v	Sweep rate
XRD	X-Ray Diffraction
ω	Angular velocity
$[CO_2]_T$	Total concentration of carbonate species: $[CO_3^{2-}]$ + $[HCO_3^-]$ + $[CO_2]$ + $[CO_2]$ + $[NH_2CO_2^-]$ + any contained in metal complexes
$[NH_3]_T$	Total concentration of ammonia species: $[NH_3]$ + $[NH_4^+]$ + $[NH_2CO_2^-]$ + any contained in metal complexes
$[NH_3]$	Concentration of ammonia added as NH_4OH (excluding contribution from NH_4HCO_3 or $NH_2CO_2NH_4$)

CONTENTS

LIST OF FIGURES

LIST OF TABLES

1 INTRODUCTION

1.1 Extractive metallurgy of nickel and cobalt

The large market demand for nickel is primarily due to its widespread use in alloys such as stainless steel. Its main sources are laterite and sulfide ores. Cobalt is usually associated with nickel at an abundance of around 10% that of nickel (Han and Meng, 1993), and is therefore often produced as a valuable by-product of the nickel processing industry (Kerfoot and Weir, 1988). Its main applications are high-performance alloys, pigments, lithium batteries and catalysis.

Although laterite ores contain more nickel (around 1.5-2.5%) than sulfide ores (around 0.3-1.2%), it is extracted primarily from the latter, which can be beneficiated by flotation to form concentrates of around 6 to 25% (Berezowsky, 2004) prior to transport and refining. The nickel concentrates are then processed by pyrometallurgy (smelting to high-grade matte) and hydrometallurgy. Examples of the latter include high pressure sulfuric acid leaching, bioleaching, Sherrit-Gordon ammoniacal pressure leaching, Falconbridge hydrochloric acid leaching and chloride or chlorine leaching (Burkin, 1987; Kerfoot and Weir, 1988; Taylor, 2009).

Processing higher grade feed material significantly reduces reagent expenditure and separation problems, making the extraction of nickel sulfides more advantageous than that of laterites. However, the mining of sulfides is usually more costly and has a greater impact on the environment, due to the greater depth at which the deposits are found. Additionally, the number of newly-discovered deposits of accessible sulfide ore is decreasing, leading to the prediction that the growing demand of nickel will in future be met by an increase in its extraction from laterites (Dalvi et al., 2004).

The various metallurgical processes applied to nickel laterites are usually chosen according to the specific mineral composition of the ore feed. Energy intensive pyrometallurgical processes are more suitable for saprolitic ores because their higher silica and magnesia content allows the formation of a suitable slag, whereas hydrometallurgical processes are applied to limonites and the upper portion of saprolites. The acid leaching techniques are generally more suitable for ores with lower magnesium content, due to reagent consumption. Some of the commercially applied hydrometallurgical processes for the extraction of nickel from laterite ores are listed in Table 1.1.

Table 1.1 Hydrometallurgical nickel laterite processes

Name	Description	Locations
Caron	Combined pyro-hydrometallurgical process (reductive roast followed by ammoniacal leach at atmospheric pressure)	Active: Yabulu (Australia), Niquelandia (Brazil), Nicaro and Punta Gorda (Cuba) Inactive: Sered (Slovakia), Sudbury (Canada), Surigao (Philippines), Las Camariocas (Cuba)
High Pressure Acid Leach (HPAL)	High temperature and pressure sulfuric acid leach developed for low magnesia limonites	Active: Moa (Cuba), Goro (New Caledonia), Murrin Murrin (Australia), Rio Tuba (Philippines) Inactive: Bulong, Cawse (Australia), Verhelmo (Brazil)
Enhanced Pressure Acid Leach (EPAL)	Enhanced pressure acid leach (AL for saprolitic portion combined with HPAL for limonitic portion)	Active: Ravensthorpe (Australia)
Atmospheric Leaching (AL)	Direct atmospheric leach with sulfuric acid, suitable for saprolites	Project in Weda Bay, Indonesia
Sulfation Atmospheric Leach (SAL)	Sulfation of limonitic portion for better selectivity during subsequent atmospheric sulfuric acid leach.	Project in Fenix (Guatemala)
Atmospheric Chloride Leach	Hydrochloric acid – chloride leach, suitable for both ore types	Various projects (Guatemala, Australia, Canada, South Africa, Austria)
Nitric Acid leaching	Atmospheric pressure nitric acid leach suitable for both ore types	Project by Direct Nickel (Western Australia)
Heap Leaching (HL)	Sulfuric acid leach, suitable for hematitic ore	Projects in Caldag (Turkey), Murrin Murrin, Nornico, Lucky Break (Australia), Acoje (Philippines), Piauí (Brazil), Larco (Greece)

(Dalvi et al., 2004; Prado, 2004; Taylor, 2009)

Various other processing techniques have also been proposed over the years, including sulfation roasting, segregation roasting, hydrothermal sulfidisation oxidation – high temperature cementation in pulp (HSO-HTCP), aqueous chlorination, nitric acid leaching, carbonyl extraction, sulfur dioxide leaching, reduction roast – sulfuric acid leaching, gas phase sulfation with SO_2/air-water leach and submerged lance smelting (Taylor, 2009).

The newer generation leaching technologies being developed aim at being able to treat both ore types with greater extraction efficiency whilst lowering energy and reagent consumption.

Generally, the more common acid leaching techniques achieve relatively high nickel and cobalt extractions of around 90% (Dalvi et al., 2004). However, they are affected by some drawbacks, mainly due to the ores containing significant amounts of acid-consuming species and to the dissolution of impurities such as iron. These drawbacks inevitably result in increased costs due to the high reagent consumption and to problems associated with separation and purification.

1.2 The Caron process

The Caron process overcomes both major problems associated with acid leaching techniques by using a lixiviant that not only dissolves nickel and cobalt with greater selectivity, but can also be regenerated for recycling into the leach circuit. The process was patented by Martinus Hendricus Caron in 1924 (Caron, 1924) as a further development of an earlier patent (Caron, 1920) in which the inventor proposed a combined pyro-hydrometallurgical method for processing nickel oxide and hydrated silicate ores. This consisted of a reductive roast, followed by cooling under non-oxidising conditions and leaching in an acid or salt solution. The 1924

patent proposed a significant improvement of the previously proposed process by using a significantly more selective solution of ammonia and ammonium carbonate, which minimised the dissolution of unwanted species and reagent consumption. Further modifications, improvements and additions to this process have been patented by different inventors over the years.

The Australian plant known as the Queensland Nickel (QN) refinery located in Yabulu, near Townsville, has been operating the Caron process since 1974, originally processing laterites from the Greenvale Nickel Mine. Since the late '80s, the plant has been processing ores imported from Indonesia, New Caledonia and the Philippines, as well as some others of different origin (Fittock, 2007). A flowsheet of the QN refinery is shown in Figure 1.1.

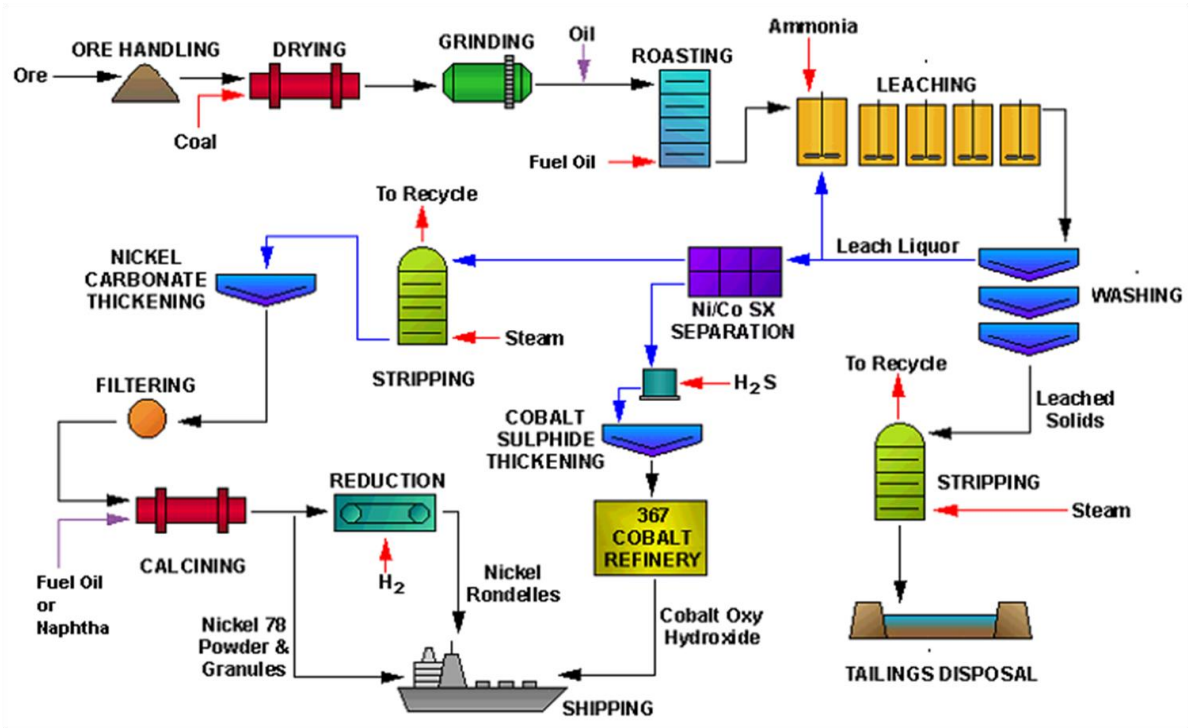

Figure 1.1 Schematic diagram of the Yabulu QN operation, from BHP Billiton (Rhamdhani et al., 2009b).

Prior to reaching the leaching stage, the dried and ground ore is pre-treated by roasting at about 750°C with a sulfur-containing heavy fuel oil as reducing agent, then cooled to below 250°C. As the reduced material is prone to re-oxidation to form insoluble oxides during cooling (Boldt and Queneau, 1967; Chander and Sharma, 1981), this step is carried out under non-oxidising conditions. The reduced material, in which around 80% of the nickel and cobalt have been converted to the metallic state, is then fed into what is known as the quench tank under air-free conditions (Fittock, 2007). This contains ammoniacal-carbonate solution which has already passed through the leaching stage and is being recirculated from the counter-current decantation circuit. It therefore already contains various dissolved species including nickel, cobalt and at times copper ions. The solid material is then fed from the quench tank into the aerated leaching tanks, and subsequently into the counter-current decantation washing circuit.

The advantages of this process compared to the more common acid-based techniques are its greater selectivity towards the metal values and the fact that the ammonia and carbon dioxide can be recovered to regenerate the lixiviant and recycle it into the leach circuit, thereby minimising reagent consumption. However, despite these advantages, the Caron process is currently employed only at a few other locations around the world, which are Nicaro and Punta Gorda, in Cuba, and Niquelandia, in Brazil (Table 1.1). This lack of popularity is due to its typically low metal value recoveries, which at the QN refinery are around 80-82% nickel and 50-60% cobalt. The reasons behind such low extractions have been investigated over the years. However, there is a significant lack of fundamental knowledge, with the actual causes of the observed behaviour being still unclear and subject of on-going investigations. A deeper understanding of the factors and mechanisms which are

currently limiting the extraction efficiency of the process may make it possible to provide solutions that could help optimise current operations and achieve higher nickel and cobalt recoveries.

1.3 The importance of iron

One of the major issues affecting the processing of laterites is their high content of iron, which in the ore processed at the QN refinery, is typically around 40%. During the pyrometallurgical pre-treatment step of the process, about 20% of the iron is inevitably reduced to the metallic state (Fittock, 2009). As a result, the material transferred to the quench tank contains significant amounts of metallic iron, and the metallic nickel and cobalt are mainly present as alloys with the iron (Canterford, 1978; Fittock, 2009; Prado and Dempsey, 1986; Queneau and Weir, 1986; Rhamdhani et al., 2009a). The dissolution behaviour of various alloys containing iron, nickel, cobalt or copper in ammoniacal-carbonate solutions has been investigated over the years by various researchers (Jandová and Pedlik, 1991; Jandová and Pedlik, 1994; Nicol, 1975; Nikoloski, 2002; Senaputra, 2010).

Comparison of the reduction and leaching efficiencies of the Caron process appears to indicate that the nickel extraction is limited mainly by the reductive roast and the ore mineralogy, which result in around 20% of the nickel not being reduced to the metallic phase. On the other hand, it appears that the low cobalt extractions are mainly due to the issues related to the leaching stage.

A study of the behaviour of sintered iron-cobalt mixtures highlighted how metallic iron plays a key role in the dissolution of cobalt, potentially being responsible for its low extraction efficiency. It has become evident that even though the Caron process aims at selectively dissolving only nickel and cobalt, the dissolution of iron is also

necessary in order to liberate the metal values. There has therefore been a strong focus on the behaviour of pure iron, particularly with regards to its passivation due to the formation of a protective oxide layer, which is considered to have a negative effect on the efficiency of the process (Kho et al., 1992; Kim et al., 1991; Lee et al., 1985; Nikoloski et al., 2003). The passivation of iron was observed during potentiodynamic experiments in all of these studies, but only in one of them it was found to take place spontaneously in Caron-type solutions (Nikoloski et al., 2003).

Under the conditions of the process, the anodic dissolution of metallic iron is known to occur during the initial oxygen-free stage which takes place in the quench-tank. This has been confirmed by open circuit potential measurements conducted on metallic iron in the quench slurry from the Yabulu QN plant, which showed that it remained active during a two hour period of immersion (Nicol et al., 2004). The dissolved iron(II) then precipitates as iron(III) at a later stage in the bulk solution as it becomes aerated in the main leaching tanks, allowing its separation from the metal values, which in principle remain in solution. In practice, nickel and cobalt adsorption or co-precipitation phenomena are known to take place as the iron(III) hydroxides are formed, and may be partially responsible for the low recoveries of the process (Boldt and Queneau, 1967; Han et al., 1982; Mackenzie and Lumsdaine, 2002; Su, 2011).

As the reduced ore feed is transferred from the quench tank to the aerators, the anodic dissolution of metallic iron and of its alloys is incomplete. Passivation of the metallic iron and of its alloys at this stage of the process could possibly account for the further loss of any nickel and in particular cobalt, as these may remain locked within the solid matrix. Studies have shown that the passivation of iron and its alloys does indeed take place spontaneously in solutions prepared in order to simulate those

employed in the Caron process (Nicol et al., 2004; Nikoloski and Nicol, 2006; Nikoloski et al., 2003). However, little is known about which species and reactions are actually involved in the passivation mechanism.

The composition of the leach solution coming into contact with the reduced ore both during the oxygen-free and the aerated phase is quite complex. Many of the species present in solution play a significant role in the dissolution behaviour of iron and it is therefore necessary to further investigate the heterogeneous interactions which may take place. Due to its relatively low reduction potential, many interactions are expected to take place at the metallic iron surface. It is therefore important to identify the dissolved species which have a significant effect on the anodic behaviour of iron, in particular to shed some light on the mechanisms responsible for its passivation.

1.4 The formation of secondary metal sulfides on the dissolving iron surface

In previous studies, it was suggested that a secondary metal sulfide layer forms on the iron surface during the early oxygen-free stage of the leach (Nicol et al., 2004; Nikoloski and Nicol, 2006; Nikoloski et al., 2003). The importance of this layer goes beyond its involvement in the mechanism of passivation of iron. The potential loss of dissolved metal values into a poorly soluble sulfide layer may in itself be another factor responsible for the low extraction efficiency of the process. In order to have a better understanding of how the interaction of metallic iron with typical Caron leach solutions results in the formation of metal sulfides on its surface, it is first necessary to investigate the origin of the key species involved, the thiosulfate ions.

The reductive pre-treatment step of the Caron process is carried out using a heavy fuel oil containing around 3% sulfur. This results in the formation of some metal

sulfides within the pre-reduced material being transferred to the leaching stage. The dissolution of these sulfides in ammoniacal solution initially results in the formation of thiosulfate ions, which are slowly further oxidised to sulfite and then sulfate ions (Fittock, 2007). Therefore, under the conditions of the quench and leaching steps, thiosulfate is thought to be present in a metastable state (Queneau and Weir, 1986). In the quench tank, it was suggested that the thiosulfate ions may be reduced by metallic iron to sulfide, which would precipitate some of the dissolved nickel and cobalt as sulfides. However, studies conducted at the Caron plant in Nicaro, Cuba, indicated that the thiosulfate ions were more likely to disproportionate than to be reduced by metallic iron.

Nevertheless, studies conducted at room temperature using a rotating disk electrode made of metallic iron in a solution simulating the Caron leach liquor resulted in the formation of a mixed nickel and cobalt sulfide layer on the iron surface (Nikoloski et al., 2003). This is consistent with the reduction of thiosulfate by metallic iron with precipitation of metal sulfides taking place under conditions similar to those of the Caron process.

The surface layer was observed by SEM/EDX and found to contain around 40% sulfur, 20% cobalt, 10% nickel, despite the solution containing over an order of magnitude more nickel than cobalt. This was attributed to the lower solubility of cobalt sulfide compared to that of nickel sulfide, for which the solubility products were reported as being 2×10^{-25} for CoS and 3×10^{-21} for NiS (Nikoloski et al., 2003). However, characterisation of the layer gave no exact information on the stoichiometry of the species formed, nor did it provide confirmation that the surface species was indeed a sulfide. Its formation is therefore worthy of further

investigation, in particular with regards to its possible involvement in the mechanism of passivation of iron. The fact that it appears to contain a significant portion of the total cobalt present compared to that of nickel, suggests that it may also be responsible for further cobalt losses from the leach solution. This may be of significant importance in the case that the layer does not re-dissolve during the time of the leach. For this reason, it would be particularly useful to gain a better understanding of the nature of this layer, and of whether it is likely to re-dissolve under the Caron leach conditions, in order to assess its potential effect on the process efficiency.

1.5 Aims of the project

It has been established that the behaviour of metallic iron and its interaction with the Caron leach solution has the potential to significantly affect the process efficiency. However, due to the complexity of the system, there is little information on which species have an important effect and the fundamental reactions in which they are involved. This thesis proposes to gain a better understanding of some of these aspects, aiming to do as follows:

- review previous studies related to the Caron process, with a particular focus on the transformations undergone by the ore during the reductive pre-treatment and the leaching reactions undergone by the metallic phases thereby formed
- identify which factors may be responsible for the relatively poor efficiency of the process, with particular regards to which specific stage of the process may be held accountable with respect to which metal and possible reasons

- identify conditions and variables likely to have an effect on the dissolution of metallic iron in ammoniacal solution and on the formation of secondary sulfides on its surface
- determine which species or combination of species cause the passivation of iron
- observe and understand the changes taking place on the iron surface following interaction with the solution species, characterising the solid layers formed
- monitor and explain changes in the electrochemical behaviour over time during interaction with the solution species
- study the effect of concentration of various dissolved species
- identify the possible reactions responsible for the observed behaviour
- assess the dissolution behaviour of the secondary sulfide species formed on the iron surface

Some of the methods employed and variables investigated as part of this thesis are listed in Table 1.2.

Table 1.2 Methods employed and variables investigated as part of this thesis

Methods	**Variables**
- OCP measurement of iron RDE - cyclic voltammetry - SEM/EDX surface characterisation - XRD	- presence of dissolved species (Ni, Co, Cu, $S_2O_3^{2-}$ and various combinations) - [Cu], [Co], [$S_2O_3^{2-}$], [NH_3]$_T$ and [CO_2]$_T$ - immersion time
- Re-immersion of RDE in barren solution and ICP-OES determination of [Co], [Ni], [Cu] and [S] over time	- Co/Ni/Cu sulfide formed on RDE
- Cyclic voltammetry of Ni_3S_2	- potential scan rate, rotation speed

2 LITERATURE REVIEW

2.1 Ore mineralogy and grade

Nickeliferous laterites are formed from the weathering of ultramafic rocks such as peridotite. During this process, the minor nickel and cobalt content of the olivine minerals [$(Mg,Fe,Ni)_2SiO_4$] is enriched by factors of 3 to 30 times (Steyl et al., 2008). The actual mineralogical composition of laterite deposits varies considerably depending on the parent rock characteristics and weathering conditions. A broad distinction can be made between wet laterites, found in humid tropical to sub-tropical regions, and dry laterites, found for example in some parts of Australia. The latter generally contain less nickel and more clay minerals, making them more difficult to process. An idealised cross-section of a laterised deposit is shown in Figure 2.1.

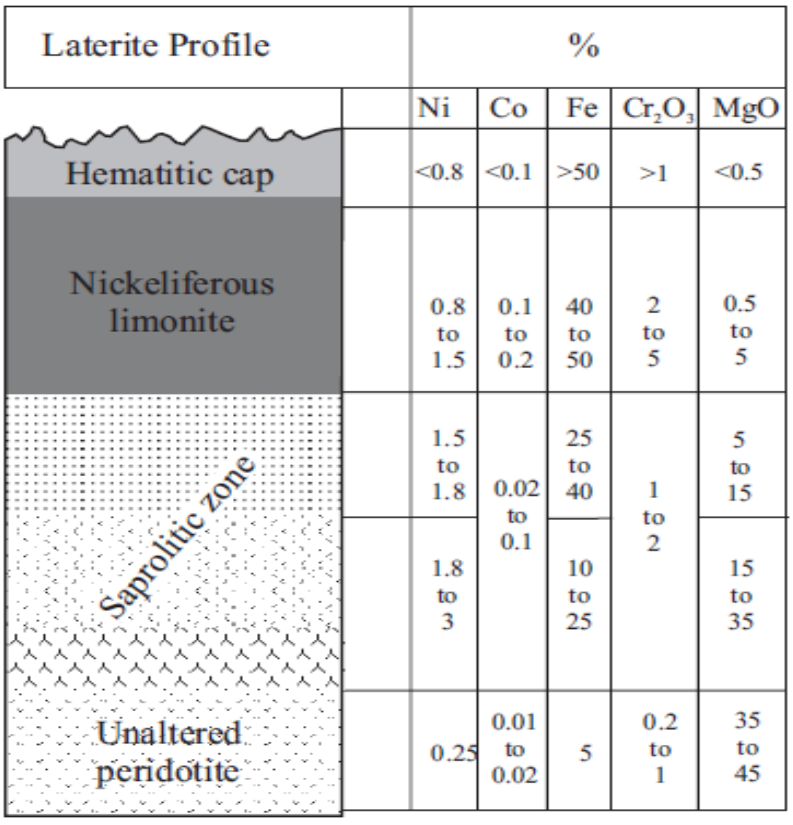

Figure 2.1 Idealised cross section of a lateritic nickel deposit, from Falconbridge Dominicana (Lewis et al., 2006).

Generally the laterisation process occurs as rainwater and decomposing organic matter form a mildly acidic solution which leaches nickel, magnesium and silica out of the ultramafic rock carrying it downwards, whilst the iron and aluminium oxides tend to remain in the upper portion. The two distinct ore types that are formed as a result of this process are limonitic and saprolitic ores. Limonitic or oxide-hydroxide ores are found closer to the surface and are richer in iron, with a typical nickel content of about 0.8-1.5%. Saprolitic ores are found at greater depths and consist primarily of silicates. These are richer in magnesium and have a typical nickel content of 1.5-3% (Queneau and Weir, 1986; Steyl et al., 2008).

In the limonitic zone, the nickel is finely dispersed within a mixture of iron oxides, and is thought to be present mainly in goethite, either as a substitution as in (Fe,Ni)O(OH) or weakly adsorbed (Swamy et al., 2003). In the saprolitic zone, nickel tends to substitute magnesium in silicates such as serpentine, as in $(Mg,Fe,Ni)_3Si_2O_5(OH)_4$ or chlorite, as in $(Ni_5Al)(AlSi_3O_{10})(OH)_8$, and it forms nickel rich garnierite pockets and veins.

Because of its intimate association with unwanted elements, for both ore types it is practically impossible to physically upgrade the ore prior to extraction, since this would require a chemical transformation.

The cobalt in laterite ores is thought to be present mainly in asbolane (Queneau and Weir, 1986), which may be written as $(Co,Ni)(MnO_2)_2(OH)_2{\cdot}xH_2O$. Studies conducted on laterites from the Greenvale Mine in Queensland, indicated that more than 70% of the cobalt was associated with the high-nickel limonitic fraction of the ore, mainly in conjunction with manganese dioxide and goethite. The amount of cobalt in the silicate minerals was found to be extremely low (<0.03%), and where

higher, it was associated with the iron possibly due to enrichment by precipitation of iron and cobalt hydroxides (Roach, 1977b).

Due to the broad variation in the composition of laterite ore feeds, numerous studies have been conducted on the effect of the mineralogy on extraction efficiency, some specifically relating to the Caron process (Borjas, 2004; Canterford, 1978; Caron, 1950; Roach, 1977b). As consistent with these studies, plants employing the Caron process are expected to achieve significantly higher nickel recoveries from limonitic than from saprolitic ores, as observed in the case of the Yabulu QN refinery (Reid and Fittock, 2004).

The QN plant was originally constructed in the early 1970's to process nickel laterite ore from the Greenvale Mine in Queensland. Although initially both the limonitic and the saprolitic portion of the ore had been found to contain 1.6% nickel and 0.12 % cobalt, the nickel grade fell rapidly over the following years, leading to closure of the mine in the early 1990's. In 1986, the QN refinery began processing imported ores from a number of mines in New Caledonia, Indonesia and the Philippines, which currently constitute the main ore-feed for the operation. Switching to the imported ores resulted in an increase in nickel production not only due to the higher grade of the feed, but also because it was possible to achieve higher recoveries by processing predominantly limonitic ore (Reid and Fittock, 2004).

Mineralogical characterisation studies have been conducted on typical 'wet' laterite ores from New Caledonian and Indonesian mines (Chen et al., 2004). The former were found to be predominantly limonitic, with the nickel present mainly in goethite, serpentine and manganese oxide and the cobalt mainly in goethite and manganese oxide. The latter was found to be predominantly saprolitic, with the nickel present

mainly in serpentine, olivine, chlorite and amphibole, and in smaller amounts in goethite and manganese oxide, while cobalt was detected in the manganese oxide. However, the Indonesian ore currently processed at the Yabulu QN comes from a different deposit, which contains both saprolitic and limonitic laterites. Overall, the imported ore mixture is a combination of high-iron limonitic ore, manganese-iron oxides, and high-magnesium, high-silica saprolitic ore, of variable nickel and cobalt association with each ore type (Fittock, 2007). The most important mineral phases found in the Yabulu QN ore feed are summarised in Table 2.1, and its typical elemental composition is given in Table 2.2.

Table 2.1 Mineral phases of the the imported nickel laterite ore processed at the Yabulu QN refinery

Ore type	Main Ni and Co bearing minerals		Minor Ni bearing minerals	
LIMONITIC	Goethite*	(Fe,Ni)O(OH)	Magnetite*	$(Fe,Ni)O{\cdot}Fe_2O_3$
	Asbolane**	$(Co,Ni)(MnO_2)_2(OH)_2{\cdot}xH_2O$	Chromite*	$(Fe,Mg)O{\cdot}(Cr,Al,Fe)_2O_3$
SAPROLITIC	Lizardite*	$(Mg,Fe,Ni)_3Si_2O_5(OH)_4$	Olivine*	$(Mg,Fe,Ni)_2SiO_4$

(***from Rhamdhani et al., 2009a; **from Fittock 2007)**

Table 2.2 Typical elemental composition of imported laterite ore processed at the Yabulu QN refinery

Moisture (% wet weight)	Chemical analysis (% w/w dry basis)											
	Ni	Co	Fe	Si	Mg	Mn	Cu	Zn	Ca	Al	Cr	S
35	1.6	0.15	37	7.2	5.2	0.8	0.01	0.05	0.1	2.1	1.2	0.2

(Fittock, 2007)

2.2 Reductive pre-treatment

The reductive roast step of the Caron process aims at selectively reducing the nickel and cobalt in the ore by mixing it with 2.5% w/w heavy fuel oil and heating it to temperatures up to 750°C. The reducing atmosphere, consisting of carbon monoxide and hydrogen, is provided by the fuel itself, which is combusted under oxygen-deficient conditions. Ideally, the pre-treatment step should result in the reduction of over 90% of the nickel and cobalt according to processes which may be described by reactions 2.1 and 2.2. Also under ideal conditions, the iron should not be reduced beyond the magnetite form, as in reactions 2.3 and 2.4 (Queneau and Weir, 1986).

$$(Ni,Co)O + CO \rightarrow Ni, Co + CO_2 \quad (2.1)$$

$$(Ni,Co)O + H_2 \rightarrow Ni, Co + H_2O \quad (2.2)$$

$$3Fe_2O_3 + CO \rightarrow 2Fe_3O_4 + CO_2 \quad (2.3)$$

$$3Fe_2O_3 + H_2 \rightarrow 2Fe_3O_4 + H_2O \quad (2.4)$$

However, it has been reported that due to practical limitations, around 5-15% of the iron is also inevitably reduced to the metallic state via reactions 2.5 - 2.8 (Queneau and Weir, 1986).

$$Fe_3O_4 + CO \rightarrow 3FeO + CO_2 \quad (2.5)$$

$$FeO + CO \rightarrow Fe + CO_2 \quad (2.6)$$

$$Fe_3O_4 + H_2 \rightarrow 3FeO + H_2O \quad (2.7)$$

$$FeO + H_2 \rightarrow Fe + H_2O \quad (2.8)$$

At the Yabulu QN plant, it has been reported that around 80% of the nickel and cobalt are reduced to the metallic state (Fittock, 2009). The amount of iron which is also reduced to the metallic state has been reported as being less than 20%, with the majority being present in the pre-treated ore as magnetite (Fittock, 2007). Studies of reduced calcines obtained from Greenvale ore originally being processed at Yabulu showed that any metallic nickel was always present as a ferronickel alloy (Canterford, 1978). This was confirmed by further studies conducted on Albanian laterites and on synthetic Ni and Co enriched goethites (Jandová and Pedlík, 1991). It was reported that in the limonitic ores, the alloy formed discrete small blebs within the goethite grains, whereas in the silicate ores it was distributed throughout the grains with no segregation (Canterford, 1978). No metallic nickel was observed in any case, as consistent with thermodynamic calculations, which predict that the completely selective reduction of nickel oxide over iron oxide is not possible (Canterford and Turnbull, 1980). It is currently widely accepted that iron-nickel alloy is the main metallic nickel-bearing phase in the reduced ore (Bunjaku, 2013; Fittock, 2007; Jandová and Pedlik, 1994; Rhamdhani et al., 2009a)

Detailed characterisation studies have been carried out on the imported laterite ore currently being processed at the Yabulu QN refinery, with a focus on the phase transformations occurring during the reductive roast and the ammoniacal leaching steps of the process (Rhamdhani et al., 2009 a,b). Based on XRD and SEM-EDX studies the authors confirmed the formation of iron-nickel alloy, thought to form from the nickel-containing goethite according to reactions 2.9 and 2.10.

$$6(Fe,Ni)O(OH) \rightarrow 2(Fe,Ni)_3O_4 + 3\ H_2O + ½\ O_2 \quad (2.9)$$

$$(Fe,Ni)_3O_4 \rightarrow 2(Ni,Fe)_{alloy} + 2O_2 \quad (2.10)$$

The metallisation of nickel from the silicate fraction of the ore is known to be more complicated and problematic (Caron, 1950; Prado and Dempsey, 1986; Roach, 1977b). Based on the studies conducted on the reduced ore from Yabulu it was suggested that the nickel-containing serpentine undergoes a transformation to olivine, according to reaction 2.11 (Rhamdhani et al., 2009a).

$$2(Mg,Fe,Ni)_3Si_2O_5(OH)_4 \rightarrow 3(Mg,Fe,Ni)_2SiO_4 + SiO_2 + 4H_2O \quad (2.11)$$

A major problem associated with the reductive pre-treatment is thought to be the formation of a very stable forsterite-type structure (Mg_2SiO_4). Once this is formed, any trapped nickel cannot be reduced unless much higher temperatures than those of the process are used (Prado and Dempsey, 1986). It was suggested that this may be prevented by adding sulfur to the roast, resulting in the formation of a nickel sulfide, thereby sequestering any nickel that would otherwise become trapped in the forsterite. The so-formed sulfides are then thought to dissolve in the ammoniacal leach resulting in overall enhanced nickel extractions (Caron, 1950). Regardless of the use of sulfur as an additive, the formation of metal sulfides during the reductive roast takes place by reaction of the ore with the 3% sulfur content of the fuel oil or with any sulfur originally present in the ore (Queneau and Weir, 1986). This may be described by reactions 2.12 to 2.14.

$$S + H_2 \rightarrow H_2S \quad (2.12)$$

$$(Ni,Co)O + H_2S \rightarrow (Ni,Co)S + H_2O \quad (2.13)$$

$$2FeO(OH) + 2H_2S + H_2 \rightarrow 2FeS + 4H_2O \quad (2.14)$$

The reduced ore and in particular the iron-rich alloys have a strong tendency to react with oxygen and passivate by forming insoluble oxides, making it essential that the

cooling and handling prior to the ammoniacal leaching stage takes place under non-oxidising conditions (Boldt and Queneau, 1967; Caron, 1950; Chander and Sharma, 1981). Therefore, the reduced ore processed at the Yabulu QN is cooled to below 250°C and transferred to the quench tank in the absence of any oxygen (Fittock, 2007).

2.3 Ammoniacal leach

2.3.1 Leaching in the quench tank

After cooling, the freshly reduced ore first comes into contact with the ammoniacal leach solution in the quench tank under oxygen-free conditions. The leaching reactions are exothermic, and the temperature of the resulting slurry is aimed at being around 42°C throughout the entire leaching stage, with allowable fluctuations between 40°C and 60°C (Fittock, 2009). Since the solution fed into the quench tank is being recycled from the counter-current decantation circuit, as described in Figure 2.2, temperature control is achieved by cooling it to around 25°C prior to it coming into contact with the reduced feed in the quench tank.

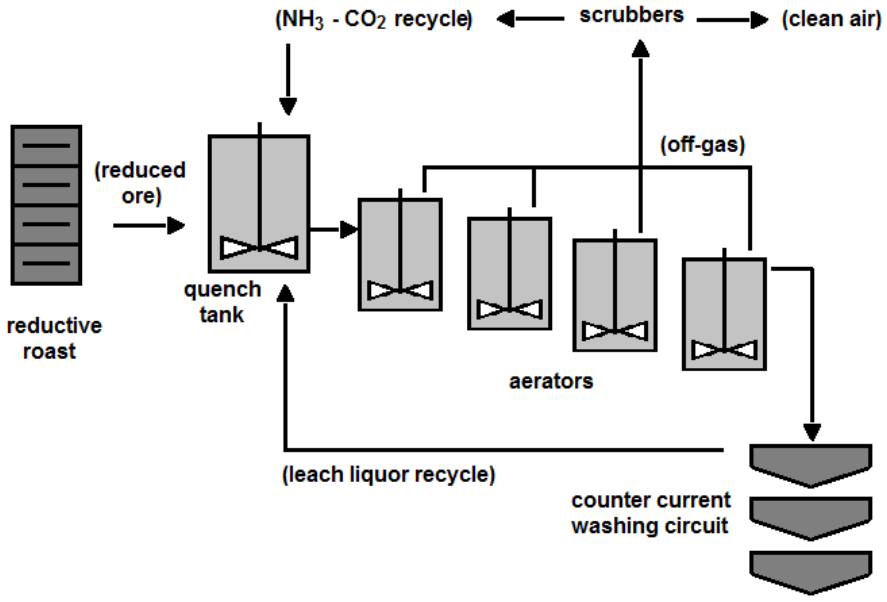

Figure 2.2 Simplified flow-sheet of the leaching stage of the Yabulu QN refinery.

Dissolved nickel and cobalt species are already present in the recycled solution at the concentration ranges given in Table 2.3, which also summarises the total ammonia and total carbonate concentrations, referred to as $[NH_3]_T$ and $[CO_2]_T$ respectively, employed at the Yabulu QN and at two other Caron plants. The required total ammonia and carbonate concentrations are achieved by the addition of recycled ammonia gas and carbon dioxide which has been recovered by scrubbing the off-gas from the aerated leaching tanks.

Table 2.3 Typical solution species concentrations at Yabulu QN and other Caron plants

[species] (g/L)	Yabulu*	Punta Gorda**	Niquelandia**
$[NH_3]_T$	75 - 95	60 - 68	82 – 85
$[CO_2]_T$	40 - 65	30 - 35	60 – 65
$[Ni]_T$	9.7 - 12.8		
$[Co]_T$	0.37 - 0.63		
$[Fe]_T$	1 - 2 (in quench tank)		
$[S_2O_3^{2-}]$	2.5***		

*(Fittock, 2009); **(Chang Cardona and Rojas Vargas, 2009); ***(Nicol et al., 2004)

Any dissolved oxygen present in the leach solution being recycled into the quench tank is rapidly consumed by the reduced material. Therefore, the initial dissolution of nickel, cobalt and iron takes place in the absence of any oxygen and may be described by reactions 2.15 to 2.18 (Queneau and Weir, 1986).

$$Ni + 2NH_4^+ + 4NH_3 + CO_3^{2-} \rightarrow Ni(NH_3)_6^{2+} + CO_3^{2-} + H_2 \quad (2.15)$$

$$Co + 2NH_4^+ + 3NH_3 + CO_3^{2-} \rightarrow Co(NH_3)_5^{2+} + CO_3^{2-} + H_2 \quad (2.16)$$

$$Fe + 2NH_4^+ + 2NH_3 + CO_3^{2-} \rightarrow Fe(NH_3)_4^{2+} + CO_3^{2-} + H_2 \quad (2.17)$$

$$Fe + 2H_2O \rightarrow Fe(OH)_2 + H_2 \quad (2.18)$$

In practice, the oxidative dissolution of these metals also involves various other oxidising species present in the recycled leach solution. One of these is thiosulfate, which originates from the ammoniacal dissolution of the metal sulfides which are formed during the reductive pre-treatment step. Although the so-formed thiosulfate ions are slowly further oxidised to other oxysulfur anions, they are known to be metastable under the conditions of the quench and aerated leaching tanks (Fittock, 2007; Queneau and Weir, 1986). The relative stability of thiosulfate ions at pH 10 can be seen from Figure 2.3 as explained by Molleman and Dreisinger (2002).

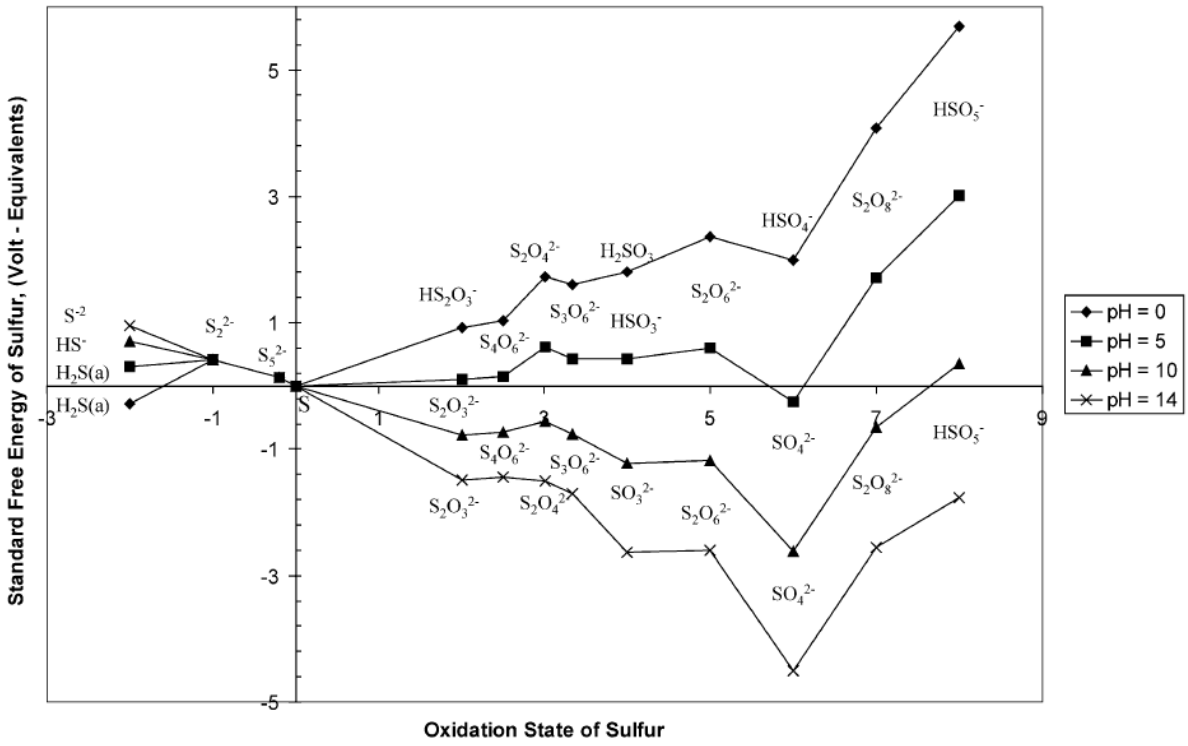

Figure 2.3 Oxidation state diagram for sulfur at several pH values (Molleman and Dreisinger, 2002).

It was suggested that in the quench tank, thiosulfate ions may be reduced to sulfide by reaction with metallic iron (reaction 2.19) and then precipitate dissolved nickel and cobalt as sulfides, according to reactions 2.20 and 2.21 (Queneau and Weir, 1986).

$$4Fe + 10NH_4^+ + S_2O_3^{2-} + 4CO_3^{2-} + 2NH_3 \rightarrow 4Fe(NH_3)_2^{2+} + 4NH_4^+ + 4CO_3^{2-} + 3H_2O + 2S^{2-} \quad (2.19)$$

$$2NH_4^+ + S^{2-} + Ni(NH_3)_6^{2+} + CO_3^{2-} \rightarrow NiS + 6NH_3 + 2NH_4^+ + CO_3^{2-} \quad (2.20)$$

$$2NH_4^+ + S^{2-} + Co(NH_3)_5^{2+} + CO_3^{2-} \rightarrow CoS + 5NH_3 + 2NH_4^+ + CO_3^{2-} \quad (2.21)$$

However, measurement showing a decrease in nickel, cobalt and sulfur concentrations and a simultaneous increase in sulfate concentration in the quench tank indicated that thiosulfate is more likely to undergo disproportionation reaction, as described by reactions 2.22 and 2.23 (Queneau and Weir, 1986).

$$Ni(NH_3)_6^{2+} + S_2O_3^{2-} + H_2O \rightarrow NiS + 2NH_4^+ + SO_4^{2-} + 4NH_3 \quad (2.22)$$

$$Co(NH_3)_5^{2+} + S_2O_3^{2-} + H_2O \rightarrow CoS + 2NH_4^+ + SO_4^{2-} + 3NH_3 \quad (2.23)$$

2.3.2 Leaching and precipitation in the aerated tanks

The oxidative dissolution reactions (2.15-2.17) do not go to completion in the quench tank, and the feed is then transferred to the aerated leaching tanks. The oxidative dissolution of the metals and metal sulfides in the aerated tanks also involves oxygen, as described by reactions 2.24 to 2.28 (Fittock, 2009). Metallic copper is also thought to be leached at this stage according to similar reactions. The

oxygen also further oxidises dissolved metals such as cobaltous ammines, as described by reaction 2.29 (Queneau and Weir, 1986).

$$Ni + 4NH_3 + (NH_4)_2CO_3 + \tfrac{1}{2} O_2 \rightarrow Ni(NH_3)_6^{2+} + CO_3^{2-} + H_2O \quad (2.24)$$

$$Co + 4NH_3 + (NH_4)_2CO_3 + \tfrac{1}{2} O_2 \rightarrow Co(NH_3)_6^{2+} + CO_3^{2-} + H_2O \quad (2.25)$$

$$Fe + 2NH_3 + (NH_4)_2CO_3 + \tfrac{1}{2} O_2 \rightarrow Fe(NH_3)_4^{2+} + CO_3^{2-} + H_2O \quad (2.26)$$

$$2FeS + 6NH_3 + (NH_4)_2CO_3 + 2O_2 \rightarrow 2Fe(NH_3)_4^{2+} + CO_3^{2-} + H_2O + S_2O_3^{2-} \quad (2.27)$$

$$2NiS + 10NH_3 + (NH_4)_2CO_3 + 2O_2 \rightarrow 2Ni(NH_3)_6^{2+} + CO_3^{2-} + H_2O + S_2O_3^{2-} \quad (2.28)$$

$$4Co(NH_3)_5H_2O^{2+} + 4NH_4^{+} + O_2 + 6CO_3^{2-} \rightarrow 4Co(NH_3)_5H_2O^{3+} + 6CO_3^{2-} + 4NH_3 + 2H_2O \quad (2.29)$$

The so-formed cobaltic ammines then also act as oxidants in the electrochemical dissolution of the metallic phases, by which they are reduced back to cobaltous ammine complexes. These are then re-oxidised by oxygen, re-generating the cobaltic ammines which can continue to act as oxidants, thereby taking up a redox-mediator role in the oxidation of the metallic phases during the leach (Nicol et al., 2004).

The ferrous ammines are also further oxidised by oxygen, resulting in the formation of ferric or ferrous-ferric hydroxide precipitates, as described by reactions 2.30 and 2.31 (Queneau and Weir, 1986):

$$4Fe(NH_3)_{2+x}^{2+} + 10H_2O + O_2 + 4CO_3^{2-} \rightarrow 4Fe(OH)_3 + 8NH_4^{+} + 4CO_3^{2-} + 4xNH_3 \quad (2.30)$$

$$3Fe(NH_3)_{2+x}^{2+} + 7H_2O + \tfrac{1}{2}O_2 + 3CO_3^{2-} \rightarrow 4Fe_3(OH)_8 + 6NH_4^{+} + 3CO_3^{2-} + 3xNH_3 \quad (2.31)$$

These hydroxides have been described as a gelatinous deposit forming on the reduced ore-particles in the aerator tanks of the Caron plant in Nicaro, Cuba (Boldt and Queneau, 1967).

Freshly formed hydrated oxides of iron(III) and manganese(II) are known to adsorb and co-precipitate nickel and in particular cobalt (reactions 2.32 and 2.33), having a negative effect on the extraction efficiency of the leaching stage of the process (Fittock, 2009; Han et al., 1982; Su, 2011).

$$x\mathrm{Fe(OH)_3} + \mathrm{Co(NH_3)_5CO_3} + 2\mathrm{H_2O} \rightarrow [\mathrm{Fe(OH)_3}]_x[\mathrm{Co(OH)_2}] + 2(\mathrm{NH_4})_2\mathrm{CO_3} + 3\mathrm{NH_3} \quad (2.32)$$

$$x\mathrm{Mn(OH)_2} + \mathrm{Co(NH_3)_5CO_3} + 2\mathrm{H_2O} \rightarrow [\mathrm{Mn(OH)_2}]_x[\mathrm{Co(OH)_2}] + 2(\mathrm{NH_4})_2\mathrm{CO_3} + 3\mathrm{NH_3} \quad (2.33)$$

This was found to be even more significant when the hydroxides were in a partially reduced state, and when dehydration to hematite (reactions 2.34- 2.36) took place whilst the nickel and cobalt were still adsorbed (Queneau and Weir, 1986; Weir and Sefton, 1979). It was suggested that lower nickel and cobalt extractions observed at higher temperatures (Reid, 1983) were possibly due to faster dehydration kinetics of the hydroxides, which resulted in more of the metal values being trapped in the solid phase (Queneau and Weir, 1986; Weir and Sefton, 1979).

$$2\mathrm{Fe(OH)_3} \rightarrow \mathrm{Fe_2O_3}\cdot n\mathrm{H_2O} + (3- n)\mathrm{H_2O} \quad (2.34)$$

$$2[\mathrm{Fe(OH)_3}]_x[\mathrm{Ni(OH)_2}] \rightarrow (\mathrm{Fe_2O_3}\cdot n\mathrm{H_2O})_x(\mathrm{NiO}\cdot y\mathrm{H_2O}) + z\mathrm{H_2O} \quad (2.35)$$

$$2[\mathrm{Fe(OH)_3}]_x[\mathrm{Co(OH)_2}] \rightarrow (\mathrm{Fe_2O_3}\cdot n\mathrm{H_2O})_x(\mathrm{CoO}\cdot y\mathrm{H_2O}) + z\mathrm{H_2O} \quad (2.36)$$

The leached slurry is then separated from the leach liquor and transferred to the thickeners, which form part of the counter-current decantation circuit (Figure 2.2), for washing of the solid residue to recover more dissolved metal values (Fittock, 2009). Measurements conducted in the thickeners at the Yabulu QN refinery indicated that cobalt which had been adsorbed and co-precipitated in the aerators continued to leach, or rather become desorbed, during washing in the counter-current decantation circuit (Mackenzie and Lumsdaine, 2002; Reid, 1983).

2.3.3 Leaching efficiency

Nickel recoveries at the Yabulu QN refinery are reported as being around 80-82% (Fittock, 2007), which corresponds to a 100% recovery during the leaching stage, if only the nickel which is reduced to the metallic state is considered to be leachable. However, other phases such as olivine or metal sulfides formed during the reductive roast may also contribute to the recoveries, as these are also thought to be leachable in ammoniacal solutions. Therefore, due to the complexity of the system it is not certain whether the dissolution of nickel from the extractable metallic phases does in fact go to completion. Nickel recoveries of close to 100% have been reported for the leaching of limonitic materials, whereas much lower recoveries were reported for the serpentinic material, specifically 50-60% which could be improved to 80-85% with the use of sulfur as an additive (Roach, 1977b). Although the evidence indicates that nickel recoveries at the Yabulu QN refinery are limited mainly by the mineralogy of the ore and its incomplete reduction during the pre-treatment step, losses which may also take place during the leach are not to be completely excluded.

The even lower cobalt recoveries, of up to 50-60% (Fittock, 2007), are thought to be mainly due to the leaching stage of the process, since incomplete reduction during

the roast can only be partially held responsible for a loss of around 20%. During the early stages of the plant operation, when the Greenvale ore was being processed, it was noted that although the cobalt was initially in the limonitic fraction of the ore, in the tailings it was associated mainly with the silicate fraction (Roach, 1977b). This was explained in terms of adsorption of the dissolved cobalt onto the silicate, based on the lower recoveries observed when quench solution (Table 2.4) was used instead of fresh ammoniacal-carbonate solution, as shown in Figure 2.4 (Roach, 1977b).

Table 2.4 Composition of fresh and quench ammoniacal-carbonate leach liquor during the early stages of the Yabulu QN refinery operation

[species] (g/L)	$[NH_3]_T$	$[CO_2]_T$	$[Ni]_T$	$[Co]_T$
fresh leach liquor	100	90	0	0
quench leach liquor	100	90	10	0.3

(Roach, 1977a; Roach, 1977b)

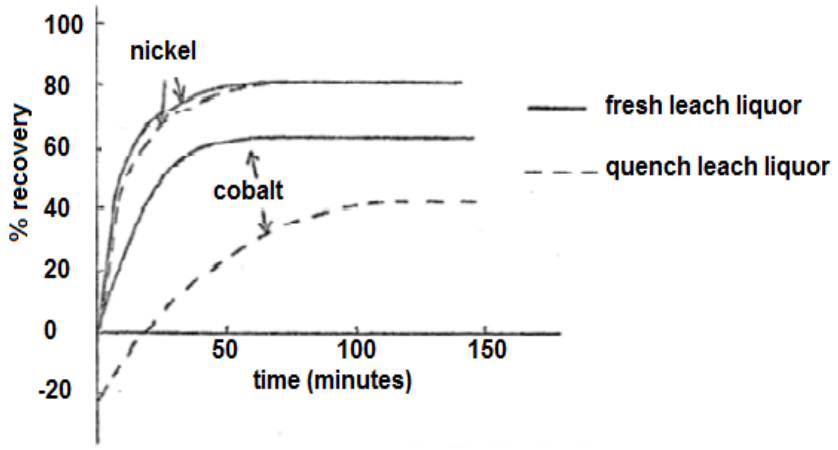

Figure 2.4 Leaching of the reduced ore in fresh and quench leach liquors at the concentrations given in Table 2.4 (Roach, 1977b).

Characterisation studies of the Caron tailings from the Yabulu QN confirmed that the adsorption of cobalt took place predominantly onto iron containing phases (Mackenzie and Lumsdaine, 2002). These studies also resulted in the identification of a manganese oxide phase strongly associated with nickel and especially cobalt, as $(Co,Ni)Mn_2O_4(OH)_2.xH_2O$. However, the existence of such phase was found to make only a very small contribution to the overall cobalt loss to tailings. Based on this investigation, it was not possible to quantify the contribution of cobalt adsorption and co-precipitation to the cobalt losses, and no conclusions were drawn as to whether the low cobalt recoveries are due to the leach or to incomplete reduction during the roast.

It is therefore evident that there is a significant lack of understanding and a strong need for further investigation into the possible mechanisms responsible for the low cobalt recoveries suffered by this process.

2.4 Thermodynamics of iron, cobalt, nickel and copper in ammoniacal solutions

In order to gain a better understanding of the processes taking place in a hydrometallurgical system, it is important to conduct a thorough thermodynamic investigation of the reactions thought to take place, so that their feasibility can be assessed, and the conditions under which they are favoured, identified.

Numerous studies have been conducted on the thermodynamics of metal-ammonia systems relevant to the Caron process (Asselin, 2008; Nazari and Asselin, 2010; Osseo-Asare, 1980; Osseo-Asare, 1981a; Osseo-Asare, 1981b; Osseo-Asare, 1981c; Osseo-Asare and Asihene, 1979; Osseo-Asare and Fuerstenau, 1978; Richardson et al., 1981). Many of these, not only investigate the thermodynamics of the nickel and cobalt metal values in the ammoniacal leach system, but also of iron, due to the considerations discussed in section 1.3, and of copper. The imported ore being processed at the Yabulu QN refinery is known to contain relatively low amounts of copper, which according to the elemental analysis reported in Table 2.2 (section 2.1) is 0.01% by weight (Fittock, 2007). Even though the dissolved copper concentration in the plant's leach liquor is thought to be very low, reaching maximum values of around 0.25 mM (Nikoloski, 2002), the variability of the ore feed may possibly result in the presence of more significant amounts, and concentrations as high as 8 to 16 mM have also been reported (Nikoloski, 2002; Senanayake et al., 2010). It is therefore important to also consider the thermodynamics of copper in ammoniacal leach systems.

2.4.1 The Nernst equation

As is the case for many hydrometallurgical systems, the reactions responsible for the dissolution of metals during the leaching stage of the Caron process, described in section 2.3, consist of redox processes.

In the simplified case in which only a single redox couple is present in a solution, as for example a metal M in equilibrium with its ions in solution (2.37), the reduction potential (E) is described by the Nernst equation (2.38), in which R is the universal gas constant, n is the number of electrons, F is the Faraday constant, a_x the activity of species x and $E°$ is the standard electrode potential, defined as its potential at an absolute temperature (T) of 298 K and unit activities of all species. Considering that the activity of a pure solid is always unity, in the case of reaction 2.37, equation 2.38 can be re-written as equation 2.39.

$$M^{n+} + ne^- \rightleftharpoons M \tag{2.37}$$

$$E = E° - \frac{RT}{nF} ln \left[\frac{a_M}{a_{M^{n+}}}\right] \tag{2.38}$$

$$E = E° + \frac{RT}{nF} ln\ a_{M^{n+}} \tag{2.39}$$

This is also known as the equilibrium potential for the given redox couple, and it is useful in order to predict which of two species, both present in the same solution or in electrical contact with each other, will act as the oxidant and which will act as the reductant. In a spontaneous redox reaction between two species, the favoured direction of electron transfer is from the reduced form of the couple with a more negative equilibrium potential, to the oxidised form of the couple with a more positive equilibrium potential. Therefore, the equilibrium potentials of redox

couples of interest are often used as a useful prediction tool in the study of hydrometallurgical systems, in particular by using them to construct potential-pH diagrams, which will be discussed in relation to the Caron process in section 2.4.3.

In the case that the leach solution also contains ligands, such as ammonia in the Caron process, which can form thermodynamically favoured complexes with the metal ions (M^{n+}) of interest, the activity of the latter ($a_{M^{n+}}$) is effectively reduced due to the competing equilibrium described by reaction 2.40.

$$M^{n+} + mL \rightleftharpoons ML_m^{n+} \quad (2.40)$$

As a result, the electrode potential of the couple is shifted in the negative direction, and a new reduction potential can be defined for the M/ML_m redox couple (2.41), as described by equation 2.42.

$$ML_m^{n+} + ne^- \rightleftharpoons M + mL \quad (2.41)$$

$$E = E° - \frac{RT}{nF} ln \left[\frac{{a_L}^m}{{a_{ML_m}}^{n+}} \right] \quad (2.42)$$

Therefore, the presence of ligands such as ammonia in the Caron leach liquor is a driving force for the leaching reactions. Complexation of the oxidised metal ions results in more stable species, thereby making the metal M more easily oxidised by a suitable oxidant as its equilibrium reduction potential is made more negative. It is therefore important to have an understanding of which metal complex ions may form during the leach by studying their thermodynamic stability, as discussed in detail for those relevant to the Caron process in the next section.

2.4.2 Stability constants of metal complexes relevant to Caron leach solution

The thermodynamic stability of metal ion complexes is usually expressed in terms of their consecutive (K_m) or cumulative (β_m) stability constants, defined in equations 2.43 and 2.44 respectively.

$$ML_{(m-1)}^{n+} + L \rightleftharpoons ML_m^{n+} \qquad K_m = \frac{a_{ML_m^{n+}}}{a_{ML_{(m-1)}^{n+}} \cdot a_L} \qquad (2.43)$$

$$M^{n+} + mL \rightleftharpoons ML_m^{n+} \qquad \beta_m = \frac{a_{ML_m^{n+}}}{a_{M^{n+}} \cdot a_L^m} \qquad (2.44)$$

Stability constants of a number of metal complexes which may form during the dissolution of metals in Caron leach solutions are available in the literature. Logarithms of the cumulative stability constants for cobalt, nickel and copper ammonia complexes at room temperature and an ionic strength of 0.5 are given in Table 2.5 (Smith and Martell, 1976). For the cobaltous ammine complexes, values were also calculated from data obtained at different temperatures in 5 M ammonium nitrate (Isaev et al., 1990b; Nazari and Asselin, 2010) and are given in Table 2.6. Stability constants for ferrous ammine complexes in aqueous 5 M ammonium nitrate solutions at different temperatures are also available in the literature (Isaev et al., 1990a; Nazari and Asselin, 2010), and are given in Table 2.7.

Table 2.5 Comparison of logβ_m values for different metal ions in different oxidation states*

complex	logβ_m for different values of *m*					
	1	**2**	**3**	**4**	**5**	**6**
$Co(NH_3)_m^{2+}$	2.1	3.67	4.78	5.53	5.75	5.14
$Co(NH_3)_m^{3+}$	-	-	-	25.6	30.7	35.2
$Ni(NH_3)_m^{2+}$	2.81	5.08	6.85	8.12	8.93	9.08
$Cu(NH_3)_m^{+}$	5.93	10.6	-	-	-	-
$Cu(NH_3)_m^{2+}$	4.24	7.83	10.8	13.0	12.4	-

***at 25°C and ionic strength = 0.5 (Smith and Martell, 1989)**

Table 2.6 Effect of temperature on the logβ_m values of $Co(NH_3)_m^{2+}$ complexes*

T (°C)	logβ_m for different values of *m*					
	1	**2**	**3**	**4**	**5**	**6**
5	2.40	4.34	5.73	6.73	7.14	6.94
25	2.31	4.14	5.43	6.36	6.68	6.38
50	2.18	3.89	5.05	5.83	6.01	5.51
75	1.93	3.35	4.23	4.73	4.63	-
100	1.66	2.78	3.41	3.61	-	-
125	1.40	2.27	2.67	2.57	-	-

***in aqueous 5 M ammonium nitrate solutions at different temperatures (Isaev et al., 1990b; Nazari and Asselin, 2010)**

Table 2.7 Effect of temperature on the logβ_n of $Fe(NH_3)_n^{2+}$ complexes*

T (°C)	logβ_m for different values of *m*				
	1	**2**	**3**	**4**	**5**
15	1.77	2.97	3.76	4.19	4.14
25	1.73	2.88	3.63	4.00	3.90
35	1.68	2.79	3.49	3.82	3.68
45	1.64	2.70	3.36	3.64	3.46
55	1.59	2.61	3.22	3.46	3.23

*** in aqueous 5 M ammonium nitrate solutions at different temperatures (Isaev et al., 1990a; Nazari and Asselin, 2010)**

The thermodynamic data presented in Tables 2.5, 2.6 and 2.7 indicate that in Caron-type solutions, the dominant metal-ammine species are likely to be the hexammine for Ni(II) and Co(III), the pentammine for Co(II), the tetrammine for Cu(II) and Fe(II), and the diammine for Cu(I).

It is important to keep in mind that Caron solutions also contain carbonate species, which may also act as ligands. Based on thermodynamic data available in the literature (Caldeira et al., 2008; King, 1998) it appears that ferrous ions form relatively stable complexes with carbonate or bicarbonate ligands (Table 2.8). It is therefore a possibility that in Caron-type solutions, ferrous ions may also form carbonate complexes or mixed complexes with both ammonia and carbonate ligands. However, there appears to be no thermodynamic data available in the literature for any mixed carbonate-ammonia complex of iron, cobalt, nickel or copper ions. Data available in the literature for carbonate or bicarbonate complexes formed with cobalt,

nickel and copper ions is also included in Table 2.8. Although the existence of the cobaltous complex $Co(CO_3)_2^{2-}$ has been reported in the literature (Calderón et al., 2008; Davies and Burstein, 1980b), there appears to be no thermodynamic data available for it.

Table 2.8 Logarithms of the equilibrium constants for the formation of metal-carbonate complexes*

Metal ion	reaction	logK
Fe(II)	$Fe^{2+} + CO_3^{2-} \rightarrow FeCO_3^0$	5.69[a]
	$Fe^{2+} + HCO_3^- \rightarrow FeHCO_3^+$	1.47[a]
	$Fe^{2+} + 2CO_3^{2-} \rightarrow Fe(CO_3)_2^{2-}$	7.45[a]
	$Fe^{2+} + CO_3^{2-} + OH^- \rightarrow FeCO_3(OH)^-$	9.97[a]
Co(II)	$Co^{2+} + CO_3^{2-} \rightarrow CoCO_3^0$	3.1[b]
	$Co^{2+} + HCO_3^- \rightarrow CoHCO_3^+$	1.4[b]
Ni(II)	$Ni^{2+} + CO_3^{2-} \rightarrow NiCO_3^0$	3.6[b]
	$Ni^{2+} + HCO_3^- \rightarrow NiHCO_3^+$	1.6[b]
Cu(II)[c]	$Cu^{2+} + CO_3^{2-} \rightarrow CuCO_3^0$	6.75[c]
	$Cu^{2+} + 2CO_3^{2-} \rightarrow Cu(CO_3)_2^{2-}$	9.92[c]

***at 25°C and ionic strength = [a]0 (Caldeira et al., 2008; King, 1998); [b]0.7, [c]0 (Smith and Martell, 1989)**

Since the Caron leach liquor is also known to contain thiosulfate ions, albeit at significantly lower concentrations than the ammonia or carbonate species, it is important to also consider the possibility of complexation of the metal ions by thiosulfate ligands. In particular, copper is known to form stable complexes with thiosulfate, for which the stability constants are given in Table 2.9.

Table 2.9 Logβ_m values for Cu(I) and Cu(II) thiosulfate complexes*

complex	logβ_m for different values of *m*		
	1	2	3
$Cu(S_2O_3)_m^{1-2m}$	10.4[a]	12.3[a]	13.7[b]
$Cu(S_2O_3)_m^{2-2m}$	2.40[c]	5.20[c]	

*at 25ºC and ionic strength = [a]0.8, [b]1.2, (Sillen and Martell, 1964); [c]0.2 (Senanayake, 2005)

At the high ammonia concentrations of the Caron leach liquor, copper complexes with thiosulfate are not likely to be formed, as the dominant species are expected to be the complexes with ammonia mentioned above. However, it should be kept in mind that, for the copper(I) oxidation state, the stability of thiosulfate complexes appears to be comparable or greater than that of the ammonia complexes (Table 2.5). In any case, the possibility of formation of mixed complexes with both ammonia and thiosulfate ligands should not be completely excluded, as these are known to form when both ammonia and thiosulfate ions are present in solution (Byerley et al., 1973a; Breuer and Jeffrey, 2003). However, the thermodynamic data available in the literature for these mixed complexes is very limited (Senanayake, 2004).

2.4.3 Potential-pH diagrams relevant to the Caron process

As discussed in section 2.4.1, the leaching reactions taking place in the Caron process are electrochemical in nature. Therefore, their thermodynamic feasibility is often assessed with the aid of potential-pH (Eh-pH) diagrams, which are constructed for each particular metal-lixiviant system from the available thermodynamic data. Several potential-pH diagrams have been constructed as part of thermodynamic studies relevant to the Caron process (Asselin, 2008; Osseo-Asare, 1980; Osseo-Asare, 1981a; Osseo-Asare, 1981b; Osseo-Asare, 1981c; Osseo-Asare and Asihene, 1979; Osseo-Asare and Fuerstenau, 1978; Richardson et al., 1981). Diagrams for the nickel-ammonia and cobalt-ammonia systems have also been constructed to support kinetic studies conducted on the leaching of nickel (Bhuntumkomol et al., 1980), nickel sulfides (Senaputra et al., 2008), cobalt (Vu and Han, 1977), cobaltous and cobaltic oxides (Vu et al., 1980) in ammoniacal solutions.

Potential-pH diagrams constructed for nickel, cobalt and copper in ammoniacal solution at a temperature of 60°C, which is the upper temperature limit of the Caron leach, are shown in Figure 2.5, A, B and C respectively (Osseo-Asare, 1981a). For the iron-ammonia system, the only diagrams available in the literature were at a temperature of 25ºC, as the one shown in Figure 2.5, D (Queneau and Weir, 1986).

According to Figure 2.5 (A), nickel hexammine is the stable oxidation product of metallic nickel in the pH range of approximately 8 to 11.5, with its formation taking place at a potential of around -0.7 V. At pH values above 11.5 nickel oxide is the dominant oxidation product, and at potentials above around 0 V the diagram shows regions of stability for Ni_3O_4, Ni_2O_3 and NiO_2.

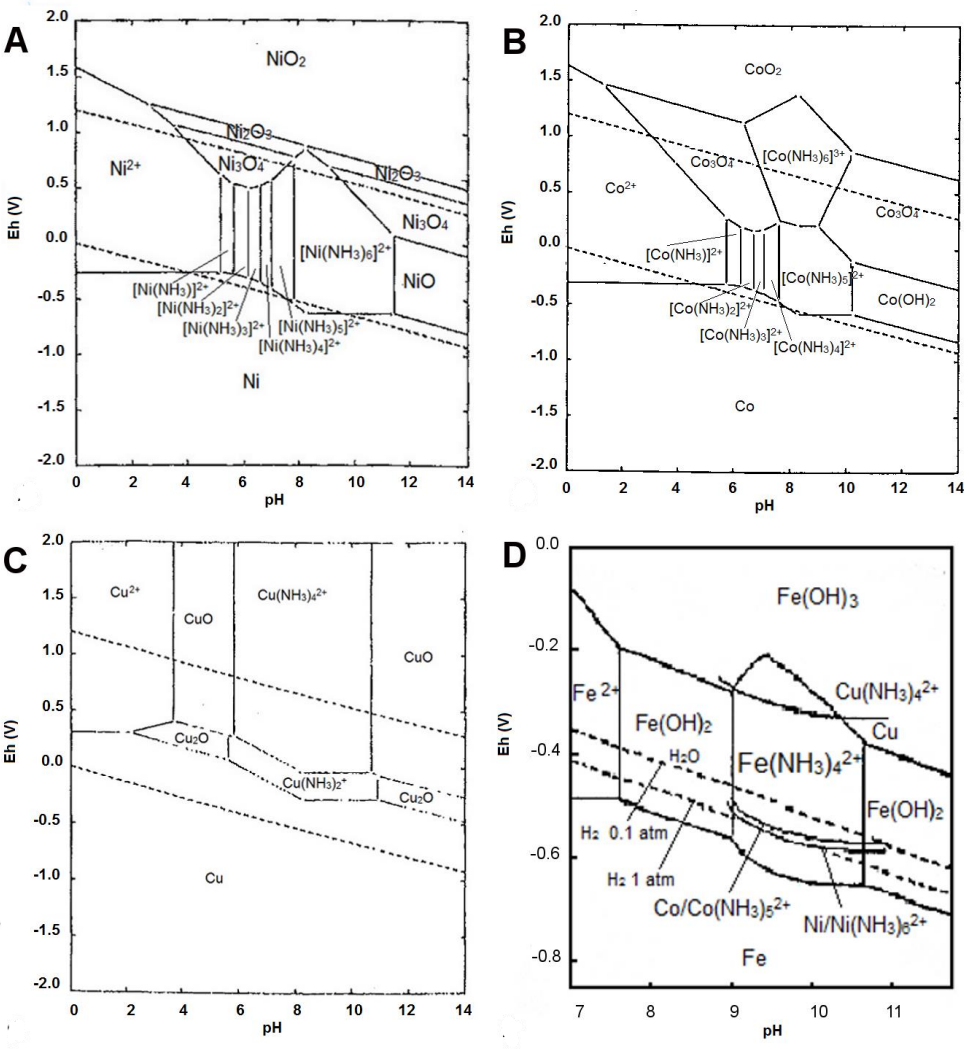

Figure 2.5 Eh-pH diagrams for the M-NH_3-H_2O system at 60°C for M = Ni (A), Co (B), Cu (C), at ammonia activity of 5 and metal activity of 0.1 (Osseo-Asare, 1981a); at 25°C for M = Fe (D) at the following species concentrations: 0.01 M Fe(II); 5 M [NH_3]; 0.2 M Ni; 2 mM Co; 0.001 mM Cu (Queneau and Weir, 1986).

As can be seen in Figure 2.5 (B), under the conditions of the Caron process, cobaltous pentammine is the dominant product of the oxidative dissolution of metallic cobalt, which takes place at potentials of around -0.6 V. However, the cobaltous pentammine appears to be stable only up to a pH of around 10.2, with cobaltous hydroxide becoming the dominant oxidation product at higher pH values. At more positive Eh values, above around 0.2 V, cobaltic hexammine becomes the dominant species up to pH values between 9 and 10. From the diagram it is evident

that cobaltic hexammine can oxidise metallic cobalt resulting in the formation of cobaltous ammine as both the oxidation and reduction product. At higher pH there is also a region of stability for Co_3O_4, which may exist at Eh values above around -0.2 V in the pH range of the process, while CoO_2 may exist at Eh values above around 0.7 V.

Copper is more noble than nickel and cobalt, and its oxidative dissolution to cuprous diammine at around -0.3 V, in the pH region of 8 to 11, may be brought about by molecular oxygen (Figure 2.5, C). As the potential increases above 0 V, cupric tetrammine becomes the dominant dissolved copper species, and this may oxidise metallic copper to form cuprous diammine as both the oxidation and reduction product. At pH values above 11, Cu_2O is stable up to around 0 V, and CuO is the stable phase at higher potentials.

According to Figure 2.5 (D), the potential region of stability of the ferrous tetrammine complex under the given conditions is in the pH region of around 9 to 10.7, between potentials of approximately -0.7 V and a maximum of around -0.2 V at pH 9.4. It should be noted that ferrous ammine species with less than four ammonia ligands appear not to have been taken into consideration for the construction this diagram. Although these may well exist lower pH values and ammonia concentrations, the thermodynamic data presented in Table 2.7 indicates that ferrous tetrammine is the most stable ferrous-ammonia complex under the conditions of the Caron process. In the process pH range of around 10 to 10.5, the equilibrium boundary between metallic iron and the ferrous tetrammine is around -0.7 V. In this region, metallic iron can be dissolved oxidatively by the reduction of hydrogen from ammonium ions in solution, even under a hydrogen gas

pressure of 1 atm. As the potential is increased to more positive values, above around -0.3 V, solid ferric hydroxide becomes the dominant stable species.

For comparison, this diagram also shows the equilibrium boundaries of nickel, cobalt and copper metals with nickel(II) hexammine, cobalt(II) pentammine and copper(II) tetrammine respectively, at given concentrations. It indicates that metallic nickel and cobalt cannot be oxidised by protons at 1 atm hydrogen pressure, whereas this becomes feasible for both metals at a tenfold lower hydrogen pressure. On the other hand, the diagram indicates that copper leaches only at significantly higher potentials. However, it should be noted that only the equilibrium between metallic copper and cupric tetrammine has been included, whereas cuprous diammine is also a stable species in this system, as consistent with the data given in Table 2.5 and the Cu-NH_3-H_2O Eh-pH diagram, which is not expected to differ significantly form 25°C data (Figure 2.5, C). The equilibrium boundary between metallic copper and cuprous diamines should therefore be taken into consideration when discussing the dissolution of metallic copper, which is therefore expected to take place at a more negative potential, as consistent with Figure 2.5 (C).

Further examination of Figure 2.5 (D) indicates that the dissolution of iron via metal displacement reactions by copper(II), nickel(II) or cobalt(II) ammines, resulting in the cementation of metallic copper, nickel or cobalt onto the iron, is thermodynamically feasible for all three metals.

Potential-pH diagrams have also been constructed for iron in the presence of both ammonia and carbonate species (Kho, 1989), as shown in Figure 2.6 (A), and in the presence of carbonate species with no ammonia, also taking into account metastable species (Caldeira et al., 2008), as shown in Figure 2.6 (B).

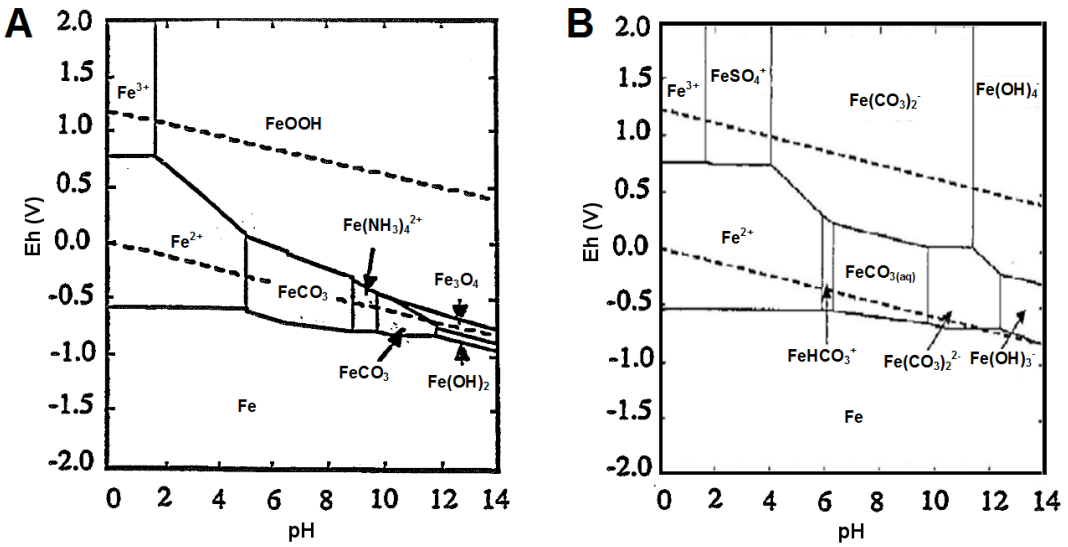

Figure 2.6 Eh-pH diagrams at 25°C for: A) Fe-NH_3-CO_3^{2-}-H_2O- system at total species concentrations of 0.1 mM Fe, 4 M $[NH_3]_T$, 1 M $[CO_2]_T$ (Kho, 1989); B) metastable Fe-S-CO_3^{2-}-H_2O system at 8 mM Fe, 0.1 M $[CO_2]_T$, 0.017 M $[S]_T$ (Caldeira et al 2008).

As can be seen from Figure 2.6 (A), in the presence of carbonate species, the stability region of ferrous tetrammine exists only up to a pH of around 9.7, with ferrous carbonate becoming the dominant stable ferrous species at higher pH values. It should be noted that, for this diagram, the total ammonia concentration is 4 M, around 20% lower than under Caron process conditions. The diagram shown in Figure 2.6 (B) displays the regions of prevalence of a number of iron-carbonate complexes, for which the equilibrium constants are given in Table 2.8. Due to the high relative stability of these species, it is important to also keep in mind their possible existence in ammoniacal-carbonate solutions.

A potential-pH diagram for the Ni-NH_3-H_2O system (Figure 2.7 B) has also been constructed for a temperature of 45°C, at a lower nickel concentration of 0.02 M (Senaputra, 2010), which are conditions more relevant to the Caron leach operated at the Yabulu QN plant.

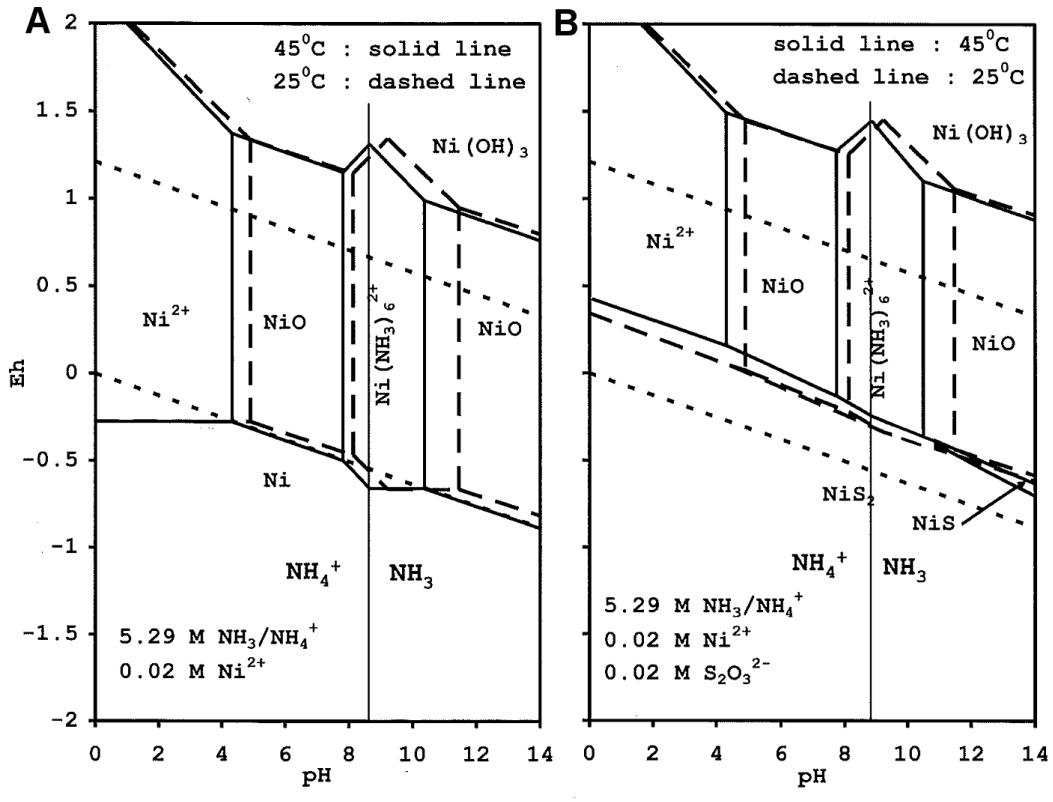

Figure 2.7 Eh-pH diagrams for the Ni-NH_3-H_2O system (A) and the Ni-S-NH_3-H_2O system (B) under Caron process conditions (Senaputra, 2010).

Although nickel ammine complexes with less than six ammonia ligands were not taken into consideration in the construction of the diagrams shown in Figure 2.7, the stability regions of these ammines exist at lower pH values than those relevant to the Caron process (Figure 2.5, A), so they are not thought to affect the stability region of the dominant nickel hexammine species. As consistent with the 60°C data (Figure 2.5, A), the oxidative dissolution of metallic nickel to nickel(II) hexammine takes place at a potential of around -0.7 V. However, from the diagrams shown in Figure 2.7 it appears nickel(II) hexammine is thermodynamically favoured only up to a pH of approximately 10.5, as opposed to 11.5 in the 60°C diagram (Figure 2.5, A). This is not consistent with the expected decrease in the nickel hexammine stability region for increasing temperatures (Osseo-Asare, 1981a; Osseo-Asare and Asihene, 1979;

Senaputra, 2010), and it is unclear which set of thermodynamic data is the most reliable. According to Figure 2.7, as well as the oxidation of nickel to form the hexammine, the formation of nickel oxide, with subsequent passivation, is also thermodynamically favourable under the conditions of the Caron process, with the boundary between this phase and the nickel hexammine being at around the pH of the leach solution.

Due to the presence of thiosulfate ions in the Caron leach liquor and the resulting possible formation of secondary sulfides, as discussed in section 2.3.1, it is also important to consider the Ni-S-NH_3-H_2O system, for which the 45ºC Eh-pH diagram is shown in Figure 2.7 (B). According to this diagram, which shows the regions of stability of NiS and NiS_2, the oxidation of the latter to nickel(II) hexammine under the conditions of the process occurs at a potential around -0.4 V, whereas NiS is stable only above pH 11 in a very small potential region in the -0.5 V to -0.7 V range.

To date, there appear to be no potential-pH diagrams for the Co-S-NH_3-H_2O available in the literature, whereas several diagrams have been constructed for the Cu-S-NH_3-H_2O, although none specifically for the conditions of the Caron process, as for example the one shown in Figure 2.8 (Aylmore and Muir, 2001).

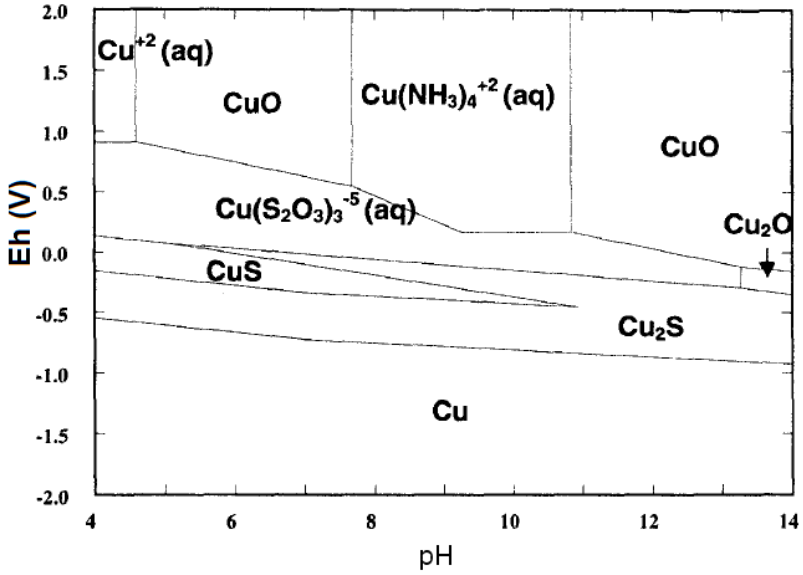

Figure 2.8 Eh-pH diagram for the Cu-NH_3-$S_2O_3^{2-}$-H_2O system at 25°C, 0.05 M Cu(II), 1 M $[NH_3]_T$, 1 M $S_2O_3^{2-}$ (Aylmore and Muir, 2001).

As can be seen from Figure 2.8, the stability region of Cu_2S at the given species concentrations extends across the entire pH range of 4-14, in an intermediate potential region between that of metallic copper and of the copper(I) thiosulfate complex, $Cu(S_2O_3)_3^{5-}$. According to the diagram, the potential boundaries of Cu_2S at pH 10.5 are around -0.8 V and -0.2 V respectively. A very narrow stability region for CuS also exists in this pH region, at potentials around -0.4 V. It should be noted that under the conditions of the Caron process, the concentration of thiosulfate ions is significantly lower (22 mM), and $[NH_3]_T$ higher (5 M), favouring the formation of ammonia complexes, or possibly mixed ammonia-thiosulfate complexes, rather than complexes containing only thiosulfate ligands. However, there appears to be limited information on the thermodynamic stability of mixed ammonia-thiosulfate copper complexes (Senanayake, 2004).

2.5 Electrochemical principles

2.5.1 Mixed potential theory

Due to the electrochemical nature of the reactions which take place during the leaching stage of the Caron process, electrochemistry is a particularly useful tool in the study of these reactions, where the dissolving solid phases act as electrodes interacting with the leach solution.

As mentioned earlier, the Nernst equation can be used to determine the equilibrium potential of a single redox couple under specific conditions, in order to predict the thermodynamic feasibility and direction of the reaction in that system, when compared to other redox couples. However, it does not account for the effect of two or more redox couples, as for example in the oxidative or reductive dissolution reactions typical of many hydrometallurgical processes. A better model of such systems may be provided by the 'mixed potential theory', first described by Wagner and Traud (Wagner and Traud, 1938). The theory describes the potential of an electrode on which two or more electrochemical processes are taking place simultaneously. Under spontaneous, or 'open circuit' conditions, the total anodic current is equal to the total cathodic current, resulting in a net current of zero. The potential assumed by the electrode is often referred to as mixed, rest or corrosion potential, and is at an intermediate value between the equilibrium potentials of the redox couples involved. However, its value is not determined by the individual thermodynamic equilibrium potentials, but rather by their reaction kinetics, and is closer to the equilibrium potential of the fastest reacting species. The mixed potential has in fact been defined as *"a complex function of the forward and reverse rate constant for each half-cell, as well as reactant and product concentrations and the cathodic/anodic area ratio"* (Miller, 1979).

In practice, the mixed potential is determined by measuring the voltage between the electrode of interest and a standard reference electrode in contact with the same solution, and is hence also referred to as the open circuit potential (OCP). Mixed potential theory can therefore help rationalise observed OCP values and leaching behaviour based on comparison with thermodynamic data. More importantly, it is useful in understanding the kinetics of oxidative and reductive leaching processes from a qualitative point of view, as well as quantitatively, if the kinetics of each individual electrode reaction are known (Li et al., 1992).

According to Faraday's law, the mass of a substance reacted in an electrochemical reaction is directly proportional to the number of electrons transferred at the electrode, and therefore the rate of reaction (r, in mol/s) is directly proportional to the current (I), as described by equation 2.45 (Hibbert, 1993). Since the current of an electrode is also proportional to its surface area, it is often useful to refer to the current per unit area, or current density (i) defined by equation 2.46.

$$r = \frac{I}{nF} \tag{2.45}$$

$$i = \frac{I}{A} \tag{2.46}$$

In order to measure a net current on an electrode, it is necessary to perturb it from its spontaneous mixed potential by applying a potential known as 'overpotential'. This can be done in practice using 'potentiodynamic polarisation' techniques.

The fundamental relationship between the net measured current on an electrode and the applied overpotential (η, given by $E - E_{mix}$) is described by the Butler-Volmer equation (2.47), where I_0 is known as the exchange current and α is the transfer coefficient, which has a value between 0 and 1 (Bard and Faulkner, 1980).

$$I = I_0\{[\exp\left[-\frac{\alpha nF\eta}{RT}\right] - \exp\left[\frac{(1-\alpha)nF\eta}{RT}\right]\} \quad (2.47)$$

The resulting current consists of the sum of the cathodic current (I_c, equation 2.48) and the anodic current (I_a, equation 2.49).

$$I_c = I_0 \exp\left[-\frac{\alpha nF\eta}{RT}\right] \quad (2.48)$$

$$I_a = I_0 \exp\left[\frac{(1-\alpha)nF\eta}{RT}\right] \quad (2.49)$$

As the applied potential is shifted in the positive direction, the anodic current becomes dominant, resulting in a positive net current. Likewise, when the applied potential is shifted in the negative direction, the cathodic component becomes dominant, resulting in a net negative current. This is shown for a single redox couple in Figure 2.9 (Bard and Faulkner, 1980). From the figure it can also be seen that as the overpotential increases beyond a certain value, either in the positive or the negative direction, the increase in current begins to level off, no longer following equations 2.48 and 2.49. At this point, the very fast electrochemical reaction is no longer controlling the overall reaction rate, which becomes limited by the diffusion of either the reactants to the electrode surface or the products away from it. The maximum achievable current is known as the limiting current (I_L) as discussed in more detail in section 2.5.2.

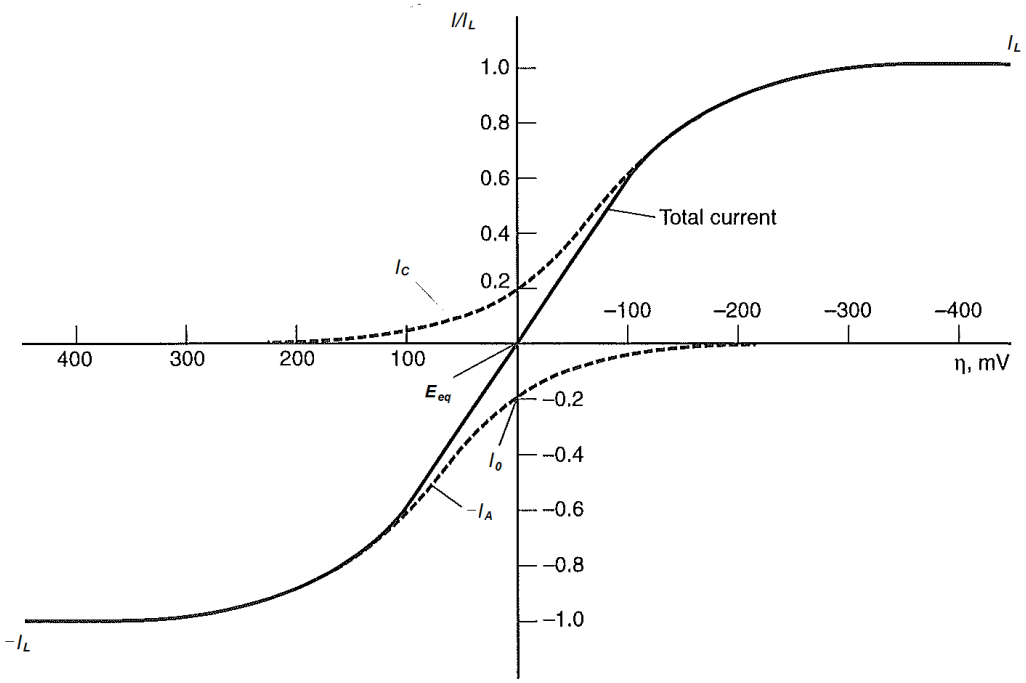

Figure 2.9 Current-overpotential curves for a single redox couple, with α = 0.5, T = 298 K (Bard and Faulkner, 1980).

At the equilibrium potential, the applied overpotential is zero, so from equations 2.48 and 2.49, I_a and I_c become equal and opposite. Their absolute value is equal to I_0, the exchange current, which is proportional to the rate of the electrochemical reaction according to equation 2.45. As it is impossible to determine the anodic and cathodic currents individually, the exchange current cannot be measured directly, although there are methods by which it can be determined, which are beyond the scope of this thesis.

Introducing a second redox couple with a more positive equilibrium potential, therefore an oxidising species, results in a shift in the electrode potential to a more positive value, as illustrated in Figure 2.10. The anodic half-reaction of the first redox couple is now paired with the cathodic half-reaction of the oxidant (Ox^{n+}), as described by equation 2.50, resulting in a higher exchange current.

$$M + Ox^{n+} \rightarrow M^{n+} + Red \qquad (2.50)$$

The potential at which the anodic current is equal, and opposite, to the cathodic current is the mixed potential (E_{mix}), which lies between the equilibrium potentials of the two redox couples. In the most likely case that these have differing reaction kinetics, the mixed potential lies closer to the equilibrium potential of the couple with faster reaction kinetics.

As illustrated in Figure 2.11, an increase in concentration of the oxidant generally causes a greater positive shift in the mixed potential, as well as a greater increase in the exchange, or corrosion, current.

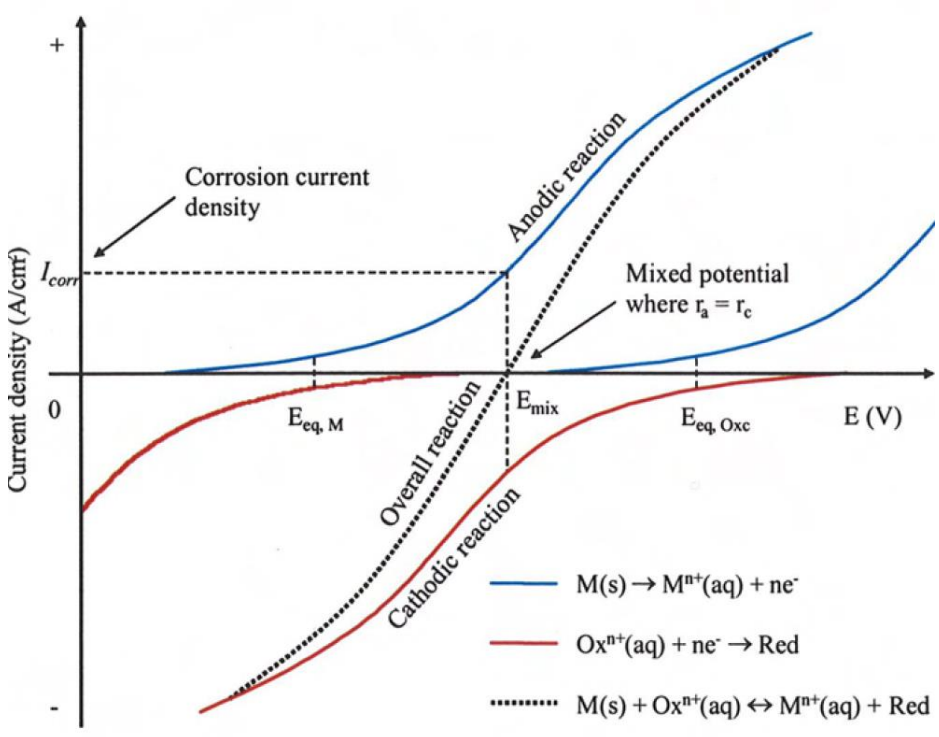

Figure 2.10 Mixed potential diagram for two paired redox couples (Nikoloski, 2002).

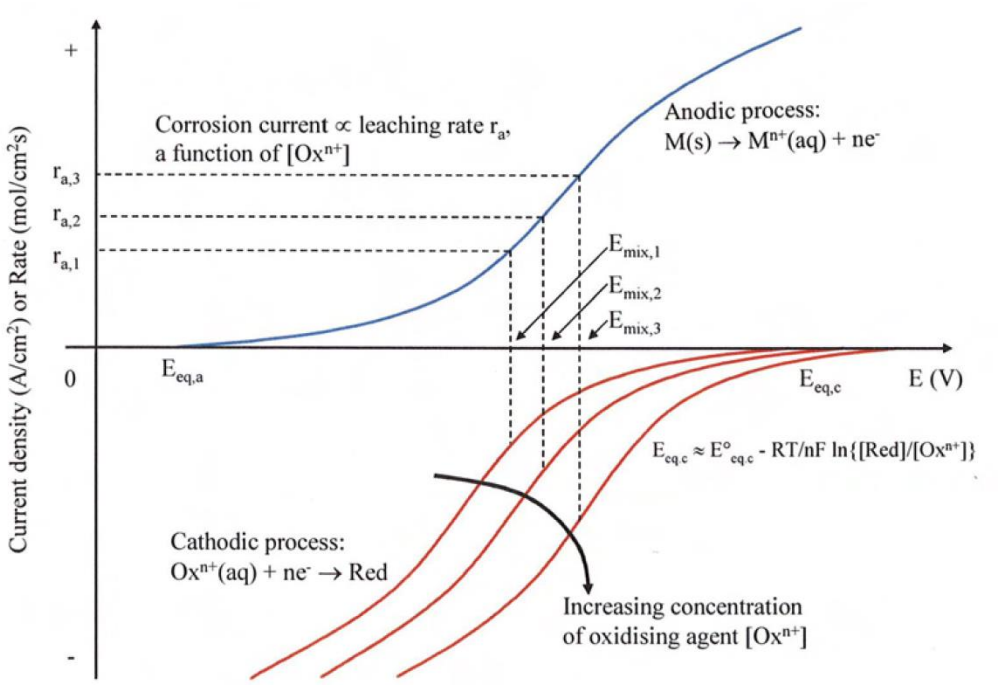

Figure 2.11 Mixed potential diagram for two paired redox couples with increasing concentrations of oxidant (Nikoloski, 2002).

2.5.2 Solution hydrodynamics

The electrochemical dissolution of a solid in a lixiviant takes place via three main steps:

- diffusion of the reactants from the bulk solution to the solid surface
- electrochemical reaction at the surface-solution interface
- diffusion of the products from the solid surface into the bulk solution

When the mixed potential of a solid is in a region where the electrochemical reaction is very fast and no longer limiting the overall rate of dissolution, the process is said to be under diffusion or mass-transport control. Under these conditions, the concentration of the reactant approaches zero at the electrode-solution interface and it asymptotically approaches the bulk concentration at increasing distance from it. The region in the vicinity of the electrode in which the concentration is significantly lower than in the bulk of the solution is known as the diffusion layer (δ), of which

the thickness is defined arbitrarily. This is shown in Figure 2.12 for the Nernst diffusion layer (IUPAC, 1997), where c_o is the concentration in the bulk of the solution and c_e is the concentration at the electrode.

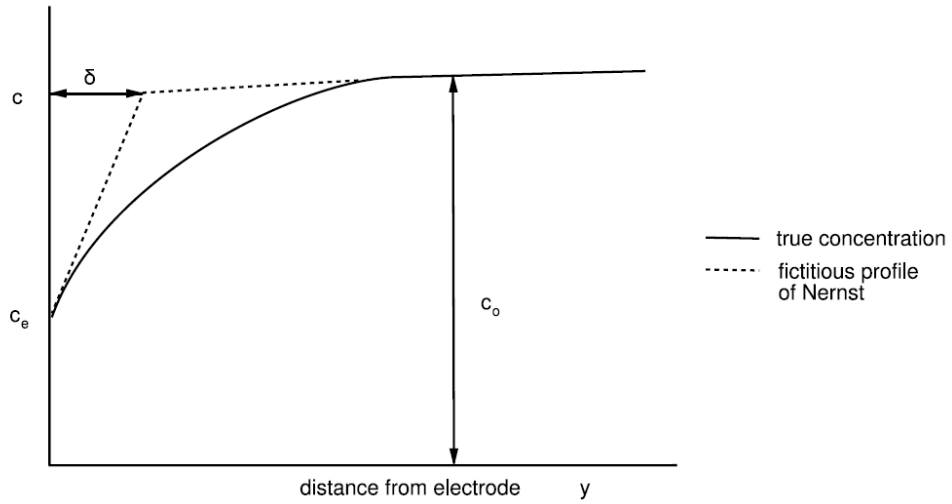

Figure 2.12 Nernst diffusion layer (IUPAC, 1997).

The use of a rotating disk electrode (RDE) for the electrochemical studies ensures a laminar flow of the reactant to the electrode surface, as shown in Figure 2.13.

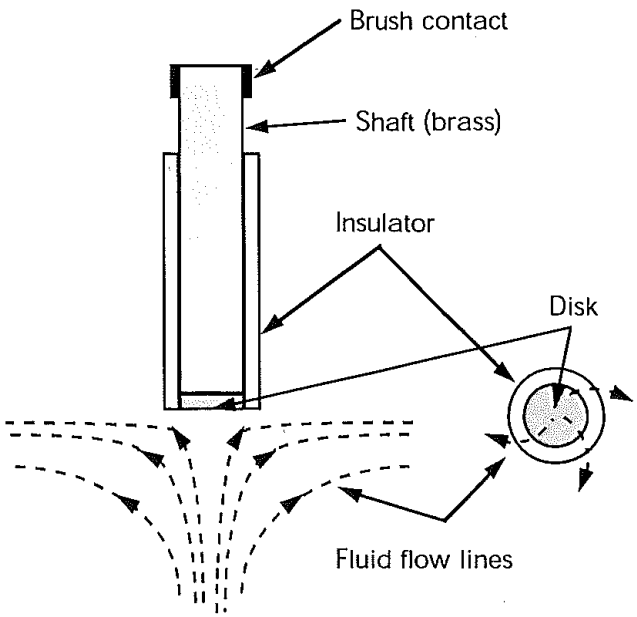

Figure 2.13 Schematic diagram of a rotating disk electrode showing laminar flow of the solution (Drok et al., 1998).

Under the controlled hydrodynamic conditions of a rotating disk electrode, the diffusion layer thickness (δ) is equal at all points of the electrode surface and inversely related to the electrode rotation speed, or angular velocity (ω), according to equation 2.51 (Bard and Faulkner, 1980), where ν is the kinematic viscosity of the solution and *D* the diffusion coefficient of the reactant in the solution.

$$\delta = 1.61 \frac{\nu^{1/6} D^{1/3}}{\omega^{1/2}} \tag{2.51}$$

When the overpotential applied to a rotating disk electrode is increased beyond a certain point, at which the reaction rate becomes limited by diffusion, the current reaches a steady value, displaying a sigmoidal shape (Figure 2.14) typical of polarisation measurements conducted on rotating disk electrodes.

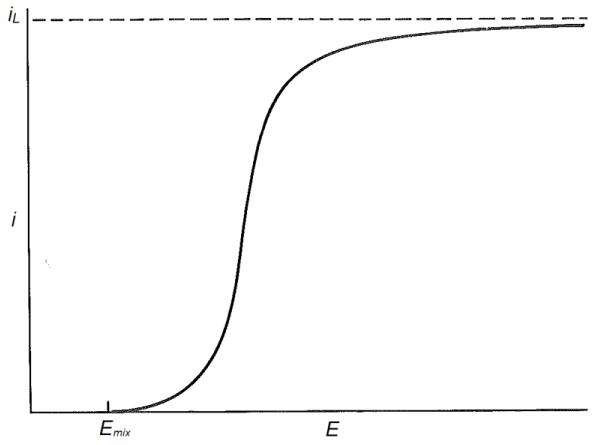

Figure 2.14 The current at an electrode as a function of potential (adapted from Hibbert, 1993).

The maximum achievable current density for any given concentration of reactant is known as the limiting current density (i_L), which is dependent on the rotation speed of the electrode according to equation 2.52, which is known as the Levich equation (Hibbert, 1993).

$$i_L = 0.62\, nF\omega^{1/2}\nu^{-1/6}D^{2/3}c_o \tag{2.52}$$

For some experiments, it is also useful to introduce a second working electrode in the form of a ring around the rotating disk electrode. This is known as a rotating ring-disk electrode (RRDE), which needs to be operated by a bipotentiostat, which is capable of controlling two working electrodes. The use of a RRDE enables the study of the products of electrochemical reactions taking place at the rotating disk electrode, in the case that these consist of solution species. The laminar flow produced by rotation of the RRDE (Figure 2.13) ensures that the species formed at the disk reach the ring electrode in a controlled manner. Detection of these species as they react at the ring electrode often provides additional information which is particularly useful in the elucidation of electrochemical reaction mechanisms.

2.5.3 Linear sweep voltammetry

When the potential applied to an electrode is varied linearly over time, the resulting current response may be plotted against the potential, effectively taking a diagonal slice out of a three dimensional current - potential - time surface (Bard and Faulkner, 1980; Hibbert, 1993). This type of experiment is known as linear sweep voltammetry, which can be conducted in the positive (anodic) or in the negative (cathodic) direction, and ideally results in a current response similar to the one shown in Figure 2.15.

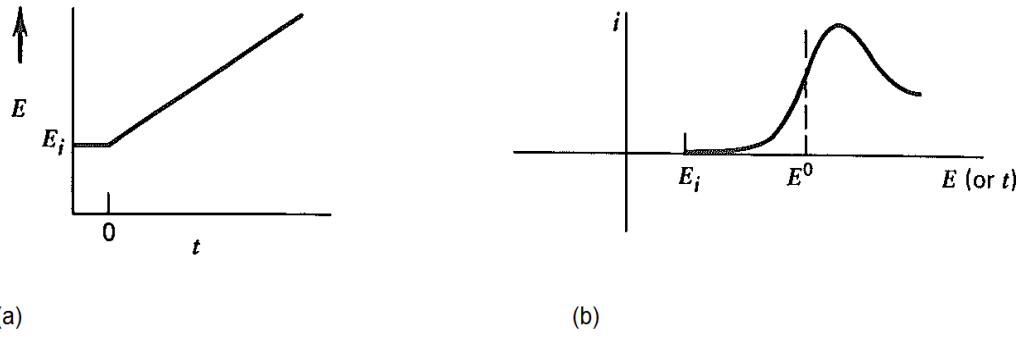

Figure 2.15 Linear potential sweep starting at E_i (a) and the resulting current response (b) (Bard and Faulkner, 1980).

For a Nernstian (reversible) reaction, the peak current is dependent on the square root of the sweep rate (v), according to the Randles-Sevcik equation, which at 25°C takes the form of equation 2.53 (Bard and Faulkner, 1980), where *A* is the area of the electrode and *c* the reactant concentration.

$$I_p = (2.69 \times 10^5)\, n^{3/2} A D^{1/2} v^{1/2} c \qquad (2.53)$$

The peak potential (E_p) is independent of the sweep rate if the reaction is reversible, and the half-peak potential ($E_{p/2}$), at which I = ½ I_p, is related to the peak potential according to Equation 2.54.

$$\left|E_p - E_{p/2}\right| = 2.2\ \frac{RT}{nF} \qquad (2.54)$$

Therefore, linear sweep voltammetry can be used to determine whether a reaction is reversible, if the above conditions are obeyed.

2.5.4 Cyclic voltammetry

In cyclic voltammetry, the applied potential is swept linearly in the anodic or the cathodic direction until it reaches a certain limit, at which its direction is inverted towards the opposite direction at the same rate, as shown in Figure 2.16 (a). The resulting current response is then plotted against the potential, resulting in a cyclic voltammogram (Figure 2.16, b), for which there are two conventions, one with increasingly positive potentials towards the right and anodic currents upwards, and the other with increasingly negative potentials towards the right and cathodic currents upwards. In the work presented in this thesis, the former convention has been adopted.

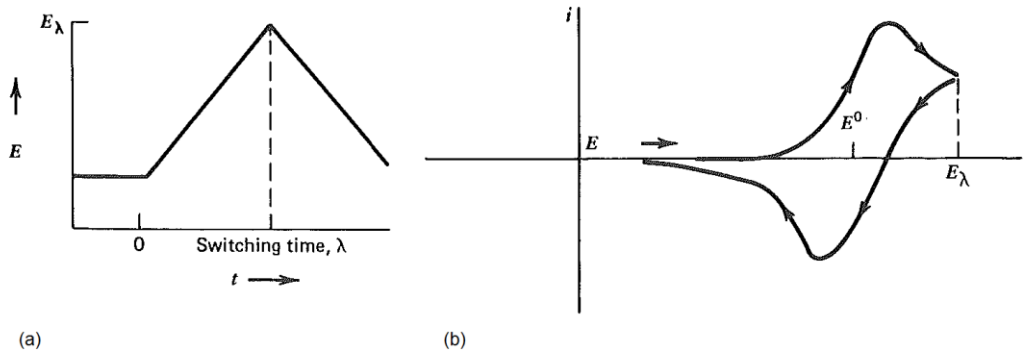

Figure 2.16 Cyclic voltammetry sweep (a) and resulting cyclic voltrammogram (b) (Bard and Faulkner, 1980).

As can be seen from Figure 2.16 (b), scanning the applied potential in the positive direction results in an anodic current which, in the case of an inert electrode, is due to the oxidation of a species present in solution. Similarly, scanning the potential in the negative direction, results in a cathodic current which is due to the corresponding reduction reaction. This type of measurement is generally conducted on a stationary electrode, which results in an anodic or cathodic current peak, depending on the direction of the sweep, arising as the current becomes limited by the availability of the reactant at the electrode interface. It should be noted that in the case of a rotating disk electrode, the current peaks shown in Figure 2.16 (b) may not be observed, and diffusion limited reactions generally result in the sigmoidal behaviour described in section 2.7 (Figure 2.14).

If the reaction is reversible, the anodic and cathodic peak potentials (E_{pa} and E_{pc}, respectively) are independent of the sweep rate, and the distance between the anodic and cathodic peaks obeys equation 2.55.

$$E_{pa} - E_{pc} = 2.303\ \frac{RT}{nF} \qquad (2.55)$$

Most of the electrochemical investigations relevant to this thesis have been focussed on more complex, generally irreversible, heterogeneous electrochemical processes. They have therefore been conducted mainly on non-inert electrodes consisting of the material being studied. In this type of voltammetric measurement, the electrode itself is oxidised or reduced as the applied potential is varied. As a result, the observed currents are mainly due to the anodic or cathodic behaviour of the electrode itself, rather than to the homogeneous redox reactions of species present in solution. A number of linear sweep and cyclic voltammetry studies conducted by various authors using non-inert electrodes in solutions relevant to this thesis are described in more detail in sections 2.8 and 2.9.

2.5.5 The passivation of metals

As discussed in section 2.5.1, a positive shift in the overpotential applied to a metal electrode is expected to result in an increase in the anodic current, hence the corrosion rate. However, this is not always the case, due to the possibility of other reactions which may become thermodynamically favourable as the applied potential becomes more positive. In the case that these reactions result in the formation of a non-reactive solid product, which inhibits further oxidation of the metal, effectively protecting it from further corrosion, passivation of the metal is said to occur. In this case, increasing the applied potential above a certain value, known as the passivation potential, results in the anodic current dropping rapidly to negligible values, as shown in Figure 2.17 (Bockris and Reddy, 1970).

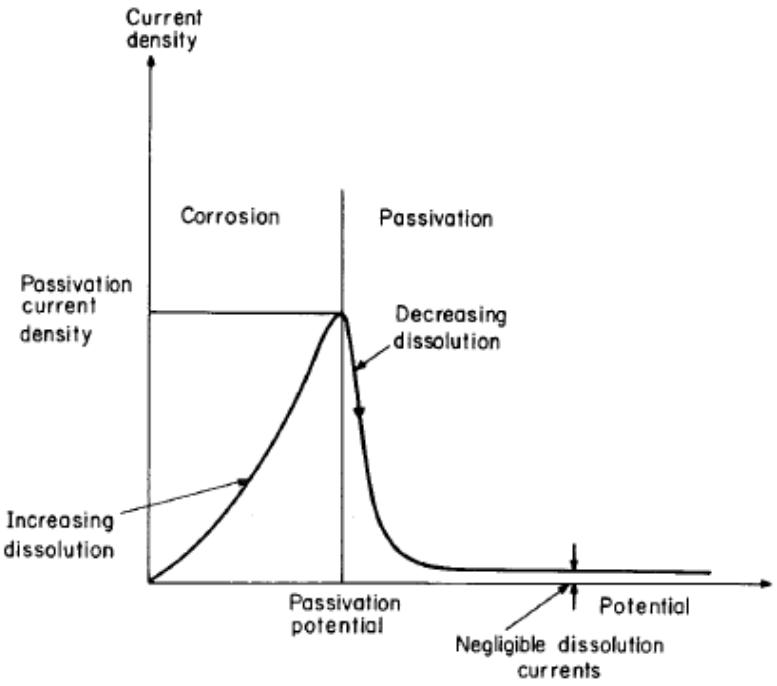

Figure 2.17 Current-potential profile for a metal which undergoes passivation when the applied potential is increased above the passivation potential (Bockris and Reddy, 1970).

The passivation of a metal can therefore be brought about by applying a sufficiently positive overpotential, either potentiostatically or during a linear sweep or cyclic voltammetry scan. However, there are some cases in which the passivation of a metal may take place spontaneously, under open-circuit conditions, therefore in the absence of any applied overpotential. This may occur at a high enough concentration of an oxidising species, which, as consistent with Figure 2.11, is capable of increasing the corrosion current density above the critical passivation current density necessary for the formation of a protective oxide layer (Bockris and Reddy, 1970).

2.6 Electrochemical investigations relevant to the Caron leach system

2.6.1 The electrochemical behaviour of metallic iron

a) Ammoniacal-carbonate solutions

There have been several investigations into the electrochemical behaviour of iron in ammoniacal-carbonate solutions similar to those employed in the Caron process, even though these were all carried out at 25°C (Kho et al., 1992; Kim et al., 1991; Lee et al., 1985; Nikoloski et al., 2003). Some studies were also conducted on various alloys of iron with nickel, cobalt and copper (Jandová and Pedlik, 1991; Nikoloski, 2002; Nikoloski and Nicol, 2006), as discussed separately in section 2.6.5. Unless otherwise stated, the potentials referred to throughout this thesis are relative to the standard hydrogen scale (SHE).

The electrochemical investigations consistently showed that metallic iron and its alloys dissolve anodically in ammonia-ammonium carbonate solutions, both in the presence and in the practical absence of dissolved oxygen. As consistent with the thermodynamic studies (section 2.4, Figure 2.5, D) the OCP of iron in ammoniacal-carbonate solutions not containing any other species is in the region of -0.7 V, reaching approximately -0.5 V in the presence of other species typically encountered in Caron leach solutions (Nikoloski, 2002). In the absence of any other oxidant, metallic iron is thought to be oxidised by the reduction of H^+ from ammonium ions to hydrogen gas.

It has been suggested that the dissolution of metallic iron occurs initially via the oxidative adsorption of hydroxyl ions, according to reactions 2.56 to 2.59 (Kho, 1989).

$$Fe + OH^- \rightarrow (FeOH)_{ad} + e^- \quad (2.56)$$

$$(FeOH)_{ad} \rightarrow FeOH^+ + e^- \quad (2.57)$$

$$FeOH^+ + NH_3 \rightarrow FeNH_3^{2+} + OH^- \quad (2.58)$$

$$FeNH_3^{2+} + 3NH_3 \rightarrow Fe(NH_3)_4^{2+} \quad (2.59)$$

Potentiodynamic studies have consistently shown that iron passivates as the applied potential is increased above a value which depends on the solution composition (Kho et al., 1992; Kim et al., 1991; Osseo-Asare et al., 1983). It was also noted that the presence of dissolved cobalt, mainly as cobaltic hexammine, increased the tendency of iron to form passive films and bulk reaction products (Lee et al., 1985).

Cyclic voltammograms of iron in ammoniacal-carbonate solutions at room temperature are shown in Figure 2.18.

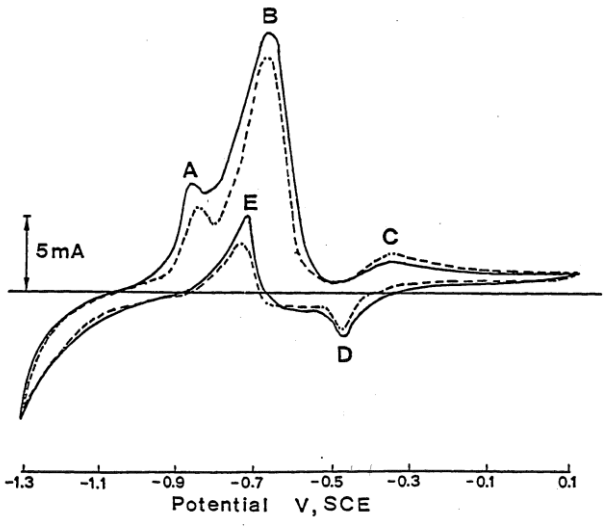

Figure 2.18 Cyclic voltammogram of iron in 4 M $[NH_3]_T$ and 1 M $[CO_2]_T$ (pH 9.8) at 50 mV/s; solid and dashed lines represent first and sixth cycle respectively, measured against a saturated calomel electrode (Kho, 1989).

The appearance of peak A was assigned to the oxidation of adsorbed hydrogen, as it was only observed when the electrode was pre-treated at a potential more negative than the hydrogen evolution potential. Peak B was assigned to the anodic dissolution of iron according to reactions 2.56 - 2.59. It was suggested that the passivation of iron observed as the potential was increased beyond peak B, took place via the formation of an iron carbonate pre-passive layer, as described by reactions 2.60 - 2.62 (Kho, 1989).

$$Fe(NH_3)_4^{2+} + HCO_3^- \rightarrow FeCO_3 + 3NH_3 + NH_4^+ \quad (2.60)$$

$$Fe(NH_3)_4^{2+} + 2OH^- \rightarrow Fe(OH)_2 + 4NH_3 \quad (2.61)$$

$$Fe(OH)_2 + HCO_3^- \rightarrow FeCO_3 + H_2O + OH^- \quad (2.62)$$

The iron carbonate precipitate was then thought to either re-dissolve (reaction 2.63) or undergo further oxidation (reaction 2.64).

$$FeCO_3 + HCO_3^- \rightarrow Fe(CO_3)_2^{2-} + H^+ \quad (2.63)$$

$$FeCO_3 + 4OH^- \rightarrow Fe_3O_4 + 3HCO_3^- + H^+ + 2e^- \quad (2.64)$$

Peak C (Figure 2.18) was assigned to the oxidation of iron(II) in the passive layer to iron(III) and peak D, observed during the cathodic scan, was assigned to the corresponding reduction. The anodic peak (E) also observed during the cathodic scan was thought to correspond to the reactivation of the anodic dissolution of iron through the passive layer.

However, the spontaneous passivation of iron in ammonia-ammonium carbonate solutions has only been observed under highly specific conditions (Kasherininov, 1960; Nikoloski et al., 2003), described as follows.

Kasherininov (1960) found that at room temperature and in the presence of atmospheric oxygen, iron powder dissolved rapidly in ammonia-ammonium carbonate solution, but became passive when dissolved cobalt was also present. It was not stated in the text whether the solution was aerated nor whether the cobalt, which had been dissolved from the metallic powder, was present as cobalt(II) or cobalt(III). Based on the concentrations given as normality (N) it appeared that an oxidation state of +2 was assumed, even though for one set of data, the author referred to the cobalt in the leach solution as being trivalent. Since the experiments were conducted in the presence of air and over extended periods of time, it is likely that the dissolved cobalt was present mainly in the +3 oxidation state.

As can be seen from Figure 2.19, the iron OCP in the absence of dissolved cobalt was found to be around -0.5 V (converted to the SHE scale), which is the potential region for the active dissolution of iron to ferrous tetrammine (Figure 2.5, D). At dissolved cobalt concentrations of 0.5 mM and 5 mM, the OCP was found to drop from an initial value of around -0.1 V to around -0.5 V, during the first day of measurement. After that, it remained for several days in this region, before increasing steeply to potentials above 0 V, during the 4^{th} day at a dissolved cobalt concentration of 5 mM, and during the 7^{th} day at 0.5 mM. In the presence of 50 mM dissolved cobalt, the initial drop in OCP was not observed, and the potential increased gradually to 0 V within one day, continuing to increase over the 9 day period of the measurement.

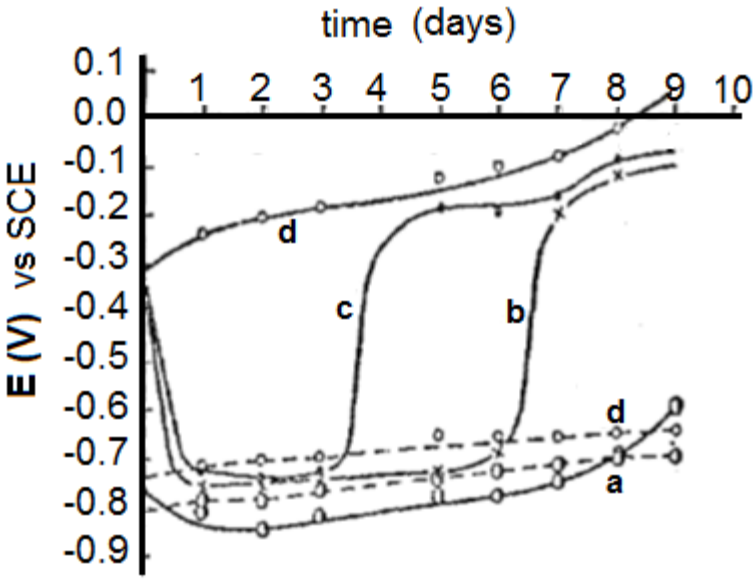

Figure 2.19 OCP over time of iron (solid lines) and cobalt (dashed lines) measured against a saturated calomel electrode in solutions containing 5 M $[NH_3]_T$ and 1 M $[CO_2]_T$ at the following dissolved cobalt concentrations: a) no cobalt; b) 0.5 mM; c) 5 mM; d) 50 mM (Kasherininov, 1960).

Nikoloski found that iron passivated spontaneously following several hours of immersion in ammoniacal carbonate solutions simulating the composition of the loaded Caron leach liquor at the Yabulu QN refinery, for which the total species concentrations are given in Table 2.10 (Nikoloski, 2002; Nikoloski et al., 2003).

Table 2.10 Composition of the loaded Caron leach liquor*

[species]	Concentration (M)
$[NH_3]_T$	5.28
$[CO_2]_T$	1.02
[Ni(II)]	0.15
[Co(II)]	0.012
$[S_2O_3^{2-}]$	0.022

***from Yabulu QN refinery (Nikoloski, 2002)**

The analysis of the iron surface by SEM/EDX, following its passivation in the above solution, revealed the presence of a mixed nickel and cobalt sulfide layer. The formation of this layer was found to lead to a gradual decrease in the rate of dissolution of iron and eventually passivation of the iron surface (Nikoloski et al., 2003). Simultaneous measurements of the dissolution rate of iron and of its OCP showed that as the passivation was taking place, an increase in the OCP to potentials above 0.1 V was observed.

The passivation of iron in these solutions was found to take place both in the presence and in the practical absence of dissolved oxygen. In the absence of any thiosulfate ions, passivation was only observed in solutions which had been sparged with oxygen (Nikoloski, 2002).

The studies reviewed so far have focused primarily on the interaction between metal ions and ammonia, whereas little has been said about the role of carbonate species which are also present in the Caron leach system. It was observed that the potentiodynamic polarisation of iron in ammonia-ammonium carbonate solutions resulted in a yellow precipitate identified by XRD as a basic ferrous ammonium carbonate, $(NH_4)_2Fe_2(OH)_4(CO_3)_2 \cdot H_2O$, which formed on the iron surface as the potential was scanned in the positive direction through the active dissolution region (Lee et al., 1985). It was also suggested elsewhere that that the bicarbonate ion is involved in the mechanism of passivation of iron in ammoniacal solutions by forming a ferrous carbonate pre-passive layer (Kho, 1989).

b) Ammonia-free carbonate solutions

The electrochemical behaviour of iron in ammonia-free carbonate/bicarbonate solutions has been studied extensively by numerous research groups (Armstrong and Coates, 1974; Blengino et al., 1995; Castro et al., 1986; Castro and Vilche, 1991; Castro et al., 1991; Davies and Burstein, 1980a; Jayalakshmi and Muralidharan, 1991; Valentini et al., 1983; Valentini et al., 1985).

It has been suggested that the anodic dissolution of iron in bicarbonate solutions takes place according to reactions 2.65 - 2.68, based on studies conducted at pH 8.8 and total carbonate-bicarbonate concentrations in the range of 0.1 M to 1.5 M (Davies and Burstein, 1980a).

$$Fe + 2H_2O \rightarrow Fe(OH)_2 + 2H^+ + 2e^- \quad (2.65)$$

$$Fe + HCO_3^- \rightarrow FeCO_3 + H^+ + 2e^- \quad (2.66)$$

$$Fe(OH)_2 + HCO_3^- \rightarrow FeCO_3 + H_2O + OH^- \quad (2.67)$$

$$FeCO_3 + HCO_3^- \rightarrow Fe(CO_3)_2^{2-} + H^+ \quad (2.68)$$

Formation of the ferrous carbonate complex is thought to drive the dissolution of iron. This is consistent with the observed increased solubility of iron and anodic currents with increasing bicarbonate concentration and electrode rotation speed. The formation of this complex is also considered responsible for the pitting of iron, and whilst in aerated solutions the complex is oxidised to insoluble ferric species, these are thought to cover the pits without preventing their growth (Davies and Burstein, 1980a). The formation of $Fe(CO_3)_2^{2-}$ was also suggested by other workers (Jayalakshmi and Muralidharan, 1991), as was the formation of bicarbonate complexes $FeHCO_3^+$ and $Fe(HCO_3)_2$ (Castro et al., 1991), $FeCO_3^0$ and $Fe(OH)CO_3^-$

(Caldeira et al., 2008), for which the thermodynamic data are given in Table 2.8 and Figure 2.6, B.

The observed OCP of iron in bicarbonate solutions is around -0.6 V (Davies and Burstein, 1980a), which is in good agreement with the thermodynamic data presented in Figure 2.6 (B).

The spontaneous passivation of iron has not been observed in carbonate-bicarbonate solutions, even under air-saturated conditions. Passivation was achieved through an anodic pre-treatment, which resulted in an OCP above 0 V, but this was reverted spontaneously in deoxygenated solutions, with reactivation of the dissolution of iron (Davies and Burstein, 1980a).The applied potentials necessary for passivation to take place were found to be dependent on pH but independent of the carbonate-bicarbonate concentration, which suggests that passivation is due to the formation of an oxide or hydroxide. Based on ring-disk measurements showing that Fe(II) species were produced by reduction of the passive film, the passive layer was suggested to be an Fe(III) oxide or hydroxide, possibly Fe_2O_3 (Armstrong and Coates, 1974).

Potentiodynamic polarisation and cyclic voltammetry studies have consistently shown the presence of up to three anodic peaks, depending on conditions (Castro et al., 1991; Davies and Burstein, 1980a; Simpson and Melendres, 1996; Valentini et al., 1985). Typical polarisation curves are shown in Figure 2.20, where the oxidation of iron to ferrous hydroxide (equation 2.65) is thought to dominate up to the potential region of peak A.

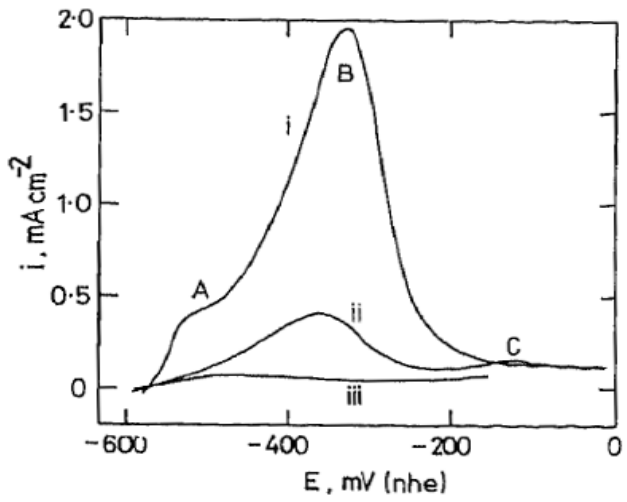

Figure 2.20 Anodic polarization of Fe in 0.75 M $KHCO_3$, 0.75 M K_2CO_3 (pH 8.8) at 10 mV/s. (i) ω = 58.3 Hz; (ii) ω = 0; (iii) ω= 58.3 Hz, solution saturated with Fe(II) 4.4 mM (Davies and Burstein, 1980a).

As the potential is increased, the iron is thought to dissolve through the ferrous hydroxide layer, resulting in the formation of a heterogeneous surface film of ferrous hydroxide and ferrous carbonate in the region between peaks A and B (Davies and Burstein, 1980a).

The appearance of peak C, at potentials above -0.2 V when the electrode was not rotated (Figure 2.20) was also observed by other workers using stationary electrodes (Valentini et al., 1985). This was attributed to the oxidation of ferrous carbonate remaining on the surface to an iron(III) species (Davies and Burstein, 1980a).

The electrochemical observations are consistent with XRD studies reporting the formation of both ferrous hydroxide and ferrous carbonate (Jayalakshmi and Muralidharan, 1991). In general, the corrosion product layers formed on iron during its active dissolution in carbonate-bicarbonate solutions are thought to contain iron carbonate, oxides and hydroxycarbonates (Blengino et al., 1995; Legrand et al., 2001a; Legrand et al., 2001b; Legrand et al., 2000; Savoye et al., 2001). The

formation of iron carbonate appears to be favoured by the absence of oxygen in solution.

Studies conducted using X-ray Photo-electron Spectroscopy (XPS) indicated the presence of Fe_2O_3 and no carbonate in the passive layer formed on iron at high anodic potentials (Castro et al., 1991). Moreover, combined electrochemical and in-situ Surface-Enhanced Raman Spectroscopy (SERS) studies suggested that ferrous carbonate does not play any significant role in the passivation process, and that ferrous hydroxide is the species which undergoes a transformation to the passivating iron(III) containing layer (Simpson and Melendres, 1996). Therefore, whereas carbonate and bicarbonate ions are involved in the formation of solid corrosion films on iron, they appear to be enhancing corrosion by forming soluble complexes, as reported in Table 2.8. The conditions which favour passivation are therefore more likely to be those which favour the formation of ferrous hydroxide (reaction 2.65) over that of ferrous carbonate species (eg. reactions 2.66 and 2.68).

2.6.2 The electrochemical behaviour of metallic cobalt

a) Ammoniacal-carbonate solutions

In ammonia-ammonium carbonate solutions similar to those employed in the Caron process (see Table 2.10 for composition), metallic cobalt dissolves anodically to form a cobaltous ammine ion at an observed OCP of around -0.5 V (Kasherininov, 1960; Nikoloski, 2002). This is consistent with the stability region of cobaltous pentammine ion shown in Figure 2.5 (B), in section 2.4.

Upon aeration, the cobaltous complexes undergo further oxidation by dissolved oxygen to cobaltic ammines, which participate as oxidants in the leaching process, functioning as redox mediators (Nicol et al., 2004), as described in section 2.3.2.

Anodic polarisation curves obtained for cobalt in ammoniacal-carbonate solutions representative of the Yabulu QN Caron leach liquor are shown in Figure 2.21. In all of the solutions, the anodic current density began to increase more steadily at potentials around -0.4 V, resulting in broad peak in the region of -0.2 V. A steep decay typical of passivation was not observed, with the current density decreasing gradually thereafter, and was reported to reach values close to zero up to the oxygen evolution region. Another study, conducted in barren ammoniacal-carbonate solution (Osseo-Asare et al., 1983), reported a breakdown of passivity, with a resulting increase in anodic current, as the applied potential was scanned above 0.8 V.

Although passivation of metallic cobalt was observed in both studies during potentiodynamic polarisation measurements (Nikoloski and Nicol, 2006; Osseo-Asare et al., 1983), it was not found to take place spontaneously, in the absence of any applied current, under the conditions of the Caron process (Kasherininov, 1960; Nikoloski and Nicol, 2006).

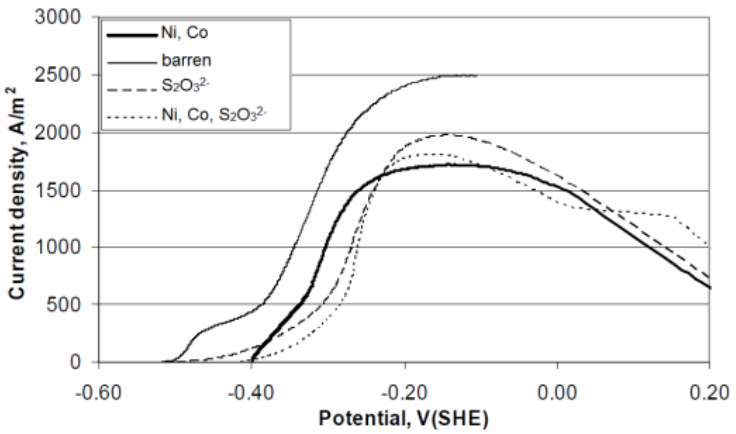

Figure 2.21 Anodic behaviour of a cobalt RDE (500 rpm) scanned at 1 mV/s in aerated solutions containing 5.28 M $[NH_3]_T$, 1.02 M $[CO_2]_T$, and the species indicated in the legend at the following concentrations: [Ni(II)] = 0.15 M, [Co(II)] = 0.012 M and $[S_2O_3^{2-}]$ = 0.022 M (Nikoloski and Nicol, 2006).

The passive layer formed on cobalt during the potentiodynamic polarisation experiments appeared to be less stable than the one formed on iron. This was evident from the relatively high anodic currents measured in the passive region and the observed breakdown of passivity (Osseo-Asare et al., 1983). It was also supported by the observation that following an anodic polarisation scan, the reactivation of metallic cobalt was found to take place readily during the cathodic sweep, at potentials close to the passivation potential (Nikoloski and Nicol, 2006), or even spontaneously, once the applied current was switched off (Kasherininov, 1960). In one study, the passive layer formed on cobalt was identified using X-ray diffraction (XRD) as being Co_3O_4 (Lee et al., 2003), which is consistent with the thermodynamic data presented in Figure 2.5 (B). However, it was not possible to access the full details of this work.

Several studies have also shown that the anodic behaviour of cobalt in ammoniacal-carbonate solutions is significantly affected by the behaviour of iron (Kasherininov, 1960; Lee et al., 1985; Osseo-Asare et al., 1983). It was found that in powder mixtures containing metallic cobalt and iron as separate phases in contact with each

other, the dissolution of cobalt was prevented by the presence of iron until most of the latter had dissolved (Kasherininov, 1960). This was explained in terms of the iron-cobalt galvanic cell in which the iron, being less noble, acted as the anode, dissolving preferentially, while the metallic cobalt acted as a cathode, remaining un-dissolved. It was also observed that the passivation of iron, induced by the presence of dissolved cobalt (see section 2.6.1) resulted in greater dissolution of cobalt. Again, this was explained in terms of the cobalt-iron corrosion couple, in which the passivation of iron resulted in the cobalt becoming the anode and dissolving preferentially, with the passive iron acting as the cathode. This was also thought to take place when the metallic cobalt was in contact with iron-cobalt alloys which had passivated and thereby acted as cathodes, while pure cobalt acted as the anode and dissolved.

b) Ammonia-free carbonate solutions

There have been several studies on the electrochemical behaviour of metallic cobalt in carbonate-bicarbonate solutions (Burstein and Davies, 1980; Calderón et al., 2008; Davies and Burstein, 1980b; Gervasi et al., 1989; Real et al., 2008). The observed OCP of cobalt in these solutions at pH 8.8 and 0.8 $[CO_2]_T$ was found to be around -0.5 V (Davies and Burstein, 1980b), and cyclic voltammetry studies have consistently shown an anodic peak in the -0.4 V to 0 V potential region, followed by a less prominent peak or shoulder just below 0.4 V (Davies and Burstein, 1980b; Gervasi et al., 1989). It was suggested that the anodic dissolution of cobalt in bicarbonate solutions takes place according to reactions 2.69 - 2.72 (Davies and Burstein, 1980b).

$$Co + HCO_3^- \rightarrow CoCO_3 + H^+ + 2e^- \quad (2.69)$$

$$Co + H_2O \rightarrow CoO + 2H^+ + 2e^- \quad (2.70)$$

$$CoO + HCO_3^- \rightarrow CoCO_3 + OH^- \quad (2.71)$$

$$CoCO_3 + HCO_3^- \rightarrow Co(CO_3)_2^{2-} + H^+ \quad (2.72)$$

At potentials closer to the OCP, it was suggested that the formation of cobalt(II) carbonate (reaction 2.69) took place faster than the formation of cobalt oxide (reaction 2.70), and that its redissolution via reaction 2.72 is limited by the diffusion of the complex away from the electrode. Similarly to the case of iron, the formation of cobalt carbonate is also thought to be preceded by the oxidative adsorption of hydroxyl ions onto the cobalt surface, with its sequential oxidation to $Co(OH)_{ads}$ and then $Co(OH)^+$, prior to the latter reacting with the carbonate anion to form the salt (Real et al., 2008). The formation of a $CoHCO_3$ intermediate adsorbed on the cobalt surface has also been proposed, thought to be followed by the simultaneous formation of the $Co(CO_3)_2^{2-}$ complex and a non-protective CoO film, favoured as the potential was increased (Calderón et al., 2008). Polarisation of a cobalt electrode in the region of the anodic peak resulted in a high density of pits, while no pitting was observed at a potential above 0.3 V (Davies and Burstein, 1980b). This was consistent with bicarbonate being more aggressive towards the CoO formed in the lower potential region, and less aggressive towards the Co(III)-containing film formed in the higher potential region. This was thought to consist mainly of Co_2O_3, as supported by an Auger electron spectroscopy (AES) study (Burstein and Davies, 1980). Its passivity towards bicarbonate ions was attributed to its inability to form complexes with cobalt(III). Nevertheless, following passivation by anodic treatment, the passive layer was found to break down spontaneously, with reactivation of the cobalt within a few minutes (Davies and Burstein, 1980b).

2.6.3 The electrochemical behaviour of metallic nickel

a) Ammoniacal-carbonate solutions

The anodic dissolution of metallic nickel in ammoniacal-carbonate solutions to form nickel hexammine takes place at an OCP of around -0.4 V, at the species concentrations given in Table 2.10 (Nikoloski, 2002). Potentiodynamic studies have shown that the passivation of nickel occurs at significantly higher applied potentials than those required for iron to passivate (Nicol, 1975; Nikoloski and Nicol, 2006). Measurements conducted in ammoniacal solutions representative of the Yabulu QN Caron leach liquor can be seen in Figure 2.22.

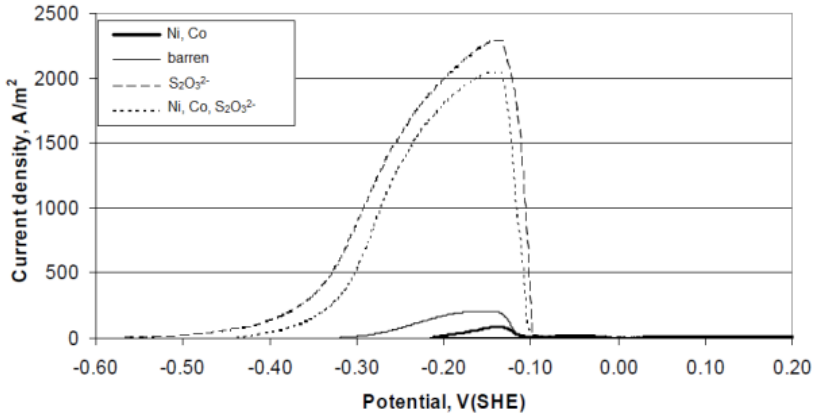

Figure 2.22 Anodic behaviour of a nickel RDE scanned at 1 mV/s in aerated solutions containing 5 M $[NH_3]_T$, 1 M $[CO_2]_T$, and the species indicated in the legend at the following concentrations: [Ni(II)] = 0.15 M, [Co(II)] = 0.012 M and $[S_2O_3^{2-}]$ = 0.022 M (Nikoloski and Nicol, 2006).

The passivation of nickel was not found to take place spontaneously in ammoniacal-carbonate solutions with and without cobalt(II) and/or thiosulfate ions. However, based on ring-disk dissolution experiments, the spontaneous passivation of nickel was observed in 1 M ammonium carbonate solutions, under the following conditions: in the presence of 6 mM copper(II), when the solution pH was adjusted to pH 10 by addition of NaOH, and in the presence of 1.6 mM copper(II), when the solution pH was adjusted to pH 9 (Nicol, 1975). The so-formed passive layer was

found to re-dissolve spontaneously during 1 hour of immersion in deoxygenated ammonium carbonate solutions.

b) Ammonia-free carbonate solutions

Cyclic voltammetric studies conducted on metallic nickel in carbonate solutions in the $8.35 < pH < 11.7$ range have shown an anodic peak between -0.5 V and -0.3 V (Bohe et al., 1984; Bohe et al., 1990). This was attributed to the oxidation of metallic nickel to nickel(II) by two competing processes: the formation of a thin hydrated $Ni(OH)_2$ layer, thought to dominate at lower potentials (reaction 2.73) and the formation of nickel carbonate according to reaction 2.74 (Bohe et al., 1984).

$$Ni + 2H_2O \rightarrow Ni(OH)_2 + 2H^+ + 2e^- \quad (2.73)$$

$$Ni + CO_3^{2-} \rightarrow NiCO_3 + 2e^- \quad (2.74)$$

In a later study it was suggested that both species formed part of a pre-passive layer on the nickel surface, where the formation of a thin $Ni(OH)_2$ film was disrupted by the precipitation of $NiCO_3$ according to reactions 2.75 and 2.76 (Bohe et al., 1990).

$$Ni(OH)_2 + CO_3^{2-} \rightarrow NiCO_3 + 2OH^- \quad (2.75)$$

$$Ni(OH)_2 + HCO_3^- \rightarrow NiCO_3 + OH^- + H_2O \quad (2.76)$$

The cyclic voltammetry measurements also resulted in an anodic peak occurring at significantly more positive applied potentials, above 0.7 V. This was attributed to the oxidation of nickel(II) to nickel(III) species according to reaction 2.77 (Bohe et al., 1984).

$$Ni(OH)_2 + OH^- \rightarrow NiOOH + H_2O + e^- \quad (2.77)$$

Since the formation nickel carbonate is thought to interfere with the formation of $Ni(OH)_2$ on the nickel surface, as in the case of iron, the presence of carbonate ions may potentially disrupt rather than favour the passivation of nickel, which in any case would require highly oxidising conditions to occur.

2.6.4 The electrochemical behaviour of copper

a) Ammoniacal-carbonate solutions

In aerated ammoniacal-carbonate solutions, metallic copper dissolves readily according to reaction 2.78. The so-formed cupric tetrammine can also oxidise metallic copper to cuprous diammine (reaction 2.79), which in the presence of oxygen is rapidly reoxidised to cupric tetrammine (reaction 2.80), thereby completing an autocatalytic redox cycle (Nicol, 1975). This is consistent with the thermodynamic data shown in Figure 2.5 (C) and discussed in section 2.4.3.

$$Cu + 4NH_3 + ½O_2 + H_2O \rightarrow Cu(NH_3)_4^{2+} + 2OH^- \quad (2.78)$$

$$Cu + Cu(NH_3)_4^{2+} \rightarrow 2Cu(NH_3)_2^{+} \quad (2.79)$$

$$2Cu(NH_3)_2^{+} + 4NH_3 + ½O_2 + H_2O \rightarrow 2Cu(NH_3)_4^{2+} + 2OH^- \quad (2.80)$$

Similarly, it was suggested that the cupric tetrammine acted as a redox mediator in the oxidative dissolution of nickel, copper-nickel alloys (Nicol, 1975), and iron-nickel alloys (Senanayake et al., 2010).

The OCP of metallic copper in aerated ammoniacal-carbonate solutions simulating the Caron leach liquor from the Yabulu QN refinery was found to be around -0.3 V (Nikoloski, 2002). This is also consistent with the thermodynamic data presented in Figure 2.5, C.

Voltammetric measurements conducted on a copper RDE in aerated ammoniacal-carbonate solutions in the presence of different species are shown in Figure 2.23 (Nikoloski and Nicol, 2006).

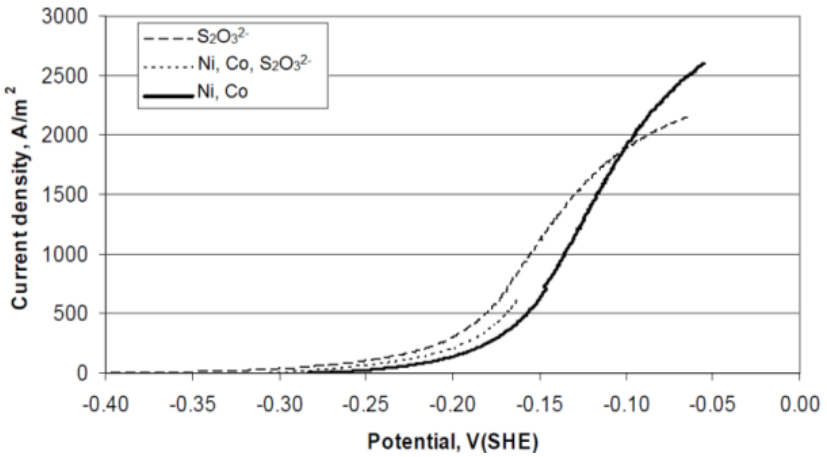

Figure 2.23 Anodic behaviour of copper at 1 mV/s in aerated solutions containing 5.28 M $[NH_3]_T$, 1.02 M $[CO_2]_T$, and the species indicated in the legend at the following concentrations: [Ni(II)] = 0.15 M, [Co(II)] = 0.012 M and $[S_2O_3^{2-}]$ = 0.022 M (Nikoloski and Nicol, 2006).

The measurements showed no evidence of passivation of the copper electrode in any of the solutions, as the applied potential was increased within the range studied. As can be seen from Figure 2.23, the behaviour of copper did not seem to be significantly affected by the presence of nickel, cobalt and/or thiosulfate ions. These results also indicated that the significantly more positive region of active dissolution of copper compared to that of metallic iron (see section 2.6.1) could potentially result in the copper cementing onto the iron, as consistent with the thermodynamic considerations discussed in section 2.4.3.

The cementation of copper was experimentally observed during the anodic dissolution of Cu-Co-Fe-Pb alloys in ammonia/ammonium chloride solutions (Burzynska et al., 2008). It was also suggested that copper cementation took place during the dissolution of iron-nickel alloys under the conditions of the Caron

process, resulting in a decrease in nickel leaching in deoxygenated solutions containing low concentrations of copper (Senanayake et al., 2010). This was attributed to the surface of the alloy becoming blocked by the cemented copper, following the displacement of nickel by copper according to reaction 2.81, for which the logK at 45°C was reported to be 14.7.

$$Cu(NH_3)_4^{2+} + 2NH_3 + Ni \rightarrow Cu + Ni(NH_3)_6^{2+} \quad (2.81)$$

In the presence of dissolved oxygen, the faster leaching observed was due to the regeneration of the cupric tetrammine (reaction 2.80), which in turn re-oxidised the cemented copper (reaction 2.79), thus completing the redox cycle and allowing the dissolution of nickel (reaction 2.81) to continue.

Even though the cementation of copper onto iron has been exploited for centuries and studied extensively in view of a wide variety of applications, most investigations have been conducted in non-ammoniacal, usually acidic solutions (Agrawal and Kapoor, 1982; Biswas and Reid, 1972; Karavasteva, 2005; Rickard and Fuerstenau, 1968). On the other hand, the electrodeposition of copper from ammoniacal solutions onto substrates other than iron has been studied extensively.

Based on thermodynamic and electrochemical studies, numerous authors agree that the electrodeposition of copper from ammoniacal solutions of different compositions occurs via the reduction of cupric tetrammine to cuprous diammine, which is then further reduced to metallic copper (Darchen et al., 1997; Giannopoulou et al., 2009; Graham et al., 2002; Grujicic and Pesic, 2005; Nila and González, 1996a; Nila and González, 1996b; Ramos et al., 2001; Vazquez-Arenas et al., 2007a; Vazquez-Arenas et al., 2007b). At more negative applied potentials, direct reduction of cupric tetrammine to metallic copper is also thought to take place (Grujicic and Pesic,

2005). It was also suggested that the anodic dissolution of metallic copper in ammoniacal solution takes place as a two-electron oxidation process to cupric tetrammine, which might be the case when the oxidant is dissolved oxygen and no cupric tetrammine is initially present in the solution. However, in the presence of cupric tetrammine, it is generally believed that dissolution takes place via the oxidation of metallic copper by cupric tetrammine to form cuprous diammine, according to reaction 2.69 (Darchen et al., 1997; Grujicic and Pesic, 2005; Nicol, 1975; Nikoloski and Nicol, 2006; Ramos et al., 2001).

In the presence of thiosulfate ions, there is also the possibility of a homogeneous redox reaction between cupric species and thiosulfate ions. In the absence of ammonia this is thought to be preceded by the formation of a $Cu(S_2O_3)_2^{2-}$ complex anion intermediate, and to result in the formation of a stable cuprous thiosulfate complex, according to reaction 2.82 (Rábai and Epstein, 1992).

$$2Cu(S_2O_3)_2^{2-} \rightarrow 2Cu(S_2O_3)^{-} + S_4O_6^{2-} \quad (2.82)$$

When more copper than thiosulfate is present, side reactions such as the disproportionation of cuprous ions (2.83) or of thiosulfate ions (2.84) are also thought to take place (Rábai and Epstein, 1992).

$$2Cu^{+} \rightarrow Cu^{2+} + Cu \quad (2.83)$$

$$2Cu^{+} + S_2O_3^{2-} + H_2O \rightarrow Cu_2S + SO_4^{2-} + 2H^{+} \quad (2.84)$$

However, these are not likely to take place in the presence of ammonia, due to the relatively high stability of cuprous ammine complexes.

The oxidation of thiosulfate by cupric ammines has been studied extensively due to its relevance to the ammoniacal leaching of metal sulfides and to the thiosulfate

leaching of gold, which is known to be enhanced by the addition of copper(II) and ammonia (Breuer and Jeffrey, 2003; Byerley et al., 1973a; Byerley et al., 1973b; Byerley et al., 1975; Senanayake, 2004). The experimental evidence is consistent with the redox process being an inner-sphere reaction, in which thiosulfate first coordinates as a ligand to the Cu(II) complex before being oxidised to tetrathionate, which then undergoes further oxidative degradation to various other oxysulfur species. Depending on the relative concentrations of ammonia and thiosulfate, the resulting cuprous species may consist of ammonia, thiosulfate or mixed complexes such as $Cu(NH_3)(S_2O_3)^-$ and $Cu(NH_3)(S_2O_3)_2^{3-}$ (Black, 2006).

Since the cuprous species are readily re-oxidised by dissolved oxygen to cupric tetrammine, the degradation of thiosulfate is expected to be much faster in ammoniacal-copper(II) solutions contaning dissolved oxygen. Observed thiosulfate oxidation rates were found to be at least forty times faster in the presence of oxygen, which was explained in terms of the formation of a catalytically active Cu(II) - ammonia - oxygen complex (Byerley et al., 1973b; Byerley et al., 1975).

Although the oxidation of thiosulfate by copper(II) species has not been studied under the conditions of the Caron leach, its rate is known to decrease at increasing ammonia concentrations (Aylmore and Muir, 2001) and is therefore expected to be relatively low at the high ammonia concentrations employed in the process.

b) Ammonia-free carbonate solutions

Cyclic voltammetry studies conducted on metallic copper in carbonate-bicarbonate solutions in the pH 8.7 to 11.3 range have shown the presence of at least two anodic peaks (Gassa et al., 1998; Perez Sanchez et al., 1990; Tromans and Sun, 1992). The first peak, observed at potentials around 0 V, was attributed to the formation of

Cu_2O, which was suggested to take place via the initial formation of a thin CuOH layer and described overall by half-reaction 2.85 (Perez Sanchez et al., 1990; Tromans and Sun, 1992) .

$$2Cu + H_2O \rightarrow Cu_2O + 2H^+ + 2e^- \quad (2.85)$$

The second peak, in the potential region of around 0.2 V, was attributed to the formation of a composite CuO-$Cu(OH)_2$ layer, according to half-reactions 2.86, 2.87 (Perez Sanchez et al., 1990) and 2.88 (Tromans and Sun, 1992). It was also suggested that the formation of soluble Cu(II) species also contributed to the currents in this region (Gassa et al., 1998), but no reactions were suggested.

$$Cu + H_2O \rightarrow CuO + 2H^+ + 2e^- \quad (2.86)$$

$$Cu_2O + H_2O \rightarrow 2CuO + 2H^+ + 2e^- \quad (2.87)$$

$$Cu_2O + 3H_2O \rightarrow 2Cu(OH)_2 + 2H^+ + 2e^- \quad (2.88)$$

At potentials above 0.2 V, a plateau in the current density was observed in what was considered to be a passive region, thought to be due to protection of the metallic copper by a relatively unstable composite Cu_2O-CuO-$Cu(OH)_2$ layer. The anodic current in this region was found to increase for increasing carbonate-bicarbonate concentrations, resulting in a broad anodic feature thought to be related to the formation of basic copper carbonates, such as $Cu(OH)_2 \cdot CuCO_3$ and $Cu(OH)_2 \cdot 2CuCO_3$, or soluble copper carbonate species, such as $CuCO_3(OH)_2^{2-}$, $CuCO_3$ (aq) and $Cu(CO_3)_2^{2-}$ (Gassa et al., 1998; Perez Sanchez et al., 1990), for which the stability constants are given in Table 2.8.

Stirring of the solution was also found to enhance the anodic current densities at potentials above 0.1 V, which was attributed to a mass transfer effect on the

dissolution of the copper carbonate species according to reactions 2.89 and 2.90, for which the logK values (at 25°C, ionic strength = 0) are -33.78 and -45.96 respectively (Perez Sanchez et al., 1990; Smith and Martell, 1976).

$$Cu(OH)_2 \cdot CuCO_3 \rightarrow 2Cu^{2+} + 2OH^- + CO_3^{2-} \quad (2.89)$$

$$Cu(OH)_2 \cdot 2CuCO_3 \rightarrow 3Cu^{2+} + 2OH^- + 2CO_3^{2-} \quad (2.90)$$

2.6.5 The electrochemical behaviour of iron-cobalt and iron-nickel alloys in ammoniacal-carbonate solutions

As part of the study by Kasherininov on the dissolution behaviour of iron-cobalt powder mixtures in ammoniacal-carbonate solutions (Kasherininov, 1960), some observations were also made on the electrochemical and dissolution behaviour of iron-cobalt alloys. These were thought to have formed at the grain boundaries between iron and cobalt, as the metallic particles were partially sintered by heating to temperatures above 700°C. The study found that alloys of iron with 3-10% cobalt became passive by simple aeration, more readily than pure iron which required specific conditions. Passivation of the alloy and of any iron coming into contact with it was seen as beneficial to the dissolution of cobalt grains in contact with it, as it resulted in the cobalt behaving as an anode and dissolving oxidatively while the passive alloy acted as the cathode (Kasherininov, 1960). The dissolution of cobalt from these alloys was not thought to take place to any appreciable extent, as consistent with the observation by other researchers that passivation of iron had a negative effect on the extraction of cobalt from sintered iron-cobalt mixtures (Osseo-Asare et al., 1983). This was also thought to be due to the formation of iron-cobalt

alloys during sintering, as their subsequent passivation would explain the negative effect on cobalt extraction from the alloy, as opposed to the case in which its dissolution is from a separate metallic phase. Based on the concentration ratios of dissolved iron and cobalt in solution, it was suggested that the dissolution of cobalt from the iron-cobalt alloy in the active phase took place via a de-alloying or selective dissolution mechanism. However, the measured concentrations did not take into account iron and cobalt concentrations in the solid corrosion product layer, and the evidence provided was not enough to confirm de-alloying of the cobalt.

Cyclic voltammetry and OCP measurements of iron-cobalt alloys containing up to 1% cobalt have shown that they behave predominantly like pure iron, undergoing spontaneous passivation in solutions containing dissolved nickel, cobalt and thiosulfate ions at concentrations similar to those encountered at the Yabulu QN refinery (Nikoloski, 2002).

Similarly, iron-nickel alloys containing up to 45% nickel were found to exhibit an electrochemical behaviour dominated by that of pure iron, with an increasing tendency towards spontaneous passivation in deoxygenated solutions with increasing nickel content of the alloy (Nikoloski, 2002).

The cyclic voltammetric behaviour of iron alloys was found to be similar to that of pure iron (Nikoloski, 2002), except for a slight shift in anodic currents and peak potential by approximately 50 mV observed in the case of the iron-nickel alloy (Figure 2.24).

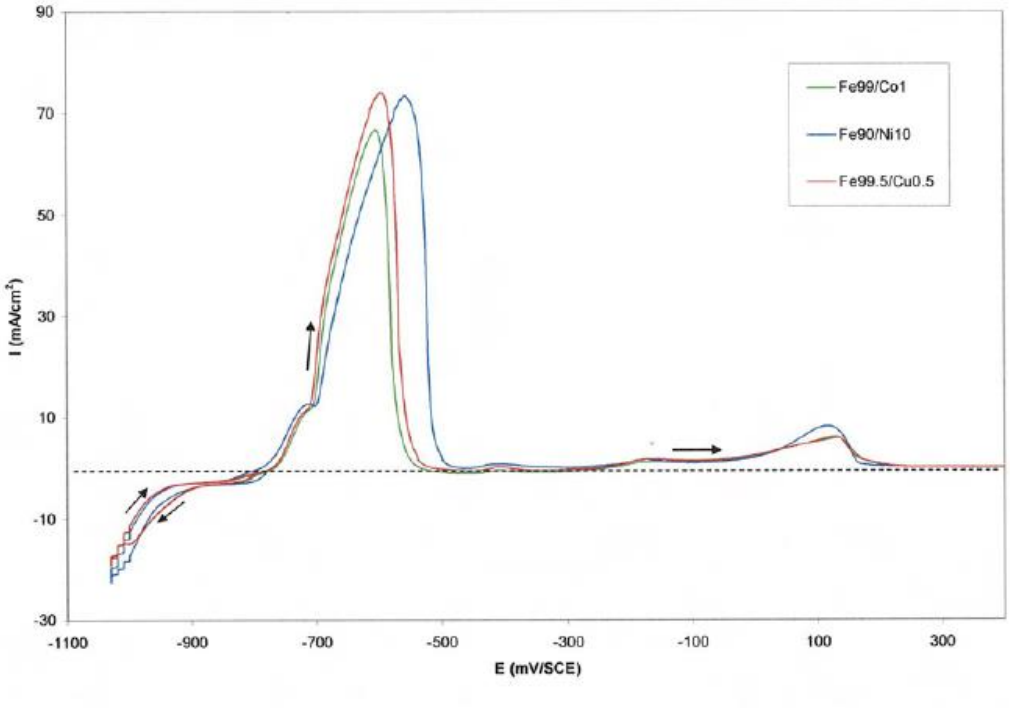

Figure 2.24 Voltammetric scans of iron-based alloys at 10 mV/s in aerated solution containing 5.28 M $[NH_3]_T$, 1.02 M $[CO_2]_T$, 0.15 M Ni(II), 0.012 M Co(II) and 0.022 M $S_2O_3^{2-}$ (Nikoloski, 2002).

2.7 The behaviour of cobalt, nickel and copper sulfides in ammoniacal solutions

To date, there appear to have been no studies conducted specifically on the dissolution or the electrochemical behaviour of cobalt sulfides in ammoniacal solutions. However, cobalt is frequently leached during the processing of nickel and copper sulfides, and this has been studied by numerous research groups over the years (Forward, 1953; Forward and Mackiw, 1955; Muir et al., 1981; Park et al., 2007).

Of these sulfides, the most extensively studied in ammoniacal solutions have been copper sulfides, with numerous investigations being relevant to the high oxygen-pressure Sheritt-Gordon process (Filmer et al., 1979b; Filmer et al., 1979c; Muir et al., 1981; Reilly and Scott, 1978; Tozawa et al., 1976). Some of these studies have also included electrochemical investigations which are also relevant to the conditions of the Caron process (Filmer et al., 1979a; Muir et al., 1981).

Linear sweep voltammetry measurements conducted on carbon paste electrodes containing Cu_2S and CuS powders in ammoniacal solution (Filmer et al., 1979a) are shown in Figure 2.25.

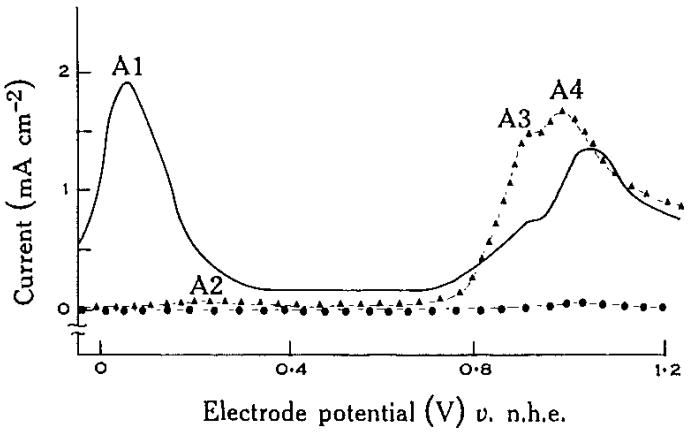

Figure 2.25 Linear sweep voltammetry (5 mV/s) on carbon paste electrodes containing 10% w/w Cu_2S (solid line), CuS (triangles) and S (dots) in unstirred 7 M NH_3 and 1.5 M $(NH_4)_2SO_4$ at pH 10.5 (Filmer et al., 1979a).

The first peak (A1), observed in the 0 to 0.1 V potential region during the anodic potential sweep conducted on the Cu_2S, was assigned to its oxidation according to reaction 2.91.

$$Cu_2S + 4NH_3 \rightarrow CuS + Cu(NH_3)_4^{2+} + 2e^- \qquad (2.91)$$

This is fairly consistent with the regions of stability of Cu_2S and CuS shown in Figure 2.8. Since the peak current was not found to be influenced by stirring the solution, the oxidation process was thought to occur via a solid-state diffusion-controlled formation of an intermediate Cu_xS species ($2 > x > 1$) which slowed the diffusion of Cu(I) to the solid liquid interface.

The much smaller anodic peak (A2) observed at around 0.2 V for the CuS electrode was assigned to its oxidation to a polysulfide species, Cu_yS ($y < 1$), while the

formation of elemental sulfur was not thought to take place. It was suggested that the anodic peaks occurring above 0.8 V for both the Cu_2S and the CuS electrodes could possibly be due to further oxidation to thiosulfate (A3) and sulfate (A4) ions, with the formation of cupric tetrammine. These processes are consistent with higher peak current densities which were observed for stirred solutions. As would be expected for a non-conductive species, the linear voltage scan of sulfur did not result in any significant current, although a very low peak was observed at around 1 V.

Comparative linear sweep voltammetry studies conducted on both CuS and NiS carbon paste electrodes (Muir et al., 1981) are shown in Figure 2.26.

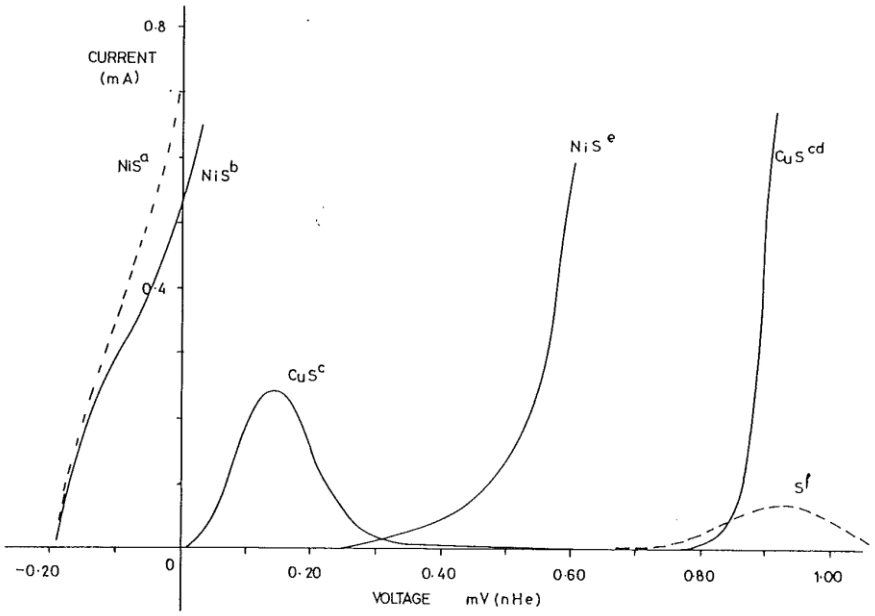

Figure 2.26 Linear sweep voltammetry (5 mV/s) of carbon paste electrodes containing 10% w/w metal sulfides (a: freshly precipitated NiS, first batch; b: freshly precipitated NiS, second batch; c: first scan of CuS; d: second and subsequent scans of CuS; e: NiS synthesised from the elements at 600°C; f: sulfur) in unstirred 7 M NH_3 and 1.5 M $(NH_4)_2SO_4$ at pH 10.5, 30°C (Muir et al., 1981).

The CuS was found to display two distinct anodic regions, one starting just above 0 V and peaking at 0.15 V and a second region above 0.8 V. The peak observed in the lower potential region was not observed in subsequent scans, which resulted only in

the currents above 0.8 V being observed. This was explained by the authors in terms of the formation of a sulfur or sulfur-rich layer resulting in the peak around 0.15 V, as consistent with the assignment of peak A2 in Figure 2.26 to the oxidation of CuS to Cu_yS ($y < 1$).

The response of NiS was found to be different depending on its preparation method, which was suggested to have an effect on the free energy and reactivity of the sulfide. Freshly precipitated NiS was found to oxidise at potentials just above -0.2 V, whereas NiS which had been synthesised at high temperature from the elements began to oxidise only above 0.25 V, reaching very high currents at potentials around 0.6 V.

Linear sweep voltammetry measurements conducted on Ni_3S_2 in ammoniacal-carbonate solutions containing various species are shown in Figure 2.27.

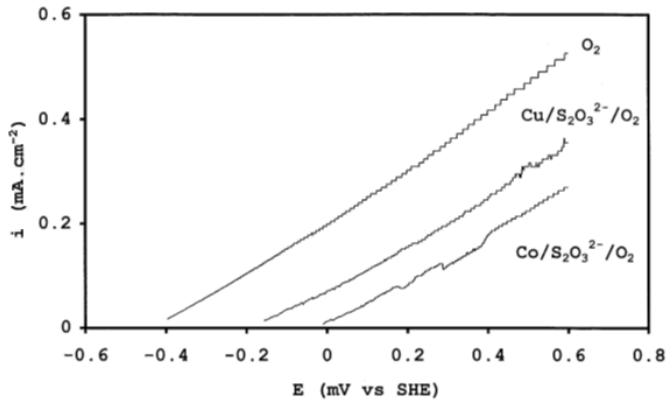

Figure 2.27 Linear sweep voltammetry of a rotating Ni_3S_2 disk in oxygenated solutions at 45°C, 5.29 M $[NH_3]_T$, 1.02 M $[CO_2]_T$, 4.72 mM Cu(II), 5.06 mM Co(III), 15.63 mM $S_2O_3^{2-}$ (Senaputra, 2010).

Although there have been numerous other electrochemical investigations on the behaviour of nickel sulfides, these have been conducted predominantly in acidic conditions (Buckley and Woods, 1991; Muir and Ho, 1996; Power, 1981; Power, 1982; Price and Davenport, 1982). Cyclic voltammograms measured in alkaline

solutions are shown in Figure 2.28, for which a fresh Ni_3S_2 surface was formed in a nitrogen atmosphere prior to each scan (Buckley and Woods, 1991).

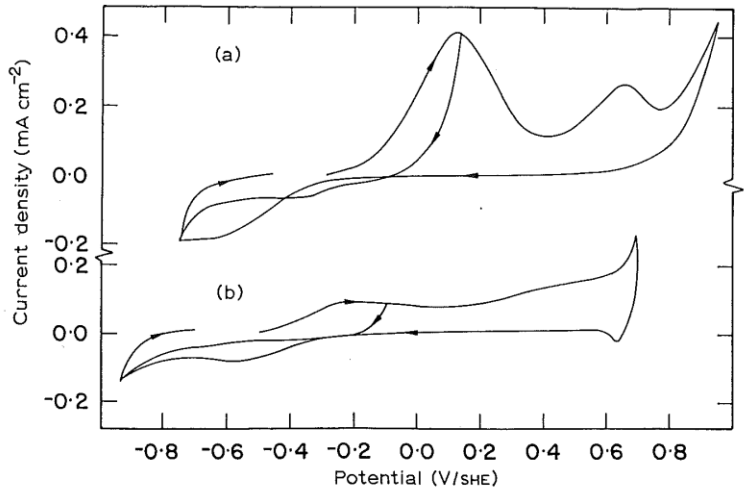

Figure 2.28 Voltammogram of Ni_3S_2 electrode at 20 mV/s scan rate in (a) sodium tetraborate solution at pH 9.2 and (b) potassium hydroxide solution at pH 13 (Buckley and Woods, 1991).

The first anodic processes observed upon scanning in the anodic direction were assigned to reaction 2.92, in which the dissolution of nickel was somewhat inhibited by the formation of nickel hydroxide. This was consistent with the significantly lower anodic peak current densities compared to those observed in acidic solutions, where the oxidative dissolution to Ni(II) was only inhibited by formation of the sulfur-rich oxidation product (Buckley and Woods, 1991).

$$Ni_3S_2 + 2xH_2O \rightarrow Ni_{3-x}S_2 + xNi(OH)_2 + 2xH^+ + 2xe^- \quad (2.92)$$

Further oxidation to NiS was also thought to take place, possibly followed by its oxidation to elemental sulfur, although no clear assignment was made to the second anodic peak observed in 0.4 V to 0.7 V potential region. The oxidation of Ni(II) to Ni(III) was not observed, as it was thought to take place at higher potentials than the upper limit of the scans.

2.8 Summary and need for further studies

- In the Caron process, ammoniacal-carbonate solutions are employed to leach nickel and cobalt from pre-reduced laterites, in which they are present in the metallic phase as iron-containing alloys (Canterford, 1978; Jandová and Pedlík, 1991; Rhamdhani et al., 2009a).
- Under the process conditions, the anodic dissolution of metallic nickel, cobalt and iron to form the corresponding metal ammine complexes is thermodynamically favoured and may be brought about by reduction of hydrogen from the ammonium ions in solution. Based on thermodynamic data, the dominant dissolved species are thought to be nickel hexammine, cobaltous pentammine and ferrous tetrammine (Isaev et al., 1990a; Isaev et al., 1990b; Osseo-Asare, 1981a; Queneau and Weir, 1986), which are all stable under the oxygen-free conditions of the initial leaching stage of the Caron process taking place in the quench tank.
- When oxygen is present in the system, ferrous tetrammine is further oxidised to hydrated ferric oxides, which precipitate out of solution. Cobaltous pentammine is further oxidised to cobaltic hexammine, which functions as a redox mediator by oxidising the metallic phases and then being regenerated by reaction with oxygen (Fittock, 2009; Queneau and Weir, 1986).
- Dissolved copper is also present in the system, at concentrations which at the Yabulu QN refinery may reach 16 mM (Nikoloski, 2002). Based on thermodynamic data, the dominant Cu(I) species is expected to be cuprous diammine and the dominant Cu(II) species is cupric tetrammine (Osseo-Asare, 1981a). The dissolution of metallic copper in the absence of any

oxygen may be brought about by the reduction of cupric tetrammine present in the recycled quench liquor, forming cuprous diammine. In the presence of oxygen, the redox cycle is completed by the regeneration of cupric tetrammine, which also functions as a redox mediator (Nicol, 1975).

- Electrochemical studies have shown that pure nickel and cobalt metals remain in an active dissolution state, whereas iron has a tendency to become passive even under open-circuit conditions (Kasherininov, 1960; Nikoloski, 2002).
- Alloys of iron with nickel and/or cobalt also show a tendency to passivate and their behaviour is strongly dominated by the behaviour of iron (Kasherininov, 1960; Nikoloski, 2002).
- Potentiodynamic passivation of iron has been studied extensively in ammoniacal-carbonate solutions (Asselin, 2008; Kho et al., 1992; Kim et al., 1991; Lee et al., 1985), but the spontaneous passivation has only been observed in a few cases (Kasherininov, 1960; Nikoloski, 2002).
- The spontaneous passivation of iron, observed at room temperature in ammoniacal-carbonate solutions simulating the loaded leach liquor at the Yabulu QN refinery, was accompanied by the formation of a surface layer containing sulfur, cobalt and nickel (Nikoloski et al., 2003).
- This surface layer was thought to consist of a sulfide species, but the only information available is its elemental composition. It would therefore be particularly useful to conduct further characterisation studies in order to shed more light on its chemical composition, which may in turn provide further information on the reaction mechanism by which it is formed.

- Examination of the surface layer following a long period of immersion after passivation indicated that a significant part of it had either re-dissolved or detached from the passive iron surface (Nikoloski et al., 2003). However, there is no published information on its redissolution behaviour, which therefore also requires further investigation.
- It is not clear which of the species present in the Caron leach liquor are specifically responsible for the passivation of iron, and in what way. Therefore, further studies are necessary in order to determine the involvement of each species, or combination of species, and their effect the anodic behaviour of iron.
- Most of the published studies were carried out at ambient temperature, so it would be useful to conduct further investigations within the temperature range of the Caron process.

3 EXPERIMENTAL METHODS AND MATERIALS

3.1 Electrochemical setup

The apparatus employed for the electrochemical investigations carried out as part of this project consisted of a Metrohm three electrode electrochemical cell connected to an EG&G Princeton Applied Research potentiostat, Model 6310. A schematic diagram of the entire setup is shown in Figure 3.1.

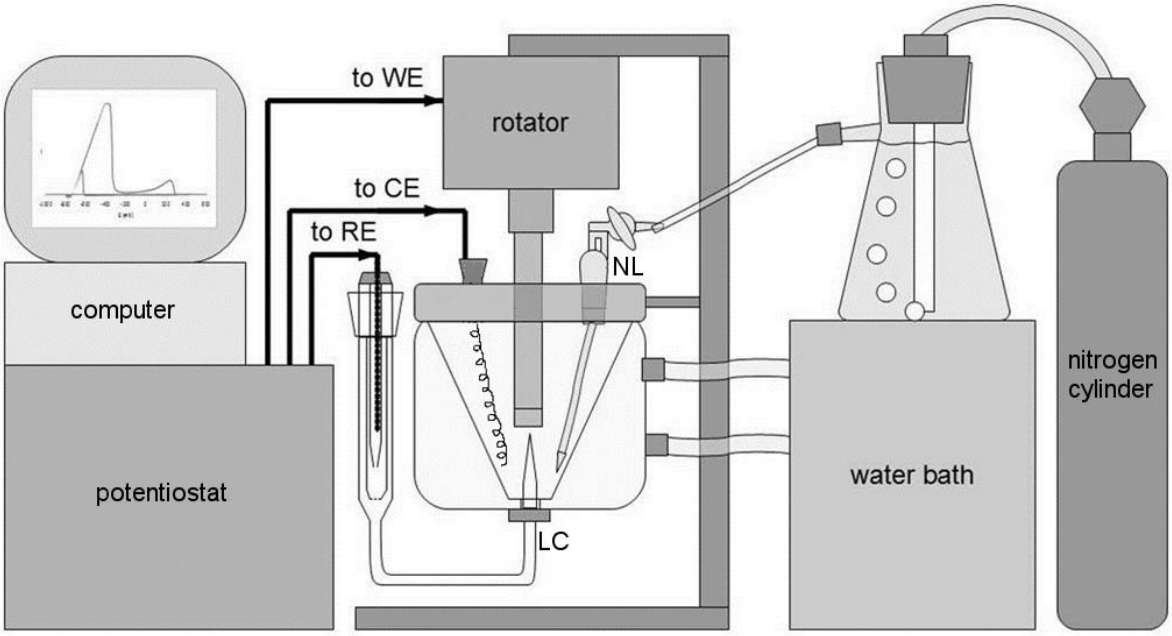

Figure 3.1 Schematic representation of the electrochemical experimental setup (WE = working electrode; CE = counter electroce; RE = reference electrode; LC = Luggin capillary; NL = nitrogen line).

In order to closely simulate the Caron process conditions, the electrochemical cell solutions, prepared as described in section 3.2, were contained within a 100 mL jacketed vessel connected to a thermostat-controlled water-bath, which was set to a temperature of 45ºC. Each measurement was carried out following a temperature equilibration delay after placing the solution in the cell. For most of the experiments the duration of this delay was 10 minutes, except for the preliminary set of measurements described in chapter 4, where the duration was 30 minutes.

The working electrode consisted of a rotating disk electrode (RDE) constructed from the material of choice and mounted onto a holder, as described in section 3.3. This was fitted to a Princeton Applied Research electrode rotator, Model 616, through which it was electrically connected to the potentiostat and rotated at a speed of 500 rpm. Immediately prior to immersion, the surface of the RDE was polished with 1200 grit silicon carbide paper wetted with ammonia-ammonium bicarbonate solution.

The counter electrode was made of a platinum wire of 0.5 mm diameter and approximately 30 cm long for all of the experiments except the preliminary measurements (chapter 4). For these, a shorter length of 18 cm was used, and in order to minimise the effect of the electrochemical deposition of solution species on the cell solution composition, the counter-electrode was placed in a salt bridge containing a portion of the cell solution. However, this was found to be unsuitable for experiments that resulted in relatively high anodic currents, as these became limited by the availability of species participating in the cathodic reactions at the counter electrode. Therefore, for most of the experiments in this study, the counter electrode was placed directly inside the cell solution.

The reference electrode consisted of a Coslow saturated calomel electrode (SCE) placed within a salt bridge containing saturated potassium chloride solution. This was in turn connected to a Luggin capillary fitted into a threaded opening on the bottom of the cell so that its tip was a few millimetres away from the surface of the working electrode. This minimised the ‘iR drop’ in potential caused by the resistance of the solution between the reference and the working electrode surface. No other form of iR correction was applied to any of the measurements. All of the potentials reported in this work have been converted to the SHE scale.

For the experiments conducted under deoxygenated conditions, nitrogen was sparged through the solution during the temperature equilibration time, unless otherwise stated. For the preliminary set of OCP measurements (chapter 4) a flowing nitrogen blanket was maintained above the cell solution to prevent oxygen from entering during the experiment. For the preliminary set of voltammetric measurements (chapter 4), nitrogen was sparged through the solutions for the entire duration of the experiments. In order to minimise the loss of ammonia, the nitrogen line was passed through a Dreshel flask containing ammoniacal-carbonate solution of approximately the same composition prior to it reaching the cell solution. However, sparging with nitrogen still resulted in an excessive loss of ammonia, making it necessary to modify the apparatus, as described in section 3.4. Since the presence of dissolved oxygen was found to have a less significant effect on the experimental results than the loss of ammonia, the solutions employed for the majority of the experiments were not sparged with nitrogen in order to maintain a more accurate control of the ammonia concentration. Therefore, the results reported generally refer to experiments conducted in solutions which were not deoxygenated, unless clearly stated in the text or the figure caption.

3.2 Solution preparation

The solutions used in this study were all prepared using deionised water and AR grade reagents, except for the Dreshel flask solutions, which were prepared from barren aqueous ammonia and ammonium carbonate recovered from the Yabulu QN plant.

All solutions were prepared in order to contain total concentrations of ammonia species, $[NH_3]_T$, and carbonate/bicarbonate species, $[CO_2]_T$, resembling those of the

plant leach liquor. The reagents used for their preparation consisted of concentrated aqueous ammonia (25-30% w/w) and either ammonium bicarbonate or an ammonium salt marketed by Sigma as ammonium carbonate. However, the latter was found to consist of an ammonium bicarbonate-ammonium carbamate double salt ($NH_4HCO_3 \cdot NH_2CO_2NH_4$) thought to result in the same species as ammonium carbonate after dissolution and equilibration. Although this reagent was used for previous studies related to the Yabulu QN refinery (Nicol et al., 2004; Nikoloski, 2002; Nikoloski and Nicol, 2006; Nikoloski and Nicol, 2010; Nikoloski et al., 2003), in the present study it was only used for the preliminary investigation (chapter 4) and for a few experiments described in chapter 5, as clearly stated in the text and figure captions. Due to the unstable nature of the double salt, known to become non-stoichiometric over time, the majority of the work conducted as part of this thesis was carried out using ammonium bicarbonate.

For consistency with the previous studies, the chosen concentrations of $[NH_3]_T$ and $[CO_2]_T$ were 5 M (90 g/L) and 1 M (45 g/L) respectively, resulting in a pH of around 11 at 25ºC and 10.5 at 45ºC. Concentrations of 6 M and 2 M, respectively, were also used for some of the investigations, in order to achieve higher solution conductivity and buffer capacity due to the slightly lower resulting pH of 10.5 at 25ºC and 10 at 45ºC. The higher concentrations were also a reflection of an increase in plant $[NH_3]_T$ to 100 g/L.

In order to study the reactions taking place in the industrial leach liquor, a simplified solution containing dissolved nickel, cobalt, copper and thiosulfate ions was used. Total concentrations considered representative of the industrial solution and generally used for this project, unless being studied as a variable, are given in Table 3.1, along with the reagents used. For simplicity, the total concentrations of the

resulting solution species are referred to throughout the text of this thesis as [Ni(II)], [Co(II)], [Cu(II)] and [$S_2O_3^{2-}$].

Table 3.1 Total species concentrations representative of the Caron leach liquor at the Yabulu QN refinery

Species	Total concentration (g/L)	Reagents used
$[NH_3]_T$	90 - 100	NH_3 + NH_4HCO_3 or $NH_4HCO_3{\cdot}NH_2CO_2NH_4$
$[CO_2]_T$	44 - 88	NH_3 + NH_4HCO_3 or $NH_4HCO_3{\cdot}NH_2CO_2NH_4$
[Ni(II)]	8.8	$NiSO_4{\cdot}6H_2O$
[Co(II)]	0.7	$CoSO_4{\cdot}7H_2O$
[Cu(II)]	0.1 - 0.8	$CuSO_4{\cdot}5H_2O$
$[S_2O_3^{2-}]$	2.5	$Na_2S_2O_3{\cdot}5H_2O$

In order to systematically investigate the effects of the species found in the Yabulu leach liquor, these were studied individually and in various combinations resulting in the solution compositions listed in Table 3.2. Each solution was prepared immediately prior to each experiment in order to minimise oxidation by air and loss of ammonia from solution.

Table 3.2 Composition of solutions used in this study

SOLUTION	Species total concentration							
	$[NH_3]_T$	$[CO_2]_T$	[Ni(II)]	[Co(II)]	[Cu(II)]	$[S_2O_3^{2-}]$	$[SO_4^{2-}]$	[Na]
	mol/L (M)		$x10^{-3}$ mol/L (mM)					
barren	5 or 6	1 or 2	_	_	_	_	_	_
Ni(II)	5 or 6	1 or 2	150	_	_	_	150	_
Co(II)	5	1	_	12	_	_	12	_
Ni(II) + Co(II)	5	1	150	12	_	_	162	_
$S_2O_3^{2-}$	5	1	_	_	_	22	_	44
Ni(II) + $S_2O_3^{2-}$	5 or 6	1 or 2	150	_	_	22	150	44
Co(II) + $S_2O_3^{2-}$	5 or 2.5	1 or 0.5	_	3 - 12	_	8 - 22	3 - 12	16 - 44
Ni(II) + Co(II) + $S_2O_3^{2-}$	5	1	150	12	_	22	162	44
Cu(II)	5	1	_	_	1 - 12	_	1 - 12	_
Cu(II) + $S_2O_3^{2-}$	6	2	_	_	1 - 12	22	1 - 12	44

3.3 Rotating disk electrode construction

In the majority of the experiments conducted as part of this study, the working electrode consisted of a rotating disk electrode made of 99.98% iron. A number of experiments were also carried out using rotating disk electrodes made from other materials, as listed in Table 3.3.

Table 3.3 Rotating disk electrodes used in this study

Electrode material	Purity/composition (%)	Diameter (mm)
iron (small)	Fe: 99.98	various, 6.00-6.35
iron (large)	Fe: 99.98	29.56
mild steel	Fe: 98.5; C: 0.5; Mn: 0.75; Si: 0.25	28.75
platinum	Pt: 99.99	2.0
nickel (small)	Ni: 99.99	6.3
nickel (large)	Ni: 99.99	39.92
iron-nickel alloy 1	Fe: 95; Ni: 5	5.95
iron-nickel alloy 2	Fe: 90; Ni: 10	5.91
iron-nickel alloy 3	Fe: 80; Ni: 20	5.94
iron-nickel alloy 4	Fe: 55; Ni: 45	12.7
iron-cobalt alloy	Fe: 99; Co: 1	5.81
graphite	C: 99.95	7.0
nickel sulfide	Ni_3S_2: 99.7	13.23

In order to construct the nickel sulfide rotating disk, synthetic Ni_3S_2 powder was first pressed into a compact pellet of the diameter given in Table 3.3, by applying a force of 10 tons.

For each of the materials used, a cylindrical specimen was glued onto a screw-fitted brass plate using a conductive adhesive. This was cast into an insulating, heat resistant epoxy-resin, leaving the screw portion out so that it could be screwed onto an epoxy-coated brass holder for mounting onto the electrode rotator (Figure 3.2).

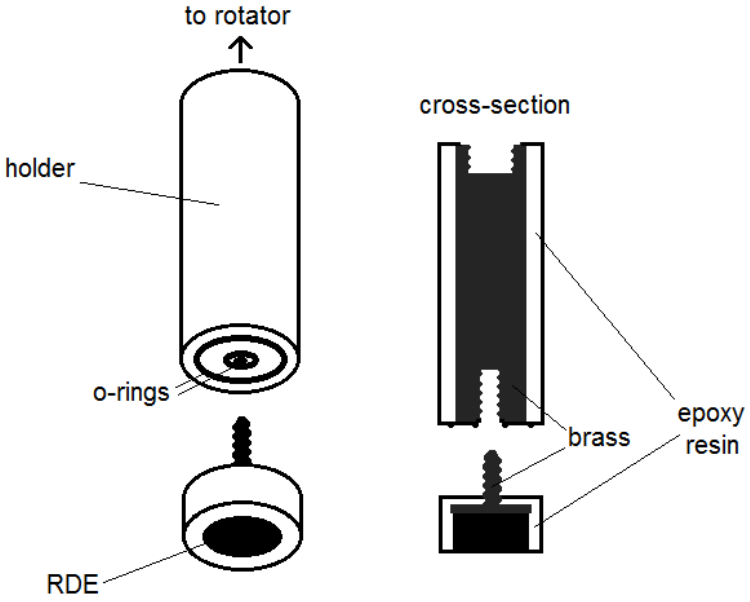

Figure 3.2 Rotating disk electrode (RDE) and holder.

3.4 Modified apparatus to minimise the loss of ammonia

In the Metrohm three electrode electrochemical equipment, the cell holder served as a lid, with an opening through which the working RDE was inserted into the cell solution. A gap around the RDE allowed it to rotate freely but was also responsible for the loss of ammonia. This problem was made worse by increasing the temperature and sparging the solution with nitrogen for long periods of time in order to exclude oxygen. Therefore, to minimise the loss of ammonia and prevent contact between the solution and atmospheric air it was necessary to modify the apparatus so that it could be sealed following an initial period of de-oxygenation where necessary. In order achieve this whilst still allowing rotation of the RDE it was necessary to design and construct a rotating paraffin seal, as described in Figure 3.3.

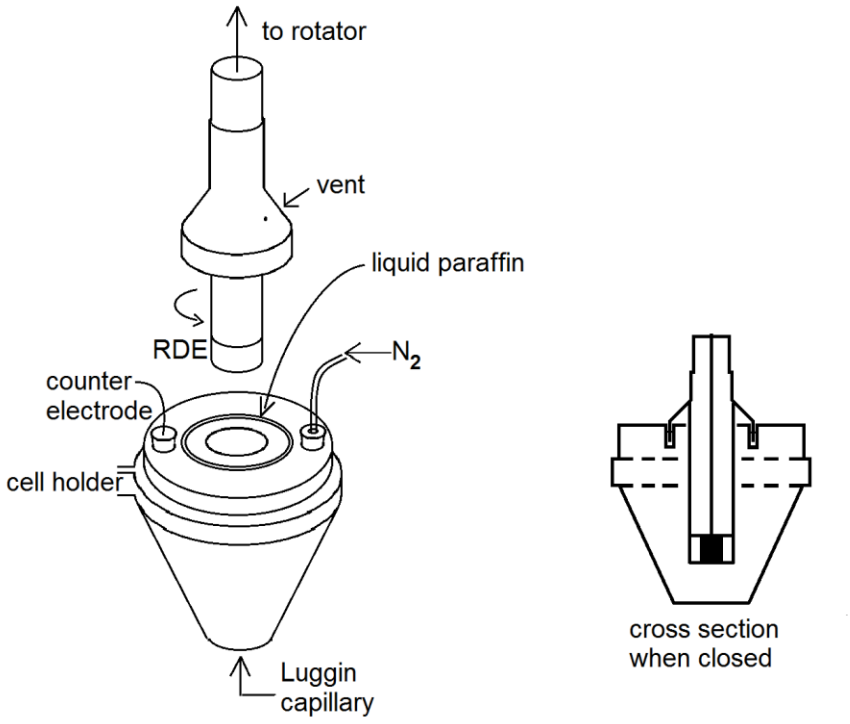

Figure 3.3 Modified rotator shaft and cell lid for sealed electrochemical cell.

Use of the rotating paraffin seal for experiments that required deoxygenated conditions allowed the nitrogen sparge to be stopped prior to each measurement. For the experiments carried out in solutions where dissolved oxygen was present, the modified setup reduced the loss of ammonia even without the use of paraffin.

3.5 Dissolution studies

Preliminary investigations into the dissolution of the sulfide layers formed on iron during its anodic dissolution were conducted using the electrochemical setup described in section 3.1. In order to evaluate the dissolution of the layers immediately after their formation, it was necessary to simultaneously use two Metrohm jacketed cells heated to 45ºC. As described in Table 3.4, the first cell (A) was used to form each sulfide layer by immersing the iron RDE in the appropriate solution. The second cell (B), used to monitor the redissolution of the freshly formed layer, was filled with barren ammoniacal carbonate solution 10 minutes prior to transferring the RDE from the cell A to cell B. Transfer of the RDE to cell B took place immediately after the OCP measurement indicated passivation, which took place in each case as described in Table 3.4. Immediately prior to re-immersion, the RDE was rinsed rapidly with deionised water. During dissolution of the layer in the cell B, the OCP of the RDE was monitored while 1 mL samples were taken at appropriate time intervals using a glass pipette. These were processed and analysed as described in section 3.6 in order to determine the total concentrations of iron, sulfur, and the relevant metal for each test (Co, Ni or Cu). The small error caused by measuring the sample volume at 45ºC was not considered significant for this set of measurements, since its aim was to obtain relative concentration values whilst minimising the effect of sampling on the total volume of the solution.

Table 3.4 Composition of solutions used for formation and dissolution studies of metal sulfides

Formation of surface layer on iron RDE (cell A)							
	$[NH_3]_T$	**$[CO_2]_T$**	**[Ni(II)]**	**[Co(II)]**	**[Cu(II)]**	**$[S_2O_3^{2-}]$**	**Method**
CoS_x	3 M	1 M	-	12 mM	-	22 mM	Immersion until spontaneous passivation of Fe
Ni_3S_2	3 M	1 M	150 mM	-	-	22 mM	Immersion until spontaneous passivation of Fe
Cu_2S	3 M	1 M	-	-	12 mM	22 mM	Potentiodynamic activation of Fe (OCP to -0.56 V at 100 mV/s); Spontaneous layer formation; potentiostatic passivation (0.4 V applied for 3 minutes)
Dissolution of surface layer (cell B)							
	$[NH_3]_T$	**$[CO_2]_T$**	**[Ni(II)]**	**[Co(II)]**	**[Cu(II)]**	**$[S_2O_3^{2-}]$**	**Method**
For each layer	6 M	2 M	-	-	-	-	Solution sampling for analysis of dissolved species

3.6 Solution elemental analysis and characterisation studies

The elemental analysis of the solution samples from the redissolution and leaching studies was carried out by Inductively Coupled Plasma – Optical Emission Spectroscopy (ICP-OES) on an Agilent Technologies 700 series spectrometer. Prior to the analysis, each accurately measured sample volume was diluted and acidified to below pH 2 using an accurate volume of hydrochloric acid. For the experiments in which the concentration of sulfur species was also determined, each solution was oxidised with an accurate volume of hydrogen peroxide solution prior to the acidification step. This was done in order to oxidise all sulfur species to sulfate and avoid losing any sulfur as hydrogen sulfide gas.

The UV-Visible spectrophotometric studies were carried out using a HP 8453 spectrophotometer. Most of the measurements were conducted using a quartz cell of 1 cm path length. When it was necessary to conduct the measurements at higher analyte concentrations, a quartz cell of 0.1 cm path length was used.

3.7 Solid phase characterisation studies

The microscope images and elemental analyses were obtained using a Philips XL20 scanning electron microscope (SEM) combined with an Oxford Link ISIS 5175 energy dispersive X-ray spectroscopy (EDX) detector.

Standard X-ray diffraction (XRD) patterns were recorded on a GBC EMMA diffractometer, using Cu k-alpha radiation. This instrument was used mainly to characterise precipitated material when it was present in sufficient amounts. Attempts were also made to use it for the study of thin surface layers formed on the iron RDE, for which it was necessary to construct a custom-built holder that allowed

the analysis to be carried out directly on the electrode. However, this technique was found to be unsuitable for the study, due to the surface layers being too thin and the resulting diffraction patterns resulting mainly from the underlying iron. For this reason, most of the diffraction patterns shown in this work were obtained by grazing-incidence X-ray diffraction (GIXRD) conducted on a Panalytical Empyrean diffractometer, also using Cu k-alpha radiation. In order to obtain patterns of the thin surface layers formed on the iron, it was necessary to cut off a thin slice off the RDE for it to be placed inside the instrument for analysis.

4 PRELIMINARY INVESTIGATION ON THE BEHAVIOUR OF IRON AND NICKEL IN AMMONIACAL-CARBONATE SOLUTIONS

4.1 Introduction

The leaching stage of the Caron process is a complex system in which numerous reactions are taking place simultaneously. Previous studies (Nicol et al., 2004; Nikoloski et al., 2003) have suggested that, during the initial stage of the leach, metallic iron surfaces become covered by a sulfide layer which appears to play an important role in the iron passivation mechanism, as described in chapter 2.

In the above mentioned studies, formation of this sulfide layer and the passivation of iron were observed at 25°C in ammoniacal-carbonate solutions containing nickel(II), cobalt(II) and thiosulfate ions at concentrations typically encountered at the Yabulu QN refinery (see section 2.8.1,a). As part of the present study, a preliminary investigation was conducted with the aim to isolate and identify the species responsible for the behaviour observed in the previous study (Nicol et al., 2004; Nikoloski et al., 2003). In order to do so, a simplified system consisting of metallic iron and solutions containing the above species was used, at a temperature of 45°C in order to more closely represent the Caron plant conditions. The solution composition was varied systematically in order to contain all possible combinations of the species used in the previous study. This way it was possible to assess their separate and combined effects on the electrochemical behaviour of iron and the corresponding surface changes. A few experiments were also carried out using metallic nickel, in order to check whether analogous interactions took place.

Further investigations were carried out in the same set of solutions using a platinum electrode, in order to study the cathodic processes separately from the interference of metallic iron.

Since copper(II) species were not present in the solutions employed for the previous study (Nicol et al., 2004; Nikoloski et al., 2003), their effect on the behaviour of iron was not studied as part of this preliminary work, but investigated separately as described in chapters 5 and 8.

4.2 Metallic iron

4.2.1 OCP measurements

The OCP behaviour of a 99.98% iron RDE was measured during 3 hour immersion periods in a set of solutions containing 5 M $[NH_3]_T$, 1 M $[CO_2]_T$ and various combinations of dissolved species commonly encountered in the Caron leach liquor. These were varied systematically in order to observe both their separate and combined effects, resulting in the set of solutions listed in Table 4.1. For all of the measurements reported in this section, nitrogen was flowed above the solution throughout the duration of the experiment.

Table 4.1 OCP of Fe RDE at different solution compositions

solution*	species concentration (mM)			OCP** (V)
	[Ni(II)]	[Co(II)]	$[S_2O_3^{2-}]$	
barren	_	_	_	-0.71
Ni(II)	150	_	_	-0.69
Co(II)	_	12	_	-0.63
Ni(II) + Co(II)	150	12	_	-0.62
$S_2O_3^{2-}$	_	_	22	-0.64
Ni(II) + $S_2O_3^{2-}$	150	_	22	-0.51
Co(II) + $S_2O_3^{2-}$	_	12	22	-0.52
Ni(II) + Co(II) + $S_2O_3^{2-}$	150	12	22	-0.49

*** all solutions also contained 5 M $[NH_3]_T$ and 1 M $[CO_2]_T$**
**** average value over first 100 minutes of immersion**

In all of the solutions studied, the iron OCP was generally found to remain in the -0.7 V to -0.5 V potential region, at least during the initial 2 hours of immersion, and in most cases for longer, as shown in Figures 4.1, 4.2 and 4.3. As discussed in chapter 2, the anodic dissolution of iron in ammoniacal solutions is generally thought to involve the formation of ferrous ammine complexes (Kim et al., 1991; Lee et al., 1985; Nikoloski and Nicol, 2006; Senanayake et al., 2010). As can be seen from the Fe-NH_3-H_2O Eh-pH diagram shown in Figure 2.5 (section 2.4), the measured OCP is consistent with the potential region in which the active dissolution of metallic iron to ferrous tetrammine is expected to take place. In the presence of dissolved oxygen, this may be described by reaction 2.26 (section 2.3.2), while in its absence the

oxidation may be coupled with the reduction of ammonium ions to hydrogen gas, as described by reaction 2.17 (section 2.3.1). A more detailed discussion of the anodic dissolution of metallic iron in ammoniacal solutions and its equilibrium potential under the experimental conditions of this study is provided in section 5.7.

As shown in Figure 4.1, the presence of thiosulfate ions resulted in the measured OCP being 50 mV more positive than in the barren solution, as consistent with the mixed potential being shifted by the introduction of a more oxidising species, as discussed in section 2.5. On the other hand, the presence of nickel was not found to have a significant effect on the OCP measurement, except when thiosulfate ions were also present. In this case, the OCP was around 0.2 V more positive than in the barren solution. This may be due to an interaction taking place between the nickel and thiosulfate ions.

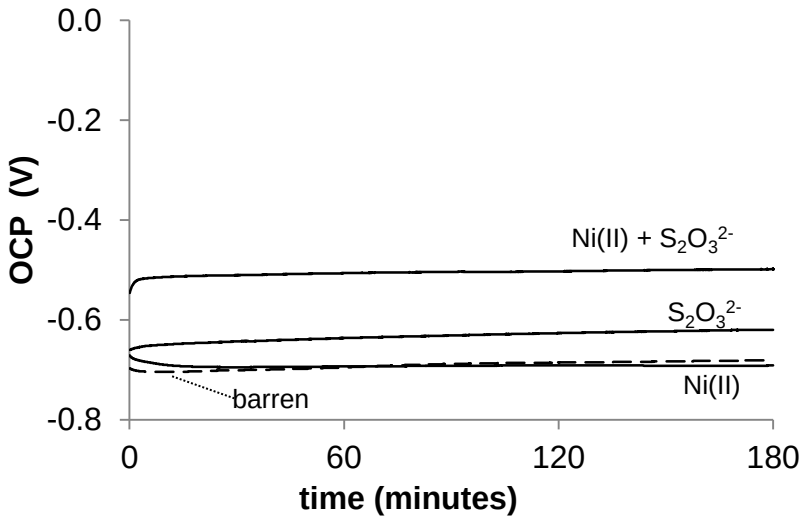

Figure 4.1 OCP of the Fe RDE in solutions containing 5 M $[NH_3]_T$, 1 M $[CO_2]_T$ with no other species (dashed line) and in the presence of 150 mM Ni(II) and/or 22 mM $S_2O_3^{2-}$, as indicated for each line.

As can be seen from Figure 4.2, in the absence of thiosulfate ions, the presence of dissolved cobalt resulted in the OCP being 50 mV more positive than in the barren solution. Similar to the case of nickel, the presence of both cobalt and thiosulfate ions resulted in the OCP being almost 200 mV more positive than in the barren solution, again suggesting some interaction between thiosulfate and, in this case, dissolved cobalt. However, after approximately 2 – 2 ½ hours of immersion in this solution, the OCP also underwent a transition to potentials above 0 V. This was thought to correspond to the passivation of the iron RDE surface, due to the formation of a protective oxide layer which caused the oxidative dissolution of the underlying metallic iron to cease. This potential region, thought to correspond to the passive state of iron, is consistent with the thermodynamic stability region of ferric hydroxide shown in Figure 2.5, section 2.4.

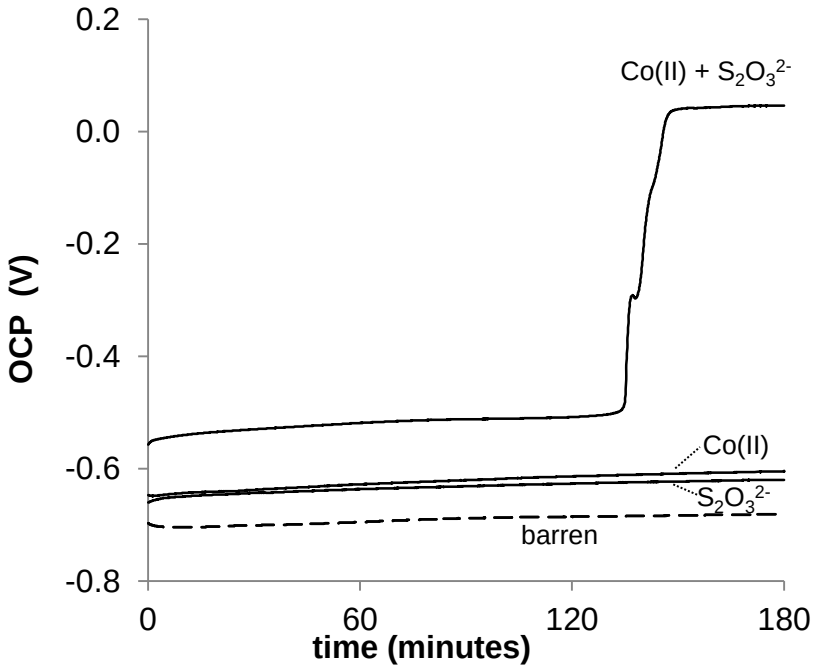

Figure 4.2 OCP of the Fe RDE in solutions containing 5 M $[NH_3]_T$, 1 M $[CO_2]_T$ with no other species (dashed line) and in the presence of 12 mM Co(II) and/or 22 mM $S_2O_3^{2-}$, as indicated for each line.

As can be seen from Figure 4.3, the OCP behaviour of iron in the presence of both nickel and cobalt ions was found to be similar to the behaviour observed in the solutions containing cobalt, with and without thiosulfate ions. Therefore, no significance could be attached to the presence of dissolved nickel, and the OCP transition observed in the presence of all three species was attributed to the effect of cobalt and thiosulfate ions. Since the composition of this solution simulated the loaded leach liquor from the Yabulu QN refinery, this observation confirmed the possibility of metallic iron passivation under the plant conditions.

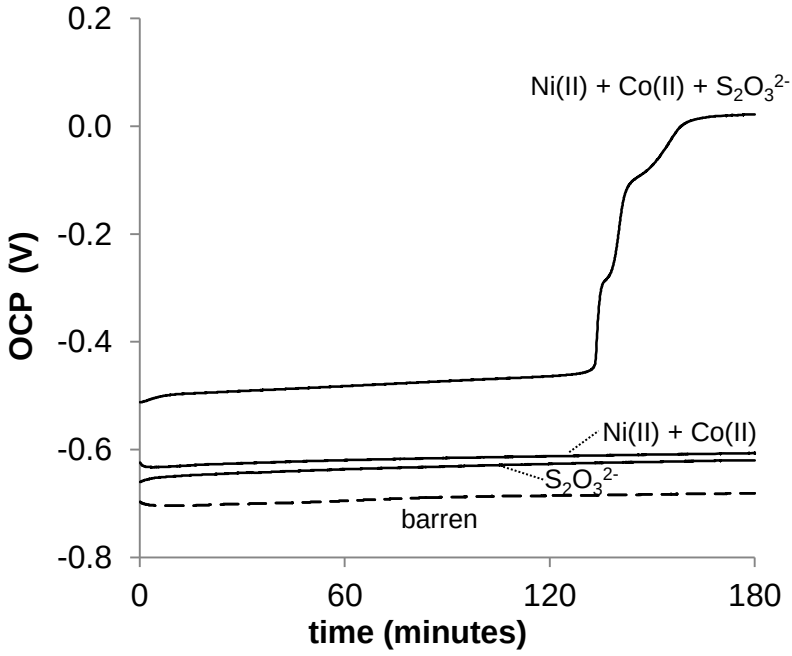

Figure 4.3 OCP of the Fe RDE in solutions containing 5 M $[NH_3]_T$, 1 M $[CO_2]_T$ with no other species (dashed line) and in the presence of 150 mM Ni(II), 12 mM Co(II) and/or 22 mM $S_2O_3^{2-}$ (as indicated for each solid line).

4.2.2 SEM/EDX surface analysis

Following each OCP measurement in the solutions listed in Table 4.1, the iron RDE surface was removed from solution, gently rinsed and analysed by SEM-EDX spectroscopy in order to gain further information on the heterogeneous processes taking place. Immersion in the solution containing only Ni(II) resulted the detection of around 20 atomic % (at%) of nickel. A possible explanation for this was the displacement of metallic iron by dissolved nickel, resulting in the cementation of metallic nickel onto the RDE surface, according to reaction 4.1.

$$Ni(NH_3)_6^{2+} + Fe \rightarrow Ni + Fe(NH_3)_4^{2+} + 2NH_3 \quad (4.1)$$

The standard Gibbs free energy ($\Delta G°$) of reaction 4.1 was calculated to be -42 kJ/mol, based on thermodynamic data available in the literature (Asselin, 2008), indicating that it is thermodynamically feasible under standard conditions. Considering that under the experimental conditions there is no dissolved iron initially present in solution, reaction 4.1 is all the more driven in the forward direction, supporting the possible cementation of metallic nickel.

Following immersion of the iron RDE in the solution containing both Ni(II) and $S_2O_3^{2-}$, SEM observation of its surface revealed the presence of small particles (Figure 4.4, a) and the EDX analysis indicated the presence of significant amounts of nickel (up to 30 at%) and sulfur (up to 25 at%). A significantly thicker deposit, covered with similar small particles, was observed following immersion in the solutions containing both Co(II) and $S_2O_3^{2-}$, with and without Ni(II) (Figure 4.4, b). The EDX analysis indicated the presence of up to 12 at% cobalt, 21 at% sulfur for the former case, and 7 at% nickel, 12 at% cobalt, 30 at% sulfur for the latter case.

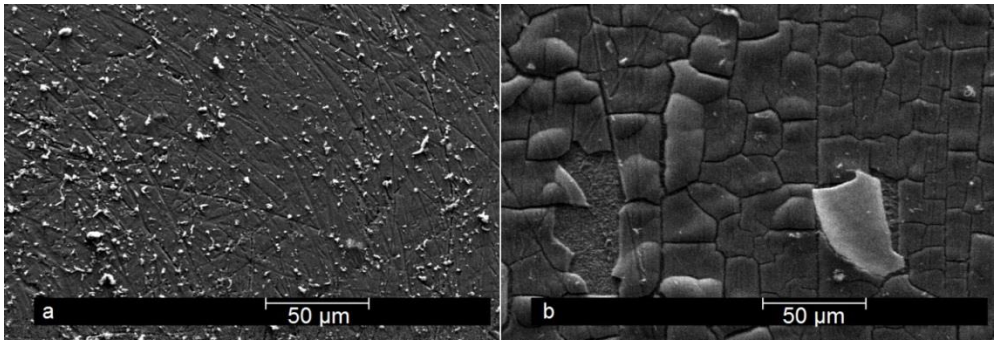

Figure 4.4 SEM images of the iron RDE following 3 hours of immersion in solutions containing 5 M $[NH_3]_T$, 1 M $[CO_2]_T$ and a) 150 mM Ni(II) and 22 mM $S_2O_3^{2-}$; b) 150 mM Ni(II), 12 mM Co(II) and 22 mM $S_2O_3^{2-}$.

The OCP measurements and surface characterisation studies indicated that the species responsible for the passivation of iron were cobalt and thiosulfate ions, but only when they were both present in solution. Therefore, the processes taking place on the iron RDE during the OCP transition were further investigated by SEM observation of its surface following different periods of immersion in the presence of both these species.

During the initial stages of immersion, small particles, surrounded by a ring of similar appearance, began to appear and increase in number, as can be seen in the SEM images taken at 20 minutes and 1 hour of immersion (Figure 4.5). These appear to indicate localised corrosion resulting in the precipitation of solid product possibly consisting of an iron oxide-hydroxide or carbonate, as consistent with previous studies discussed in section 2.6.1(b). In the image taken following 1 hour of immersion, it is also possible to see a more uniform but cracked layer, which became even more clearly visible in the image taken after 2 hours of immersion, following the OCP transition to the passive potential region. This cracked layer was thought to consist of a cobalt sulfide or polysulfide layer (CoS_x) which was further investigated as described in chapter 6.

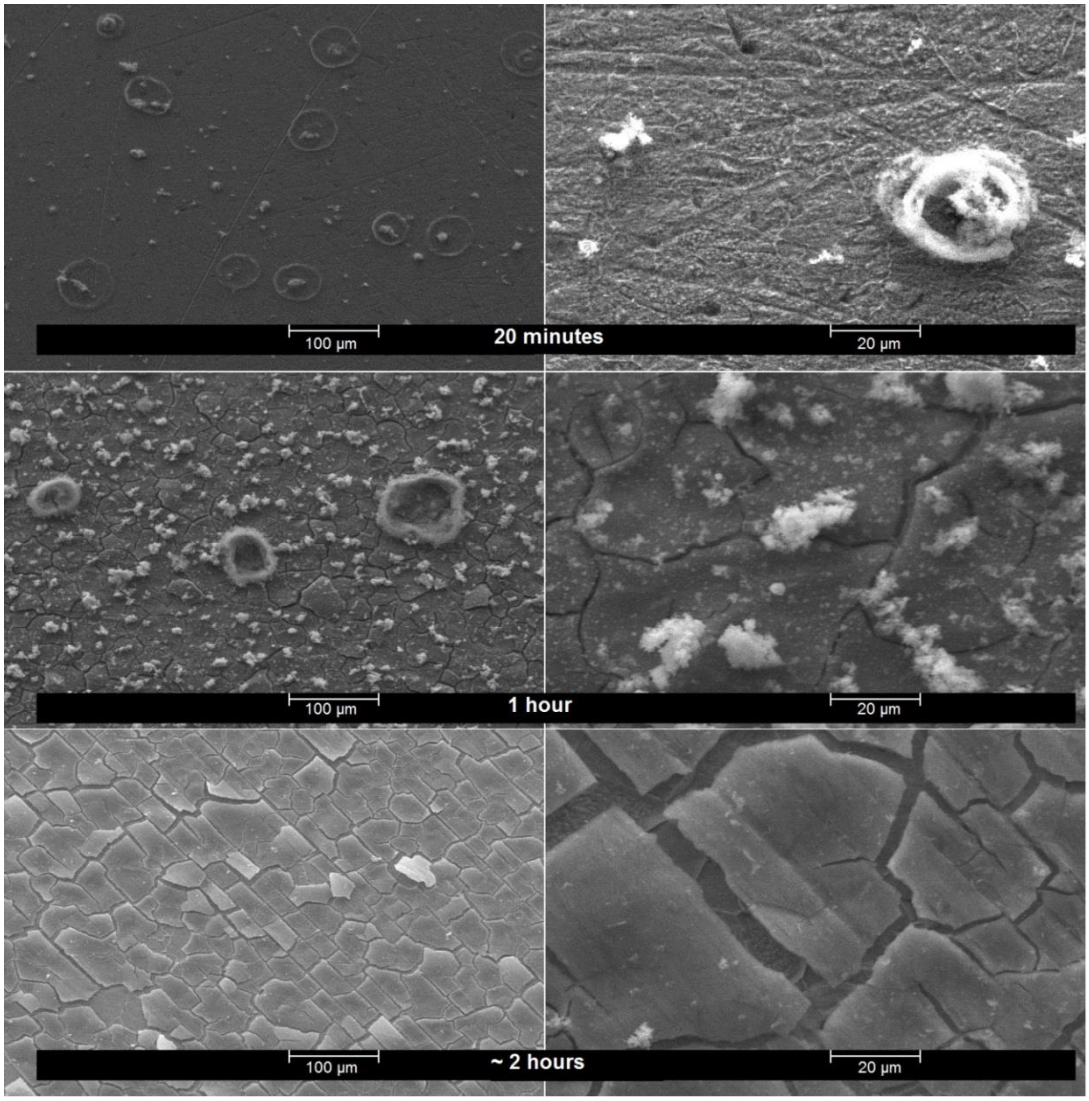

Figure 4.5 SEM images of the iron RDE surface following different periods of immersion in ammoniacal-carbonate solution containing 5 M $[NH_3]_T$, 1 M $[CO_2]_T$, 12 mM Co(II) and 22 mM $S_2O_3^{2-}$.

4.2.3 Rotating disk cyclic voltammetry

The iron RDE was immersed for 1 hour in a set of solutions containing the combinations of nickel, cobalt and thiosulfate ions listed in Table 4.2. Cyclic voltammetric measurements were then taken by scanning the potential in the positive direction from the OCP to 0.74 V and back, at a rate of 10 mV/s. For each solution composition, the corresponding cyclic voltammetry curves are shown in the figures listed in Table 4.2, along with the anodic peak potentials and current densities. As can be seen from Figure 4.6, the behaviour of iron was found to be fairly similar in

all of the solutions not containing any thiosulfate ions, with an anodic current peak being observed at around -0.4 V (peak A). This current was attributed to the dissolution of metallic iron to ferrous tetrammine, as discussed in more detail in chapter 5, section 5.7.

Table 4.2 Anodic peak potentials (E_{pa}) and current densities (i_{pa}) in different solutions*

solution	species concentration (mM)			E_{pa} (V)	i_{pa} (mA/cm²)	Figure no.
	[Ni(II)]	[Co(II)]	[$S_2O_3^{2-}$]			
barren	_	_	_	-0.40	28	4.6 a
Ni(II)	150	_	_	-0.33	25	4.6 b
Co(II)	_	12	_	-0.40	22	4.6 c
Ni(II) + Co(II)	150	12	_	-0.41	20	4.6 d
$S_2O_3^{2-}$	_	_	22	-0.11	224	4.7
Ni(II) + Co(II) + $S_2O_3^{2-}$	150	12	22	-0.16	148	4.8

*Fe RDE, at 10 mV/s, following 1 hour immersion; solutions also contain 5 M $[NH_3]_T$ and 1 M $[CO_2]_T$

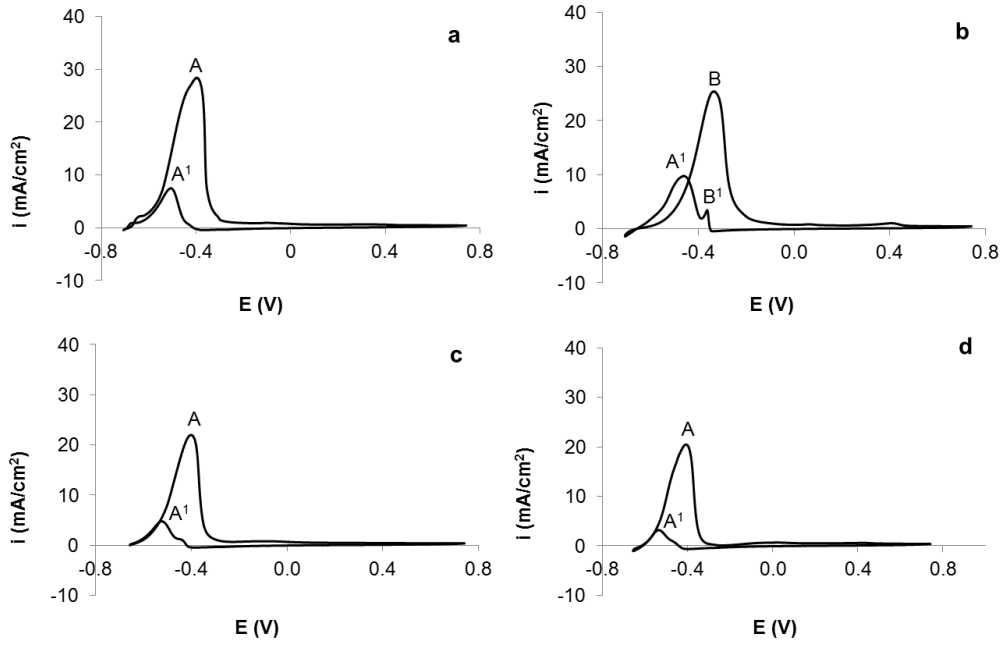

Figure 4.6 Rotating disk cyclic voltammetry of Fe RDE at 10 mV/s, following 1 hour immersion in deoxygenated solutions containing 5 M $[NH_3]_T$, 1 M $[CO_2]_T$ and: a) no other species; b) 150 mM Ni(II); c) 12 mM Co(II); d) 150 mM Ni(II) and 12 mM Co(II).

Following the steep decrease in current density, ascribed to the passivation of metallic iron, no significant currents were observed up to the inversion potential. During the reverse scan, reactivation of the anodic dissolution of metallic iron (A^1) was observed in all solutions, as the potential was scanned negative to -0.4 V.

The peak current densities observed during the anodic scans were slightly lower in solutions containing Ni(II) and in particular Co(II) ions, compared to those measured in the barren solution, as can be seen from Table 4.2. When only Ni(II) species were present, the potential region of peak A was shifted by about 50 mV in the anodic direction (Figure 4.6 b, peak B). This may be related to the cementation of metallic nickel onto the iron surface resulting in an iron-nickel alloy which was slightly more noble than iron. During the reverse scan, the small anodic peak preceding the reactivation of the iron at around -0.4 V could possibly be attributed to the reactivation of the dissolution of metallic nickel from the passivated alloy (Figure 4.6 b, peak B^1).

Cyclic voltammetry measurements taken in the presence of thiosulfate ions resulted in significantly larger anodic currents, which dropped sharply as the applied potential approached 0 V (Figures 4.7 and 4.8). When all three species were present in the solution which simulated the loaded leach liquor at the Yabulu QN refinery, a second anodic process peaking at around 0.5 V (Figure 4.8, peak C) was observed. This was attributed to the oxidation of a metal sulfide layer formed on the iron during its anodic dissolution under open circuit conditions, as consistent with the SEM/EDX studies described in section 4.1.1. Further investigations of the voltammetric behaviour of iron in solutions containing thiosulfate and either cobalt or nickel ions separately, are described in chapters 6 and 8 respectively.

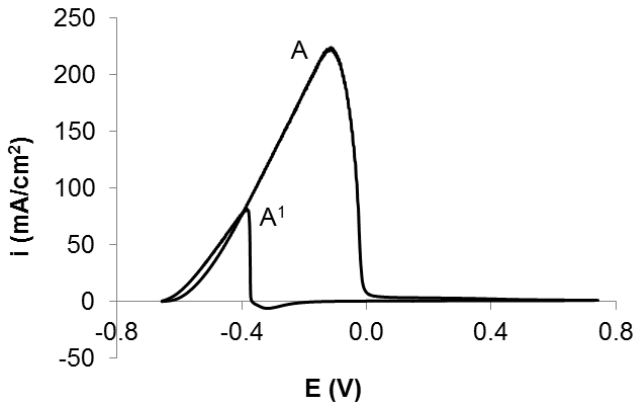

Figure 4.7 Rotating disk cyclic voltammetry of Fe RDE at 10 mV/s, following 1 hour of immersion in deoxygenated solution containing 5 M $[NH_3]_T$, 1 M $[CO_2]_T$ and 22 mM $S_2O_3^{2-}$.

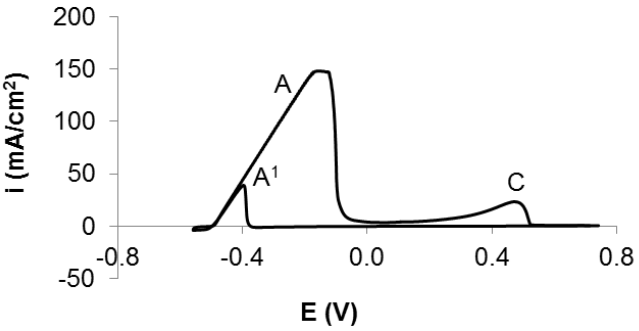

Figure 4.8 Rotating disk cyclic voltammetry of the Fe RDE at 10 mV/s, following 1 hour immersion in deoxygenated solution containing 5 M $[NH_3]_T$, 1 M $[CO_2]_T$, 0.15 M Ni(II), 12 mM Co(II) and 22 mM $S_2O_3^{2-}$.

4.2.4 The effect of iron purity

The behaviour of iron in ammoniacal-carbonate solutions containing both cobalt and thiosulfate under a nitrogen flow was not found to be significantly affected by its purity. As can be seen from Figure 4.9, the OCP of a mild steel electrode (98.5% Fe, 0.75% Mn, 0.5% C and 0.25 % Si) displayed a similar behaviour to that of the pure iron electrode, except for the transition to the passive potential region taking place sooner.

However, the timing of the onset of passivation cannot be related with certainty to the lower purity of the RDE due to the possibility of it being influenced by other factors. As further discussed in chapters 5 and 6, lower concentrations of ammonia

have been found to result in the passivation of iron taking place sooner. Due to the larger size of the mild steel electrode, it required a wider opening in the cell lid, which caused a more significant loss of ammonia from the solution.

The EDX analysis of the mild steel surface following immersion resulted in the detection of lower amounts of cobalt and sulfur (approximately 7 at% and 10 at%, respectively) than in the case of pure iron, which was consistent with the layer also appearing thinner upon visual inspection. A possible explanation for this was the shorter period of active dissolution during which formation of the layer took place.

On the other hand, the slightly longer pause during the OCP transition, observed at around -0.3 V, is possibly related to the lower purity of the electrode. One explanation for the observed behaviour is the presence of a more noble element which begins to dissolve only after the iron becomes passive.

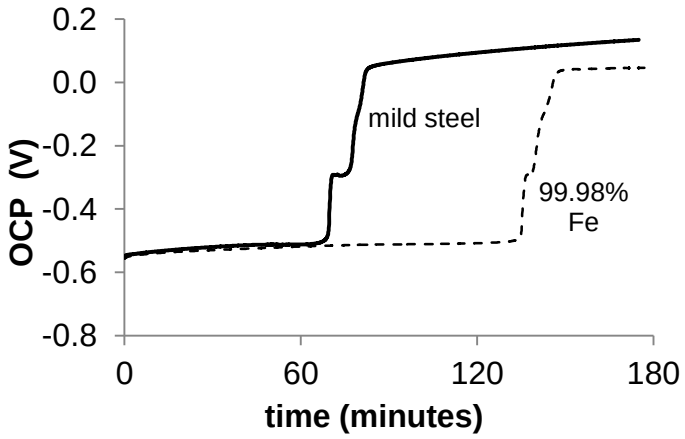

Figure 4.9 OCP of a mild steel RDE (solid line) and a pure iron RDE (dashed line) in solutions containing 5 M $[NH_3]_T$, 1 M $[CO_2]_T$,12 mM Co(II) and 22 mM $S_2O_3^{2-}$, under a N_2 flow.

4.3 Metallic nickel

4.3.1 OCP and SEM/EDX surface analysis

The OCP of a large nickel RDE (see Table 3.3 in section 3.3) was measured in deoxygenated ammoniacal-carbonate solutions containing cobalt and thiosulfate ions (Figure 4.10). The measurement was taken over a period of 6 hours, during which a nitrogen flow was maintained above the solution. Following an initial increase by about 0.1 V which took approximately 1.5 hours, the OCP was found to stabilise at -0.36 V for the remainder of the measurement period.

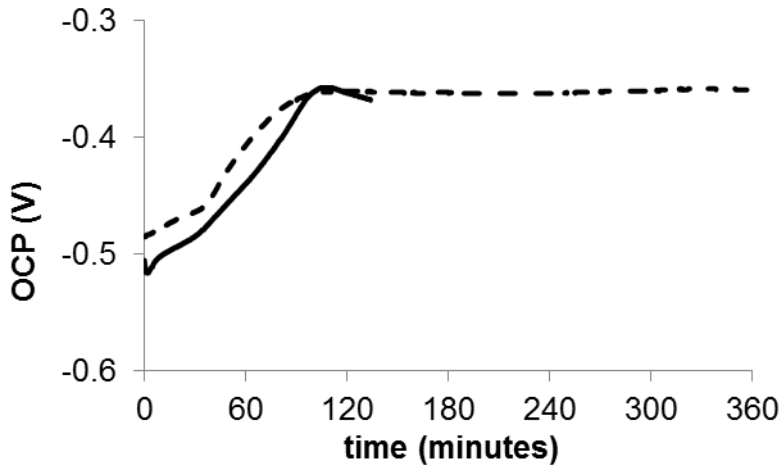

Figure 4.10 OCP of the Ni RDE in solutions containing 5 M $[NH_3]_T$, 1 M $[CO_2]_T$, 12 mM Co(II) and 22 mM $S_2O_3^{2-}$; under a N_2flow (dashed line) or sparge (solid line).

Following immersion for 2 hours in a solution deoxygenated by sparging nitrogen the electrode surface was a shiny bronze colour, whereas after the 6 hour measurement, it was covered with a dark brown-black layer. However, as soon as the electrode was exposed to air after rinsing with deionised water, part of the layer appeared to decompose as the water evaporated, giving way to the small spots in which the metallic nickel surface beneath became visible. Inspection of the RDE surface using an optical microscope revealed evidence of pitting corrosion. As can

be seen from the SEM images (Figure 4.11) the RDE surface appeared to be covered by a cracked layer similar to the one observed on iron. The EDX analysis resulted in the detection of up to 20 at% cobalt and 30 at% sulfur. On the other hand, analysis of the RDE by XRD did not result in any diffraction peaks other than from the underlying metallic nickel, suggesting that the surface layer may be either too thin or amorphous. Based on the EDX results, the surface layer is thought to consist of a cobalt-containing sulfide or polysulfide similar to the one formed on metallic iron.

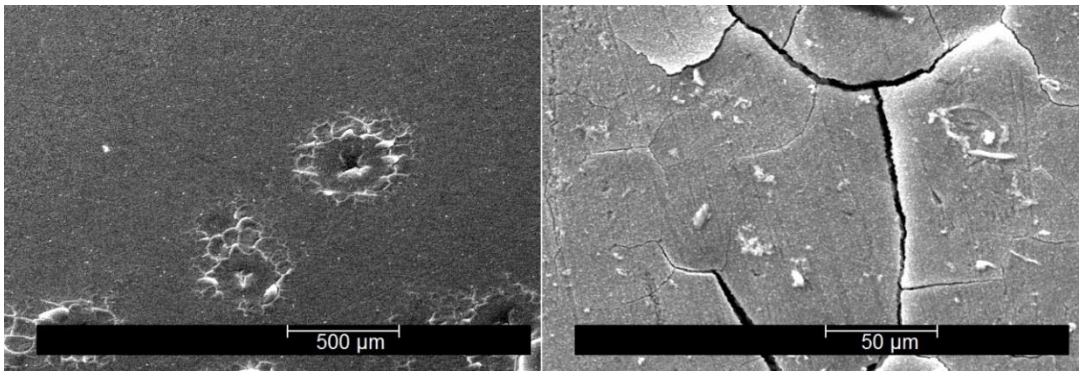

Figure 4.11 SEM images of the nickel RDE following 6 hours of immersion in deoxygenated 5 M $[NH_3]_T$, 1 M $[CO_2]_T$, 12 mM Co(II) and 22 mM $S_2O_3^{2-}$.

4.3.2 Rotating disk cyclic voltammetry

A smaller nickel RDE (see Table 3.3 in section 3.3) was immersed for 3 hours in deoxygenated ammoniacal-carbonate solution containing Ni(II), Co(II) and $S_2O_3^{2-}$. As shown in Figure 4.12, the OCP was found to be more negative than the measurement shown in Figure 4.10, remaining below -0.4 V throughout the 3 hours of immersion.

Cyclic voltammetry measurements conducted following this immersion period by scanning the applied potential in the anodic direction and back for two cycles, at a scan rate of 10 mV/s, are shown in Figure 4.13. The first increase in anodic current (D), attributed to the oxidation of metallic nickel to nickel hexammine, peaked and

dropped sharply as the applied potential reached values above 0.2 V, indicating a sudden cessation of the dissolution of nickel, consistent with its passivation. However, the current density only reached approximately half the peak value, before a second increase took place, peaking just below 0.6 V (E). This was attributed to the oxidation of the surface layer formed on the nickel. During the reverse scan, reactivation of the anodic dissolution of nickel took place as the potential was scanned below 0 V (D^1). The second cycle was consistent with the behaviour of metallic nickel with no surface layer on it, with the current increasing steadily up to the potential at which it became limited by the currents sustained at the counter-electrode.

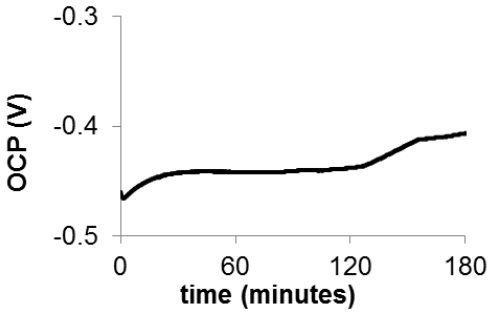

Figure 4.12 OCP of a Ni RDE in deoxygenated solution containing 5 M $[NH_3]_T$, 1 M $[CO_2]_T$, 150 mM Ni(II), 12 mM Co(II) and 22 mM $S_2O_3^{2-}$.

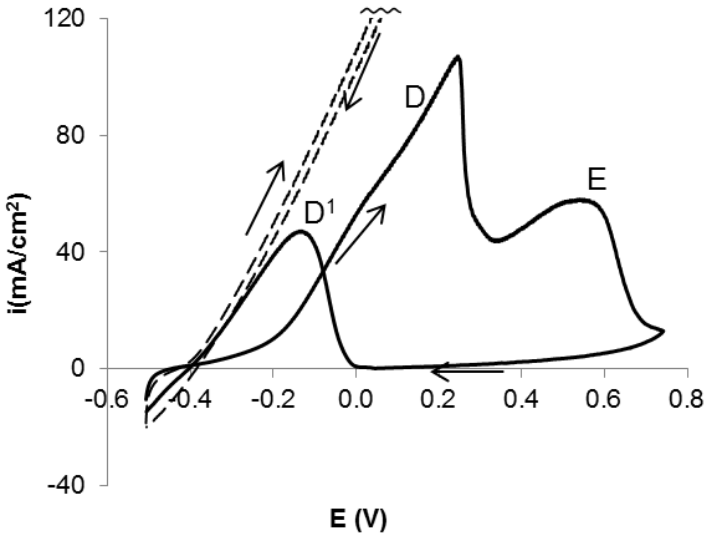

Figure 4.13 Rotating disk cyclic voltammetry of a Ni RDE at 10 mV/s following immersion for 3 hours in deoxygenated solution containing 5 M $[NH_3]_T$, 1 M $[CO_2]_T$, 150 mM Ni(II), 12 mM Co(II) and 22 mM $S_2O_3^{2-}$. Solid line: first cycle; dashed line: second cycle.

4.4 Polarisation studies conducted on platinum

4.4.1 Potentiostatic polarisation and EDX surface analysis

Further preliminary studies were conducted by polarising a platinum RDE in the same set of solutions and under the same conditions as the study conducted on iron (section 4.2.1). The applied potentials, shown in Table 4.3, were chosen to be approximately the same as the mixed potential of the iron RDE in each of the solutions (Table 4.1). The potentials were applied for periods of 3 hours in each solution, after which the RDE was removed, gently rinsed with deionised water and dried with air. The RDE surface was then analysed by SEM/EDX, which resulted in the detection of the elements listed for each solution in Table 4.3.

Table 4.3 Potentials applied to Pt RDE in different solutions and resulting elements detected on surface*

solution	species concentration (mM)			applied potential (V)	elements detected by EDX
	[Ni(II)]	[Co(II)]	[$S_2O_3^{2-}$]		
barren	_	_	_	-0.7	-
Ni(II)	150	_	_		nickel
Co(II)	_	12	_	-0.6	-
Ni(II) + Co(II)	150	12	_		-
$S_2O_3^{2-}$	_	_	22		sulfur
Ni(II) + $S_2O_3^{2-}$	150	_	22	-0.5	-
Co(II) + $S_2O_3^{2-}$	_	12	22		sulfur, cobalt
Ni(II) + Co(II) + $S_2O_3^{2-}$	150	12	22		sulfur, cobalt, nickel

* potentiostatic polarisation for 3 hours; all solutions also contain 5 M $[NH_3]_T$ and 1 M $[CO_2]_T$

As can be seen from Table 4.3, polarisation at -0.7 V in the presence of Ni(II) resulted in the deposition of nickel onto the platinum surface, while polarisation in solutions containing cobalt did not result in the detection of any cobalt except when thiosulfate ions were also present. This suggested that metal displacement of iron by cobalt resulting in its cementation is unlikely to take place under the conditions of this study, as consistent with the results reported in section 4.2. Polarisation in the presence of both cobalt and thiosulfate ions resulted in the detection of both cobalt and sulfur, as well as nickel when this was also present in solution. This is consistent with the possible formation of a cobalt sulfide or polysulfide species during polarisation of the platinum in the presence of both dissolved cobalt and thiosulfate ions. However, even though sulfur was also detected on the RDE surface following polarisation in the solution containing only thiosulfate ions, neither sulfur nor nickel were detected following polarisation in the presence of nickel and thiosulfate ions when no cobalt was present. This appears to indicate that in this solution, the polarisation did not result in the formation of any surface species. However, this is in contrast with the findings observed for the other solutions, and a more plausible explanation may be that the sulfide layer formed re-dissolved rapidly after the applied potential was switched off, during the short delay immediately before its removal from solution. This was consistent with the layer being stable only while the negative potential was applied to the platinum, and similarly on the actively dissolving metallic iron. This can be explained in terms of the cathodic protection, provided by either the metallic iron or the negatively polarised platinum, with respect to the oxidative dissolution of the layer. Switching off the potential applied to the platinum was thought to have resulted in redissolution of the layer, which did not take place in the case of metallic iron, as this remained active until removed from

solution. On the other hand, the cobalt sulfide or polysulfide species formed on the polarised platinum or on the actively dissolving metallic iron did not dissolve as readily as the nickel sulfide, even after the applied potential was switched off and after passivation of the iron.

4.4.2 Rotating disk cyclic voltammetry

Cyclic voltammetric measurements were conducted on the platinum RDE following polarisation for 3 hours under the same conditions as the study conducted on iron (section 4.1) at the potentials listed in Table 4.4. The applied potential was then scanned in the anodic direction at a rate of 10 mV/s, up to the inversion potential of 0.75 V, and back to the original applied potential. For each solution composition, the corresponding cyclic voltammetry curves are shown in the figures listed in Table 4.4, along with the anodic peak potentials (E_{pa}) and current densities (i_{pa}). However, it should be kept in mind that in the solutions containing thiosulfate ions, platinum is not to be considered completely inert due to the possibility of reaction with thiosulfate, poisoning by sulfide species or formation of platinum sulfide (Anthony and Williams, 1994; Ijzermans, 1969a; Ijzermans, 1969b; Najdeker and Bishop, 1973; Ramasubramanian, 1975).

No significant anodic currents were observed following the polarisation of platinum in the absence of thiosulfate ions, except for those measured in the solution containing Ni(II), as shown in Figure 4.14. During the first cyclic voltammetry scan measured following the potentiostatic polarisation an anodic peak (B) was observed at -0.37 V. This was assigned to the oxidation of metallic nickel to nickel hexammine, as consistent with its deposition taking place during the potentiostatic polarisation and with its region of thermodynamic stability given in the Eh-pH

diagram shown in Figure 2.5 (A), section 2.4. No significant peak was observed in subsequent scans or when the electrode was polarised for only one hour.

In solutions containing thiosulfate ions, a broad anodic feature was observed at potentials above 0.4 V, as shown in Figure 4.15 (peak F) for the experiment carried out in the absence of any dissolved nickel or cobalt. This was thought to be due to an interaction between the platinum and thiosulfate ions, and the possibility of formation and oxidation of a platinum sulfide layer is not to be excluded.

Table 4.4 Potentials applied to the Pt RDE in different solutions and resulting E_{pa} and i_{pa}*

solution	species concentration (mM)			applied potential (V)	E_{pa} (V)	i_{pa} (mA/cm^2)	Figure no.
	[Ni(II)]	[Co(II)]	[$S_2O_3^{2-}$]				
barren	_	_	_	-0.7	_	_	_
Ni(II)	150	_	_		-0.37	5.2	4.14
Co(II)	_	12	_	-0.6	_	_	_
Ni(II) + Co(II)	150	12	_		_	_	_
$S_2O_3^{2-}$	_	_	22		0.63	2.5	4.15
Ni(II) + $S_2O_3^{2-}$	150	_	22	-0.5	0.62	1.9	_
Co(II) + $S_2O_3^{2-}$	_	12	22		0.31 0.62	1.8 4.0	_
Ni(II) + Co(II) + $S_2O_3^{2-}$	150	12	22		0.39 0.49	21.5 14.7	4.16

* potentiostatic polarisation for 3 hours, followed by scan in the anodic direction at 10 mV/s; all solutions also contain 5 M $[NH_3]_T$ and 1 M $[CO_2]_T$.

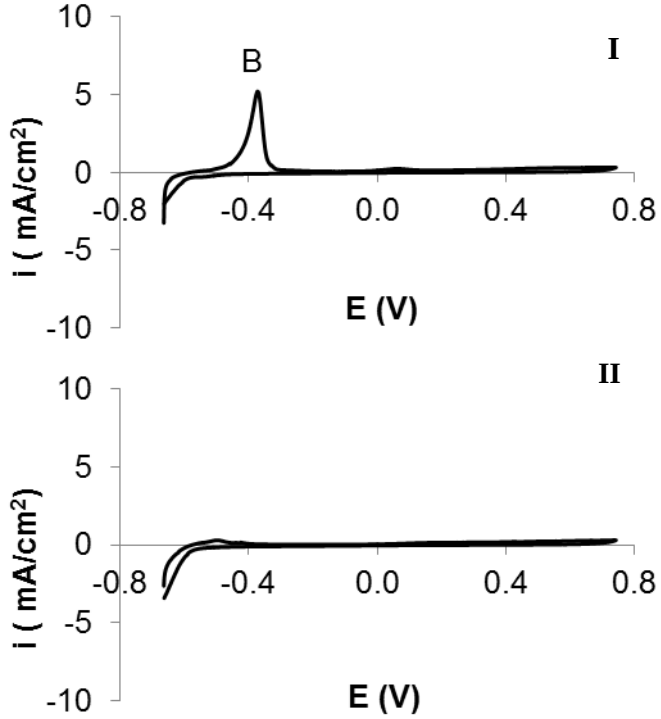

Figure 4.14 Rotating disk cyclic voltammetry (10 mV/s) of Pt RDE following 3 hours polarisation at -0.7 V in deoxygenated solution containing 5 M $[NH_3]_T$, 1 M $[CO_2]_T$ and 150 mM Ni(II), first cycle (I) and second cycle (II).

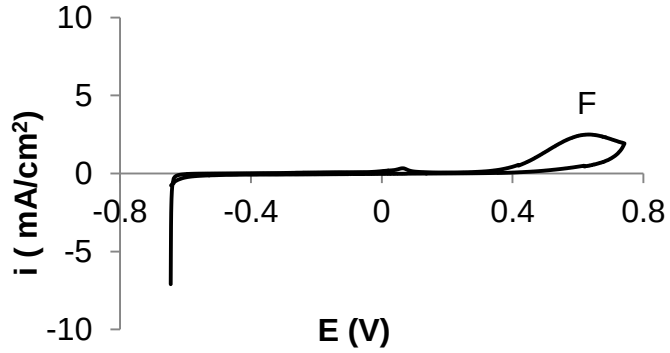

Figure 4.15 Rotating disk cyclic voltammetric measurement (10 mV/s) of a Pt electrode following 3 hours potentiostatic polarisation at -0.6 V in deoxygenated solution containing 5 M $[NH_3]_T$, 1 M $[CO_2]_T$ and 22 mM $S_2O_3^{2-}$.

In the presence of nickel, cobalt and thiosulfate ions, more significant peaks were observed in the 0.4 V potential region, but their reproducibility was poor. Curves obtained during two subsequent scans in the presence of all three species are shown in Figure 4.16. These showed the presence of multiple peaks, which during the subsequent scan, were replaced by a single peak around 0.4 V.

Following this preliminary work, the platinum RDE was not considered to be suitable for further investigations, as these were to be carried out in solutions containing thiosulfate ions, therefore under conditions in which platinum is not to be considered completely inert.

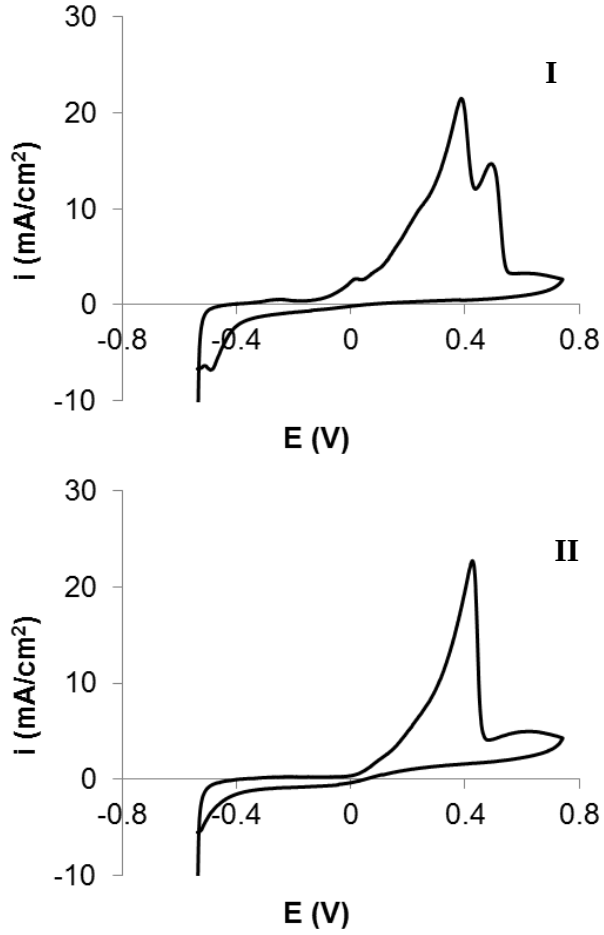

Figure 4.16 Rotating disk cyclic voltammetric measurements (10 mV/s) of the Pt RDE following 3 hours of potentiostatic polarisation at -0.5 V in deoxygenated solutions containing 5 M $[NH_3]_T$, 1 M $[CO_2]_T$, 150 mM Ni(II), 12 mM Co(II) and 22 mM $S_2O_3^{2-}$, first (I) and second (II) cycle.

4.5 Summary

Based on this preliminary set of experiments, it was found that the presence of both cobalt(II) and thiosulfate ions in ammoniacal-carbonate solutions simulating the Caron leach liquor resulted in the passivation of iron within less than 3 hours of immersion. This was accompanied by the deposition of a visible surface layer containing cobalt and sulfur, based on its analysis by SEM/EDX, thought to contain a cobalt sulfide or polysulfide species. Immersion of the iron RDE in the presence of nickel(II) ions resulted in the detection of nickel on its surface, possibly resulting from the displacement of metallic iron by nickel hexammine. This was found to be consistent with thermodynamic calculations and with polarisation experiments conducted on platinum. The presence of both nickel(II) and thiosulfate ions in solution resulted in the detection of some nickel and sulfur on the iron surface following its immersion for 3 hours. Based on SEM/EDX analysis, this was thought to possibly consist of a nickel sulfide species, which however appeared to be visibly thinner than the cobalt sulfide layer. In this case, the passivation of metallic iron was not observed, indicating that the behaviour observed in the previous studies by Nikoloski (2003) was likely to be due to the co-presence of cobalt(II) and thiosulfate ions, and the resulting cobalt sulfide or polysulfide layer, with little or no involvement of the nickel(II) ions.

5 THE BEHAVIOUR OF IRON IN AMMONIACAL-CARBONATE SOLUTIONS CONTAINING COPPER(II) IONS

5.1 Introduction

The Caron leach liquor from the Yabulu QN refinery contains low concentrations of dissolved copper, which can reach a maximum of 0.6 mM, depending on the ore feed being processed (Fittock, 2014). However, more significant amounts may be found at plants which process ores with a higher copper content, such as the Niquelandia Caron plant in Brazil (Fittock, 2014).

As consistent with the thermodynamic data discussed in section 2.4, it has been suggested that metallic copper is likely to cement onto metallic iron (Nikoloski and Nicol, 2006), nickel and iron-nickel alloys (Senanayake et al., 2010) under the conditions of the Caron process (see Table 2.3 in chapter 2 for details). However, the focus of previous studies conducted on iron has been on its behaviour in solutions containing nickel, cobalt and thiosulfate ions in the absence of copper(II) ions (Nicol et al., 2004; Nikoloski, 2002; Nikoloski and Nicol, 2006; Nikoloski and Nicol, 2010; Nikoloski et al., 2003). For this reason, it was useful to investigate the effect of dissolved copper species on the anodic dissolution of iron in ammoniacal-carbonate solutions.

In the present study, the behaviour of metallic iron in solutions containing copper(II) ions was investigated by means of electrochemical measurements and SEM-EDX studies of the surface changes at different immersion times. Other variables studied included the concentration of copper(II) species, $[NH_3]_T$ and $[CO_2]_T$. The investigation was extended to an iron-nickel and an iron-cobalt alloy in order to

check whether their behaviour was analogous to that of pure iron. The study was conducted at 45°C in order to more closely represent the process temperature.

5.2 Open circuit behaviour and SEM/EDX surface analysis

The open circuit potential of an iron RDE was measured over 3 hours in an aqueous solution of ammonia and ammonium bicarbonate - ammonium carbamate double salt, at 5 M $[NH_3]_T$, 1 M $[CO_2]_T$, and 0.2 mM copper sulfate. The potential was found to increase slowly from just above -0.7 V, reaching -0.6 V after 3 hours (Figure 5.1). The electrode was then taken out of solution, rinsed immediately with deionised water and gently dried with air. The surface was analysed by scanning electron microscopy / energy dispersive X-ray spectroscopy (SEM/EDX), which revealed the presence of a dendritic copper deposit (Figure 5.2, a). The experiment was then repeated at a higher copper(II) concentration of 12 mM. In this case, the OCP was found to initially increase slowly at potentials around -0.5 V, followed by a sharp increase after about 5 minutes (Figure 5.1). Following a brief pause at around -0.25 V, which lasted a few minutes, the OCP increased to a higher potential of 0.1 - 0.2 V, where it remained for the rest of the 3 hour measurement period (Figure 5.1). This is within the stability region of an iron(III) oxide or hydroxide, as consistent with Eh-pH diagrams (Figures 2.5 and 2.6) discussed in chapter 2. Analysis for the electrode surface by SEM/EDX indicated only the presence of iron, which is consistent with there being a thin undetectable oxide layer on the surface of the metallic iron.

The processes occuring on the RDE surface during the OCP transition from the lower to the higher potential region were further studied by conducting SEM/EDX analyses on the electrode taken out at different immersion times. The results,

summarised in Figure 5.1, revealed the presence of an adherent, thick but porous, copper deposit during the initial phase of increase in the potential (insert A) which appeared thinner at the OCP shoulder at around -0.25 V (insert B) and was no longer detectable at potentials above 0 V (insert C).

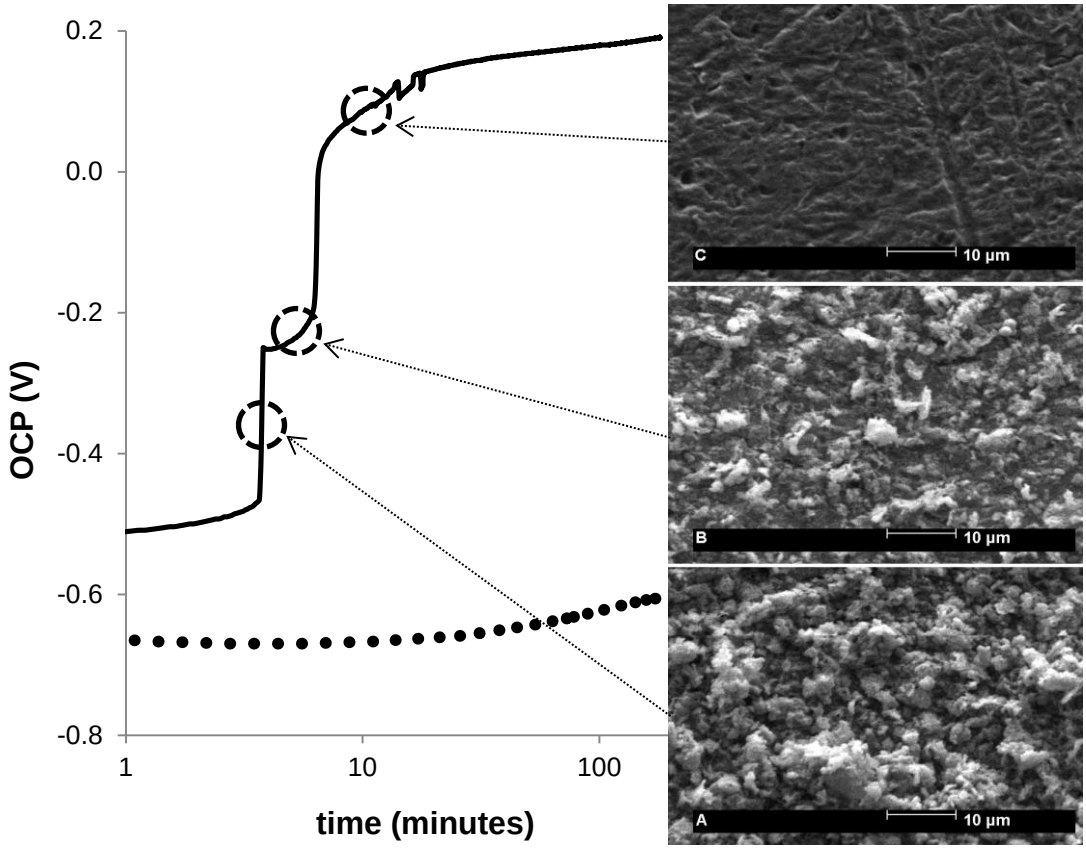

Figure 5.1 OCP of the Fe RDE in ammonia - ammonium bicarbonate/carbamate ($NH_4HCO_3/NH_2CO_2NH_4$) solutions at 5 M $[NH_3]_T$, 1 M $[CO_2]_T$, 12 mM Cu(II) (solid line) and 0.2 mM Cu(II) (dotted line), and the corresponding surface changes during the potential transition from -0.6 V to above 0.1 V.

The OCP behaviour of the iron RDE in solutions containing varying concentrations of copper ions displayed relative consistency in terms of the transition from active to passive with a shoulder at around -0.25 V. This appeared to be the case irrespective of whether oxygen was present in the solution or not and whether the solution was prepared using ammonia and ammonium bicarbonate or ammonia and ammonium bicarbonate-carbamate double salt. However, the morphology of the copper deposit

was found to change from dendritic (Figure 5.2, A) to botroydal (Figure 5.2, B and C) when the solution was prepared using ammonium bicarbonate instead of the double salt. It is well known that the morphology of this kind of deposit is sensitive to the conditions under which it was formed, in particular to variables such as temperature, rotation speed, pH, concentration of depositing ion and anions present (Power and Ritchie, 1975). In the ammonia-carbonate solutions employed in this study, a number of species such as NH_3, NH_4^+, CO_3^{2-} HCO_3^- and $NH_2CO_2^-$ exist in a complex equilibrium with each other (Mani et al., 2006; Wen and Brooker, 1995). The metal complex speciation is also rather complicated. The observed change in copper deposit morphology is likely to have been caused by a variation in the ratios of the species present affecting the nucleation mechanism and subsequent crystal growth.

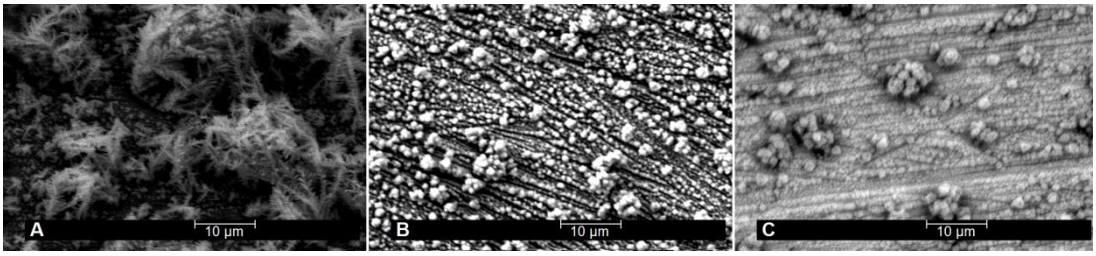

Figure 5.2 SEM image of the Fe RDE following immersion in solutions containing 5 M $[NH_3]_T$, 1 M $[CO_2]_T$ and a) 0.2 mM Cu(II), immersed for 3 hours (solution prepared using $NH_4HCO_3/NH_2CO_2NH_4$); b) 0.2 mM Cu(II), immersed for 3 hours (solution prepared using NH_4HCO_3; c) 12 mM Cu(II), immersed for a few minutes (solution prepared using NH_4HCO_3), under deoxygenated conditions.

5.3 Rotating disk cyclic voltammetry

Potentiodynamic studies were conducted in ammonia – ammonium bicarbonate solutions containing 6 mM copper(II) ions. Following a 2 minute immersion of the iron RDE under open circuit conditions, the potential was scanned in the anodic direction at a rate of 10 mV/s from the OCP to +0.24 V, and then back in the cathodic direction to -0.56 V. The resulting current density response is shown in

Figure 5.3. The first anodic peak (A) observed close to -0.43 V during the positive sweep is assigned to the anodic dissolution of metallic iron, followed by a second anodic peak (B) around -0.13 V, assigned to the redissolution of cemented copper. This is discussed in more detail in section 5.7. During the cathodic scan, a small negative current becomes visible at potentials below 0 V, with the anodic dissolution of iron resuming just above -0.4 V and peaking at -0.47 V (A^1).

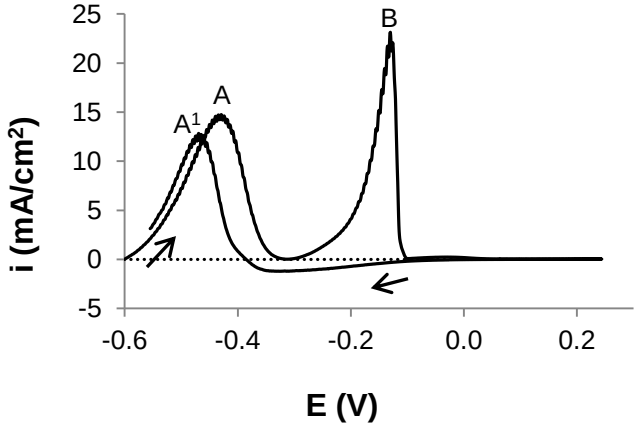

Figure 5.3 Cyclic voltammogram (10 mV/s) of the Fe RDE in ammonia - ammonium bicarbonate solution at 5 M $[NH_3]_T$, 1 M $[CO_2]_T$ and 6 mM Cu(II).

In order to confirm that the spontaneous transition of the iron OCP to the higher potential region was due to the formation of a stable passive layer, potentiodynamic experiments were conducted following the OCP increase to above 0 V. The applied potential was scanned from the final OCP to + 0.24 V and then back in the cathodic direction to -0.56 V. The measurements were conducted in ammonia – ammonium bicarbonate solutions containing 6 mM copper(II) ions, both under normal and deoxygenated conditions. As can be seen in Figure 5.4, no significant anodic current was observed in either scan direction until the applied potential became negative enough to re-activate the anodic dissolution of iron, resulting in peak A^1. Prior to reaching this point, the cathodic scan again resulted in a negative current, visible

between 0.1 V and -0.4 V. No anodic peak attributable to the dissolution of copper was observed, which was consistent with the fact that once the OCP of the iron RDE reached the passive potential region all the cemented copper had re-dissolved.

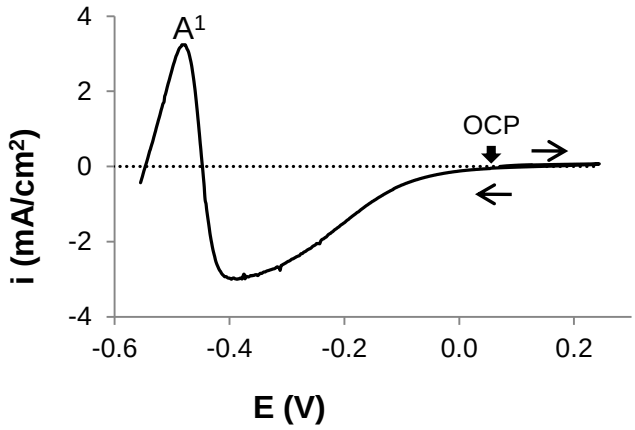

Figure 5.4 Cyclic voltammogram (10 mV/s) of the Fe RDE in deoxygenated ammonia - ammonium bicarbonate solution at 5 M $[NH_3]_T$, 1 M $[CO_2]_T$ and 6 mM Cu(II), following its transition to the passive state.

5.4 The effect of copper(II) concentration on the passivation time

A study of the effect of the copper(II) concentration in ammonia - ammonium bicarbonate solutions, on the immersion time required for passivation of the iron RDE, was conducted at copper concentrations ranging from 1 mM to 12 mM. The results indicated a trend by which the passivation time increased with decreasing copper(II) concentration, as shown for some of the concentrations studied in the presence of oxygen in Figure 5.5, and in deoxygenated solutions in Figure 5.6. Such trend can be clearly seen for all of the copper(II) concentrations studied in Figure 5.7, which shows the dependence on copper(II) concentration of the time between immersion and the first and second increase in potential, above E_1 = -0.4 V and E_2 = -0.2 V respectively.

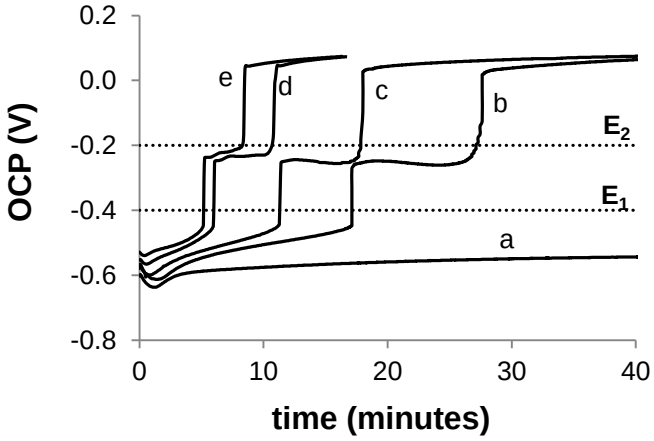

Figure 5.5 The variation over time of the OCP of the Fe RDE in ammonia - ammonium bicarbonate solutions at 5 M $[NH_3]_T$, 1 M $[CO_2]_T$ and [Cu(II)] = a) 1 mM; b) 2 mM; c) 3 mM; d) 6 mM; e) 10 mM.

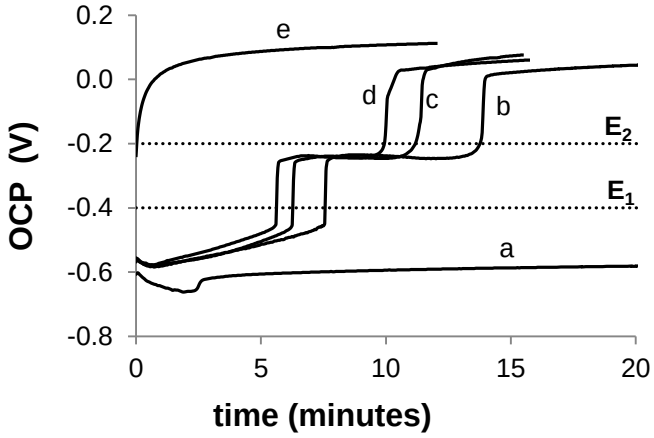

Figure 5.6 The variation over time of the OCP of the Fe RDE in deoxygenated ammonia - ammonium bicarbonate solutions containing 5 M $[NH_3]_T$, 1 M $[CO_2]_T$ and [Cu(II)] = a) 1 mM; b) 3 mM; c) 4 mM; d) 5 mM; e) 6 mM.

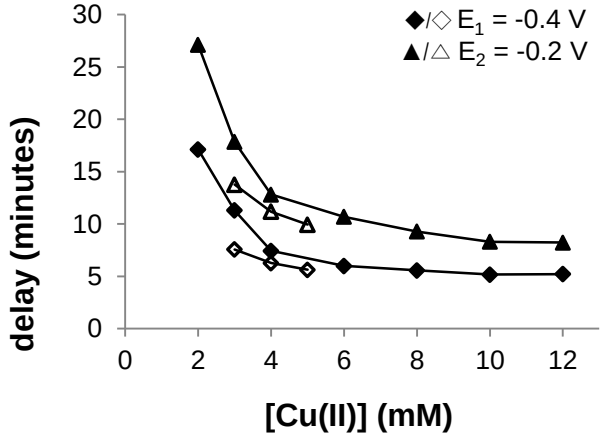

Figure 5.7 The dependence on [Cu(II)] of the time delay between immersion of the Fe RDE and the potential increase above E_1 = -0.4 V and E_2 = -0.2 V in the presence (solid symbols) or absence (outline symbols) of dissolved oxygen.

5.5 The effect of $[NH_3]_T$ and $[CO_2]_T$ on the passivation time

The effect of varying the ammonia concentration on the time required for passivation was studied without de-oxygenating the solutions, in order to better control the ammonia concentration. Due to the complex equilibria and the unstable nature of ammonia and ammonium bicarbonate solutions at 45°C, investigating the effect of $[NH_3]_T$ and $[CO_2]_T$ as independent variables resulted in poorly reproducible results. Nevertheless, the passivation time was found to be less sensitive to changes in the ammonia concentration at a constant $[CO_2]_T$, than it was to changes in $[CO_2]_T$ at a constant $[NH_3]_T$. The passivation time was found to increase with increasing ammonium bicarbonate concentration, as shown in Figure 5.8, where $[NH_3]$ represents the concentration of ammonia added, excluding the contribution from NH_4HCO_3.

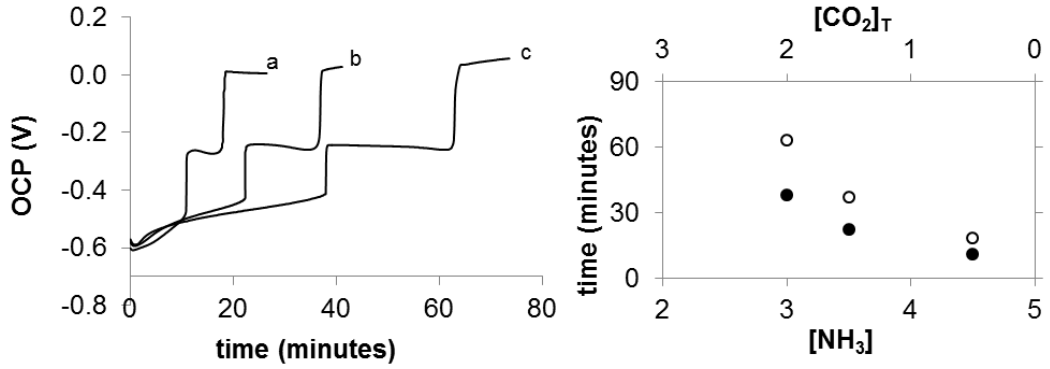

Figure 5.8 Left: the variation over time of the OCP of the Fe RDE in solutions containing 2 mM Cu(II), 5 M $[NH_3]_T$ and $[CO_2]_T$ = a) 0.5 M; b) 1.5 M; c) 2 M. Right: the effect of $[NH_3]$ and $[CO_2]_T$ on the time delay from immersion to the first OCP transition to above -0.4 V (solid circles) and to the second OCP transition to above -0.2 V (outline circles).

This is consistent with the ammonium bicarbonate playing an important role in preventing or delaying the passivation of iron. It should also be noted that in the complete absence of ammonium bicarbonate, iron was found to be passive

immediately upon immersion irrespective of the ammonia concentration, even at copper concentrations as low as 0.2 mM, as shown in Figure 5.9.

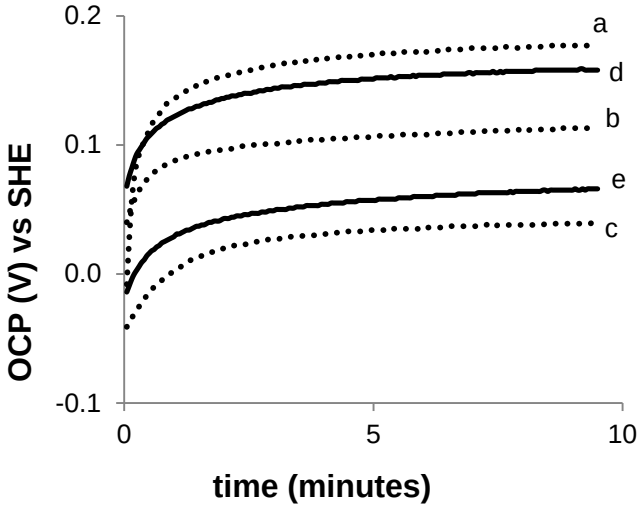

Figure 5.9 The variation over time of the OCP of the Fe RDE in ammonia solutions at 0.2 mM Cu(II) (dotted lines) and [NH_3] = a) 0.1 M; b) 1 M; c) 5 M; at 1 mM Cu(II) and [NH_3]= d) 1 M; e) 5 M.

The results shown in Figure 5.9 are included only for comparison, since ammoniacal leaching systems operate at a lower pH due to the addition of an ammonium salt, which is necessary for the active dissolution of the metals. A more relevant study was conducted on the dependence of the passivation time on both $[NH_3]_T$ and $[CO_2]_T$ varied at a constant molar ratio of 5 to 1. This had the additional advantage of maintaining the pH close to 10.5 for all of the measurements, therefore removing additional variables able to affect the passivation time. In this set of measurements, more clear trends were obtained, as shown for a copper(II) concentration of 2 mM in Figures 5.10 and 5.11.

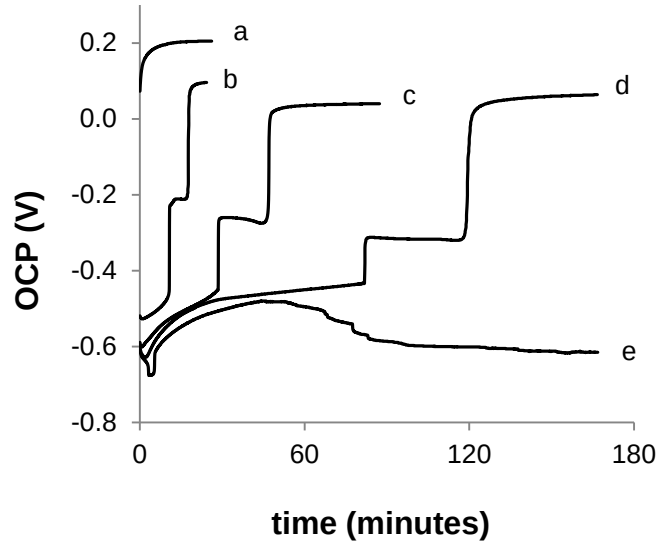

Figure 5.10 The variation over time of the OCP of the Fe RDE in ammonia – ammonium bicarbonate solutions at 2 mM Cu(II), $[NH_3]_T$: $[CO_2]_T$ = 5 : 1, and $[NH_3]_T$ = a) 1 M; b) 2 M; c) 5 M; d) 7 M; e) 8 M.

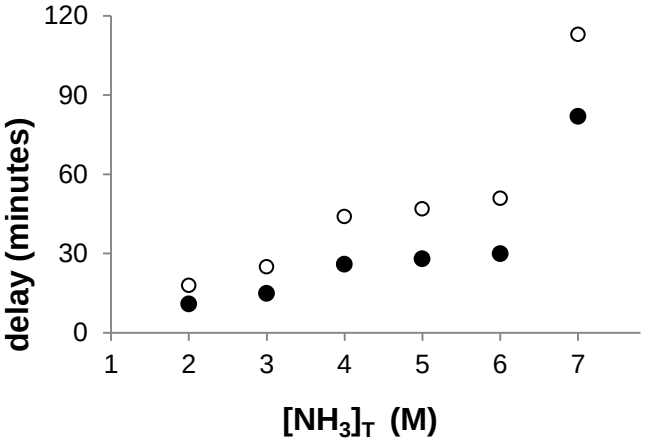

Figure 5.11 The dependence on $[NH_3]_T$ of the time delay between immersion of the Fe RDE and the first increase in potential to above -0.4 V (solid circles) and to above -0.2 V (outline circles), at 2mM Cu(II) and $[NH_3]_T$: $[CO_2]_T$ = 5 : 1.

As it can be seen in Figures 5.10 and 5.11, the higher the concentration of ammonia and ammonium carbonate, the longer the immersion time required for passivation to occur. At 1 M $[NH_3]_T$ the OCP appears to be dominated by the effect of ammonia and is consistent with the behaviour shown in Figure 5.9. This suggests that below a certain concentration, the ammonium bicarbonate becomes ineffective at preventing the passivation of iron. On the other hand, at high enough $[NH_3]_T$, passivation does

not occur at all, and copper continues to cement onto the dissolving iron for longer than 16 hours. These results are also consistent with ammonium bicarbonate playing a significant role in preventing the passivation of iron.

5.6 Iron-nickel and iron-cobalt alloys

Measurements of the OCP of an 80% iron - 20% nickel alloy and a 99% iron - 1% cobalt alloy showed behaviours very similar to that of iron under the same conditions (Figure 5.12). This confirmed that the findings regarding the behaviour of iron apply to the alloys of iron with nickel and cobalt, which appear to undergo passivation via a similar mechanism.

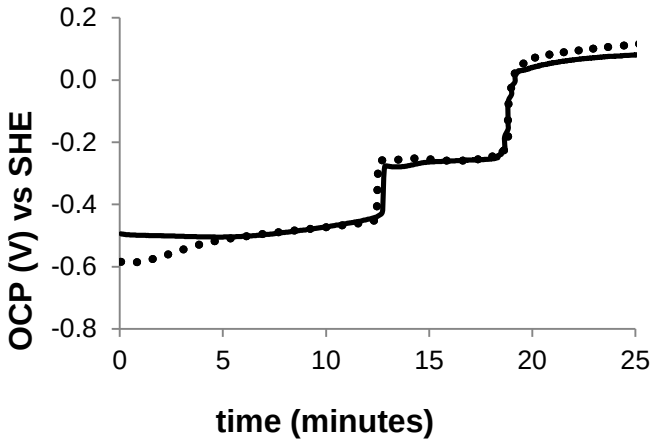

Figure 5.12 The variation over time of the OCP of an 80% Fe – 20% Ni alloy RDE (solid line) and a 99% Fe - 1% Co alloy RDE (dotted line) in 4 mM Cu(II), $[NH_3]_T$ = 5 M and $[CO_2]_T$ = 1 M.

5.7 Discussion of reactions

As discussed in chapter 2 , the anodic dissolution of iron in ammoniacal-carbonate solution is generally thought to result in the formation of ferrous tetrammine complexes (Kim et al., 1991; Lee et al., 1985; Nikoloski and Nicol, 2006; Senanayake et al., 2010), although ferrous pentammine complexes have also been suggested as a dominant species (Asselin, 2008). As discussed in section 2.4,

published thermodynamic data (Isaev et al., 1990a) suggests that the most stable ferrous ammine complex is the tetrammine. The anodic dissolution of metallic iron in ammoniacal solutions may therefore be described by half-reaction 5.1.

$$Fe + 4NH_3 \rightarrow Fe(NH_3)_4^{2+} + 2e^- \quad (5.1)$$

Based published on standard Gibbs free energy of formation ($\Delta_f G°$) data (Asselin, 2008), the standard reduction potential for half-reaction 5.1 was calculated to be E° = -0.5 V. More negative values have also been published, namely -0.57 V (Senanayake et al., 2010), -0.58 V (Nikoloski and Nicol, 2006), -0.586 V (Kim et al., 1991) and -0.548 V (Lee et al., 1985). It should be noted that calculations carried out directly from the iron ammine stability constants (Isaev et al., 1990a) also result in a more negative value for the standard reduction potential of half-reaction 5.1. This varies depending on the $\Delta_f G°$ value chosen for the aqueous ferrous ion, for which different values are available in the literature. In order to ensure that the following argument holds valid for all of the available data, the calculations that follow were based on the more positive standard reduction potential, calculated from the most recently published data (Asselin, 2008), since the same line of reasoning will also apply for more negative values.

The dependence of the equilibrium potential of ferrous tetrammine / iron half-reaction on the ferrous tetrammine and ammonia activities at 45°C was calculated by applying the Nernst equation (5.2), as shown in Figure 5.13.

$$\boldsymbol{E = E° - 0.0137 ln \left[\frac{a_{NH_3}{}^4}{a_{Fe(NH_3)_4}{}^{2+}} \right]} \quad (5.2)$$

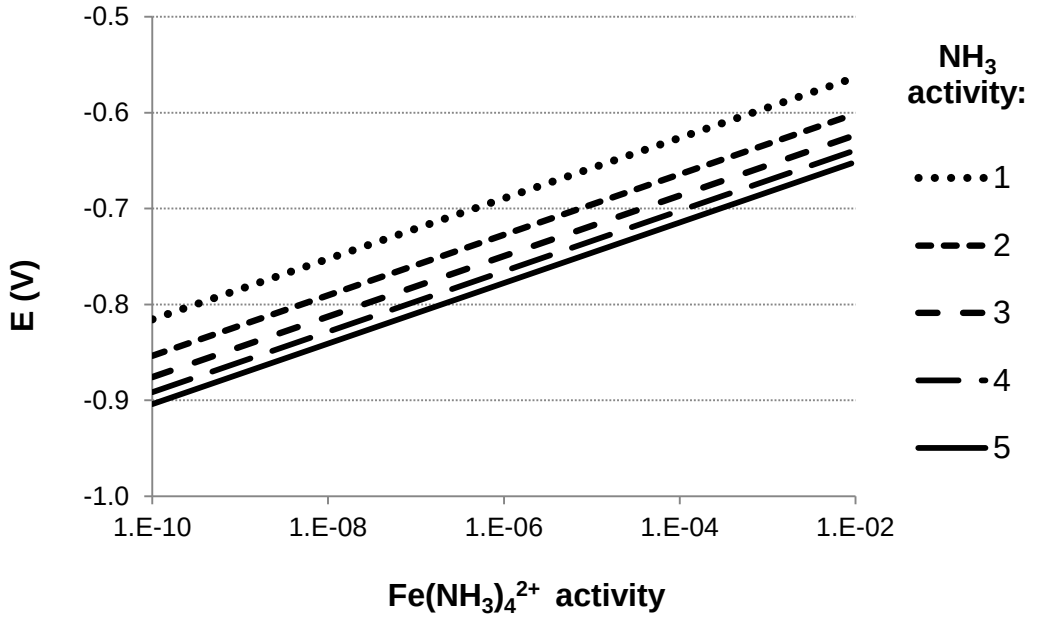

Figure 5.13 The dependence of the equilibrium potential of the iron / ferrous tetrammine half-reaction on iron tetrammine and ammonia activities at 45°C.

The observed OCP of iron in each of the solutions used in this study was always more positive than the equilibrium potential of the iron / ferrous tetrammine half-reaction at 45°C, in the likely ferrous ion activity and ammonia activity ranges encountered in each experiment. Therefore, the experimental values are thermodynamically consistent with the iron oxidation being coupled with a higher redox potential oxidant such as oxygen or copper ions. According to the mixed potential theory (Wagner and Traud, 1938), the OCP of the electrode, on which the anodic and cathodic sites are short circuited, is dependent not only on the concentrations of the reactants and products of each half-cell and on the cathodic/anodic area ratio, but also on the kinetics of each half-cell reaction (Miller, 1979). Thus, based on the observed OCP alone, it is not possible to draw any conclusion as to which reduction half-reaction is coupled with the anodic dissolution of iron.

The standard potentials of some copper-reduction half-reactions which may be coupled with the iron oxidation half-reaction were calculated using HSC 7 software, based on data available in its database (Roine, 2009) and are given in Table 5.1.

Table 5.1 Reduction half-reactions and E° calculated from HSC 7 data (Roine, 2009)

Copper ammine reduction half-reactions		**E°**
$Cu(NH_3)_2^+ + e^- \rightarrow Cu + 2NH_3$	(5.3)	- 0.124 V
$Cu(NH_3)_4^{2+} + 2e^- \rightarrow Cu + 4NH_3$	(5.4)	- 0.023 V
$Cu(NH_3)_4^{2+} + e^- \rightarrow Cu(NH_3)_2^+ + 2NH_3$	(5.5)	0.078 V

The dependence of the equilibrium potentials of half-reactions 5.3 and 5.4 (equations 5.6 and 5.7 respectively) on the copper ammine and ammonia ammonia activities at 45°C is shown in Figure 5.14.

$$\boldsymbol{E = E^\circ - 0.0274 ln \left[\frac{a_{NH_3}{}^2}{a_{Cu(NH_3)_2}{}^+} \right]} \quad (5.6)$$

$$\boldsymbol{E = E^\circ - 0.0137 ln \left[\frac{a_{NH_3}{}^4}{a_{Cu(NH_3)_4}{}^{2+}} \right]} \quad (5.7)$$

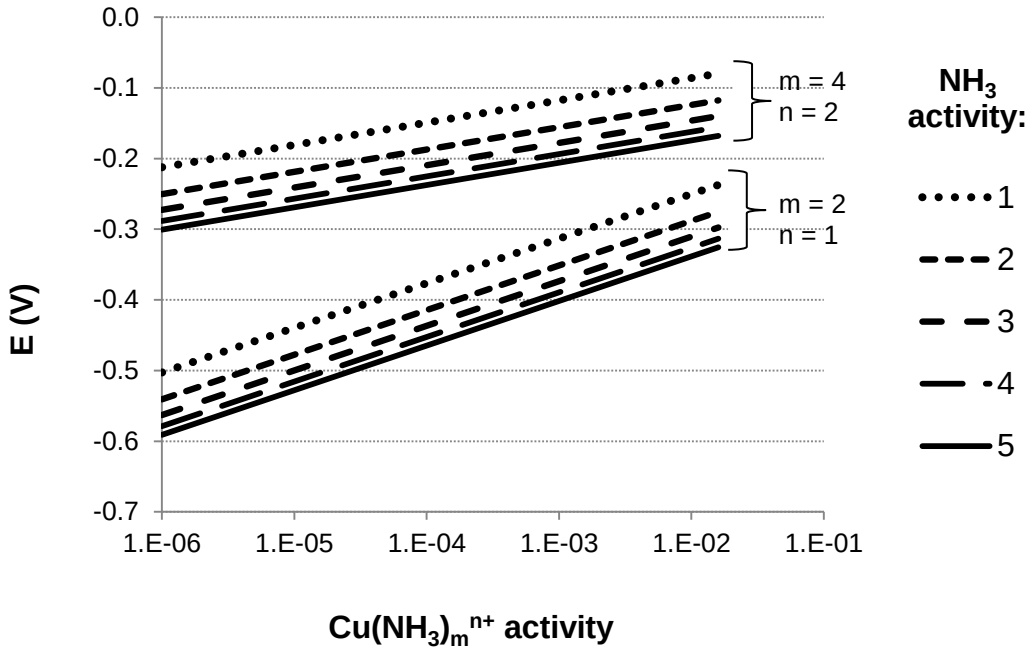

Figure 5.14 The dependence of the potentials of the copper / copper ammine half-reactions on copper ammine and ammonia activities at 45°C.

The observed cementation of copper onto iron confirms that the overall reduction of copper(II) to metallic copper, possibly via the formation of a cuprous ammine, takes place at the iron surface during its anodic dissolution. By comparison of Figure 5.14 with Figure 5.13 it can be seen that the oxidation of iron by either cupric tetrammine or cuprous diammine is thermodynamically feasible under the Caron process conditions. In the latter case, the oxidant would form via the initial coupling of half-reaction 5.5, of even higher standard reduction potential, with half-reaction 5.1.

After the iron dissolution ceases, the cemented copper is no longer cathodically protected and there is a sharp rise in OCP to around -0.25 V (Figure 5.1), which indicates a change in behaviour of the metallic copper from cathodic to anodic, as it is above the equilibrium potential for the cuprous diammine/copper reaction. The same may not be said for the cupric tetrammine/copper reaction, which occurs at potentials higher than the measured OCP. This suggests that the cemented copper re-

dissolves anodically by initially forming cuprous diammine. This can be brought about by a reproportionation reaction (5.8) in which the cupric tetrammine oxidises metallic copper to form cuprous diammine, according to reaction 5.8.

$$Cu + Cu(NH_3)_4^{2+} \rightarrow 2Cu(NH_3)_2^{+} \quad (5.8)$$

This reaction is thermodynamically favoured, with a $\Delta G°$ value of -19.4 kJ/mol and a logK value of 3.4 at room temperature, and 3.9 at 45°C, based on data from HSC 7 (Roine, 2009).

From the OCP measurements at different copper(II) concentrations (Figures 5.5 and 5.6) it can be observed that in the presence of oxygen, the time delay from immersion to the first rapid increase in potential is longer than the delay between the first and the second potential increase. In deoxygenated solutions, this difference is much less pronounced. This may suggest that the deposition of metallic copper takes longer, and its redissolution is faster, in the presence of dissolved oxygen, which is consistent with oxygen participating in the process either by directly oxidising metallic copper or by regenerating the cupric ammine oxidant.

During the observed cementation of copper onto the iron surface, the anodic sites at which iron is actively dissolving progressively decrease in area, while the cathodic sites at which metallic copper is being deposited increase. Due to the porous morphology of the deposit, which allows the dissolution of iron to continue, the cathodic area continues to increase leading to a very small anodic to cathodic area ratio. As a result, the oxidative current densities experienced by the anodic sites may oxidise the iron at the solution interface to a non-reactive oxide such as, for example, magnetite. A possible half-reaction which may describe this process is given by

equation 5.9, for which the standard reduction potential was calculated to be -0.77 V, using the HSC 7 database and software (Roine, 2009).

$$3Fe + 4OH^- + 4NH_3 \rightarrow Fe_3O_4 + 4NH_4^+ + 8e^- \quad (5.9)$$

The passivation process is likely to involve the initial formation of ferrous hydroxide following the oxidative adsorption of hydroxyl ions, favoured by an increase in localised pH which may result from the de-coordination of ammonia ligands by the cathodic reactions (5.3-5.5). In this case, the passive layer may form on the iron surface according to the reaction 5.10, for which the standard Gibbs free energy change was calculated from HSC 7 data (Roine, 2009) to be $\Delta G° = -146.1$ kJ/mol.

$$3Fe(OH)_2 + 2Cu(NH_3)_4^{2+} \rightarrow Fe_3O_4 + 2Cu(NH_3)_2^+ + 2NH_3 + 2NH_4^+ + 2H_2O \quad (5.10)$$

As the thin oxide layer prevents further dissolution of metallic iron, the deposited copper is no longer cathodically protected and begins to re-dissolve anodically, exposing small fractions of the iron surface at a time, which passivate immediately upon contact with the solution. Once all the copper is re-dissolved, the iron surface is completely covered by the thin oxide layer, which is consistent with the observed increase in the OCP and the drop in current observed in the potentiodynamic measurements.

The presence of copper(II) ions in solution is therefore responsible for the passivation of iron under conditions in which it would otherwise continue to dissolve anodically. The presented results show that the higher the copper(II) concentration in solution, the sooner the passivation takes place. On the other hand, varying $[NH_3]_T$ and $[CO_2]_T$ at a constant molar ratio has the opposite effect, whereby lower concentrations appear to promote the passivation of iron, even though it does not

take place in their complete absence. This trend is likely to be due to the effect of $[NH_3]_T$ on the stability of the metal complexes formed and on the rate of the metal displacement reaction leading to passivation. However, the passivation reaction itself is likely to be favoured by an increase in ammonia concentration if the ammonium bicarbonate concentration is maintained constant, due to the resulting increase in hydroxyl ion concentration. This may be a contributing factor to the lack of a clear trend when the ammonia concentration is varied at a constant $[CO_2]_T$. It is also consistent with the observed effect of the ammonium bicarbonate concentration varied at constant $[NH_3]_T$, which appears to reflect the effect of pH on the passivation reaction. Varying the ammonia and the ammonium carbonate at a constant molar ratio removes the pH as an additional variable, and the increase in the time required for passivation as $[NH_3]_T$ and $[CO_2]_T$ increase is attributed mainly to the increased stability of the copper complexes and the reduced rate of metal displacement. It follows that the ammonia and ammonium bicarbonate concentrations determine the critical copper(II) concentration at which iron will passivate immediately upon immersion and, as demonstrated by this work, at very low $[NH_3]_T$ the critical copper concentration can be very low also, as can be seen for example in Figure 5.10.

5.8 Summary

The presence of copper(II) ions in ammoniacal solutions was found to promote the passivation of iron, which occurs more readily at higher [Cu(II)] and lower $[NH_3]_T$. The mechanism of passivation was found to initially involve the cementation of copper onto the actively dissolving iron surface, which subjects the anodic sites to increasingly higher anodic current densities due to the progressively smaller anodic to cathodic area ratio. This eventually leads to conditions under which the favoured

product of the iron oxidation reaction is no longer a soluble complex ion, but an insoluble protective oxide compound. The iron passivation process then continues during the redissolution of the cemented copper, which takes place once the copper is no longer cathodically protected by metallic iron, as consistent with thermodynamic calculations.

An analogous process is likely to take place on iron-nickel and iron-cobalt alloys, both of which display a similar OCP behaviour to that of iron. It is therefore possible that this mechanism of passivation may be responsible for the incomplete dissolution of metal values from alloys being leached in the Caron process. However, further work is required in order to assess whether the passivation also takes place in the presence of other solution species encountered in the Caron leach liquor. A study of the behaviour of iron in the presence of Cu(II) and thiosulfate ions is described in chapter 7.

6 THE BEHAVIOUR OF IRON IN AMMONIACAL-CARBONATE SOLUTIONS CONTAINING COBALT(II) AND THIOSULFATE IONS

6.1 Introduction

Previous studies by Nikoloski (2002) have shown that alloys containing iron, nickel and cobalt undergo passivation under conditions which cause pure iron to passivate. In the present study, this was also observed in ammoniacal-carbonate solutions containing copper(II) ions, in which iron-nickel and iron-cobalt alloys were found to undergo passivation in the same way as pure iron (section 5.6), due to the formation of an oxide layer on the surface. Due to the industrial importance of the dissolution of iron and its alloys in solutions simulating the Caron leach liquor from the Yabulu QN, the passivation observed by Nikoloski (2002) was further studied in a simplified system consisting of pure metallic iron and ammoniacal-carbonate solutions containing cobalt(II) and thiosulfate ions.

The preliminary investigation conducted in ammoniacal-carbonate solutions containing nickel(II), cobalt(II) and thiosulfate ions (chapter 4) at the concentrations specified in Table 4.1 indicated that, in the absence of copper(II) ions, the passivation of iron may only take place when both cobalt(II) and thiosulfate ions are simultaneously present in solution. It was also found that a surface layer containing cobalt and sulfur was formed on the iron surface during immersion in solutions containing both cobalt(II) and thiosulfate ions. The formation of this layer was thought to be implicated in the mechanism of passivation of the iron, but the mechanism is still unclear and in need of further investigation. In addition, the formation of this layer may also contribute to the loss of cobalt from the leach solution, thereby further affecting the cobalt extraction efficiency in the Caron process.

The aims of the work described in this chapter were to:

(i) investigate the conditions which promoted the formation of a surface layer containing cobalt and sulfur;

(ii) further study the effects of this layer on the anodic dissolution of iron;

(iii) characterise the surface layer in order to shed more light on its formation mechanism;

(iv) assess its electrochemical and dissolution behaviour.

6.2 The anodic dissolution of iron in the presence of cobalt(II) ions

6.2.1 Surface changes

The presence of cobalt(II) ions was not found to promote the spontaneous passivation of iron (chapter 4). This is in contrast to the behaviour observed in the presence of copper(II) ions, which under the same conditions were found to promote passivation even at a concentration of 2 mM (chapter 5).

As shown in Figure 4.2 (chapter 4), the measured OCP of an iron RDE immersed in a deoxygenated solution containing 5M $[NH_3]_T$, 1 M $[CO_2]_T$ and 12 mM [Co(II)] was found to remain in the -0.7 V to -0.6 V potential region, indicating active dissolution of the iron. The SEM observation of the iron surface following the immersion revealed a high density of pits (Figure 6.1), with a small amount of cobalt (< 1 at%) being detected by the EDX analysis. A similar OCP behaviour was observed at half the $[NH_3]_T$ and $[CO_2]_T$, with a precipitate also being observed on the pitted iron surface (Figure 6.2). This was thought to consist mainly of iron corrosion products, due to the fact that only iron, oxygen and carbon were detected in

significant amounts, while only small amounts of cobalt (< 1 at%) were detected. It was not possible to determine whether (i) the cobalt was present on the iron surface in the metallic state, as a result of cementation, or (ii) within the iron hydroxides and carbonates, due to adsorption or co-precipitation.

The morphology of the precipitate was found to vary depending on whether the solution had been sparged with nitrogen (Figure 6.2, a) or not (Figure 6.2, b). However, this variation is more likely to be due to the loss of ammonia during sparging than to the presence of oxygen in solution. The precipitate was not visible at the higher $[NH_3]_T$ and $[CO_2]_T$ (Figure 6.1) due to the formation of soluble complexes being favoured.

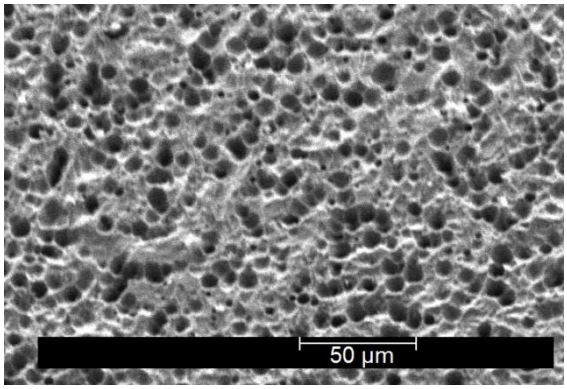

Figure 6.1 SEM image of the Fe surface following 3 hours of immersion in deoxygenated ammonia-ammonium bicarbonate solution containing 5 M $[NH_3]_T$, 1 M $[CO_2]_T$ and 12 mM Co(II).

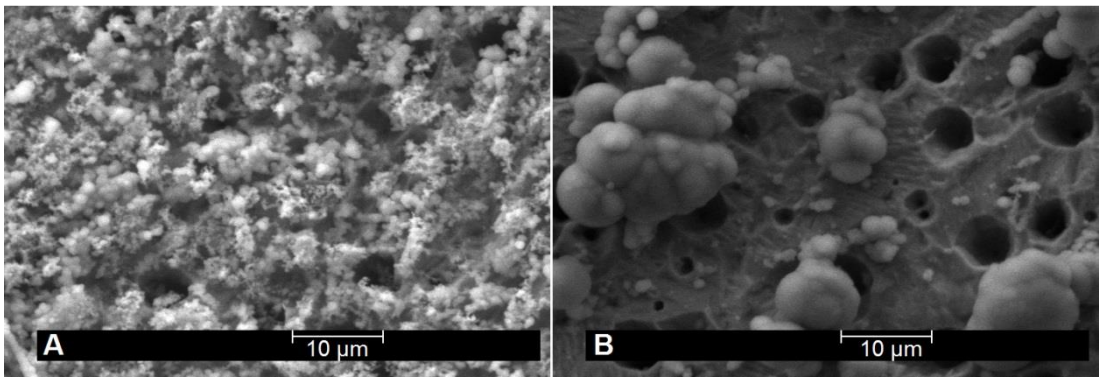

Figure 6.2 SEM image of the Fe surface following 3 hours of immersion in ammonia-ammonium bicarbonate solutions containing 2.5 M $[NH_3]_T$, 0.5 M $[CO_2]_T$ and 12 mM Co(II); a) deoxygenated; b) non deoxygenated.

The significant corrosion of iron, observed even in solutions which had been sparged with nitrogen, suggested that de-oxygenation of the solution following its preparation was not sufficiently effective at preventing the oxidation of cobalt(II) to cobalt(III). As the solution preparation took place in all cases under normal atmospheric conditions, it is likely that some cobalt(II) reacted with oxygen during preparation and prior to de-oxygenation by nitrogen sparging. It is possible that a cobaltous peroxy-dicobalt complex, $[(NH_3)_5Co–O_2–Co(NH_3)_5]^{4+}$, suggested to form during the aeration stage of the Caron leach (Fittock, 2009), may also form during the preparation of the solutions. This is followed by auto-oxidation to cobaltic pentammine upon standing, which may therefore form even after all of the free molecular oxygen has been removed from the solution by sparging with nitrogen. Therefore, although the dissolved cobalt species are referred to in this study as [Co(II)] for simplicity, it is likely that both Co(II) and Co(III) species are present in all of the solutions employed, in proportions dependant on various factors including the age of the solution and whether nitrogen sparging has been employed.

6.2.2 Rotating disk cyclic voltammetry

Cyclic voltammetric measurements conducted on an iron RDE in the presence of Co(II) species showed an anodic response typical of the behaviour of iron in ammoniacal-carbonate solutions. As the potential was scanned in the positive direction from the OCP of around -0.7 V, the anodic current increased steadily, followed by a sudden drop denoting potentiodynamic passivation of the electrode, and significantly reduced anodic currents thereafter (Figure 6.3). The anodic peak current density and the corresponding passivation potential were found both to decrease for increasing immersion times.

Small cathodic currents were also observed following reversal of the scan, possibly due to the reduction of cobalt complexes, and these currents became larger at longer immersion times. As the applied potential was further decreased below -0.4 V, reactivation of the dissolution of iron was observed.

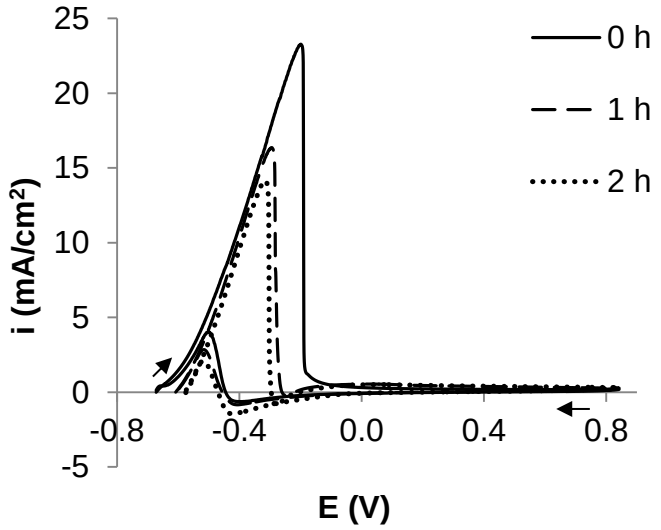

Figure 6.3 Cyclic voltammetry (10 mV/s) of the Fe RDE following different times of immersion in deoxygenated ammonia - ammonium bicarbonate solutions containing 5 M $[NH_3]_T$, 1 M $[CO_2]_T$ and 12 mM Co(II).

6.3 The behaviour of iron in the presence of cobalt(II) and thiosulfate ions

6.3.1 General comparison of reagents

The presence of metastable thiosulfate ions in ammoniacal-carbonate solutions was found to significantly enhance the dissolution of iron (Figure 4.7), with the anodic currents measured during linear polarisation reaching values an order of magnitude higher than in their absence. However, the presence of both cobalt and thiosulfate ions was also found to promote passivation. For this system, following an initial stage of active dissolution the OCP of the iron RDE was found to undergo a steep transition to values above 0 V. The co-occurrence of such an increase in potential with the passivation of iron has been shown in a previous study in which the iron

dissolution rate was also monitored by measuring changes in the iron concentration in solution (Nikoloski et al., 2003). In deoxygenated solutions containing 22 mM $[S_2O_3^{2-}]$, 5 M $[NH_3]_T$ and 1 M $[CO_2]_T$, and no cobalt(II) ions, the OCP of iron remained just above -0.7 V for over 3 hours, in the same region as in solutions containing cobalt(II) but no thiosulfate ions. When both cobalt and thiosulfate ions were present, the OCP of iron during the active dissolution stage was found to be approximately 0.1 V higher than in solutions containing either ion separately (Figure 6.4 a).

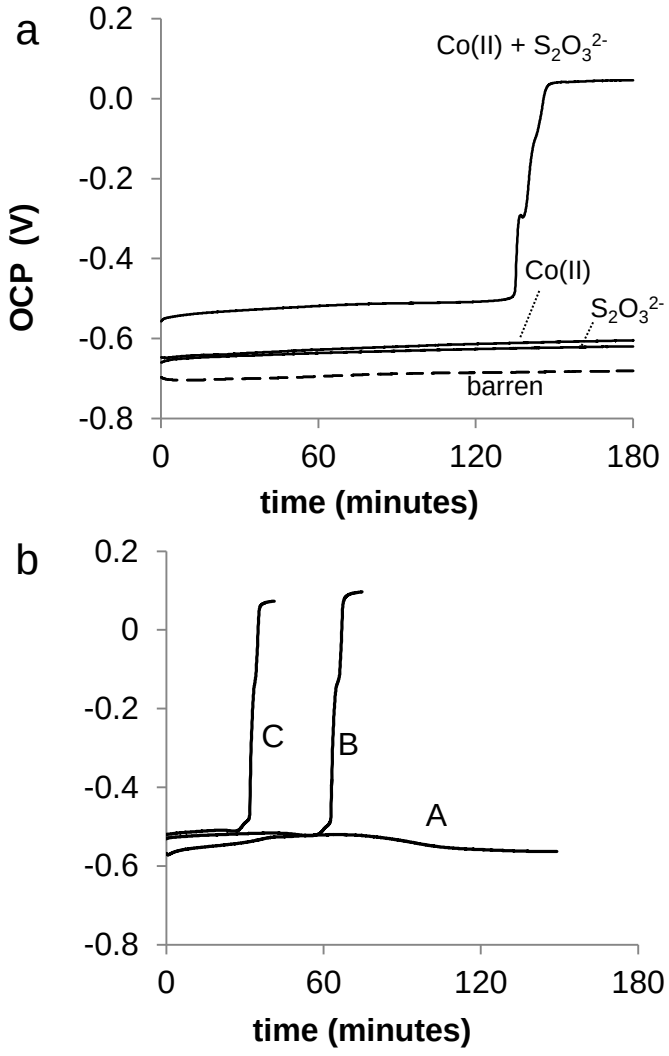

Figure 6.4 OCP of the Fe RDE in solutions containing: a) 5 M $[NH_3]_T$, 1 M $[CO_2]_T$ with no other species (dashed line), in the presence of 12 mM Co(II) and/or 22 mM $S_2O_3^{2-}$, as indicated for each line; b) 2.5 M $[NH_3]_T$, 0.5 M $[CO_2]_T$ and: A) 36 mM Co(II); B) 6 mM Co(II) and 11 mM $S_2O_3^{2-}$; C) 12 mM Co(II) and 22 mM $S_2O_3^{2-}$.

The timing of the OCP transition in solutions containing both cobalt and thiosulfate ions at 5 M $[NH_3]_T$ and 1 M $[CO_2]_T$ showed little reproducibility, attributed mainly to the difficulty in controlling the ammonia concentration accurately, in particular when nitrogen sparging was employed. Therefore, since passivation was found to take place regardless of whether the solution had been sparged with nitrogen or not, experiments in which it was important to have a more accurate control of $[NH_3]$ were conducted in solutions that had not been deoxygenated.

At half the $[NH_3]_T$ and $[CO_2]_T$, with the same [Co(II)] and $[S_2O_3^{2-}]$, passivation took place consistently after approximately ½ hour of immersion, while at half the [Co(II)] and $[S_2O_3^{2-}]$, it took place after about 1 hour (Figure 6.4). It should be noted that under the same conditions but in the absence of thiosulfate, spontaneous passivation was not observed within 2.5 hours, even at a cobalt concentration as high as 36 mM. However, these results do not exclude the possibility that even in the absence of thiosulfate ions, spontaneous passivation may still take place at high enough cobalt concentrations, lower ammonia concentrations or at significantly longer periods of immersion than those encountered in practice, as observed by Kasherininov (Kasherininov, 1960). Nevertheless, the fact that passivation was observed at significantly lower cobalt concentrations and shorter immersion times when both species were present, indicates the involvement of a different mechanism, as a result of an interaction between cobalt and thiosulfate.

6.3.2 The effect of $[NH_3]_T$ and $[CO_2]_T$ on the passivation time

The effect of $[NH_3]_T$ on the immersion time required for passivation to occur was investigated both at a constant $[CO_2]_T$ and at a constant $[NH_3]_T$: $[CO_2]_T$ molar ratio of 5:1. As can be seen from Table 6.1, increasing the amount of ammonia added to

the solution, referred to as [NH_3], whilst maintaining a constant amount of ammonium bicarbonate (part a), or increasing the amounts of both reagents at a constant molar ratio between them (part b), was found to significantly delay passivation. The trend can be seen clearly in Figure 6.5 (a, b). On the other hand, varying the amount of ammonium bicarbonate at a constant initial concentration of ammonia was not found to have any significant effect on the passivation time.

Table 6.1 Immersion times required for passivation of the Fe RDE at different $[NH_3]_T$, $[CO_2]_T$ and $[NH_3]$*

species concentrations (M)			time to passivation
$[NH_3]_T$	$[CO_2]_T$	$[NH_3]$	(minutes)
a) constant $[CO_2]_T$			
3	2	1	20
4	2	2	35
5	2	3	70
6	2	4	316
b) constant $[NH_3]_T : [CO_2]_T = 5:1$			
1	0.2	0.8	10
2	0.4	1.6	20
3	0.6	2.4	40
4	0.8	3.2	140
5	1.0	4.0	> 360
c) constant $[NH_3]_T$			
6	2	4	316
6	3	3	66
6	4	2	50

*** $[NH_3]$ refers to the concentration added as NH_4OH (excluding contribution from NH_4HCO_3); all solutions also contain 12 mM Co(II) and 22 mM $S_2O_3^{2-}$**

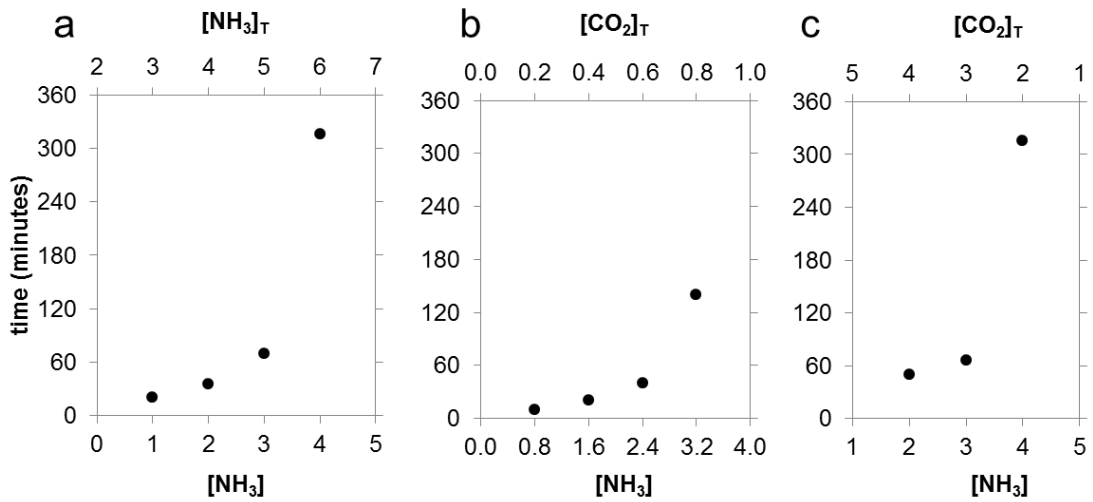

Figure 6.5 Effect of $[NH_3]_T$, $[CO_2]_T$ and $[NH_3]$ on the immersion times required for passivation of the Fe RDE at 12 mM Co(II) and 22 mM $S_2O_3^{2-}$ at: a) $[CO_2]_T$ = 2 M; b) $[NH_3]_T$: $[CO_2]_T$ = 5:1; c) $[NH_3]_T$ = 6 M.

In contrast with the behaviour of iron observed in the presence of copper ammines (section 5.5), where increasing the ammonium bicarbonate concentration at a constant $[NH_3]_T$ was found to delay passivation, in the presence of cobalt(II) and thiosulfate ions the opposite trend was observed, as can be seen from Table 6.1 and in Figure 6.5 (c). The fact that, in this case, passivation took place faster at higher ammonium bicarbonate concentration, can be attributed to the decrease in NH_3/NH_4^+ ratio and hence the pH. Whereas in solutions containing Cu(II) ions, increasing the pH appeared to promote passivation, in the presence of Co(II) and $S_2O_3^{2-}$, it appeared to inhibit passivation. However, since the effect of pH cannot be studied as an independent variable to $[NH_3]$, it cannot be ascertained whether the observed delay in passivation is due to an increase in metal complexation by the ammonia ligands or whether the increase in hydroxyl ion concentration also plays a role.

6.3.3 Linear and cyclic voltammetry in the presence of Co(II) and $S_2O_3^{2-}$

Linear sweep voltammetry measurements conducted in the deoxygenated NH_3-CO_2-Co(II)-$S_2O_3^{2-}$ system, following different times of immersion, resulted in the progressive reduction of the iron oxidation peak current density, suggesting a gradual coverage of the iron surface by a solid species hindering the dissolution process (Figure 6.6). Following longer immersion times, several other anodic processes also began to appear at more positive potentials. These are thought to correspond to the oxidation of the solid species formed on the iron surface during its anodic dissolution. These can be seen more clearly in Figure 6.7, which shows a cyclic voltammetric measurement taken following 2 hours of immersion at 24 mM [Co(II)] and 44 mM [$S_2O_3^{2-}$]. The resulting iron oxidation peak (A) was found to be significantly reduced, and followed by a slight inflection in current. A second significant increase in current density began as the potential was scanned in the positive direction above -0.3 V, with a slight inflection followed by peaks at approximately -0.1 V (B), 0 V (C) and +0.1 V (D). As the potential was further scanned above +0.2 V, again the anodic current increased steadily, reaching its maximum as the potential approached +0.4 V (E), and then dropping to significantly lower values thereafter.

Upon reversal of the scan, no significant current was observed until the potential reached values below -0.1 V, with a cathodic peak (F) being observed at a potential slightly more negative than -0.3 V. As the potential approached -0.4 V, the reactivation of metallic iron took place (A^1), resulting in a peak current density over three times larger than that observed during the anodic scan (A). These results suggest the possibility that the species hindering the dissolution of iron was reduced

during the cathodic scan resulting in peak F, thereby allowing reactivation of the metallic iron.

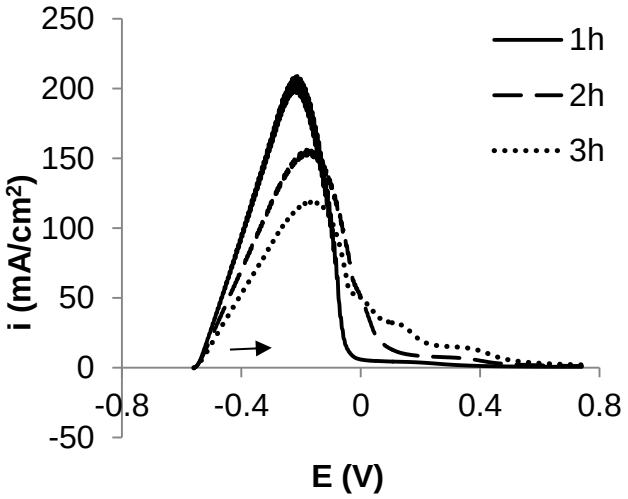

Figure 6.6 Linear sweep voltammetry (10 mV/s) of the Fe RDE following different times of immersion in deoxygenated ammonia-ammonium bicarbonate solutions containing 5 M $[NH_3]_T$, 1 M $[CO_2]_T$, 12 mM Co(II) and 22 mM $S_2O_3^{2-}$.

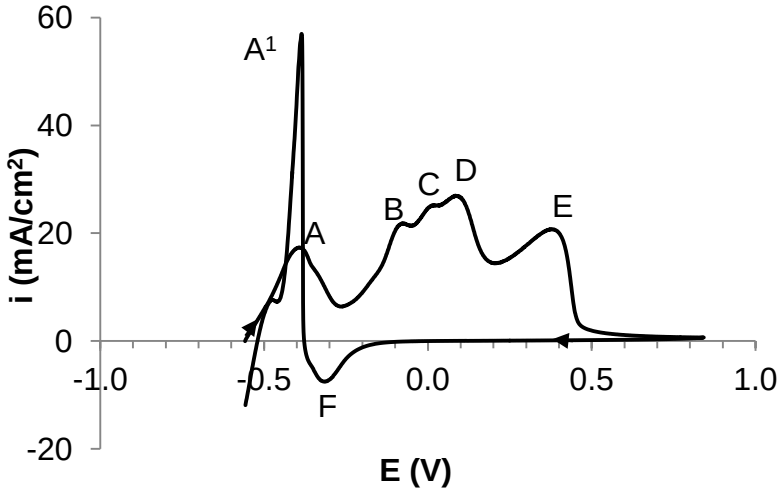

Figure 6.7 Cyclic voltammetry (10 mV/s) of the Fe RDE following a 2 hour immersion at 5 M $[NH_3]_T$, 1 M $[CO_2]_T$, 24 mM Co(II) and 44 mM $S_2O_3^{2-}$.

In order to compare the voltammetric behaviour just before and a few minutes after passivation, measurements were also taken at a slightly lower $[NH_3]_T$ of 4 M, at which the OCP transition was consistently observed after approximately 2 hours of immersion (Figure 6.8). Prior to passivation, the iron oxidation peak (A) was found

to be reduced in size, followed by a broad anodic feature with three ill-defined peaks thought to correspond to peaks B, C and D in Figure 6.7. Neither of these anodic processes was observed after passivation, as the species involved were only present at the iron surface during its active dissolution, and are likely to have either lost electrical contact or to have been oxidised during the OCP transition.

On the other hand, peak E was observed both before and after passivation, reaching a lower maximum current density at a less positive potential in the latter case. In both cases, reversal of the scan resulted in a cathodic process thought to correspond to that labelled F in Figure 6.7, although this time it did not reach a clear maximum before the reactivation of the anodic dissolution of iron prevailed (A^1).

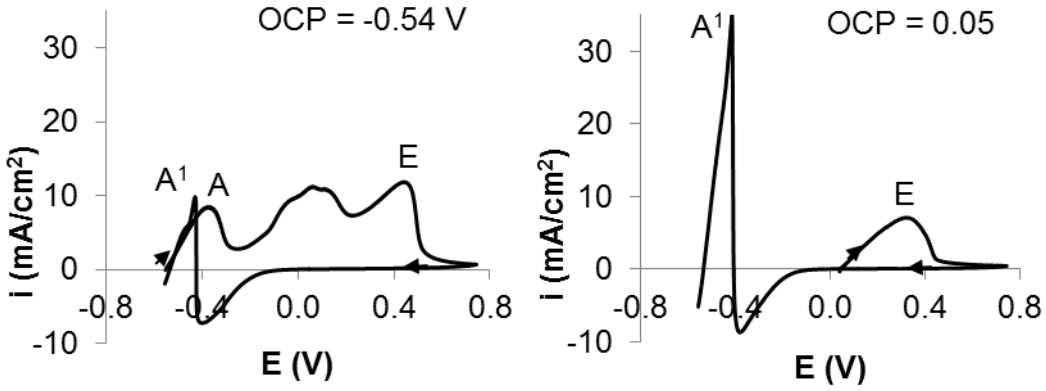

Figure 6.8 Cyclic voltammetry measurements (10 mV/s) taken a few minutes before (OCP = -0.54 V) and a few minutes after (OCP = 0.05 V) passivation of the iron RDE in ammonia-ammonium bicarbonate solutions containing 4 M $[NH_3]_T$, 0.8 M $[CO_2]_T$, 12 mM Co(II) and 22 mM $S_2O_3^{2-}$.

6.3.4 Surface changes during active dissolution at 5 M $[NH_3]_T$

In order to further investigate the surface species formed on iron during its active dissolution, a study was conducted following longer periods of active dissolution at 5 M $[NH_3]_T$, 1 M $[CO_2]_T$. As can be seen in Figure 6.9, a cyclic voltammetric measurement taken after 8.5 hours of immersion, during which the OCP remained within the active dissolution region resulted in the almost complete suppression of

peak A. At potentials more positive than -0.4 V, a broad anodic feature began to increase, with the appearance of ill-defined peaks thought to correspond to B, D and E. Upon reversal of the scan, an anodic current density of about 2 mA/cm^2 was maintained until the applied potential approached -0.2 V. As the potential was further scanned in the negative direction, a cathodic feature peaked at around -0.4 V, followed by a small anodic current peaking around -0.5 V, due to the anodic dissolution of iron (A^1). A cyclic voltammetry measurement reversed prior to reaching the potential region of peak E, taken after 4 hours of immersion, is also shown in Figure 6.9. The anodic scan resulted in peaks A, B and D, whereas following reversal of the applied potential, a cathodic current starting around 0 V resulted in peak G. No obvious reactivation of the anodic dissolution of iron was observed, probably due to the fact that the species hindering the dissolution of iron was still present at the RDE surface, following its reduction resulting in peak G.

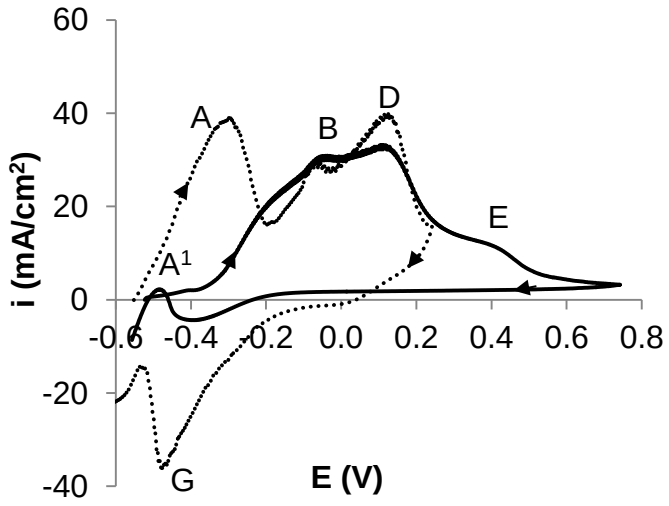

Figure 6.9 Cyclic voltammetry of the iron RDE in ammonia-ammonium bicarbonate solutions containing 5 M $[NH_3]_T$, 1 M $[CO_2]_T$, 22 mM $S_2O_3^{2-}$ and 12 mM Co(II), following 8.5 h immersion (solid line) and 4 h immersion, potential reversed at +0.24 V (dotted line).

SEM images taken after 16 hours of active dissolution revealed the presence of a thick layer (Figure 6.10), which based on EDX analyses was thought to consist mainly of iron hydroxides, oxides or carbonates, with small amounts of cobalt and sulfur present. Although it was found to suppress the dissolution of iron, this layer did not promote the passivation of iron, as consistent with the OCP remaining in the active dissolution region over the long immersion period during which it formed.

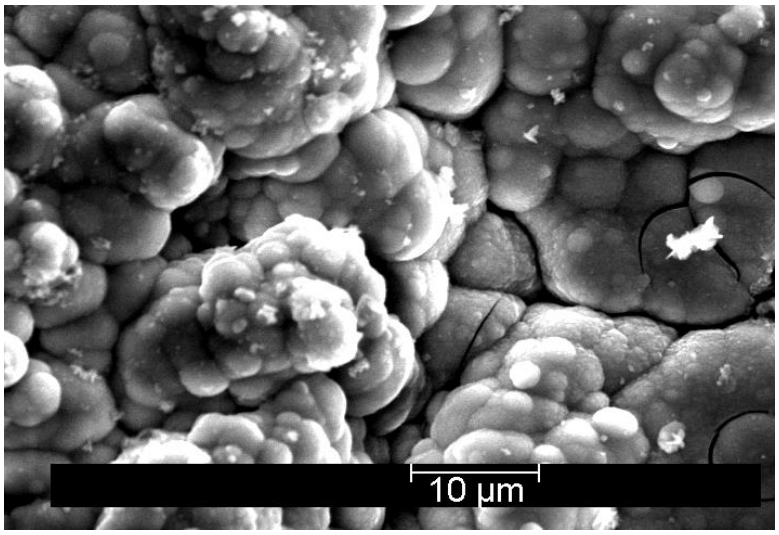

Figure 6.10 SEM image of the surface layer formed on the iron RDE following 16 hours active dissolution in ammonia - ammonium carbonate solution containing 5 M $[NH_3]_T$, 1 M $[CO_2]_T$, 22 mM $S_2O_3^{2-}$ and 12 mM Co(II).

6.3.5 Surface changes leading to passivation at 2.5 M $[NH_3]_T$

At half the $[NH_3]_T$, cyclic voltammetric measurements conducted at different immersion times prior to passivation, resulted in the intermediate peaks B, C and D being significantly reduced or absent (Figure 6.11). The progressive decrease in anodic current density at peak A and simultaneous increase at peak E became evident at shorter immersion times, indicating that the progressive suppression of the anodic dissolution of iron and simultaneous increase in surface coverage by the species being oxidised at E took place faster at lower $[NH_3]_T$. This can be seen clearly in Figure 6.12, in which the change in peak anodic current densities for peaks

A and E at different immersion times are shown for $[NH_3]_T$ of 2.5 M (6.12,a) and 5 M (6.12,b) for comparison (please note different scale for $i_{P(a)}$ and time). As can be seen from Figure 6.11, the shape of the anodic peak was also found to change progressively, with a steep drop in current typical of a passivation phenomenon being observed when the measurement was taken immediately prior to the OCP transition. The increased height of peak E and shorter delay to passivation are consistent with a surface species which, unlike the iron corrosion products observed at higher $[NH_3]_T$, promotes the passivation.

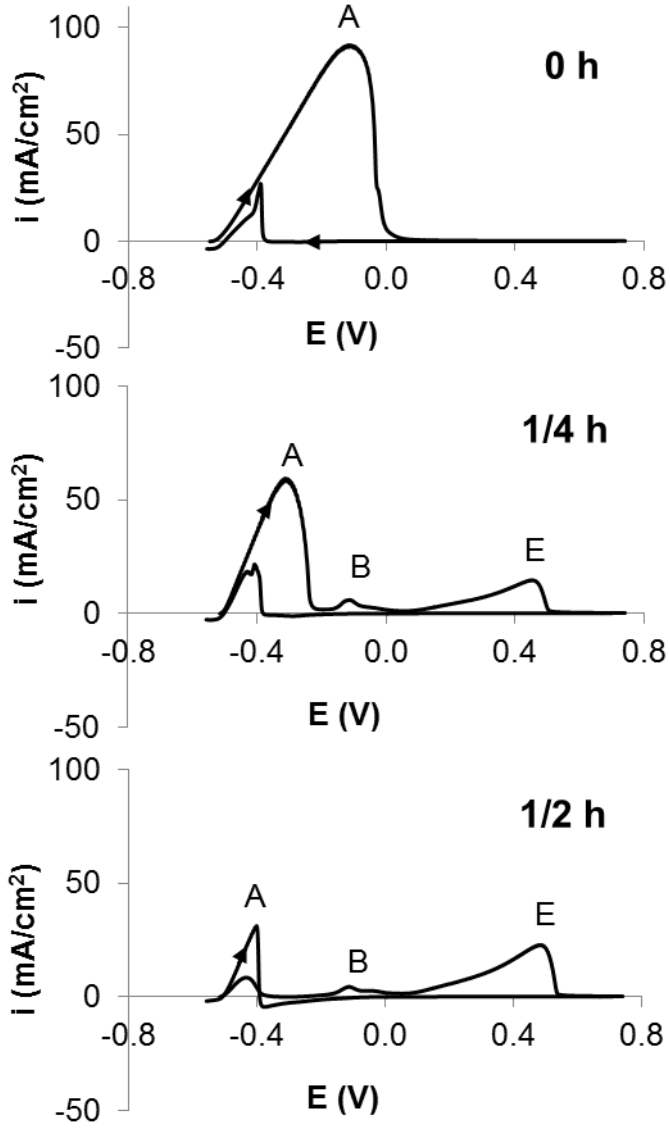

Figure 6.11 Cyclic voltammetry (10 mV/s) of the iron RDE in ammonia-ammonium bicarbonate solution containing 2.5 M $[NH_3]_T$, 0.5 $[CO_2]_T$, 22 mM $S_2O_3^{2-}$ and 12 mM Co(II), at the immersion times shown.

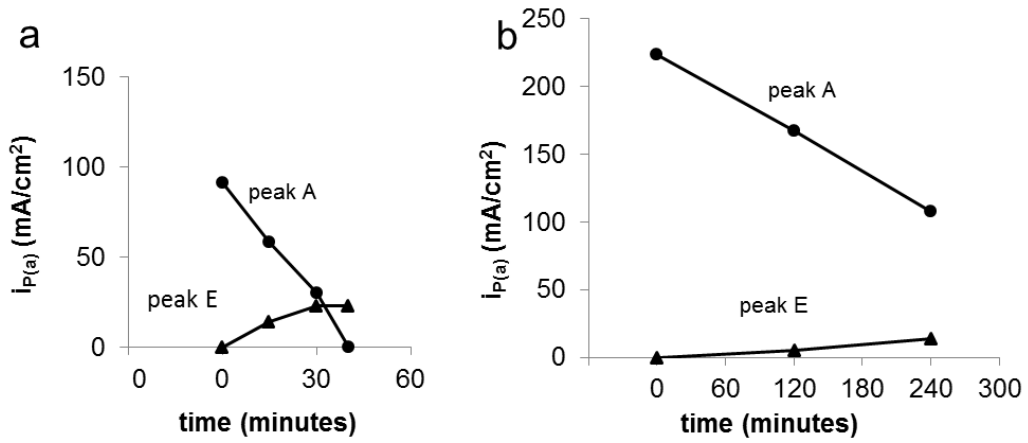

Figure 6.12 Peak anodic current densities measured at 10 mV/s following different periods of immersion at 12 mM Co(II), 22 mM $S_2O_3^{2-}$, and: a) 2.5 M $[NH_3]_T$, 0.5 M $[CO_2]_T$; b) 5 M $[NH_3]_T$, 1 M $[CO_2]_T$.

6.3.6 The effect of [Co(II)] and $[S_2O_3^{2-}]$

The immersion time required for passivation to take place was found to depend both on [Co(II)] and $[S_2O_3^{2-}]$, as shown in Figure 6.13 (a and b respectively). The slight shoulder in the OCP transition from the active to the passive potential region, visible around -0.15 V (Figure 6.4, b), became more evident for decreasing [Co(II)] concentrations. Cyclic voltammetry measurements conducted following passivation showed an increase in the current density at peak E for increasing [Co(II)] (Figure 6.14). Correlation between the height of peak E and the corresponding time required for passivation in the same solutions (Figure 6.13) confirmed that shorter delays to passivation are reflected by higher anodic current densities at peak E. Both of these quantities became less sensitive to [Co(II)] as it was increased above 9 mM (Figure 6.13, a). Measurements conducted at a fixed [Co(II)] of 12 mM showed that by increasing $[S_2O_3^{2-}]$ between 8 and 22 mM, the increase in anodic current density at peak E was less significant, as was the decrease in passivation time (Figure 6.13, b).

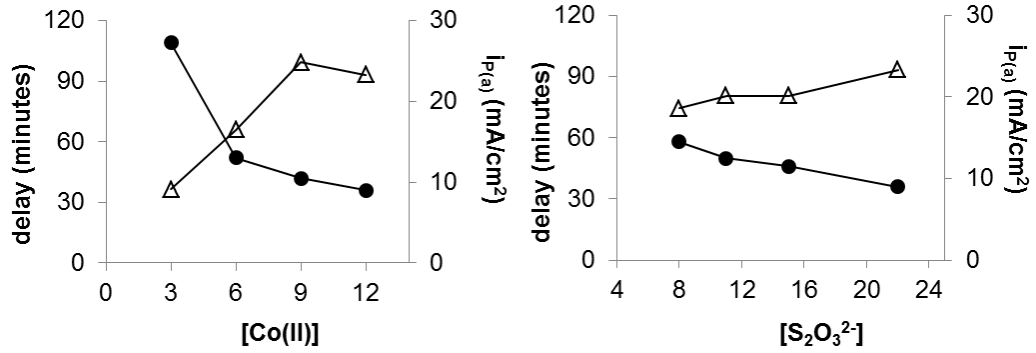

Figure 6.13 The immersion times required for passivation of the Fe RDE (solid circles) and corresponding peak anodic current densities at E (outline triangles) in each solution containing 2.5 M $[NH_3]_T$, 0.5 $[CO_2]_T$ and a) 22 mM $S_2O_3^{2-}$, at different Co(II); b) 12 mM Co(II), at different $[S_2O_3^{2-}]$.

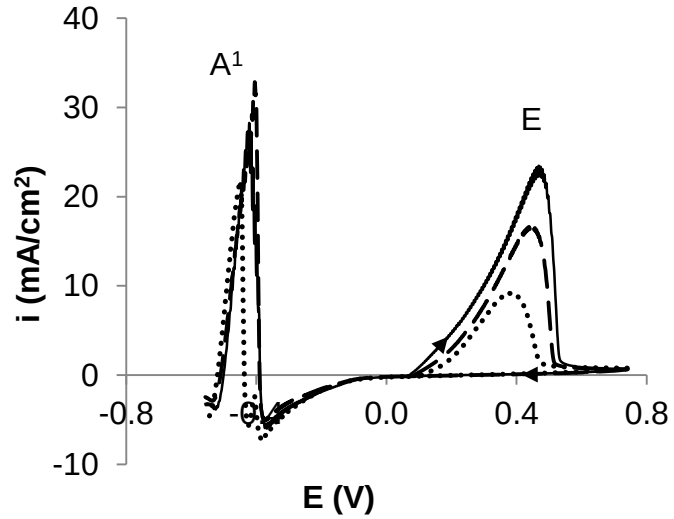

Figure 6.14 Cyclic voltammetry (10 mV/s) of the Fe RDE in ammonia-ammonium bicarbonate solutions containing 2.5 M $[NH_3]_T$, 22 mM $S_2O_3^{2-}$, and [Co(II)] = 3 mM (dotted line); 6 mM (dashed line); 12 mM (solid line).

From these results it appears that the dissolved cobalt plays an important role in the formation of the species being oxidised at peak E, which is thought to consist of a CoS_x layer deposited cathodically during the anodic dissolution of the iron. Based on the OCP and cyclic voltammetry results, there is strong evidence to suggest that formation of such layer is likely to be implicated in the mechanism of passivation of iron.

6.4 Characterisation of the CoS_x surface layer

As noted in the preliminary investigation described in chapter 4, the SEM/EDX study of the iron RDE surface following immersion and passivation in solutions containing 5 M $[NH_3]_T$, 1 M $[CO_2]_T$, 12 mM [Co(II)] and 22 mM $[S_2O_3^{2-}]$, revealed the presence of a cracked surface layer containing up to 10 at% Co and 20 at % S (Figure 6.15, a). This layer is thought to contain the species responsible for peak E and is therefore likely to be implicated in the mechanism of passivation. At lower $[NH_3]_T$, lower amounts of cobalt and sulfur were detected, possibly due to the shorter period of active dissolution of the iron, during which formation of the layer took place. In all cases, the cobalt and sulfur were generally present at an approximate ratio of 1:2. Based on SEM/EDX observation, layers formed at 2.5 M $[NH_3]_T$ and 0.5 M $[CO_2]_T$ appeared to be thinner, almost indistinguishable from the iron surface (Figure 6.15, b) and were found to contain around 3.5 at% Co and 8 at% S. The CoS_x layer was also analysed by Grazing Incidence X-ray Diffraction (GIXRD) and found to be amorphous, as can be seen from its diffraction pattern shown in Figure 6.16.

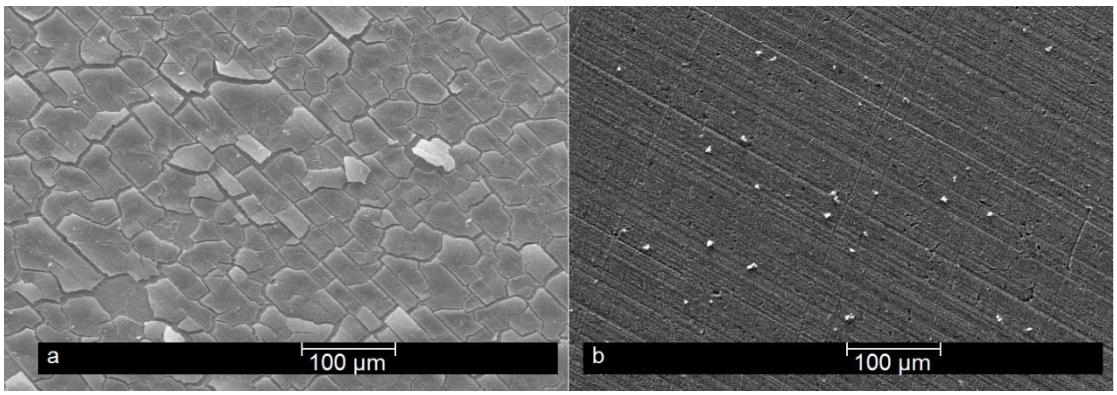

Figure 6.15 SEM image of the Fe RDE following passivation in solution containing 12 mM Co(II), 22 mM $S_2O_3^{2-}$, and: a) 5 M $[NH_3]_T$, 1 M $[CO_2]_T$, immersed for 2 hours; b) 2.5 M $[NH_3]_T$, 0.5 M $[CO_2]_T$, immersed for 40 minutes.

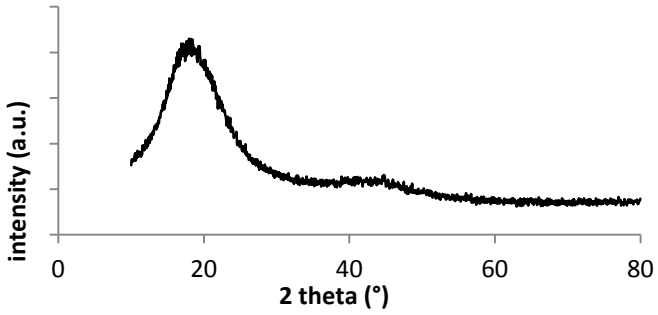

Figure 6.16 GIXRD diffraction pattern of the surface layer formed on the Fe RDE during immersion for 4.5 hours in deoxygenated solution containing 5 M $[NH_3]_T$, 1 M $[CO_2]_T$, 12 mM Co(II) and 22 mM $S_2O_3^{2-}$.

Addition of a few drops of concentrated hydrochloric acid to the surface of the iron RDE resulted in the distinctive smell of hydrogen sulfide gas, therefore indicating the presence of sulfide ions. These observations suggest that the surface species responsible for the anodic peak (E) and implicated in the mechanism of passivation, is an amorphous cobalt sulfide or polysulfide.

In order to confirm that the species responsible for peak E was not significantly affected by removal of the RDE from the solution, following passivation in a solution containing 2.5 M $[NH_3]_T$, 0.5 $[CO_2]_T$, 12 mM [Co(II)] and 22 mM $[S_2O_3^{2-}]$, the electrode was taken out, rinsed with deionised water and allowed to dry. Following SEM/EDX analysis, which confirmed the presence of approximately 3 at% cobalt and 7 at% sulfur, the electrode was re-immersed in a barren solution of the same $[NH_3]_T$ and $[CO_2]_T$, in which it had an OCP of around 0.15 V, in the same region as in the previous solution (Figure 6.17, curve a). Linear sweep voltammetry in the positive direction resulted in the anodic peak E, which was found to decrease the longer the electrode was left in the solution prior to the measurement (Figure 6.18). Following the linear sweep voltammetry scan, the OCP was found to drop within 15 minutes from an initial value of 0.3 V to values just below 0 V, and to continue to decrease slowly thereafter (Figure 6.17, curve b).

The SEM/EDX analysis of the RDE surface following the linear sweep voltammetry and OCP measurements revealed the presence of approximately 1 at% cobalt and 2 at% sulfur. Reaction with concentrated hydrochloric acid confirmed that a sulfide or polysulfide species was still present on the iron surface. When an analogous set of measurements was conducted after re-immersion of the RDE in the same solution in which it had passivated, the behaviour was found to be similar to that observed in the barren solution, except for the OCP measured after linear polarisation, which was found to relax back to the same region in which it was prior to the scan.

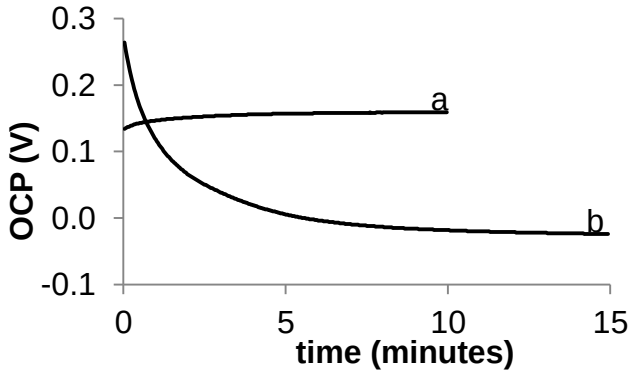

Figure 6.17 OCP during immersion of the Fe RDE in 2.5 M $[NH_3]_T$, 0.5 M $[CO_2]_T$ following its pre-treatment in 2.5 M $[NH_3]_T$, 0.5 $[CO_2]_T$, 12 mM Co(II), and 22 mM $S_2O_3^{2-}$: a) upon re-immersion; b) following linear sweep voltammetry scan to 0.74 V (Figure 6.18, a).

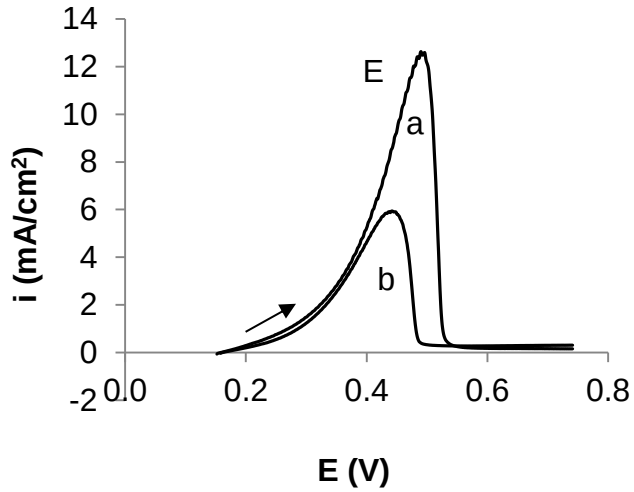

Figure 6.18 Linear sweep voltammetry of the Fe RDE in 2.5 M $[NH_3]_T$, 0.5 M $[CO_2]_T$ following its pre-treatment in 2.5 M $[NH_3]_T$, 0.5 $[CO_2]_T$, 12 mM Co(II), and 22 mM $S_2O_3^{2-}$: a) upon re-immersion; b) 10 minutes after re-immersion.

6.5 Dissolution of the CoS_x-containing surface layer

The dissolution behaviour of the CoS_x layer in barren ammoniacal-bicarbonate solution was assessed by first allowing it to form on the iron RDE at 3 M $[NH_3]_T$, 1 M $[CO_2]_T$, 12 mM [Co(II)] and 22 mM $[S_2O_3^{2-}]$. Following the passivation of iron, the RDE was removed and re-immersed in a solution containing 6 M $[NH_3]_T$ and 2 M $[CO_2]_T$, monitoring the OCP and the concentrations of dissolved cobalt, sulfur and iron over a period of 6 hours (Figure 6.19).

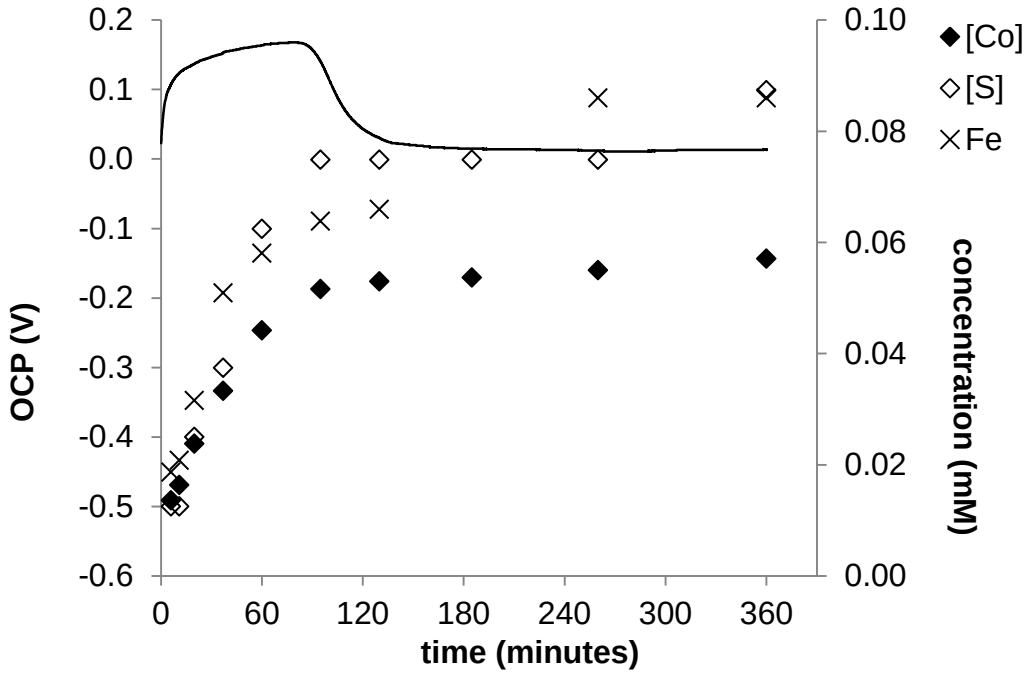

Figure 6.19 OCP and concentrations of dissolved cobalt, sulfur and iron (as indicated in the legend) during immersion of the Fe RDE in 6 M $[NH_3]_T$, 2 M $[CO_2]_T$, following its pre-treatment in 3 M $[NH_3]_T$, 1 M $[CO_2]_T$, 12 mM Co(II) and 22 mM $S_2O_3^{2-}$.

Assuming a uniformly distributed layer on the RDE surface, the initial dissolution of cobalt, sulfur and iron took place at a rate of around 3.6×10^{-10} mol s^{-1} cm^{-2}, 2.8×10^{-10} mol s^{-1} cm^{-2} and 4.6×10^{-10} mol s^{-1} cm^{-2}, respectively. Within approximately 2 hours of immersion, the increase in cobalt and sulfur concentrations began to level-off at around 0.05 mM and 0.07 mM respectively. At around this same time, the iron

OCP underwent a steep drop after reaching a maximum of around 0.17 V, thereafter decreasing gradually from around 0.02 V, to stabilise around 0.01 V. The measured dissolved cobalt and sulfur concentrations, which change from being at a 1:1 ratio to 1:4 after 2 hours, indicate that during this period the layer becomes more cobalt-deficient. The steep drop in OCP may therefore be due to the fact that after this period of time, the sulfide layer remaining on the RDE is sulfur-rich and non-conductive, no longer contributing to the measured mixed potential which then becomes dominated by that of the underlying iron oxide. This is also consistent with the difference in OCP measured before and after the anodic scan to potentials above peak E (Figure 6.17), which is assigned to the same oxidative dissolution process and formation of a sulfur-rich layer. The absence of any significant current following peak E during the voltammetric measurements (Figures 6.7, 6.8, 6.11, 6.14) is also consistent with the surface layer becoming non-conductive, and suggests that it does not undergo further oxidation even at higher applied potentials.

6.6 Electrodeposition of CoS_x on an inert substrate

In order to further study the cathodic processes taking place during immersion of the iron RDE separately from the response due to the iron species, a set of experiments was conducted in an iron-free system, using a graphite RDE. Scanning the potential in the cathodic direction resulted in a current response likely to be due to the simultaneous reduction of the various cobalt ammine and thiosulfate species present in solution. Nevertheless, it was possible to distinguish at least two diffusion limited cathodic processes (Figure 6.20), the first in the 0.1 V to -0.7 V potential region, and the second at potentials more negative than -0.7 V. The latter was attributed to the deposition of metallic cobalt, which may be described by half-reaction 6.1, for which $E°$ was calculated from available thermodynamic data (Asselin, 2008) to be -0.33 V.

$$Co(NH_3)_5^{2+} + 2e^- \rightarrow Co + 5NH_3 \quad (6.1)$$

Assuming that most of the cobalt was present in solution as the cobaltous pentammine complex, by applying the Nernst equation (6.2) to half-reaction 6.1 it is possible to estimate the potential region below which it is thermodynamically feasible:

$$\boldsymbol{E = E^{\circ} - 0.0137 ln \left[\frac{a_{NH_3}{}^5}{a_{[Co(NH_3)_5]^{2+}}} \right]} \quad (6.2)$$

In the ammonia activity range of 1 to 2.5, the equilibrium potential of half-reaction 6.1 was calculated to be between -0.39 V and -0.45 V, therefore confirming that the deposition of metallic cobalt is a feasible process likely to be contributing to the cathodic currents observed below -0.7 V. This was also confirmed upon reversal of the scan by the appearance of an anodic peak (H) around -0.4 V, which was assigned to the oxidation of metallic cobalt, by the reverse of half-reaction 6.1. This was followed by a small shoulder and prevailing cathodic currents up to potentials above 0 V. As the potential was further scanned in the positive direction, an anodic current increased at around 0.1 V, as previously observed for the iron RDE. Following a slight shoulder around 0.2 V, an anodic current peak was observed just above 0.4 V and assigned to the same process responsible for peak E observed on the iron RDE (Figure 6.20).

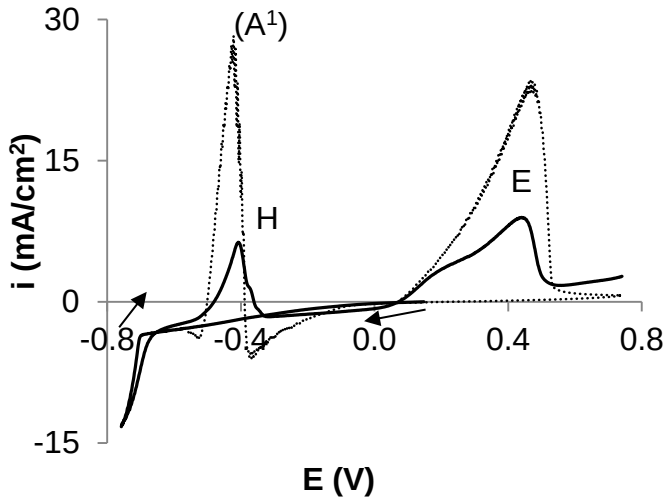

Figure 6.20 Cyclic voltammetry of the graphite RDE (solid line) and of the iron RDE following passivation (dotted line) in 2.5 M $[NH_3]_T$, 0.5 M $[CO_2]_T$, 12 mM Co(II) and 22 mM $S_2O_3^{2-}$.

Comparison of the cathodic currents obtained in solutions containing both cobalt and thiosulfate ions, with those obtained in solutions containing either ion separately (Figure 6.21) indicated that the overpotential for the deposition of metallic cobalt was significantly reduced in the presence of thiosulfate ions. In solutions containing only cobalt(II) ions, the deposition of metallic cobalt took place at potentials more negative than 0.9 V (Figure 6.21, curve b). Although the corresponding cathodic currents could not be distinguished from those due to the evolution of hydrogen, this was confirmed by stripping the metallic cobalt anodically. Measurements conducted in solutions containing only thiosulfate ions suggested the possible occurrence of a reductive process as the potential was scanned cathodically down to the hydrogen evolution region (Figure 6.21, curve a), whereas no significant anodic current was observed upon reversal of the scan.

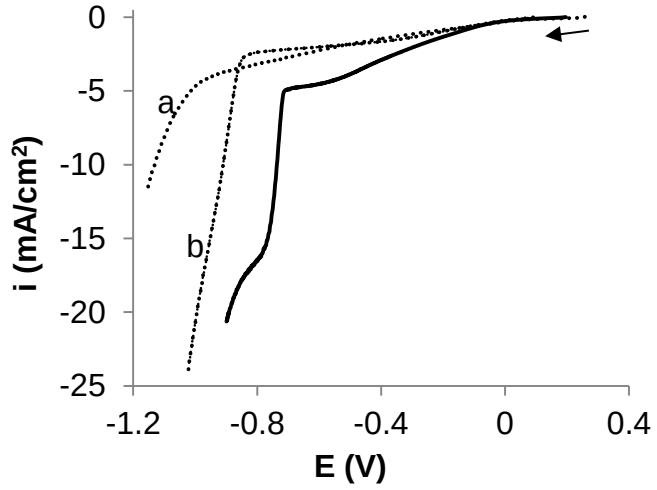

Figure 6.21 Linear sweep voltammetry of the graphite RDE in 2.5 M $[NH_3]_T$, 0.5 M $[CO_2]_T$, 12 mM Co(II) and 22 mM $S_2O_3^{2-}$ (solid line); dotted lines: a) without Co(II); b) without $S_2O_3^{2-}$.

The graphite RDE was also polarised for 30 minutes at -0.52 V, the potential corresponding to the OCP of iron during its active dissolution in the same solution. This resulted in some cobalt and sulfur being detected by EDX analysis of the graphite surface, and reaction with concentrated hydrochloric acid indicated the presence of sulfide or polysulfide ions. Cyclic voltammetry measurements conducted following the potentiostatic polarisation at both 2.5 M and 5 M $[NH_3]_T$ resulted in multiple anodic peaks in the 0 V to 0.6 V region (Figures 6.22 and 6.23) and a cathodic peak around -0.5 V (I). Second and subsequent cycles resulted in peak E being observed, with a small shoulder around 0.2 V as previously observed (Figure 6.20). Peak E was also observed when the electrode was taken out following the potentiostatic polarisation and then re-immersed in a barren solution, as shown in Figure 6.22. These results confirm that at the potential corresponding to the anodic dissolution of iron, a CoS_x species deposits onto the iron surface, as proven by the presence of peak E, resulting from its oxidation.

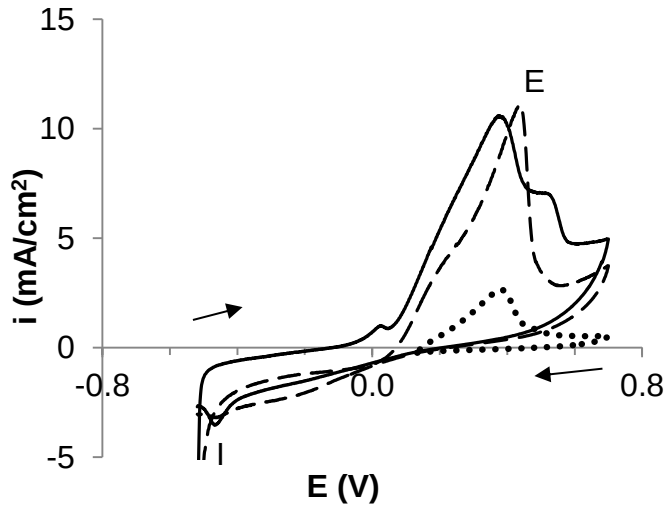

Figure 6.22 Cyclic voltammetry of the graphite RDE in 2.5 M $[NH_3]_T$, 0.5 M $[CO_2]_T$, 12 mM Co(II) and 22 mM $S_2O_3^{2-}$, following potentiostatic polarisation for 30 minutes at -0.52 V (solid line); second cycle, measured after 30 minutes (dashed line); following potentiostatic polarisation for 30 minutes at -0.52 V, and re-immersion in barren 2.5 M $[NH_3]_T$ and 0.5 M $[CO_2]_T$ solution (dotted line).

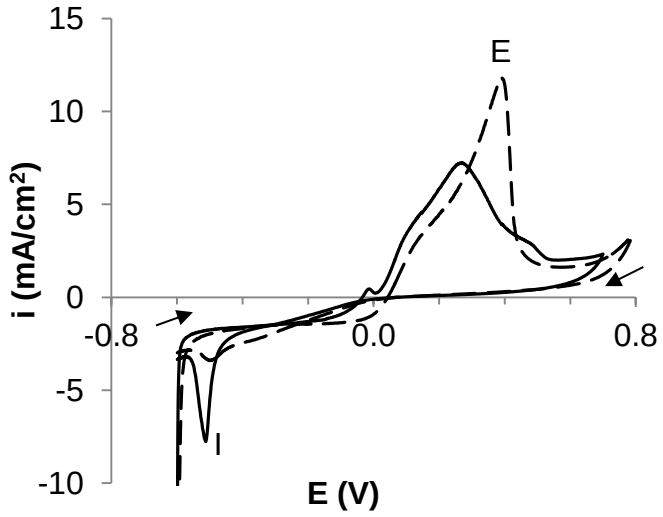

Figure 6.23 Cyclic voltammetry of the graphite RDE in 5 M $[NH_3]_T$, 1 M $[CO_2]_T$, 12 mM Co(II) and 22 mM $S_2O_3^{2-}$, following potentiostatic polarisation for 2 hours at -0.6 V (solid line); second cycle, taken immediately after (dashed line).

Two possible mechanisms have been suggested in the past for the reduction of thiosulfate ions during the first leaching stage of the Caron process (Queneau and Weir, 1986). One is the reduction to sulfide by metallic iron as it is dissolved oxidatively to form a ferrous ammine (section 2.3.1, reaction 2.19). The other is the

disproportionantion of the thiosulfate to sulfide and sulfate (section 2.3.1, reaction 2.23). This was said to be supported by measurements carried out in the plant quench tank (see section 2.3.1). In both cases the reaction is driven by the precipitation of the sulfide ions as an insoluble metal sulfide. However, in the present study it was found that the CoS_x species was formed only on the actively dissolving iron RDE and on the polarised graphite RDE, and not in the bulk of the solution. This supports the view that the reduction of thiosulfate ions to form an insoluble sulfide takes place via a redox reaction involving metallic iron as the reducing agent, and not via the disproportionation of the thiosulfate to sulfide and sulfate.

The formation of a CoS_x species both on the cathodically polarised graphite electrode and on metallic iron can be represented by half-reactions 6.3 and 6.4.

$$Co(NH_3)_5^{2+} + xS_2O_3^{2-} + 2e^- \rightarrow CoS_x + xSO_3^{2-} + 5NH_3 \quad (6.3)$$

$$Co(NH_3)_6^{3+} + xS_2O_3^{2-} + 3e^- \rightarrow CoS_x + xSO_3^{2-} + 6NH_3 \quad (6.4)$$

Based on available thermodynamic data (Isaev et al., 1990b; Roine, 2009), the standard reduction potential for half-reaction 6.3 was calculated to be -0.06 V (for $x = 2$), and -0.15 V (for $x = 1$). For half-reaction 6.4, the standard reduction potentials were calculated from the available thermodynamic data (Roine, 2009; Smith and Martell, 1976) to be 0.05 V (for $x = 2$) and -0.01 V (for $x = 1$). This indicates that the formation of both the cobalt polysulfide, CoS_2, and cobalt sulfide, CoS, by reduction of either cobaltous pentammine or cobaltic hexammine is thermodynamically feasible when coupled with the oxidation of metallic iron (equation 5.1). The formation of the polysulfide, CoS_2 or a similar species, by reduction of either cobaltous or cobaltic ammines is expected to take place more

readily than that of CoS, due to its more positive equilibrium potential, particularly in the case where cobaltous pentammine is being reduced.

6.7 Summary

During the anodic dissolution of metallic iron in ammoniacal-carbonate solutions containing both cobalt(II) and thiosulfate ions, the formation of an amorphous CoS_x species on the iron surface takes place and appears to be implicated in the passivation of iron. The presence of such species was confirmed by a combination of SEM/EDX, GIXRD and electrochemical characterisation methods.

Linear sweep and cyclic voltammetry measurements indicated that the CoS_x species undergoes an oxidative process which results in a distinctive current peak in the 0.3 V to 0.5 V potential region. The relationship between the height of this anodic peak and the immersion time required for passivation (Figure 6.12) is a clear indication that the formation of this layer plays a significant role in the mechanism of passivation of iron, which is thought to occur via the formation of a protective oxide layer, as observed in solutions containing copper(II) ions (chapter 5).

The results indicate that the formation of a CoS_x species during the leaching stage of the Caron process may potentially have a negative effect on the process efficiency by promoting the passivation of iron and its alloys with nickel and cobalt thereby preventing further dissolution of the metal values. However, the passivation of iron was not found to occur at $[NH_3]_T > 4$ M, suggesting that it is not likely to take place under the conditions of the Caron process, which employs higher ammonia concentrations. Nevertheless, the formation of CoS_x may possibly contribute to the low cobalt extractions suffered by the Caron process by causing the loss of dissolved cobalt from the leach solution as it precipitates into the layer.

7 THE BEHAVIOUR OF IRON IN AMMONIACAL-CARBONATE SOLUTIONS CONTAINING COPPER(II) AND THIOSULFATE IONS

7.1 Introduction

The investigations described in chapter 5 have shown that the presence of copper(II) in ammoniacal solutions results in the passivation of metallic iron. This is preceded by the cementation of metallic copper, which re-dissolves following the passivation of iron. As described in chapter 6, cobalt(II) ammines were not found to have the same effect in the absence of thiosulfate ions. However, when thiosulfate ions were present, the formation of a CoS_x layer took place, and this was found to gradually suppress the dissolution of iron and promote its passivation.

The presence of both cupric ammines and thiosulfate ions is also likely to result in the formation of a sulfide layer, but it is not known what effect this may have on the anodic behaviour of iron. This chapter describes an investigation into the formation of this surface layer during the immersion of iron in ammoniacal solutions containing dissolved copper(II) and thiosulfate ions. The layer was characterised by SEM/EDX and XRD methods, and its electrochemical behaviour and effect on iron dissolution was investigated using OCP measurements and rotating disk cyclic voltammetry. Additionally, since cupric ammines are also known to oxidise thiosulfate ions (Breuer and Jeffrey, 2003; Byerley et al., 1973a; Byerley et al., 1973b; Byerley et al., 1975; Rábai and Epstein, 1992) the occurrence of this homogeneous reaction in the presence of metallic iron was also investigated using of UV-visible spectrometry.

7.2 OCP Measurements

The OCP of the iron rotating disk electrode was found to remain in the active dissolution region of iron in ammoniacal–carbonate solutions, throughout a number of 3 hour measurements conducted using various copper(II) concentrations between 1 mM and 12 mM, and thiosulfate concentrations between 4 mM and 24 mM. This behaviour can be seen for example in Figure 7.1 (curve a). By comparison, the OCP behaviour with the same copper(II) concentration but with no thiosulfate (curve (b)) shows a distinct transition due to the passivation of iron (chapter 5).

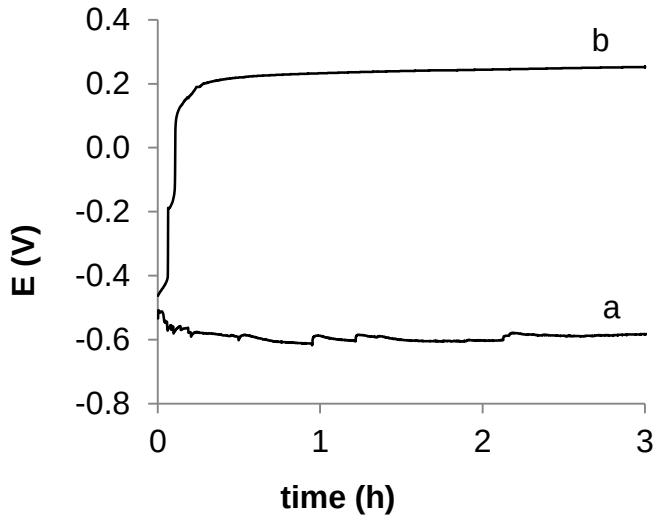

Figure 7.1 OCP of the Fe RDE in 5 M $[NH_3]_T$, 1 M $[CO_2]_T$, and a) 12 mM Cu(II), 22 mM $S_2O_3^{2-}$; b) 12 mM Cu(II).

During dissolution, the formation of a black solid on the iron surface was also observed. This was found to be non-adherent and to continuously fall off the iron surface, remaining suspended in the agitated solution. Sharp drops in the OCP of up to 50 mV were observed each time a piece of the black solid layer became detached

from the iron surface. The precipitation of significant amounts of finely divided iron(III) hydroxides was also observed.

In solutions containing cobalt(II) and thiosulfate ions, the presence of copper(II) ions, even at very low concentrations, was found to significantly delay the onset of passivation. For example, a copper concentration as low as 0.1 mM in an ammoniacal-carbonate solution containing 12 mM [Co(II)] and 24 mM [$S_2O_3^{2-}$] resulted in the passivation taking place after 2 hours of immersion, as opposed to the 30-40 minutes it took when no copper ions were added (Figure 7.2).

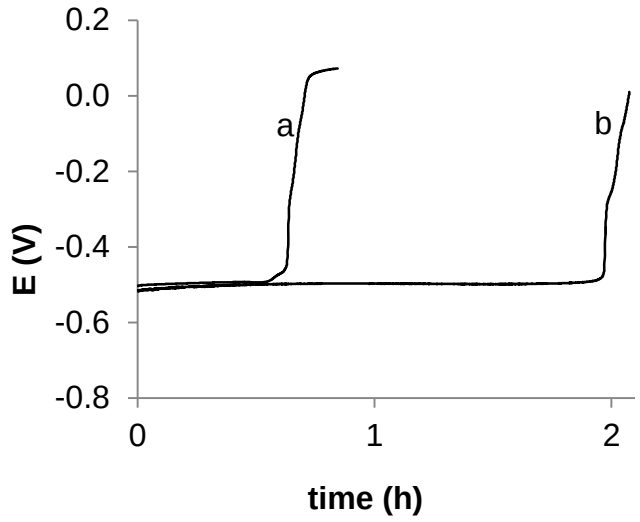

Figure 7.2 OCP of Fe in 3 M $[NH_3]_T$, 1 M $[CO_2]_T$, 12 mM Co(II), 24 mM $S_2O_3^{2-}$, and a) no Cu(II); b) 0.1 mM Cu(II).

In a final experiment, an iron RDE which had been allowed to passivate in an ammoniacal-carbonate solution containing 12 mM [Cu(II)] and no thiosulfate ions was re-immersed in a solution containing 6 M $[NH_3]_T$, 2 M $[CO_2]_T$, 4 mM [Cu(II)] and 4 mM [$S_2O_3^{2-}$]. The OCP of the iron RDE was found to remain in the passive potential region, above 0 V, indicating that re-activation of the anodic dissolution of iron is not likely to take place spontaneously in these solutions.

7.3 Surface layer characterisation

The OCP behaviour of the iron RDE did not exhibit significant differences across the concentration ranges of copper and thiosulfate, consistently behaving in the unstable manner shown in Figure 7.1 (curve a), within the potential region of active iron dissolution. Therefore, XRD and SEM/EDX analyses of the RDE surface were only carried out for one representative combination, following its immersion for 3 hours in the presence of 12 mM Cu(II) and 24 mM thiosulfate ions, at 5 M $[NH_3]_T$ and 1 M $[CO_2]_T$. The SEM-EDX analysis of its surface revealed the presence of a predominantly dendritic deposit, with an elemental analysis of approximately 30% Cu and 20% S. Analysis by GIXRD of the iron RDE, following its immersion for 4 hours, under the same conditions, revealed the presence of metallic copper and Cu_2S (Figure 7.3).

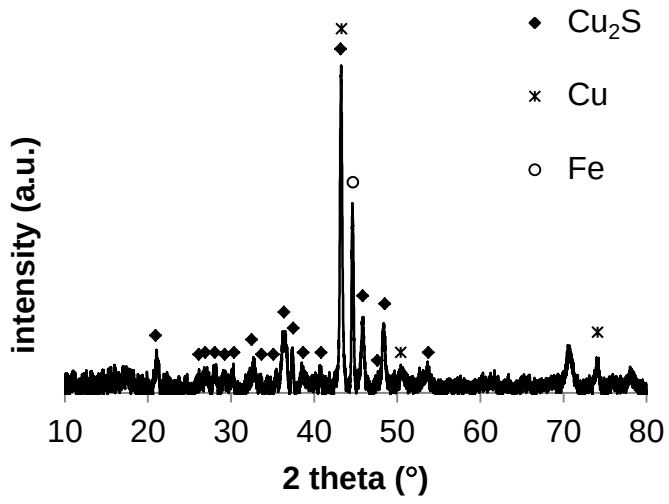

Figure 7.3 GIXRD (Cu Kα) pattern of the Fe RDE following immersion in 5 M $[NH_3]_T$, 1 M $[CO_2]_T$, 12 mM Cu(II) and 24 mM $S_2O_3^{2-}$.

The solid precipitate which formed following immersion of the iron RDE in the absence of air above the solution was also analysed. The SEM images of the filtered solid revealed a mixture of phases with different morphologies (Figure 7.4) and the

EDX elemental analysis resulted in major variations in the relative amounts of copper and sulfur in different parts of the precipitate. The XRD analysis of the solid indicated the presence of metallic copper, Cu_2O, Cu_2S, possibly $CuFe_4S_7$ and FeS (Figure 7.5).

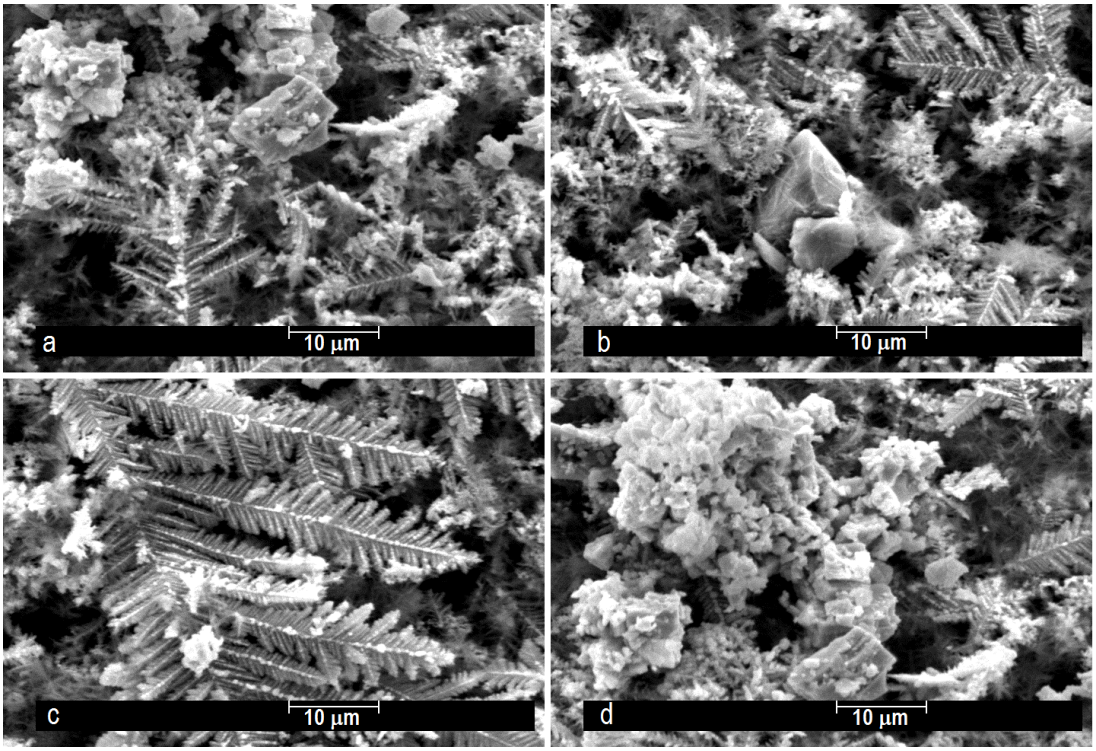

Figure 7.4 SEM images of different parts of the solid precipitate formed during dissolution of iron in 6 M $[NH_3]_T$, 2 M $[CO_2]_T$, 12 mM Cu(II) and 24 mM $S_2O_3^{2-}$.

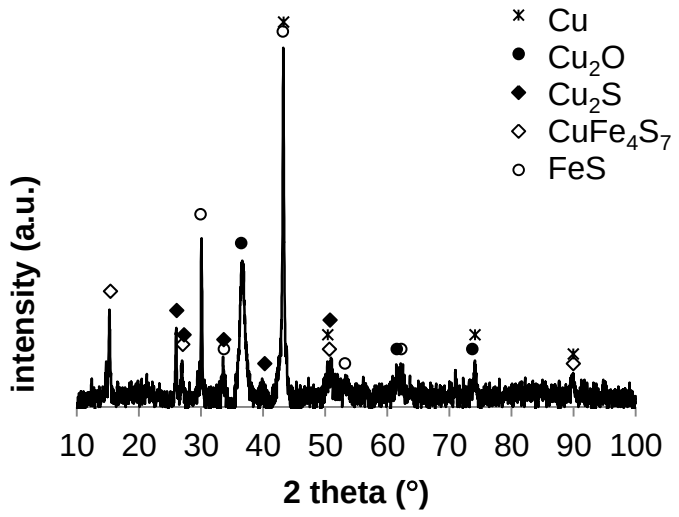

Figure 7.5 XRD (Cu Kα) pattern of the solid precipitate formed during the dissolution of iron in 6 M $[NH_3]_T$, 2 M $[CO_2]_T$, 12 mM Cu(II) and 24 mM $S_2O_3^{2-}$.

7.4 Dissolution of the Cu_2S-containing surface layer

In order to assess the dissolution behaviour of the Cu_2S-containing surface layer, it was allowed to form on an iron RDE surface immersed in 3 M $[NH_3]_T$, 1 M $[CO_2]_T$, 12 mM [Cu(II)] and 24 mM $[S_2O_3^{2-}]$ under open-circuit conditions. In order to achieve this, it was first necessary to activate the electrode, which became passive upon immersion due to the low $[NH_3]_T$, by scanning the potential from the OCP to -0.56 V at 100 mV/s. The applied potential was then switched off and the layer was allowed to form spontaneously for 10 minutes. Prior to removing the electrode from this solution, non-spontaneous passivation of the metallic iron was achieved by applying a potential of 0.4 V for around 3 minutes. The RDE was then removed and reimmersed in barren ammoniacal-carbonate solution at 6 M $[NH_3]_T$, 2 M $[CO_2]_T$, in order to monitor the change in [Cu], [S], [Fe] and the OCP, as shown in Figure 7.6.

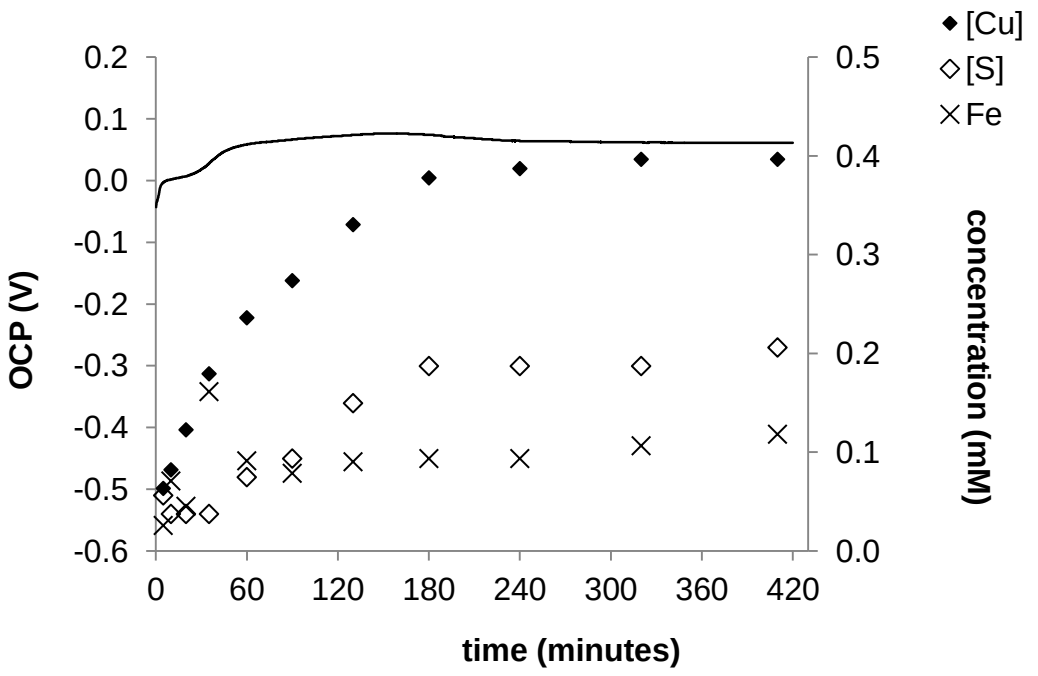

Figure 7.6 OCP and concentrations of dissolved copper, sulfur and iron (as indicated in the legend) during immersion of the Fe RDE in 6 M $[NH_3]_T$, 2 M $[CO_2]_T$, following its pre-treatment in 3 M $[NH_3]_T$, 1 M $[CO_2]_T$, 12 mM Cu(II) and 24 mM $S_2O_3^{2-}$.

Assuming a uniformly distributed layer on the RDE surface, the initial dissolution rate of copper from the layer was around 3.1×10^{-9} mol s^{-1} cm^{-2}, which is almost an order of magnitude higher than the dissolution rate of cobalt from the CoS_x layer under the same conditions, as discussed in section 6.5. Accurate dissolution rates could not be determined for sulfur and iron. However, the results indicated that overall the Cu and S dissolved at a molar ratio of approximately 2:1, which is consistent with the stoichiometric dissolution of Cu_2S to copper complexes and dissolved sulfur species. In the presence of dissolved oxygen, the overall process may be described by reaction 7.1, for which the logK at 45°C was calculated to be 114 (Roine, 2009).

$$2Cu_2S + 13NH_3 + 3NH_4^+ + 3O_2 \rightarrow 4Cu(NH_3)_4^{2+} + S_2O_3^{2-} + 3OH^- \quad (7.1)$$

7.5 UV-visible spectrophotometric studies

In order to assess whether the reduction of copper(II) by thiosulfate ions occurred to a significant extent at the ammonia concentrations used for this study, reference solutions containing ammonia, carbonate, copper(II) and/or thiosulfate ions were investigated using UV-VIS spectrophotometry. The results were treated qualitatively, due to reaction between the species during solution preparation and the uncontrolled presence of dissolved oxygen, which can re-generate copper(II) tetrammine following its reduction.

Spectra were first obtained for copper(II) in 6 M $[NH_3]_T$, 2 M $[CO_2]_T$ solution. This resulted in a maximum UV absorption at 246 nm and a broad absorption in the visible region at 630 nm, due to the formation of blue cupric ammine complexes (Figure 7.7, solid line). Spectra were then obtained for copper(II) in 24 mM aqueous

sodium thiosulfate. This resulted in a UV absorption maximum at 276 nm, ascribed to cuprous thiosulfate complexes (Figure 7.7, dotted line), formed from the reduction of copper by thiosulfate according to reaction 7.2.

$$2Cu^{2+} + (2x+2)S_2O_3^{2-} \rightleftharpoons 2Cu(S_2O_3)_x^{1-2x} + S_4O_6^{2-} \quad (7.2)$$

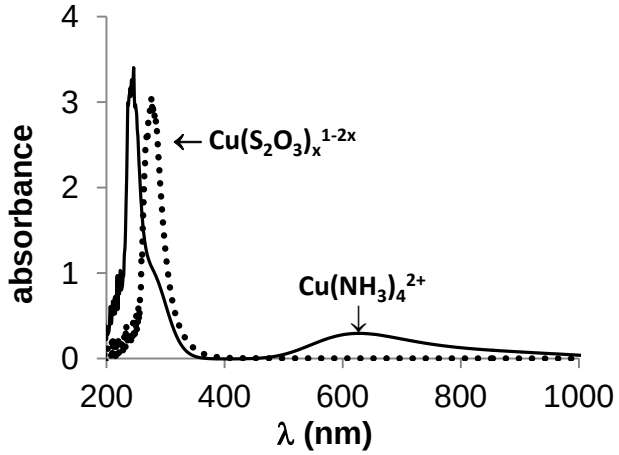

Figure 7.7 UV-VIS spectra of 4 mM Cu(II) in 6 M $[NH_3]_T$, 2 M $[CO_2]_T$ (solid line), and in 24 mM $S_2O_3^{2-}$(dotted line).

A study was then conducted for copper(II) in 24 mM $[S_2O_3^{2-}]$, 3 M $[NH_3]_T$ and 1 M $[CO_2]_T$, which corresponds to half the $[NH_3]_T$ and $[CO_2]_T$ employed in the study with an iron RDE. The spectra indicated the presence of both a copper(II) ammine complex, with a maximum absorbance at 623 nm, and a Cu(I) thiosulfate complex, with a peak at 273 nm (Figure 7.8, solid line). The intensity of these two peaks was monitored over a 2.5 hour period (Figure 7.8, dotted lines), during which the absorbance peak at 273 nm was found to decrease by over 17%, suggesting the progressive consumption of thiosulfate ions by reduction of copper(II). A decrease of just over 6% in the cupric tetrammine absorbance at 623 nm was also observed, despite its rapid regeneration by reaction with oxygen.

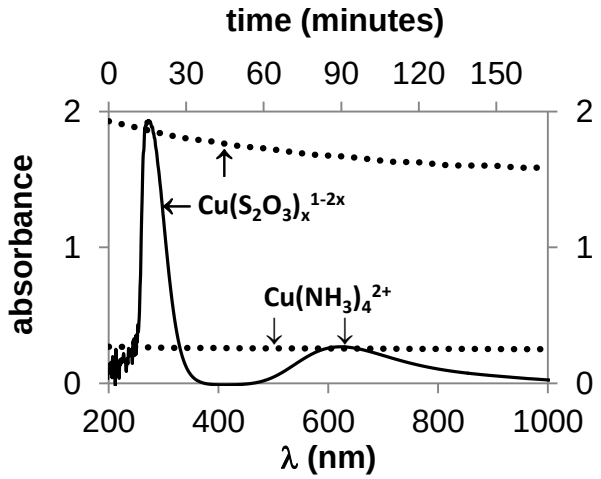

Figure 7.8 UV-visible spectrum of 4 mM Cu(II) in 24 mM $S_2O_3^{2-}$, 3 M $[NH_3]_T$ and 1 M $[CO_2]_T$ (solid line); change over time in maximum absorbance at 273 nm and 623 nm (dotted lines).

At 6 M $[NH_3]_T$, 2 M $[CO_2]_T$, the UV-visible measurements were conducted at the highest $[S_2O_3^{2-}]$ and [Cu(II)] used in the studies with an iron RDE, and in a tightly sealed cell with no air above the solution. This minimised the loss of ammonia and re-oxidation of Cu(I). The higher Cu(II) concentration made it necessary to use a shorter path-length of 0.1 cm. The spectrum (Figure 7.9, solid line) was found to be qualitatively similar to that of copper(II) in ammoniacal carbonate solutions (Figure 7.7, solid line), with no absorbance peak arising from the presence of thiosulfate ions. Despite the presence of dissolved oxygen, it was possible to observe a clear decrease over time in cupric tetrammine absorbance at 620 nm (Figure 7.9, dotted line), suggesting that the homogeneous reduction of cupric ammines by thiosulfate took place to an appreciable extent even at the high $[NH_3]_T$ employed in this study.

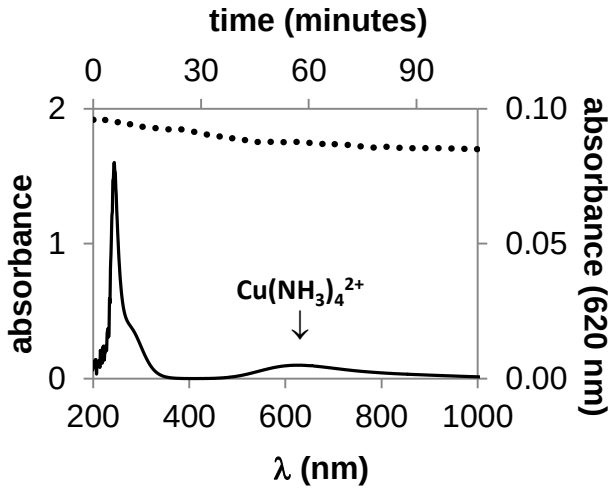

Figure 7.9 UV-VIS spectrum of 12 mM Cu(II) in 24 mM $S_2O_3^{2-}$, 6 M $[NH_3]_T$ and 2 M $[CO_2]_T$ (solid line); change over time in maximum absorbance at 620 nm (dotted line).

Spectrophotometric analysis of the solution was also carried out following the immersion of metallic iron at room temperature, with no air above the solution. Within approximately half an hour of immersion and active dissolution of the iron, the solution colour changed from deep blue to colourless, indicating the rapid reduction of most of the copper(II) ammine complexes to copper(I) species and metallic copper.

The UV-visible spectrum, measured using a 0.1 cm path length, is shown in Figure 7.10. As expected, there was no visible absorbance in the 620 nm region, indicating complete reduction of the cupric ammines. This appeared to be sustained by the iron remaining in its active dissolution state throughout the experiment, rather than by reaction with thiosulfate ions. Under such conditions, dissolved oxygen was also consumed by metallic iron, so the concentration of cupric tetrammine continued to decrease as its regeneration was not sustained by reaction with dissolved oxygen. This was supported by the colour change which was only observed when the iron

disk was activated by polishing immediately prior to immersion, a condition which replicated the initial stages of the Caron leach.

The maximum UV absorbance at 269 nm was ascribed to a cuprous thiosulfate complex, which was not observed following the homogeneous reaction in the absence of iron. This confirmed that there was practically no dissolved oxygen available to reoxidise the complex, and that the cupric ammines were reduced predominantly by iron rather than thiosulfate.

It was concluded that the homogeneous reduction of copper(II) by thiosulfate is not likely to have a significant effect on studies conducted in the presence of metallic iron, nor to take place to a significant extent during the initial stage of the Caron leach.

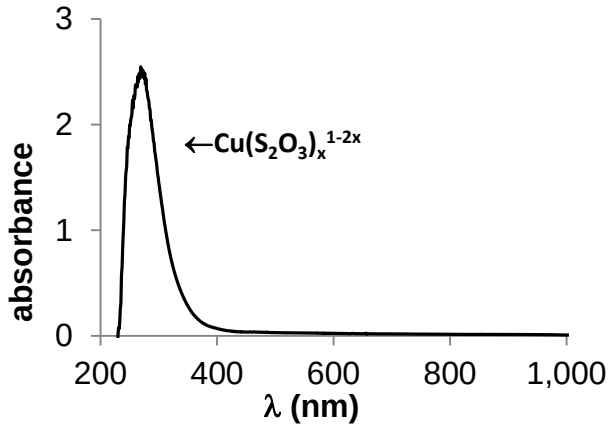

Figure 7.10 UV-VIS spectrum of 12 mM Cu(II), 24 mM $S_2O_3^{2-}$, 6 M $[NH_3]_T$ and 2 M $[CO_2]_T$ solution following reaction with metallic iron.

7.6 Rotating disk cyclic voltammetry

The voltammetric behaviour of the iron RDE was observed following 15 minutes of immersion in 6 M $[NH_3]_T$, 2 M $[CO_2]_T$ solutions at different [Cu(II)] and $[S_2O_3^{2-}]$ (Figure 7.11). For the purpose of this investigation, it was not necessary to compensate the results for the solution resistance between the tip of the Luggin capillary and the RDE surface. Therefore, high anodic currents occurr at slightly different potentials, due to changes in the solution conductivity at different species concentrations.

Scanning the potential in the positive direction from the OCP resulted in an anodic peak due to the dissolution of metallic iron (A) in the -0.6 V to -0.2 V potential region, followed by a smaller anodic process (B) in the -0.1 V to 0 V region and a third peak (C) above 0.1 V. The peak current density at A was not significantly affected by changes in [Cu(II)] and $[S_2O_3^{2-}]$, whereas increasing [Cu(II)] from 1 mM to 4 mM at constant $[S_2O_3^{2-}]$ resulted in a 7-fold increase in peak C. Further increase to 12 mM had a smaller effect on the peak current density, but resulted in a fourth anodic process (D) being observed in the 0.4 V to 0.5 V potential region, as a shoulder following peak C. On the other hand, increasing $[S_2O_3^{2-}]$ at constant [Cu(II)] resulted in a 10% decrease in the current density at peak C. These observations are consistent with peak C being due to the oxidation of a copper-containing species, such as a copper sulfide, formed during the anodic dissolution of iron. Its formation appears to be strongly dependent on the copper(II) concentration, as consistent with the change in peak current density, whereas the effect of $[S_2O_3^{2-}]$ may be explained in terms of a decrease in [Cu(II)] by reaction with thiosulfate ions. This suggests that the species responsible for peak C may possibly form as a result of copper(II) reduction to copper(I) on the iron surface. Following reversal of the

potential scan, the RDE appeared to become passive, with no significant current being observed in the cathodic direction until it reached negative values. Scanning the potential below 0 V resulted in a cathodic process, likely to be the reduction of cupric ammines, followed by a further increase in cathodic current density observed at higher [Cu(II)] as the potential approached -0.4 V. The anodic dissolution of metallic iron resumed in the region of -0.4 V (A^1), reaching higher current densities at lower [Cu(II)] and higher [$S_2O_3^{2-}$].

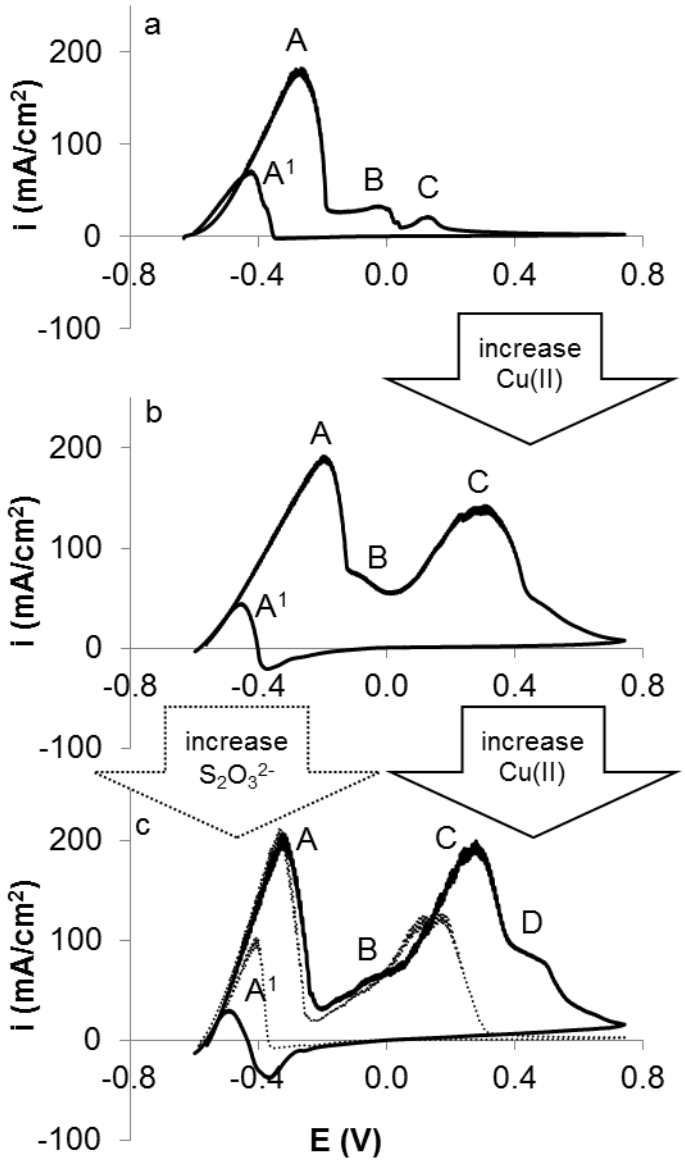

Figure 7.11 Rotating disk cyclic voltammetry (50 mV/s) of the Fe RDE following 15 minutes of immersion in 6 M $[NH_3]_T$, 2 M $[CO_2]_T$ and a) 1 mM Cu(II) and 4 mM $S_2O_3^{2-}$; b) 4 mM Cu(II) and 4 mM $S_2O_3^{2-}$; c) 12 mM Cu(II) and 4 mM $S_2O_3^{2-}$ (solid line); 4 mM Cu(II) and 24 mM $S_2O_3^{2-}$ (dotted line).

Cyclic voltammetric measurements taken after 2 hours of immersion resulted in a continued increase in anodic current density in the potential region of (C), which did not result in a peak prior to reaching the inversion potential, as shown in Figure 7.12 (b) for 4 mM [Cu(II) and 24 mM [$S_2O_3^{2-}$]. The cathodic scan, resulted in a similar but lower anodic current due to the process at C, and a negative current as the potential was decreased below 0.1. Two cathodic peaks were observed, one between 0 and -0.1 V (E) and the other just below -0.4 V (F), while the reactivation of metallic iron (A^1) was not observed in this case.

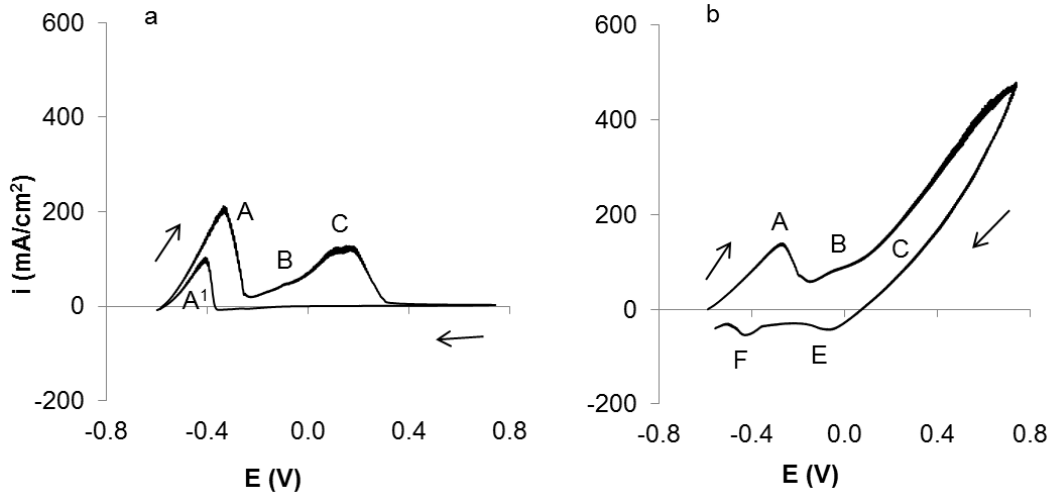

Figure 7.12 Rotating disk cyclic voltammetry (50 mV/s) of the Fe RDE in 6 M $[NH_3]_T$, 2 M $[CO_2]_T$, 4 mM Cu(II) and 24 mM $S_2O_3^{2-}$, measured after an immersion period of: a) 15 minutes; b) 2 hours.

Monitoring the voltammetric behaviour following different periods of immersion at 4 mM [Cu(II)] and 4 mM [$S_2O_3^{2-}$] showed a progressive increase in current density at C (Figure 7.13). For the 2 hour immersion, inversion of the scan at the same potential as the other measurements resulted in a similar response as that shown in Figure 7.12, although in this case the reactivation of metallic iron (A^1) was observed during the cathodic scan. As shown in Figure 7.13, by inverting the scan at a higher

potential it was possible to observe a very large peak C. These results indicate that although a substantial amount of the species being oxidised at C is formed during the anodic dissolution of iron, this does not appear to promote the passivation of iron, nor to significantly suppress its dissolution.

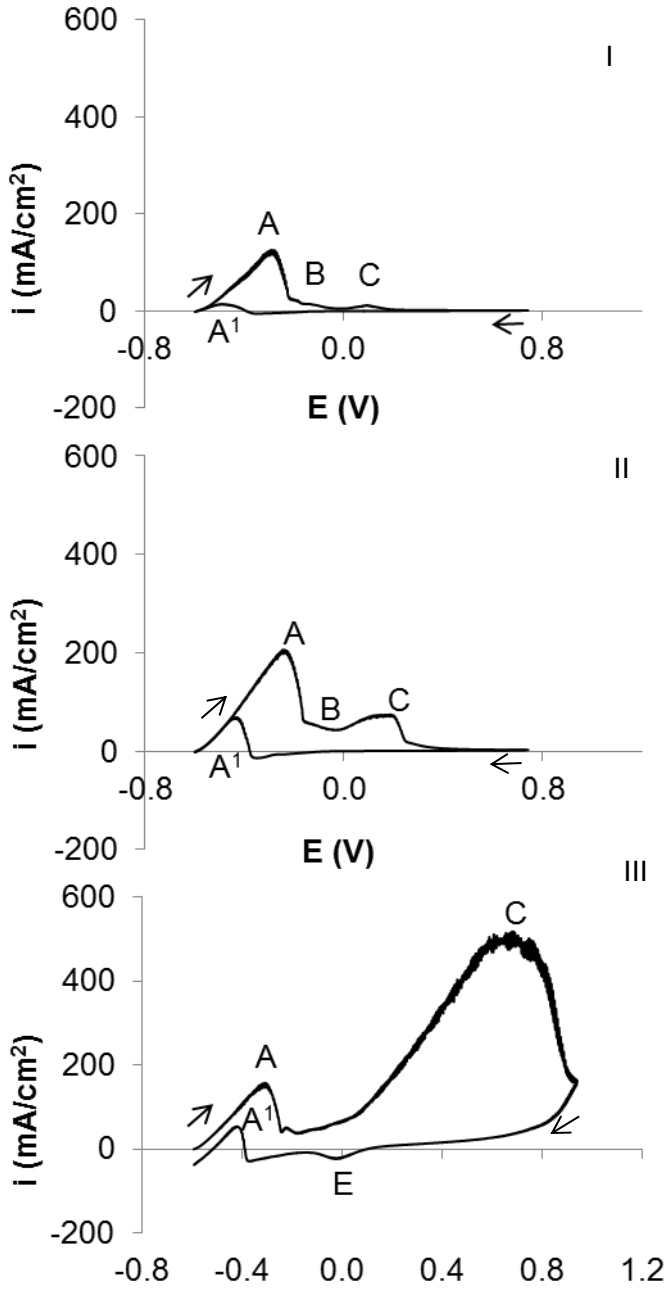

Figure 7.13 Rotating disk cyclic voltammetry of Fe RDE in 6 M $[NH_3]_T$, 2 M $[CO_2]_T$, 4 mM Cu(II) and 4 mM $S_2O_3^{2-}$ taken immediately after immersion (I), after 10 minutes of immersion (II) and after 2 hours of immersion (III).

7.7 Discussion of reactions

In the absence of thiosulfate ions, the dissolution of iron in ammoniacal-carbonate solutions containing copper(II) ions can be described by reactions 7.3-7.5. This was confirmed by experimental observations (chapter 5) and is thermodynamically feasible as discussed in detail in section 5.7.

$$Fe + 2Cu(NH_3)_4^{2+} \rightarrow Fe(NH_3)_4^{2+} + 2Cu(NH_3)_2^{+} \quad (7.3)$$

$$Fe + Cu(NH_3)_4^{2+} \rightarrow Fe(NH_3)_4^{2+} + Cu \quad (7.4)$$

$$Fe + 2Cu(NH_3)_2^{+} \rightarrow Fe(NH_3)_4^{2+} + 2Cu \quad (7.5)$$

When thiosulfate ions are present, the presence of metallic copper on the iron surface as observed by GIXRD indicates that reactions 7.3-7.5 still take place. The dissolution of iron has been found to be significantly enhanced by the presence of thiosulfate ions, as suggested by the higher resulting anodic current densities, as discussed in section 6.3. The detection of a small amount of sulfur by SEM/EDX analysis of the iron surface following immersion in the presence of thiosulfate, and the production of H_2S upon addition of HCl, indicates that some sulfide was precipitated or adsorbed on the iron surface, with the possible formation of an iron sulfide or polysulfide. It has been suggested by previous researchers (Queneau and Weir, 1986) that iron sulfide may form during the initial stage of the Caron leach either by reduction of the thiosulfate by metallic iron or via a disproportionation mechanism. The latter may be described by reaction 7.6, for which the standard Gibbs free energy ($\Delta G°$) was calculated from available thermodynamic data (Isaev et al., 1990a; Roine, 2009) to be -80 kJ/mol. Similarly, it was suggested that the precipitation of even less soluble metal sulfides took place via an analogous

mechanism involving other metal ions present in the leach solution (reactions 2.22 and 2.23 in chapter 2, section 2.3.1). However, the formation of metal sulfides was only observed on the electrode surface, suggesting that it is more likely to involve the reduction of thiosulfate by metallic iron rather than the disproportionation of thiosulfate. In such case, the formation of iron sulfide may be described by reaction 7.7, for which the $\Delta G°$ was calculated to be -68 kJ/mol (Roine, 2009).

$$Fe(NH_3)_4^{2+} + S_2O_3^{2-} + H_2O \rightarrow FeS + 2NH_4^{+} + SO_4^{2-} + 2NH_3 \quad (7.6)$$

$$Fe + S_2O_3^{2-} \rightarrow FeS + SO_3^{2-} \quad (7.7)$$

When both thiosulfate and copper(II) ions are present, the system is more complicated, due to the well known homogeneous redox reaction between copper(II) and thiosulfate ions (Breuer and Jeffrey, 2003; Byerley et al., 1973a; Byerley et al., 1973b; Byerley et al., 1975; Rábai and Epstein, 1992). This results in the formation of various cuprous thiosulfate, ammine and mixed complexes, depending on the relative ammonia and thiosulfate concentrations. This situation may be described by reactions 7.8 and 7.9, where thiosulfate is initially oxidised by cupric ammines to tetrathionate, which is then further oxidised resulting in a mixture of sulfur oxyanions. The $\Delta G°$ values for these reactions were calculated from available thermodynamic data to be -18 kJ/mol (Roine, 2009) and -34 kJ/mol (Aylmore and Muir, 2001) respectively.

$$2Cu(NH_3)_4^{2+} + 2S_2O_3^{2-} \rightarrow 2Cu(NH_3)_2^{+} + S_4O_6^{2-} + 4NH_3 \quad (7.8)$$

$$2Cu(NH_3)_4^{2+} + 4S_2O_3^{2-} \rightarrow 2Cu(S_2O_3)^{-} + S_4O_6^{2-} + 8NH_3 \quad (7.9)$$

However, in the presence of metallic iron, the copper(I) complexes are thought to result mainly from reaction 7.3, as discussed in section 7.4, for which the $\Delta G°$ was

calculated to be -129 kJ/mol (Isaev et al., 1990a; Roine, 2009). The observations described in section 7.4 also appear to indicate that under the experimental conditions the reduction of cupric ammines by metallic iron is also kinetically favoured compared to their reduction by thiosulfate ions.

The formation of Cu_2S may then take place by further reaction of cuprous complexes and disproportionation of thiosulfate according to reaction 7.10, for which $\Delta G°$ was calculated to be -159 kJ/mol (Isaev et al., 1990a; Roine, 2009). However, since the formation of Cu_2S was only observed in the presence of metallic iron, the overall process may be better described by reaction 7.11, for which $\Delta G°$ was calculated to be -147 kJ/mol (Isaev et al., 1990a; Roine, 2009). It is also possible that some Cu_2S was formed by the reduction of thiosulfate on the copper dendrites formed by reactions 7.4 and 7.5, as described by reaction 7.12, for which $\Delta G°$ was calculated to be -57 kJ/mol (Roine, 2009). Similar mechanisms may be responsible for the formation of mixed iron-copper sulfides and of various other unidentified or amorphous sulfide or polysulfide species.

$$2Cu(NH_3)_2^{+} + S_2O_3^{2-} + H_2O \rightarrow Cu_2S + SO_4^{2-} + 2NH_3 + 2NH_4^{+} \quad (7.10)$$

$$Fe + 2Cu(NH_3)_2^{+} + S_2O_3^{2-} \rightarrow Cu_2S + SO_3^{2-} + Fe(NH_3)_4^{2+} \quad (7.11)$$

$$2Cu + S_2O_3^{2-} \rightarrow Cu_2S + SO_3^{2-} \quad (7.12)$$

The Eh-pH diagrams constructed for the Cu-NH_3-CO_3^{2-}-H_2O system and the Cu-S-NH_3-CO_3^{2-}-H_2O system under the experimental conditions, without including any copper-thiosulfate complexes, are shown in Figure 7.14 (a and b respectively).

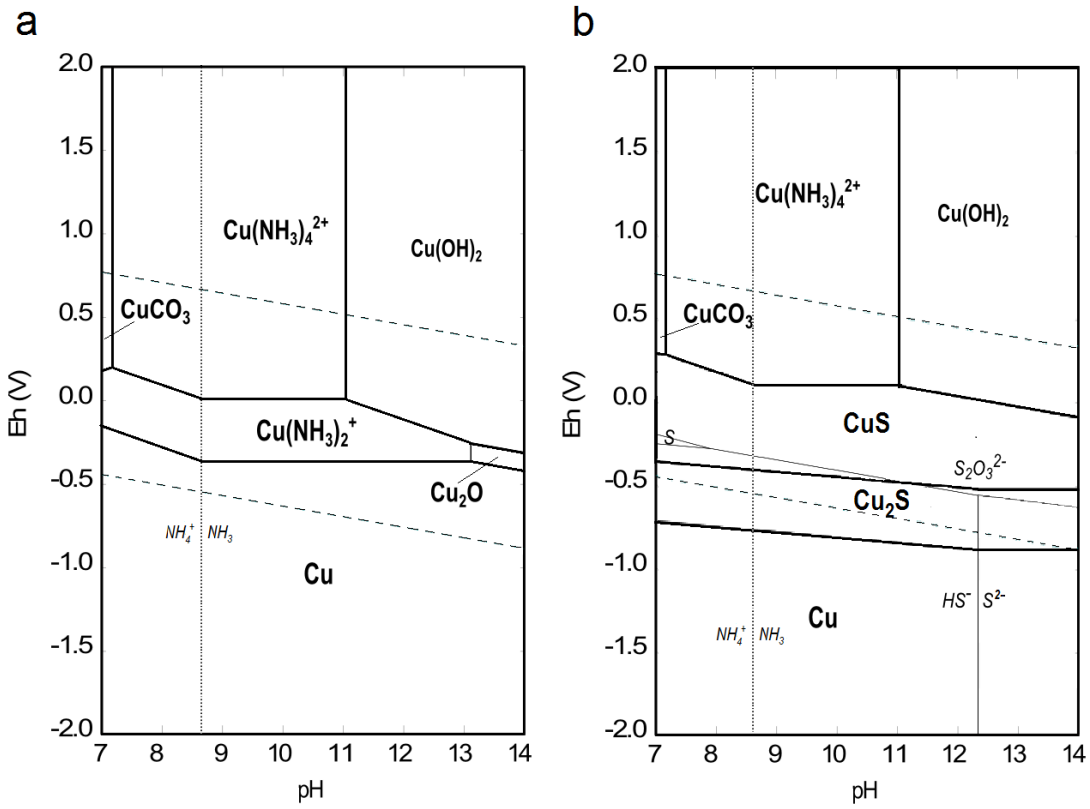

Figure 7.14 Eh-pH diagrams constructed using the HSC 7 thermodynamic database and software (Roine, 2009) for Cu-NH_3-CO_3^{2-}-H_2O (a) and Cu-S-NH_3-CO_3^{2-}-H_2O (b) at [NH_3] = 6 m, [CO_2] = 2 m, [Cu(II)] = 0.01 m, [$S_2O_3^{2-}$] = 0.02 m, 45°C. The thick lines correspond to the boundaries of the predominance regions of Cu species, the dashed lines to the H_2O limits and the dotted lines to the NH_3/NH_4^+ equilibrium boundary. Thin lines in Figure b indicate stability regions of metastable thiosulfate ions and elemental sulfur.

Comparison of the metallic copper-Cu_2S boundary in Figure 7.14 (b) with the thiosulfate stability region (thin lines) confirms that the reduction of thiosulfate by metallic copper is also thermodynamically feasible under the experimental conditions of this study. Although the diagram only shows the $S_2O_3^{2-}/HS^-$ boundary, the reduction is expected to be even more favoured if the product is solid species Cu_2S.

7.8 Summary

Although the presence of copper(II) in ammoniacal-carbonate solutions was found to promote the passivation of iron (chapter 5), the presence of both copper(II) and thiosulfate ions was found to prevent the passivation process. Throughout a number of 3 hour measurements of the OCP of iron at variable copper(II) and thiosulfate concentrations, the potential was found to remain in the active dissolution region of iron in ammoniacal–carbonate solutions.

During dissolution, a partially-adherent black solid layer was formed on the iron surface, found to contain Cu_2S and dendritic copper based on XRD characterisation studies. The effect of this layer on the electrochemical behaviour of iron was investigated using rotating disk cyclic voltammetry, which showed that a significant amount of it remained in electrical contact with the RDE surface. The most remarkable observation was that the formation of such a sulfide deposit on the iron surface did not appear to suppress its dissolution or promote its passivation, as observed when CoS_x was formed (chapter 6). This is proposed to be due to the partly crystalline and poorly-adherent nature of the deposit, as well as a disrupting effect of the cementation of copper.

8 THE BEHAVIOUR OF IRON IN AMMONIACAL-CARBONATE SOLUTIONS CONTAINING NICKEL(II) AND THIOSULFATE IONS

8.1 Introduction

The studies described in chapters 5, 6 and 7 have shown that different metal ions present as ammonia complexes in the ammoniacal-carbonate leach system have significantly different effects on the dissolution behaviour of metallic iron. Most remarkably, the presence of copper ammines even at millimolar concentrations has been found to consistently induce the passivation of metallic iron, which takes place via the cementation and subsequent dissolution of metallic copper (chapter 5). This behaviour has not been observed in solutions containing cobalt or nickel ammines, even though the latter are also thought to undergo cementation onto the dissolving iron.

When thiosulfate ions are also present, the passivation process observed in the presence of copper ammines alone was found to be disrupted, and the continued anodic dissolution of iron resulted in the precipitation of significant amounts of cuprous sulfide which prevented the passivation of iron (chapter 7).

In contrast with this, the presence of both cobalt and thiosulfate ions resulted in the formation of an amorphous CoS_x layer which caused a gradual suppression of the dissolution of iron and appeared to be implicated in its passivation, which was observed at $[NH_3]_T < 5$ M (chapter 6). Even though the passivation was consistently observed only at ammonia concentrations slightly lower than those normally encountered under the conditions of the Caron process, the loss of dissolved cobalt by precipitation into the layer itself was identified as another factor contributing to the low cobalt extractions.

The preliminary studies described in chapter 4 have shown that the presence of nickel ammines, even at concentrations of over an order of magnitude higher than the cobalt or copper ammines, is not likely to be implicated in the passivation of iron, regardless of the presence of thiosulfate ions (chapter 4). However, immersion of the iron for 3 hours in ammoniacal-carbonate solutions containing nickel(II) ions resulted in some nickel being detected by the elemental analysis of the iron surface. This is thought to be due to the cementation of nickel onto the iron surface, but further experimental work is necessary in order to confirm this. In the presence of both nickel(II) and thiosulfate ions, the elemental analysis of the iron surface also indicated the possible formation of a nickel sulfide layer. This chapter describes further investigation into the formation of such layer and its effect on the electrochemical behaviour of metallic iron. This has been carried out in order to assess whether the potential formation of this sulfide is likely to affect the metal extraction efficiency of the Caron process, either by contributing to the tendency of iron to passivate or by causing the loss of dissolved nickel from solution. The study included identification of the sulfide layer by GIXRD. This allowed further investigation into its electrochemical behaviour to be conducted using a commercially available sample of the same stoichiometry and similar diffraction pattern, thereby avoiding the interference of underlying metallic iron.

8.2 OCP and rotating disk cyclic voltammetry measurements

The OCP of iron in ammoniacal-carbonate solutions containing nickel(II) and thiosulfate ions at concentrations typically encountered in Caron process leach liquors solution has been found to remain in the active dissolution region for metallic iron. This can be seen from Figure 8.1, which shows OCP measurements taken at

0.15 M Ni(II), 22 mM $S_2O_3^{2-}$ and various $[NH_3]_T$ and $[CO_2]_T$ immediately prior to the cyclic voltammetry measurements shown in Figures 8.2 (b), 8.3 and 8.4.

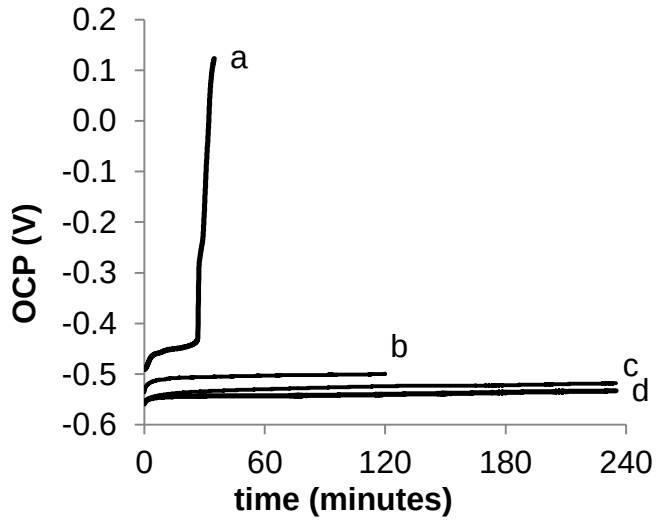

Figure 8.1 OCP of Fe RDE in solutions containing 0.15 M Ni(II), 22 mM $S_2O_3^{2-}$, and: a) 3 M $[NH_3]_T$ and 1 M $[CO_2]_T$; b) 6 M $[NH_3]_T$ and 2 M $[CO_2]_T$; c) 5.5 M $[NH_3]_T$ and 1.5 M $[CO_2]_T$; d) 5 M $[NH_3]_T$ and 1 M $[CO_2]_T$.

As can be seen from Figure 8.1, the spontaneous passivation of iron was only observed at 3 M $[NH_3]_T$ (curve a), which is lower than the typical Caron process concentrations of around 5 - 6 M.

Increasing $[NH_3]_T$ and $[CO_2]_T$ by increasing the ammonium bicarbonate concentration at a fixed initial ammonia concentration (curves b, c and d) resulted in the OCP shifting to more positive values. This is likely to be an effect of the resulting decrease in pH, from 10.5, at 5 M $[NH_3]_T$ and 1 M $[CO_2]_T$, to 10, at 5 M $[NH_3]_T$ and 1 M $[CO_2]_T$ on the mixed potential of the electrode.

The increase in $[CO_2]_T$ was found to have an even more significant effect on the voltammetric behaviour of the RDE, following each period of immersion shown in Figure 8.1, as can be seen by comparing Figures 8.2 (b), 8.3 and 8.4. At the highest $[CO_2]_T$ of 2 M, cyclic voltammetry measurements were taken upon immersion and

following 2 hours of immersion (Figure 8.2, curves a and b, respectively). Due to the higher conductivity of this solution compared to those at lower $[CO_2]_T$ it was possible to carry out these measurements at a higher scan rate of 50 mV/s without any significant current peak distortion resulting from uncompensated solution resistance.

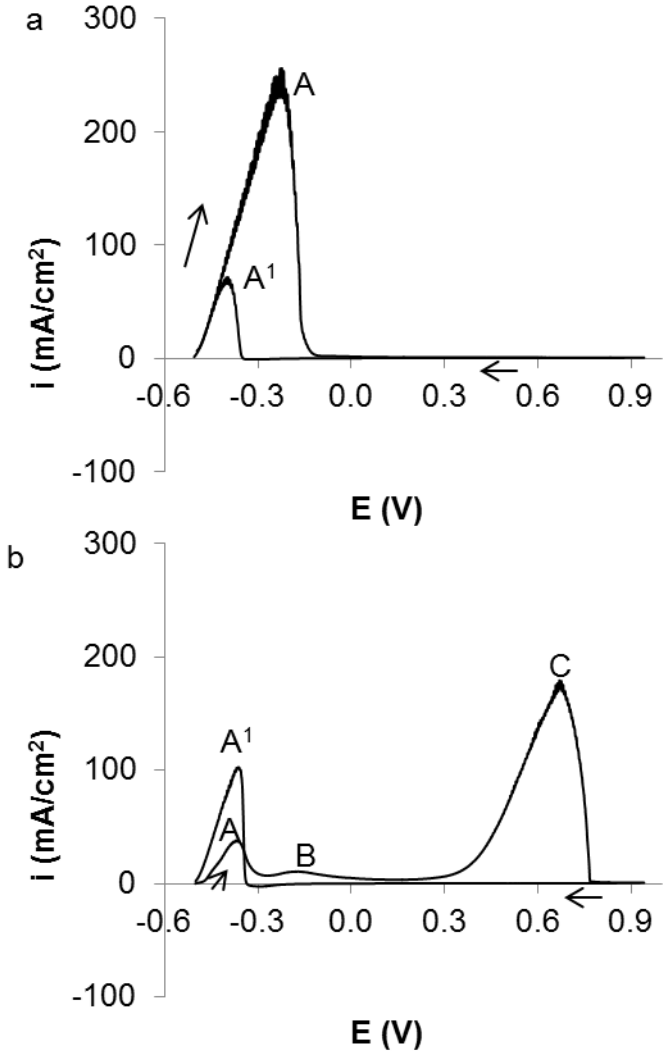

Figure 8.2 Rotating disk cyclic voltammetry (50 mV/s) of the Fe RDE in 6 M $[NH_3]_T$, 2 M $[CO_2]_T$, 0.15 M Ni(II) and 22 mM $S_2O_3^{2-}$ at different immersion times: a) upon immersion; b) following 2 hours of immersion.

Scanning the potential in the anodic direction from the OCP immediately upon immersion resulted in the anodic peak (A) assigned to the dissolution of iron to ferrous tetrammine according to half-reaction 5.1, as discussed in chapter 5.

As the applied potential was further increased, a sharp drop in current was observed at -0.4 V, with no significant currents being observed up to the inversion potential. During the cathodic scan, no significant currents were observed until the iron dissolution reaction was reactivated at potentials more negative than -0.3 V. When the same measurement was taken after 2 hours of immersion, the current densities observed during the anodic scan in the region of peak A were found to be almost an order of magnitude lower than those observed immediately upon immersion. A smaller current peak (B) was also observed around -0.18 V, followed by a much larger current which increased steeply at around 0.3 V peaking just above 0.6 V (peak C). A possible explanation for the lower currents at peak A is the formation of a surface species which covers the iron surface reducing the area of the anodic sites at which the oxidation of iron to ferrous tetrammine (half-reaction 5.1) is taking place. This is thought to consist of a nickel sulfide layer, as further discussed in sections 8.3 and 8.4, which is oxidised at more positive applied potentials resulting in peak C.

As can be seen from Figure 8.3, lower $[CO_2]_T$ at a constant $[NH_3]$ resulted in significantly smaller currents at peak C. This suggests that formation of the nickel sulfide may be favoured by higher $[CO_2]_T$ or by the resulting lower pH. This is also supported by the comparison of Figure 8.3 (b) with Figure 8.2 (b), in which immersion of the iron for only half the time at equal $[NH_3]$ and double $[CO_2]_T$ resulted in peak C being over an order of magnitude larger.

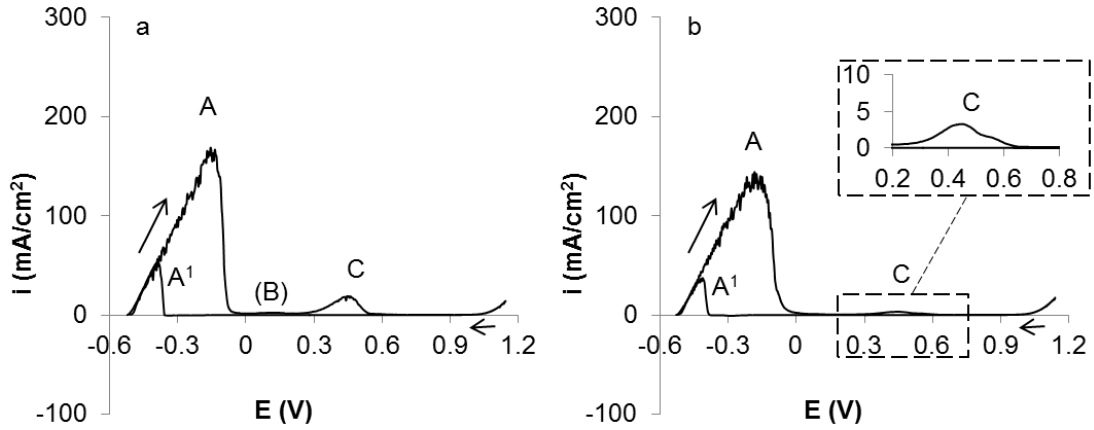

Figure 8.3 Rotating disk cyclic voltammetry (20 mV/s) of the Fe RDE following 4 hours of immersion in the presence of 0.15 M Ni(II), 22 mM $S_2O_3^{2-}$, and: a) 5.5 M $[NH_3]_T$, 1.5 M $[CO_2]_T$; b) 5 M $[NH_3]_T$, 1 M $[CO_2]_T$.

The voltammetric behaviour of the iron RDE following its passivation within 30 minutes at 3 M $[NH_3]_T$ (Figure 8.1, a) is shown in Figure 8.4. As expected, the peak due to the anodic dissolution of iron was not observed during the anodic scan, starting from the OCP of around 0.14 V, whereas peak C was visible in the 0.3 V to 0.6 V potential region. Other than the anodic current due to the evolution of oxygen observed above 1 V, no significant currents were observed until the applied potential was scanned to below -0.3 V, where reactivation of the anodic dissolution of iron (half-reaction 5.1) took place, resulting in peak A^1. The absence of peak B is consistent with the slight shoulder observed during the OCP transition (Figure 8.1, a) measured prior to the voltammetric measurement (Figure 8.4). Both the shoulder and peak B are thought to correspond to the same anodic dissolution process, which becomes thermodynamically favourable after the passivation of metallic iron takes place. In other words, the anodic dissolution process responsible for peak B is thought to take place spontaneously after metallic iron is no longer providing it with cathodic protection by acting as an anode.

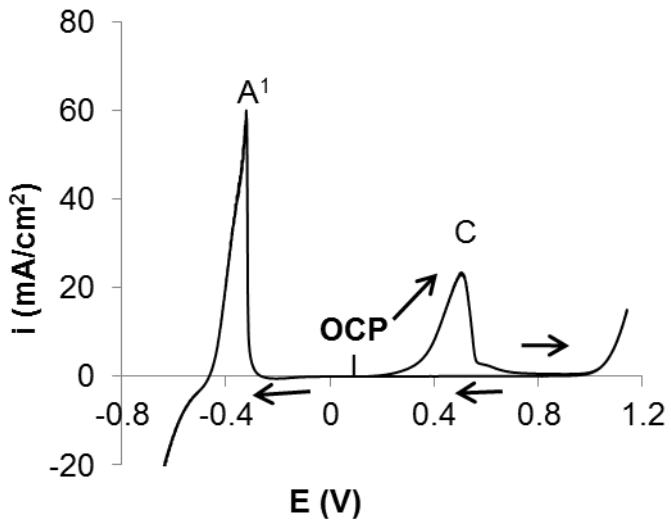

Figure 8.4 Rotating disk voltammetry (20 mV/s) of the Fe RDE following its passivation within 30 minutes immersion in 0.15 M Ni(II), 22 mM $S_2O_3^{2-}$, 3 M $[NH_3]_T$ and 1 M $[CO_2]_T$.

8.3 Surface layer characterisation and comparison with commercial Ni_3S_2

The surface of the iron RDE was immersed for 3 hours in a solution containing 5 M $[NH_3]_T$, 1 M $[CO_2]_T$, 0.15 M Ni(II) and 22 mM $S_2O_3^{2-}$. It was then rinsed with deionised water, allowed to dry in air, and analysed using SEM/EDX, which resulted in the detection of up to 29 at% nickel and 25 at% sulfur.

Further characterisation studies were conducted using GIXRD of the RDE surface following 2 hours of immersion under the conditions which had resulted in the largest observed anodic peak C (Figure 8.2, b). The resulting GIXRD pattern revealed the presence of a crystalline nickel sulfide (Ni_3S_2) within the surface layer. This is shown in Figure 8.5 (a), in which the XRD pattern of commercially available Ni_3S_2 (b) is also shown for comparison.

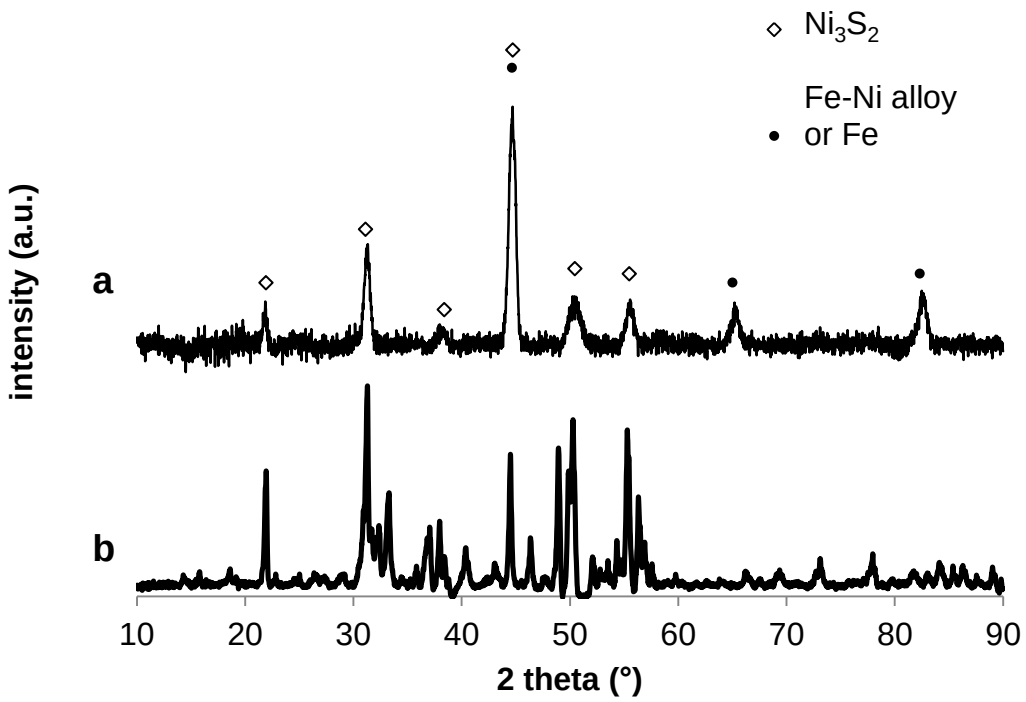

Figure 8.5 GIXRD pattern of: a) Fe RDE surface following 2 hours of immersion in 6 M $[NH_3]_T$, 2 M $[CO_2]_T$, 0.15 M Ni(II) and 22 mM $S_2O_3^{2-}$; b) XRD pattern of commercial Ni_3S_2.

The GIXRD analysis of the Fe RDE surface also indicated the presence of a strongly amorphous component affecting the baseline of the pattern, which was attributed to the RDE resin casing and subtracted from the pattern during the baseline correction. However, the existence of undetected amorphous nickel sulfide phases is not to be excluded.

The XRD pattern of commercially available Ni_3S_2 (Figure 8.5, b) was found to contain major diffraction lines which matched all six of the peaks used for the identification of Ni_3S_2 in the layer formed on the Fe RDE (Figure 8.5, a). The broader peaks observed for the latter suggest that it is likely to contain smaller crystallites than the commercial powder.

Additional diffraction peaks in the GIXRD pattern were observed at 2 theta = 45°, 65° and 82°. These may be attributed either to the underlying iron surface or to the formation of an iron-nickel alloy, identified by the XRD database comparison software as kamacite. The latter possibility was found to be consistent with some preliminary experiments conducted by immersing the iron RDE for 3 hours in a solution containing 5 M $[NH_3]_T$, 1 M $[CO_2]_T$ and 0.15 M Ni(II) and analysing its surface by SEM/EDX, which resulted in the detection of a significant amount of nickel (up to 20at%) on the iron surface.

8.4 Electrochemical response of commercial Ni_3S_2

In order to make a comparison between the electrochemical response of commercially available Ni_3S_2 and that of the layer formed on iron, a linear sweep voltammetry measurement was conducted on an RDE made of the commercially available powder pressed into a pellet. The current response obtained by scanning the applied potential in the anodic direction at 50 mV/s in 6 M $[NH_3]_T$ and 2 M $[CO_2]_T$ is shown in Figure 8.6 (curve a), with that obtained following a 2 hour immersion of the iron RDE in 6 M $[NH_3]_T$, $[CO_2]_T$, 0.15 M [Ni(II)] and 22 mM $[S_2O_3^{2-}]$ (curve b) also shown for comparison. The steeper increase in current density in curve b is consistent with a larger specific surface area due to the smaller size of the crystallites formed on the iron RDE, compared to the commercial powder, as consistent with the broader XRD peaks (Figure 8.5, a).

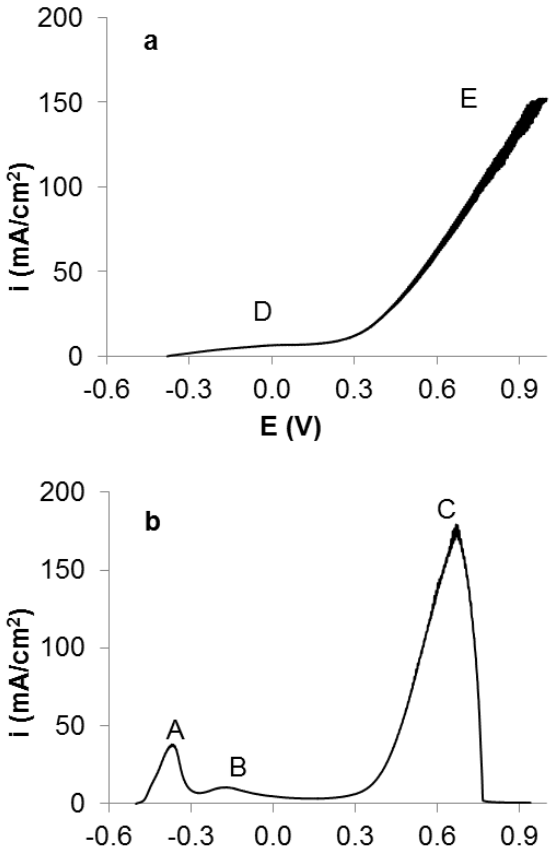

Figure 8.6 Anodic scan (50 mV/s) of: a) commercial Ni_3S_2 RDE in 6 M $[NH_3]_T$, 2 M $[CO_2]_T$; (b) Fe RDE following 2 hours of immersion at 6 M $[NH_3]_T$, 2 M $[CO_2]_T$, 0.15 M Ni(II) and 22 mM $S_2O_3^{2-}$.

Scanning the Ni_3S_2 RDE from its OCP of around -0.38 V resulted in a small increase in current density peaking slightly around 0 V (D). This was attributed to the partial oxidation of Ni_3S_2 in a process which may be described by half-reaction 8.1. A similar process is thought to be responsible for peak B observed on the iron RDE (Figure 8.6, b) and the shoulder in the OCP transition in Figure 8.1 (curve a).

$$Ni_3S_2 + 6xNH_3 \rightarrow Ni_{(3-x)}S_2 + xNi(NH_3)_6^{2+} + 2xe^- \quad (8.1)$$

As the applied potential was further scanned in the positive direction, a more significant current increase was observed at potentials above 0.2 V (E in Figure 8.6,

a). This was attributed to further oxidation of the sulfide, which overall may be described by half-reaction 8.2 or 8.3.

$$Ni_{(3-x)}S_2 + [6\cdot(3-x)]NH_3 \rightarrow (3-x)Ni(NH_3)_6^{2+} + 2S + [2(3-x)+6]e^- \quad (8.2)$$

$$Ni_{(3-x)}S_2 + 3OH^- + [6\cdot(3-x)+3]NH_3 \rightarrow (3-x)Ni(NH_3)_6^{2+} + S_2O_3^{2-} + 3NH_4^+ + [2(3-x)+6]e^- \quad (8.3)$$

The formation of elemental sulfur according to half-reaction 8.3 is consistent with previous studies in which it was found to be favoured under oxidising conditions in ammoniacal solutions at temperatures below 50ºC and pH 10.5 to 11 (Muir et al., 1981), therefore under the conditions of this study. This is further investigated and discussed in section 8.6.

A number of oxidative half-reactions which may describe some of the processes taking place on either electrode in the potential region of peaks B and D (reactions 8.4-8.7) or E (reactions 8.8-8.10) and the corresponding standard reduction potentials are given in Table 8.1.

Table 8.1 Oxidation half-reactions and corresponding standard reduction potentials*

Ni_3S_2 – NiS – NiS_2 oxidation half-reactions	**E° (V)**
$Ni_3S_2 + 6NH_3 \rightarrow 2NiS + Ni(NH_3)_6^{2+} + 2e^-$ (8.4)	-0.35
$Ni_3S_2 + 17NH_3 + NH_4^+ \rightarrow 3Ni(NH_3)_6^{2+} + HS_2^- + 4e$- (8.5)	-0.03
$Ni_3S_2 + 18NH_3 \rightarrow 3Ni(NH_3)_6^{2+} + S_2^{2-} + 4e^-$ (8.6)	0.01
$Ni_3S_2 + 3OH^- + 21NH_3 \rightarrow 3Ni(NH_3)_6^{2+} + S_2O_3^{2-} + 3NH_4^+ + 10e^-$ (8.7)	-0.29
$2NiS + 6NH_3 \rightarrow NiS_2 + Ni(NH_3)_6^{2+} + 2e^-$ (8.8)	-0.20
$NiS_2 + 6NH_3 \rightarrow Ni(NH_3)_6^{2+} + 2S + 2e^-$ (8.9)	0.15
$NiS_2 + 9NH_3 + 3OH^- \rightarrow Ni(NH_3)_6^{2+} + S_2O_3^{2-} + 3NH_4^+ + 6e^-$ (8.10)	0.30

***calculated from HSC 7 data (Roine, 2009)**

8.5 Dissolution of the Ni_3S_2-containing surface layer formed on iron

In order to assess the dissolution behaviour of the nickel sulfide surface layer formed during immersion of the iron RDE in ammoniacal-carbonate solutions containing nickel(II) and thiosulfate ions, it was allowed to form in a solution containing 3 M $[NH_3]_T$, 1 M $[CO_2]_T$, 0.15 M Ni(II) and 22 mM $S_2O_3^{2-}$. As shown in Figure 8.1 (curve a) this resulted in passivation of the iron RDE, which was removed from the solution and then re-immersed in a barren ammoniacal-carbonate solution containing 6 M $[NH_3]_T$ and 2 M $[CO_2]_T$. The concentrations of dissolved nickel, iron and sulfur species were monitored over a period of 5.5 hours, along with the OCP of the electrode (Figure 8.7).

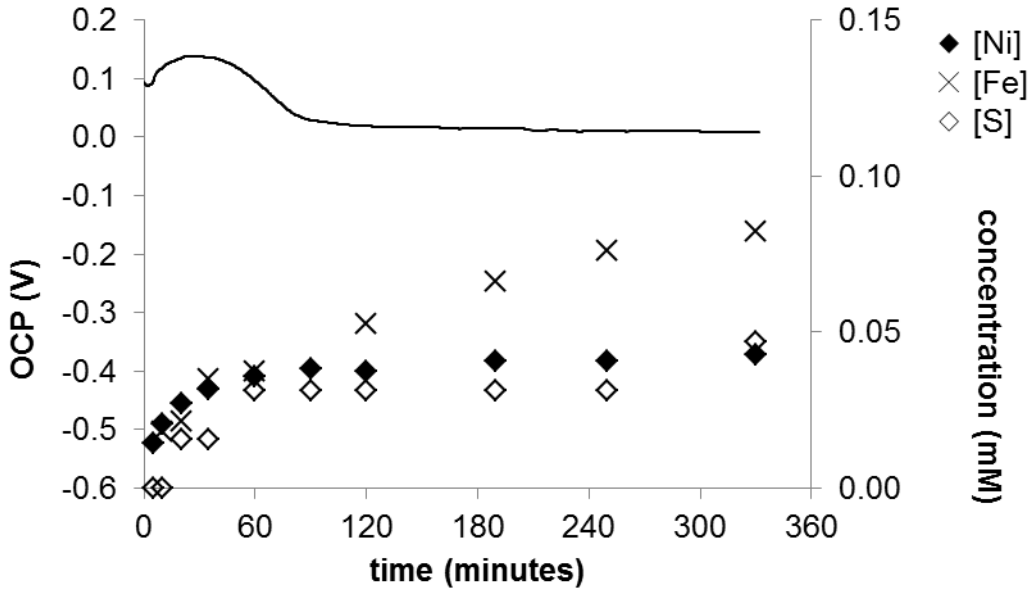

Figure 8.7 OCP and concentrations of dissolved nickel, sulfur and iron (as indicated in the legend) during immersion of the Fe RDE in 6 M $[NH_3]_T$, 2 M $[CO_2]_T$, following its pre-treatment in 3 M $[NH_3]_T$, 1 M $[CO_2]_T$, 0.15 M Ni(II) and 22 mM $S_2O_3^{2-}$.

Assuming a uniformly distributed layer on the RDE surface, the initial dissolution of nickel and iron took place at rates of around 7×10^{-10} mol s^{-1} cm^{-2} and 4×10^{-10} mol s^{-1} cm^{-2}, respectively. It was not possible to determine the initial dissolution rate of

sulfur, due to the large analytical error in the measurement of its concentration and the fact that no sulfur was detected during the first 10 minutes of immersion. After 1.5 hours, the concentration of nickel(II) was found to reach approximately 0.04 mM, ~90% of the concentration reached after 5.5 hours. The sulfur concentration also appeared level off at around the same time, but the large analytical error in its determination did not allow further conclusions to be drawn.

During the first 1.5 hours of immersion, the OCP of the electrode increased to a maximum value of around 0.14 V within the first half-hour of immersion, remaining in this region for around 20 minutes, before decreasing to values around 0.03 V over the next half-hour. For the remainder of the measurement, the OCP decreased very gradually from its value of around 0.03 V to 0.01 V. This behaviour correlates well with the initial ~1.5 hour period of faster dissolution of the nickel and sulfur, during which the mixed potential of the electrode is thought to have been influenced mainly by the surface species responsible for peak C. Beyond this period, the nickel and sulfur dissolution rates began to level off, and the mixed potential was possibly influenced mainly by the underlying iron oxide, from which the iron continued to dissolve at an approximate rate of around $5x10^{-11}$ mol $s^{-1}cm^{-2}$.

8.6 Rotating disk cyclic voltammetry of commercial Ni_3S_2

The characterisation and electrochemical results discussed in sections 8.3 and 8.4 have indicated that the commercial Ni_3S_2 powder is reasonably similar to the layer formed on iron, with the voltammetric scan resulting in anodic processes that are consistent with those observed for the layer on the iron RDE. It was therefore considered useful to further investigate the electrochemical behaviour of the Ni_3S_2 RDE under the conditions of the Caron process, in order to shed more light on the

potential implications of the formation of such layer, whilst avoiding any interference from the underlying iron.

The voltammetric behaviour of the Ni_3S_2 RDE was studied at different scan rates in solutions containing 5 M $[NH_3]_T$ and 1 M $[CO_2]_T$. At scan rates of 20 mV/s and lower, a clearly defined anodic peak (E) became visible at around 0.9 V (Figure 8.8). During the cathodic scan of the measurement conducted at 20 mV/s, an increase in cathodic current was observed in the -0.2 V to -0.6 V potential region, followed by a slightly steeper increase at more negative potentials, peaking around -0.65 V (F). Changing the rotation speed of the electrode between 100 and 700 rpm was not found to have any significant effect on peaks E and F (Figure 8.9), which is consistent with the corresponding reactions not being limited by solution-diffusion processes.

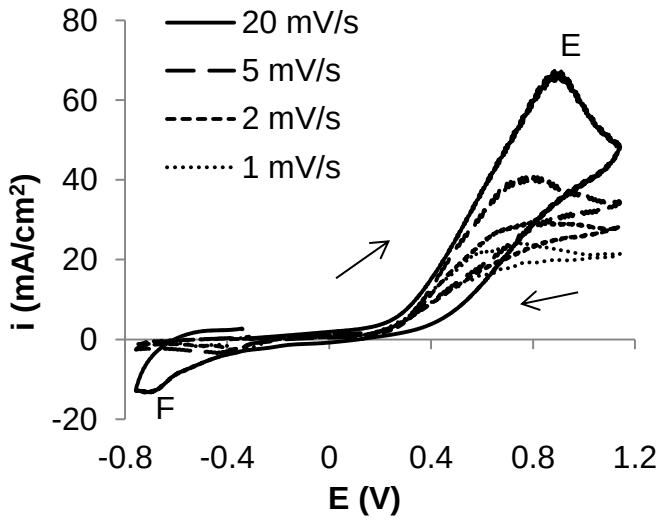

Figure 8.8 Rotating disk cyclic voltammetry of the Ni_3S_2 RDE in solutions containing 5 M $[NH_3]_T$ and 1 M $[CO_2]_T$ at different scan rates, as given in the legend.

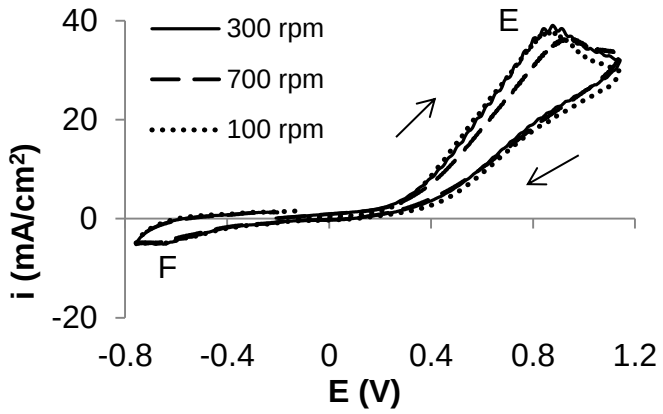

Figure 8.9 Rotating disk cyclic voltammetry (10 mV/s) of the Ni_3S_2 RDE in solution containing 5 M $[NH_3]_T$ and 1 M $[CO_2]_T$ at the different electrode rotation speeds as given in the legend.

As can be seen from Figure 8.10, which shows in more detail the cathodic part of cyclic voltammetry measurements taken at different scan rates, peak F was no longer observed at the slower scan rates of 5 and 2 mV/s, while a peak (G) became visible at around -0.4 V.

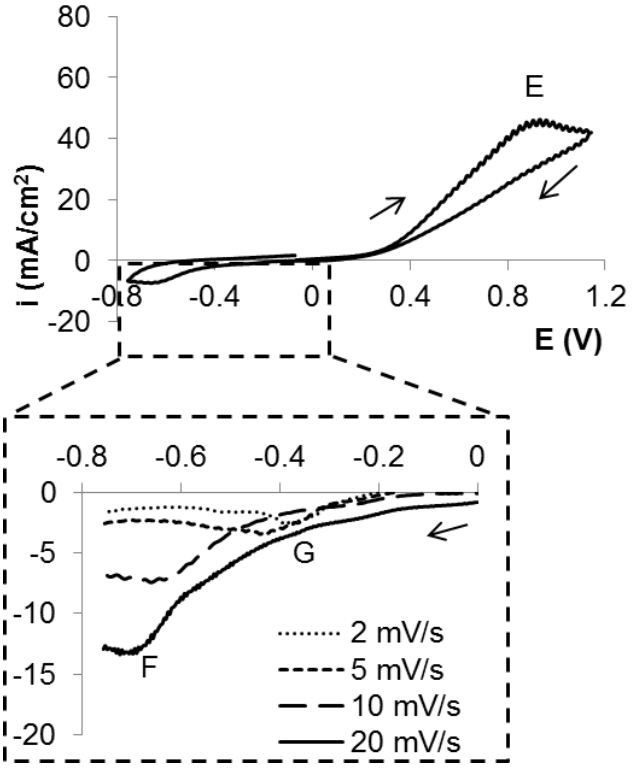

Figure 8.10 Rotating disk cyclic voltammetry (10 mV/s) of the Ni_3S_2 RDE in 5 M $[NH_3]_T$ and 1 M $[CO_2]_T$ and detail of the cathodic sweep currents at different scan rates, as given in the legend.

As shown in Figure 8.11, further decreasing the scan rate to 1 mV/s resulted in a shoulder preceding anodic peak E, at around 0.6 V (E^1). This suggested that further oxidation of the nickel-deficient sulfide formed by half-reaction 8.1 may involve the formation of an intermediate product such as NiS_2. This is described by half-reaction 8.11, to which the shoulder E^1 may possibly be attributed.

$$Ni_{(3-x)}S_2 + 6\cdot(2-x)\ NH_3 \rightarrow NiS_2 + (2-x)Ni(NH_3)_6^{2+} + 2\cdot(2-x)e^- \qquad (8.11)$$

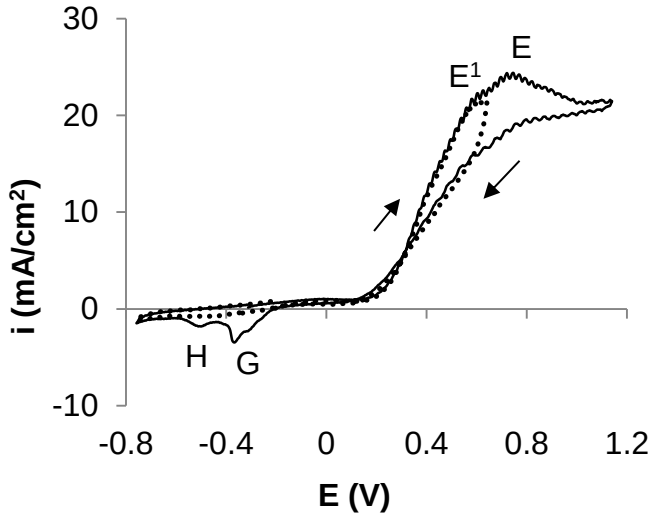

Figure 8.11 Rotating disk cyclic voltammetry of synthetic Ni_3S_2 in solution containing 5 M $[NH_3]_T$ and 1 M $[CO_2]_T$ scanned at 1 mV/s with different inversion potentials (solid line: 1.14 V; dotted line: 0.64 V).

The slower scan rate also resulted in a more clearly defined cathodic peak (G) which was followed by a second smaller peak (H) around -0.5 V. These were not observed when the potential scan was inverted immediately after E^1, prior to reaching peak E, suggesting that the process taking place at peak E resulted in the formation of a species which remained on the electrode surface, to then be reduced during the cathodic scan at peaks G and H.

A possibility is that this consists of elemental sulfur formed in the nickel deficient outer layer of the electrode at high anodic potentials, which may be reduced back to

a polysulfide first (G) and then a sulfide (H). This is consistent with the potential region in which the reduction of sulfur is expected to take place, for which a number of possible reduction reactions and corresponding E° are given in Table 8.2.

Table 8.2 Standard potentials for sulfur/polysulfide reduction half-reactions*

$S / HS_2^- / S_2^{2-}$ reduction half-reactions	**E° (V)**
$2S + NH_4^+ + 2e^- \rightarrow HS_2^- + NH_3$ (8.12)	-0.33
$HS_2^- + NH_4^+ + 2e^- \rightarrow 2HS^- + NH_3$ (8.13)	-0.34
$2S + 2e^- \rightarrow S_2^{2-}$ (8.14)	-0.41
$S_2^{2-} + 2e^- \rightarrow 2S^{2-}$ (8.15)	-0.48

*calculated from HSC 7 data (Roine, 2009)

8.7 Discussion of reactions

The observed formation of Ni_3S_2 on the iron RDE is thought to have taken place via the reduction of both nickel(II) and thiosulfate ions by the metallic iron. This may be described by half-reactions 8.16 and 8.17, for which the standard reduction potentials calculated from HSC 7 data are -0.47 V and -0.03 V respectively. These are more positive than the standard reduction potential of the ferrous tetrammine/iron couple (half-reaction 5.1, section 5.7), for which values between -0.55 V and -0.59 V have been reported (Kim et al., 1991; Lee et al., 1985; Nikoloski and Nicol, 2006; Senanayake et al., 2010). This indicates that under standard conditions, half-reactions 8.16 and 8.17 are thermodynamically feasible, if coupled to the oxidation of metallic iron to ferrous tetrammine. It should be noted that half-reaction 8.16 is also driven by the removal of HS^- from solution as it precipitates as Ni_3S_2 in half-reaction 8.17.

$$S_2O_3^{2-} + 4NH_4^+ + 6e^- \rightarrow HS_2^- + 4NH_3 + 3OH^- \quad (8.16)$$

$$3Ni(NH_3)_6^{2+} + HS_2^- + 4e^- \rightarrow Ni_3S_2 + 17NH_3 + NH_4^+ \quad (8.17)$$

Therefore, the overall process taking place on the iron surface may be described by reaction 8.18, for which the $\Delta G°$ was calculated to be -290 kJ/mol based on available thermodynamic data (Isaev et al., 1990a; Roine, 2009).

$$5Fe + 3Ni(NH_3)_6^{2+} + S_2O_3^{2-} + 3NH_4^+ \rightarrow 5Fe(NH_3)_4^{2+} + Ni_3S_2 + NH_3 + 3OH^- \quad (8.18)$$

As discussed in section 8.3, the surface layer characterisation studies also suggested the possible deposition of metallic nickel, with formation of an iron-nickel alloy. The standard potential for the reduction of nickel hexammine to metallic nickel (reaction 8.5) was calculated from available thermodynamic data to be around -0.50 V (Roine, 2009).

$$Ni(NH_3)_6^{2+} + 2e^- \rightarrow Ni + 6NH_3 \quad (8.19)$$

This value is more positive than the standard reduction potential of the ferrous tetrammine/iron couple, as discussed above, suggesting that the displacement of metallic iron by nickel, resulting in cementation of the nickel onto the iron (reaction 4.1, section 4.2.2), is also thermodynamically feasible under standard conditions. The equilibrium potential of the nickel hexammine/nickel couple under the experimental conditions is around -0.67 V, whereas that of the ferrous tetrammine/iron couple at an arbitrarily low $[Fe(NH_3)_4^{2+}]$ of 10^{-4}, 6 M $[NH_3]$ and 45°C is estimated to be around -0.77 V. This further supports the feasibility of the cementation of nickel under the conditions of the experiment. A potential-pH

diagram constructed for the Ni-NH_3-CO_3^{2-}-H_2O system under the experimental conditions is shown in Figure 8.12, a.

Depending on the relative reaction kinetics of reaction 8.18 and 8.19, it is possible that the formation of Ni_3S_2 was preceded by the cementation of metallic nickel followed by its partial re-oxidation by thiosulfate ions. This may be described by reaction 8.20, for which $\Delta G°$ was calculated to be -146 kJ/mol (Roine, 2009). In the presence of metallic iron, the process may be described by reaction 8.21, for which $\Delta G°$ was calculated to be -234 kJ/mol (Isaev et al., 1990a; Roine, 2009).

$$3Ni + 2S_2O_3^{2-} \rightarrow Ni_3S_2 + 2SO_3^{2-} \quad (8.20)$$

$$3Ni + 2Fe + S_2O_3^{2-} + 3NH_4^{+} + 5NH_3 \rightarrow Ni_3S_2 + 2Fe(NH_3)_4^{2+} + 3OH^{-} \quad (8.21)$$

An Eh-pH diagram constructed for the Ni-S-NH_3-CO_3^{2-}-H_2O system under the experimental conditions is shown in Figure 8.12 (b). The stability region of metastable thiosulfate ions under the same conditions is overlaid for comparison, as indicated by the thinner lines. Although it was not possible to show the $S_2O_3^{2-}$/Ni_3S_2 boundary on the same diagram, comparison of the thiosulfate stability region with the Ni_3S_2/Ni boundary, and with the $Fe(NH_3)_4^{2+}$/Fe equilibrium potential discussed above, supports the thermodynamic feasibility of reaction 8.21 under the conditions of the experiments.

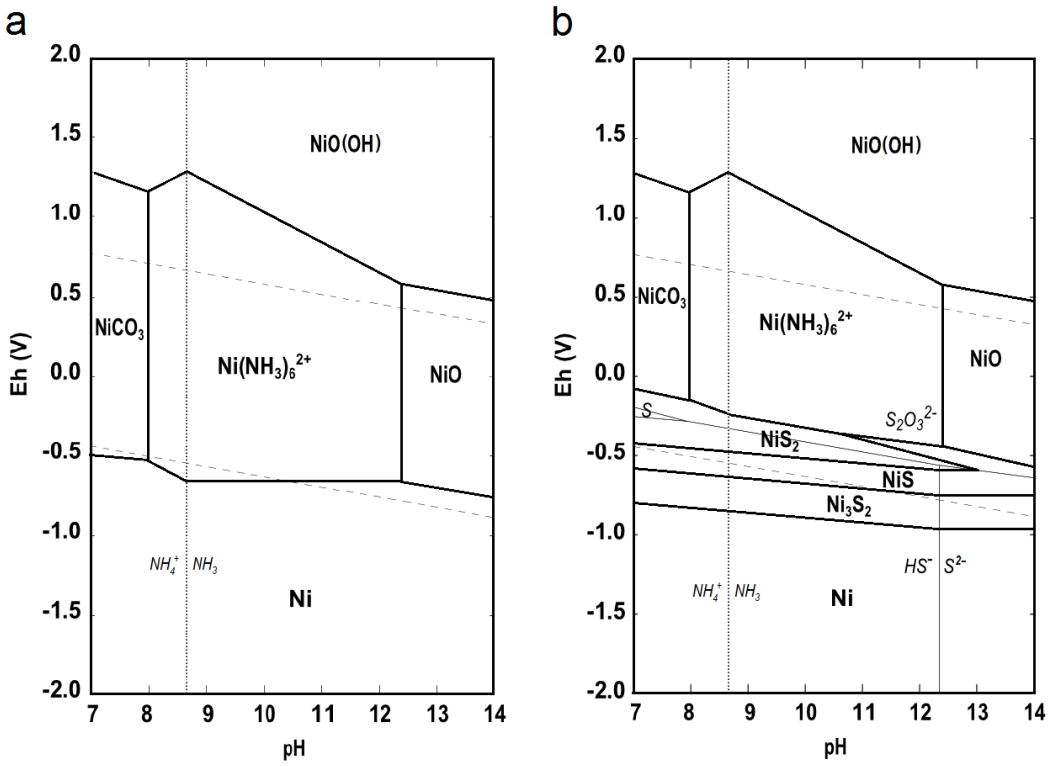

Figure 8.12 Eh-pH diagrams constructed using the HSC 7 thermodynamic database and software (Roine, 2009) for Ni-NH_3-CO_3^{2-}-H_2O (a) and Ni-S-NH_3-CO_3^{2-}-H_2O (b) at [NH_3] = 6 m, [CO_2] = 2 m, [Ni(II)] = 0.1 m, [$S_2O_3^{2-}$] = 0.02 m, 45°C. The thick lines correspond to the boundaries of the predominance regions of Ni species, the dashed lines to the H_2O limits and the dotted lines to the NH_3/NH_4^+ equilibrium boundary. Thin lines in Figure b indicate the stability regions of metastable thiosulfate ions and elemental sulfur.

These results from the rotating disk cyclic voltammetry study conducted on the Ni_3S_2 RDE indicated that, under the conditions of the Caron process, the dissolution of this sulfide was limited by the formation of a sulfur-rich layer, which may only dissolve under highly oxidising conditions. The dissolution process taking place in the lower potential region, between the OCP and 0.1 V (half-reaction 8.1) is thought to be responsible for the formation of the sulfur-rich species, which is further oxidised only at potentials above 0.2 V. However, even under highly oxidising conditions, the formation of elemental sulfur may also possibly hinder further dissolution of the nickel sulfide.

8.8 Summary

The anodic dissolution of iron in ammoniacal-carbonate solutions containing nickel(II) and thiosulfate ions results in the formation of Ni_3S_2, as supported by the GIXRD analysis of an iron RDE surface following its immersion under open circuit conditions. This was found to be consistent with thermodynamic calculations which predicted the feasibility of this spontaneous redox process.

Rotating disk cyclic voltammetry studies also supported the formation of Ni_3S_2, which was found to be favoured by increasing $[CO_2]_T$ and decreasing $[NH_3]_T$, and possibly implicated in an iron passivation mechanism which was only observed at a lower $[NH_3]_T$ of 3 M.

Even though the passivation of iron in these solutions was not observed at the higher $[NH_3]_T$ encountered in the Caron process, the formation of a Ni_3S_2 is favoured whilst metallic iron is in its active dissolution state. However, it is not expected to take place to a significant extent under the conditions of the process, particularly if lower $[CO_2]_T$ of around 1 M are employed. Therefore nickel losses into a sulfide layer are likely to be insignificant.

However, once formed, the redissolution of Ni_3S_2 is thought to be limited by the formation of a nickel-deficient nickel sulfide layer. This is likely to require strongly oxidising conditions for its dissolution to take place, as indicated by the electrochemical measurements conducted as part of this study. Further investigations are necessary in order to assess its dissolution behaviour under aerated or oxygenated conditions or in the presence of other oxidants, but these are beyond the scope of the present study, considering that the formation of Ni_3S_2 is thought to be insignificant under the conditions of the Caron process.

9 CONCLUSION

The electrochemical behaviour of metallic iron in ammoniacal-carbonate solutions such as those employed in the Caron process is known to strongly influence the dissolution behaviour of metallic nickel and cobalt. In particular, the passivation of iron and of its alloys with nickel and cobalt may be responsible, at least in part, for the incomplete dissolution of these metal values from the pre-reduced ore, especially if this passivation takes place during the early stages of the leach.

In addition to this, the presence of metallic iron has the potential to result in the formation of metal sulfides via complex redox reactions involving the reduction of the dissolved metals and of thiosulfate ions. The loss of metal values from the leach liquor as they precipitate into the so-formed sulfide layer may also further affect the metal extraction efficiency of the process, particularly if complete redissolution of the sulfide layer does not take place prior to the solid-liquid separation stage.

In the present study, both these aspects were investigated by electrochemical techniques, with the aim of identifying the specific dissolved species which caused the passivation of metallic iron and resulted in the formation of metal sulfides on its surface. The dissolved species investigated were nickel(II), cobalt(II), copper(II) and thiosulfate ions. SEM/EDX and XRD characterisation studies were carried out in order to identify the sulfide species formed on the iron surface, and the dissolution behaviour of these sulfides was also assessed, to determine the likelihood of their redissolution during the Caron leach.

Under conditions similar to those of the Caron process, the passivation of iron was not found to take place in thiosulfate-free solutions containing nickel(II) and/or cobalt(II) species, but took place readily in the presence of copper(II) ions. The

passivation was found to take place even at millimolar copper(II) concentrations, at ammonia and carbonate concentrations typically encountered at Caron plants, and it was observed for iron-nickel and iron-cobalt alloys, as well as for pure iron. The immersion time required for the passivation to take place was found to decrease for increasing [Cu(II)], and decreasing $[NH_3]_T$ and $[CO_2]_T$. Based on SEM/EDX and electrochemical studies, the passivation mechanism was found to take place via the cementation of metallic copper and its subsequent redissolution, which resulted in the formation of a stable protective oxide layer on the iron surface.

This behaviour, however, was only observed in solutions not containing any thiosulfate ions. When both copper(II) and thiosulfate ions were present, passivation of the iron was not observed, although the cementation of metallic copper was found to take place even in the presence of both species, as confirmed by the characterisation studies. UV-Visible studies of the solutions indicated that the oxidation of thiosulfate by copper(II) in the presence of metallic iron was insignificant. The reduction of both copper(II) and thiosulfate ions was found to take place on the metallic iron surface, resulting in the formation of a partially-adherent surface layer, which, based on XRD studies, was found to contain metallic copper dendrites, cuprous sulfide and cuprous oxide. The continuous formation and detachment of this layer during the active dissolution of the metallic iron was thought to interfere with the formation of a protective oxide layer, disrupting the passivation mechanism which would otherwise be expected to take place, as observed in the absence of thiosulfate ions.

On the other hand, the presence of both cobalt(II) and thiosulfate ions was found to promote the passivation of metallic iron. In this case, the formation of an adherent layer containing an amorphous CoS_x species was observed on the iron surface

following its immersion, and electrochemical studies indicated that it was likely to be implicated in the mechanism of passivation of the iron. The immersion time required for passivation to take place was found to decrease for increasing [Co(II)], decreasing $[NH_3]_T$ and, in contrast with the behaviour observed in the presence of copper(II) ions, increasing $[CO_2]_T$. In this case, passivation took several hours, compared to a few minutes in the presence of similar concentrations of copper(II). Moreover, it was consistently observed only at lower total ammonia concentrations ($\leq$4 M) than are generally encountered in the Caron leach. Nevertheless, formation of the CoS_x layer was found to result in the suppression of the anodic dissolution of iron, as indicated by rotating disk cyclic voltammetry studies.

The formation of this CoS_x layer is likely to have implications which go beyond the fact that it suppressed dissolution or promoted passivation of the metallic iron. The loss of cobalt from the leach liquor by precipitation into this layer is likely to be a contributing factor to the low cobalt extractions suffered by the Caron process.

Despite a concentration of more than an order of magnitude higher than cobalt(II) or copper(II), the presence of nickel(II), either alone or together with thiosulfate ions, was not found to have a significant effect on the behaviour of metallic iron in ammoniacal-carbonate solutions. Although it was found that some nickel is likely to cement onto the dissolving metallic iron, this was not found to result in the passivation of iron, as in the case of copper(II).

Following immersion in the presence of both nickel(II) and thiosulfate ions, GIXRD studies of the iron surface were consistent with the formation of some Ni_3S_2 by reduction of both the nickel(II) and thiosulfate ions. However, rotating disk cyclic voltammetry measurements indicated that detectable amounts were only formed at

higher $[CO_2]_T$ and lower $[NH_3]_T$ than encountered under typical Caron process conditions. At a significantly lower $[NH_3]_T$ of 3 M, the passivation of iron was also observed and thought to take place via a similar mechanism to that promoted by the CoS_x layer. However, this was not found to take place under the conditions of the Caron process, and the formation of Ni_3S_2 is not thought to take place to a significant extent, when compared to the dissolved nickel(II) concentration. Nevertheless, rotating disk cyclic voltammetry studies conducted on commercially available Ni_3S_2 suggest that once formed, its redissolution becomes limited by the formation of a sulfur-rich layer which requires highly oxidising conditions in order to be dissolved. However, in practice this is not likely to adversely affect the nickel extraction efficiency of the Caron process, as the loss of nickel(II) from the leach liquor by precipitation into the sulfide layer is expected to be insignificant.

Overall, out of the dissolved metals studied, copper(II) was found to have the greatest effect on the behaviour of metallic iron in the absence of thiosulfate ions, by readily promoting its passivation. However, this is unlikely to be one of the factors affecting the Caron process in practice, because the leach liquor usually also contains thiosulfate ions, which effectively prevent the passivation of iron caused by the presence of copper(II). Based on the results of this study, it can be concluded that the factor most likely to adversely affect the extraction efficiency of the Caron process is the formation of CoS_x, mainly due to the resulting loss of dissolved cobalt from the solution, as well as its negative effect on the dissolution of metallic iron. The conditions that promote the formation of the sulfide layer, such as increasing $[CO_2]_T$ and decreasing $[NH_3]_T$, should therefore be taken into account when considering changes to the process conditions to improve cobalt recoveries. It should be kept in mind that, whilst thiosulfate ions are responsible for the formation of the CoS_x layer,

they also play a beneficial role as oxidants in the leach, as well as preventing the passivation of iron by other mechanisms, such as in the presence of copper(II). Therefore, if formation of the cobalt-containing sulfide layer cannot be prevented, further investigations aimed at improving the cobalt recoveries should be focussed on optimising the process conditions in order to favour the redissolution of the sulfide layer following the passivation of metallic iron.

The results of this study may potentially have broader implications which go beyond the effect of iron passivation on the extraction of nickel and cobalt from laterite ores. Since steel is the material of choice for reactors used in several alkaline processes, it may be useful to extend this research to further understand and develop methods for forming a stable passive layer on iron or steel, in order to make it capable of withstanding specific harsh process conditions, hence preventing corrosion damage.

REFERENCES

Agrawal, R.D. and Kapoor, M.L., 1982. Theoretical considerations of the cementation of copper with iron. Journal of the South African Institute of Mining & Metallurgy, 82(4): 106-11.

Anthony, E.Y. and Williams, P.A., 1994. Thiosulfate complexing of platinum-group elements - implications for supergene geochemistry. American Chemical Society, pp. 551-560.

Armstrong, R.D. and Coates, A.C., 1974. The passivation of iron in carbonate/bicarbonate solutions. Journal of electroanalytical chemistry and interfacial electrochemistry, 50(3): 303-313.

Asselin, E., 2008. Thermochemical aspects of the Fe, Ni & Co - NH_3-H_2O systems relevant to the Caron process Hydrometallurgy VI. SME, Phoenix, Arizona, pp. 522-531.

Aylmore, M.G. and Muir, D.M., 2001. Thiosulfate leaching of gold—A review. Minerals Engineering, 14(2): 135-174.

Bard, A.J. and Faulkner, L.R., 1980. Electrochemical Methods: Fundamentals and Applications. John Wiley & Sons, New York.

Berezowsky, R., 2004. Nickel extraction technology development, MEMS 13th Annual Conference, Toronto, Ontario.

Bhuntumkomol, K., Han, K.N. and Lawson, F., 1980. Leaching behavior of metallic nickel in ammonia solutions. Transactions of the Institution of Mining and Metallurgy, Section C: Mineral Processing and Extractive Metallurgy, 89(March): 7-13.

Biswas, A.K. and Reid, J.G., 1972. Cementation of copper on iron, Australasian Institute of Mining and Metallurgy Conference, pp. 37-45.

Black, S.B., 2006. The thermodynamic chemistry of the aqueous copper-ammonia thiosulfate system. PhD Thesis, Murdoch University.

Blengino, J.M., Keddam, M., Labbe, J.P. and Robbiola, L., 1995. Physico-chemical characterization of corrosion layers formed on iron in a sodium carbonate-bicarbonate containing environment. Corrosion Science, 37(4): 621-643.

Bockris, J.O.M. and Reddy, A.K.N., 1970. Modern Electrochemistry, 2. Plenum Press, New York.

Bohe, A.E., Vilche, J.R. and Arvia, A.J., 1984. The potentiodynamic response of polycrystalline nickel electrodes in 0.5 M potassium carbonate. Journal of Applied Electrochemistry, 14(5): 645-52.

Bohe, A.E., Vilche, J.R. and Arvia, A.J., 1990. The electrochemical behavior of polycrystalline nickel electrodes in different carbonate-bicarbonate ion-containing solutions. Journal of Applied Electrochemistry, 20(3): 418-26.

Boldt, J.R. and Queneau, P.E., 1967. Extractive Metallurgy of Oxide Ores, The Winning of Nickel. Methuen, London, pp. 425-453.

Borjas, N.M., 2004. Ore variability influence on the metallurgical process, International Laterite Nickel Symposium. TMS, Charlotte, US, pp. 113-120.

Breuer, P.L. and Jeffrey, M.I., 2003. The reduction of copper(II) and the oxidation of thiosulfate and oxysulfur anions in gold leaching solutions. Hydrometallurgy, 70(1–3): 163-173.

Buckley, A.N. and Woods, R., 1991. Electrochemical and XPS studies of the surface oxidation of synthetic heazlewoodite (Ni_3S_2). Journal of Applied Electrochemistry, 21(7): 575-82.

Bunjaku, A., 2013. The effect of mineralogy, sulphur, and reducing gases on the reducibility of saprolitic nickel ores. PhD Thesis, Aalto University, Finland.

Burkin, A.R., 1987. Extractive Metallurgy of Nickel. John Wiley & Sons, New York.

Burstein, G.T. and Davies, D.H., 1980. The analysis of anodic films formed on cobalt in bicarbonate and borate electrolytes. Corrosion Science, 20(8-9): 989-95.
Burzynska, L., Gumowska, W., Rudnik, E. and Partyka, J., 2008. Mechanism of the anodic dissolution of Cu70-Co4-Fe14-Pb7 alloy originated from reduced copper converter slag in an ammoniacal solution: Recovery of copper and cobalt. Hydrometallurgy, 92(1-2): 34-41.
Byerley, J.J., Fouda, S.A. and Rempel, G.L., 1973a. Kinetics and mechanism of the oxidation of thiosulfate ions by copper(II) ions in aqueous ammonia solution. Journal of the Chemical Society, Dalton Transactions: 889-893.
Byerley, J.J., Fouda, S.A. and Rempel, G.L., 1973b. The oxidation of thiosulfate in aqueous ammonia by copper(II) oxygen complexes. Inorganic and Nuclear Chemistry Letters 9: 879-883.
Byerley, J.J., Fouda, S.A. and Rempel, G.L., 1975. Activation of copper(II) ammine complexes by molecular oxygen for the oxidation of thiosulfate ions. Journal of the Chemical Society, Dalton Transactions: 1329-1338.
Caldeira, C.L., Ciminelli, V.S.T. and Osseo-Asare, K., 2008. Pyrite oxidation in alkaline solutions: the carbonate effect, Hydrometallurgy IV. SME, Phoenix, Arizona, pp. 990-999.
Calderón, J.A., Barcia, O.E. and Mattos, O.R., 2008. Reaction model for kinetic of cobalt dissolution in carbonate/bicarbonate media. Corrosion Science, 50(7): 2101-2109.
Canterford, J.H., 1978. Mineralogical aspects of the extractive metallurgy of nickeliferous laterites, Australasian Institute of Mining and Metallurgy Conference, North Queensland, pp. 361-370.
Canterford, J.H. and Turnbull, A.G., 1980. The reduction of nickeliferous laterites: thermodynamic considerations, Australasian Institute of Mining and Metallurgy Conference, pp. 43-51.
Caron, M.H., 1920. Process of treating nickel ores, US Patent 1,346,175.
Caron, M.H., 1924. Process of recovering values from nickel and cobalt-nickel ores, US Patent 1,487,145.
Caron, M.H., 1950. Ammonia leaching of nickel and cobalt ores. Journal of Metals - Transactions AIME, 188: 67-90.
Castro, E.B., Valentini, C.R., Moina, C.A., Vilche, J.R. and Arvia, A.J., 1986. The influence of ionic composition on the electrodissolution and passivation of iron electrodes in potassium carbonate-bicarbonate solutions in the 8.4-10.5 pH range at 25°C. Corrosion Science, 26(10): 781-789, 791-793.
Castro, E.B. and Vilche, J.R., 1991. Electrooxidation/electroreduction processes at composite iron hydroxide layers in carbonate-bicarbonate buffers. Journal of Applied Electrochemistry, 21(6): 543-51.
Castro, E.B., Vilche, J.R. and Arvia, A.J., 1991. Iron dissolution and passivation in K_2CO_3-$KHCO_3$ solutions. rotating ring disc electrode and XPS studies. Corrosion Science, 32(1): 37-50.
Chander, S. and Sharma, V.N., 1981. Reduction roasting/ammonia leaching of nickeliferous laterites. Hydrometallurgy, 7(4): 315-327.
Chang Cardona, A.R. and Rojas Vargas, A., 2009. La lixiviación del proceso Caron: sintesis del conocimiento para su perfeccionamiento industrial. Parte I. Tecnologia Quimica, 29(1): 98-107.
Chen, T.T., Dutrizac, J.E., Krause, E. and Osborne, R., 2004. Mineralogical Characterisation of Nickel Laterites from New Caledonia and Indonesia, International Laterite Nickel Symposium. TMS, Charlotte, US, pp. 79-99.
Dalvi, A.D., Bacon, W.G. and Osborne, R.C., 2004. The past and the future of nickel laterites, PDAC 2004 International Convention, Toronto, Ontario.

Darchen, A., Drissi-Daoudi, R. and Irzho, A., 1997. Electrochemical investigations of copper etching by $Cu(NH_3)_4Cl_2$ in ammoniacal solutions. Journal of Applied Electrochemistry, 27(4): 448-454.
Davies, D.H. and Burstein, G.T., 1980a. The effects of bicarbonate on the corrosion and passivation of iron. Corrosion (Houston), 36(8): 416-22.
Davies, D.H. and Burstein, G.T., 1980b. The electrochemical behavior of cobalt in bicarbonate and borate electrolytes. Corrosion Science, 20(8-9): 973-87.
Drok, K.J., Ritchie, I.M. and Power, G.P., 1998. A simple electrochemical approach to heterogeneous reaction kinetics. Journal of Chemical Education, 75(9): 1145-1149.
Filmer, A., MacLeod, I. and Parker, A., 1979a. Oxidation of Copper Sulfides in Aqueous Ammonia. II. Electrochemical Aspects. Australian Journal of Chemistry, 32(5): 975-987.
Filmer, A., Parker, A., Clare, B. and Wadley, L., 1979b. Oxidation of Copper Sulfides in Aqueous Ammonia. III. Kinetic Characteristics. Australian Journal of Chemistry, 32(12): 2597-2609.
Filmer, A., Parker, A. and Wadley, L., 1979c. Oxidation of Copper Sulfides in Aqueous Ammonia. I. Formation of Sulfur. Australian Journal of Chemistry, 32(5): 961-973.
Fittock, J., 2009. Area 340 process description. Internal report.
Fittock, J.E., 2007. Nickel and cobalt refining by QNI Pty Ltd, Yabulu, QLD. AusIMM Monograph 19 - Mawby Volume.
Fittock, J.E., 2014. Personal communication.
Forward, F.A., 1953. Ammonia pressure leach process for recovering nickel, copper and cobalt from Sheritt-Gordon nickel sulfide concentrate. Canadian Mining and Metallurgical Bulletin, 499: 677-684.
Forward, F.A. and Mackiw, V.N., 1955. Chemistry of the ammonia pressure process for leaching Ni, Cu and Co from Sheritt-Gordon sulphide concentrate. Journal of Metals, 7: 457-463.
Gassa, L.M., Ribotta, S.B., Folquer, M.E. and Vilche, J.R., 1998. Influence of temperature on dissolution and passivation of copper in carbonate-bicarbonate buffers. Corrosion, 54(3): 179-186.
Gervasi, C.A., Biaggio, S.R., Vilche, J.R. and Arvia, A.J., 1989. The electrochemical behaviour of cobalt in carbonate-bicarbonate solutions. Corrosion Science, 29(4): 427-437.
Giannopoulou, I., Panias, D. and Paspaliaris, I., 2009. Electrochemical modeling and study of copper deposition from concentrated ammoniacal sulfate solutions. Hydrometallurgy, 99(1-2): 58-66.
Graham, L., Steinbruchel, C. and Duquette, D.J., 2002. Nucleation and growth of electrochemically deposited copper on TiN and copper from a $Cu\text{-}NH_3$ bath. Journal of the Electrochemical Society, 149(8): C390-C395.
Grujicic, D. and Pesic, B., 2005. Reaction and nucleation mechanisms of copper electrodeposition from ammoniacal solutions on vitreous carbon. Electrochimica Acta, 50(22): 4426-4443.
Han, K.N. and Meng, X., 1993. The leaching behaviour of nickel and cobalt from metals and ores - a review, The Paul E. Queneau International Symposium, TMS, pp. 709-733.
Han, K.N., Narita, E. and Lawson, F., 1982. The coprecipitation behavior of Co(II) and Ni(II) with Fe(III), Cr(III) and Al(III) from aqueous ammoniacal solutions. Hydrometallurgy, 8(4): 365-377.
Hibbert, D.B., 1993. Introduction to Electrochemistry. Macmillan Press, UK.
Ijzermans, A.B., 1969a. Poisoning effects of hydrogen sulphide on noble metal electrodes. Pt. 1. Recueil des Travaux Chimiques 88(3): 334-343.
Ijzermans, A.B., 1969b. Poisoning effects of hydrogen sulphide on noble metal electrodes. Pt. 2. Recueil des Travaux Chimiques 88(3): 344-352.

Isaev, I.D. et al., 1990a. Formation of iron(II) ammine complexes in aqueous solutions. Russian Journal of Inorganic Chemistry, 35(8): 1162 -1164.
Isaev, I.D. et al., 1990b. The influence of temperature on the formation of cobalt(II) ammines in aqueous solution. Russian Journal of Inorganic Chemistry, 35(12): 1789 - 1791.
IUPAC, 1997. Compendium of Chemical Terminology. Blackwell Scientific Publications, Oxford.
Jandová, J. and Pedlik, M., 1991. Anodic dissolution of iron-nickel, iron-cobalt, and nickel-cobalt alloys in ammoniacal ammonium carbonate solutions. Hutnicke Listy, 46(9-10): 75-81.
Jandová, J. and Pedlik, M., 1994. Leaching behavior of iron-nickel alloys in ammoniacal solution. Hydrometallurgy, 35(1): 123-8.
Jandová, J. and Pedlík, M., 1991. Examination of the metallic phase formed in reduction of lateritic FeNi ore. Metallic Materials, 29(6): 439 - 449.
Jayalakshmi, M. and Muralidharan, V.S., 1991. Passivation of iron in alkaline carbonate solutions. Journal of Power Sources, 35(2): 131-42.
Karavasteva, M., 2005. Kinetics and deposit morphology of copper cementation onto zinc, iron and aluminium. Hydrometallurgy, 76: 149-152.
Kasherininov, G.O., 1960. Behavior of iron in ammoniacal solutions during leaching of cobalt from its ores. Zhurnal Prikladnoi Khimii, 33(6): 1233-1239.
Kerfoot, D.G.E. and Weir, D.R., 1988. The Hydro and Electrometallurgy of Nickel and Cobalt, Extractive Metallurgy of Nickel and Cobalt, Phoenix, Arizona, pp. 241-267.
Kho, Y.T., 1989. Anodic behaviour of iron in aqueous ammoniacal solution. PhD Thesis, Pennsylvania State University.
Kho, Y.T., Osseo-Asare, K. and Pickering, H.W., 1992. Anodic behavior of iron in ammoniacal carbonate solution. I. Steady-state polarization and cyclic voltammetry. Journal of the Electrochemical Society, 139(1): 32-9.
Kim, H.S., Kho, Y.T., Osseo-Asare, K. and Pickering, H.W., 1991. Active and passive behavior of sintered iron in ammoniacal ammonium carbonate solution. Metallurgical Transactions B: Process Metallurgy, 22B(3): 323-32.
King, D.W., 1998. Role of carbonate speciation on the oxidation rate of Fe(II) in aquatic systems. Environmental Science and Technology, 32: 2997-3003.
Lee, J.W., Osseo-Asare, K. and Pickering, H.W., 1985. Anodic dissolution of iron in ammoniacal ammonium carbonate solution. Journal of the Electrochemical Society, 132(3): 550-5.
Lee, J.W., Pickering, H.W. and Osseo-asare, K., 2003. Anodic dissolution of cobalt in ammoniacal ammonium carbonate solution, Electrochemistry in Mineral and Metal Processing VI. Electrochemical Society, pp. 204.
Legrand, L., Abdelmoula, M., Géhin, A., Chaussé, A. and Génin, J.M.R., 2001a. Electrochemical formation of a new Fe(II)-Fe(III) hydroxy-carbonate green rust: characterisation and morphology. Electrochimica Acta, 46(12): 1815-1822.
Legrand, L., Sagon, G., Lecomte, S., Chausse, A. and Messina, R., 2001b. A Raman and infrared study of a new carbonate green rust obtained by electrochemical way. Corrosion Science, 43(9): 1739-1749.
Legrand, L., Savoye, S., Chausse, A. and Messina, R., 2000. Study of oxidation products formed on iron in solutions containing bicarbonate/carbonate. Electrochimica Acta, 46(1): 111-117.
Lewis, J.F., Draper, G., Proenza, J.A., Espillat, J. and Jimenez, J., 2006. Ophiolite-related ultramafic rocks (serpentines) in the Caribbean region: a review of their occurrence, composition, origin, emplacement and Ni-laterote soil formation. Geologica Acta, 4(1-2): 237-263.

Li, J., Zhong, T.-K. and Wadsworth, M.E., 1992. Application of mixed potential theory in hydrometallurgy. Hydrometallurgy, 29: 47-60.

Mackenzie, J. and Lumsdaine, I., 2002. Characterising cobalt losses for improved recoveries, Metallurgical Plant Design and Operating Strategies. AusIMM, Melbourne, pp. 367-372.

Mani, F., Peruzzini, M. and Stoppioni, P., 2006. CO_2 absorption by aqueous NH_3 solutions: speciation of ammonium carbamate, bicarbonate and carbonate by a 13C NMR study. Green Chemistry, 8(11): 995-1000.

Miller, J.D., 1979. Cementation. In: H.Y. Sohn and M.E. Wadsworth (Eds.), Rate processes of extractive metallurgy. Plenum, New York, pp. 197-244.

Molleman, E. and Dreisinger, D., 2002. The treatment of copper–gold ores by ammonium thiosulfate leaching. Hydrometallurgy, 66(1–3): 1-21.

Muir, D. and Ho, E., 1996. Composition and Electrochemistry of Nickel Matte: Implications for Matte Leaching and Refining in Acid Solution. In: E.J. Grimsey and I. Neuss (Eds.), Nickel '96, Mineral to Market. AusIMM, Kalgoorlie, Australia.

Muir, D.M., Parker, A.J. and Filmer, A.O., 1981. Formation of sulfur from the ammonia/oxygen leach of copper and nickel sulfides, Hydrometallurgy. Society of Chemical Industry, Manchester. UK, pp. 1-14.

Najdeker, E. and Bishop, E., 1973. The formation and behaviour of platinum sulphide on platinum electrodes. Journal of electroanalytical chemistry, 41(1): 79-87.

Nazari, G. and Asselin, E., 2010. Estimation of thermodynamic properties of aqueous iron and cobalt ammines at elevated temperatures. Metallurgical and Materials Transactions B, 41B: 520-526.

Nicol, M.J., 1975. Electrochemical investigation of the dissolution of copper, nickel, and copper-nickel alloys in ammonium carbonate solutions. Journal of the South African Institute of Mining & Metallurgy, 75(11): 291-302.

Nicol, M.J., Nikoloski, A.N. and Fittock, J.E., 2004. A fundamental study of the leaching reactions involved in the Caron process, International Laterite Nickel Symposium, pp. 369-384.

Nikoloski, A.N., 2002. The electrochemistry of the leaching of pre-reduced laterite ored in ammonia-ammonium carbonate solution. PhD Thesis, Murdoch University.

Nikoloski, A.N. and Nicol, M.J., 2006. The electrochemistry of the leaching reactions in the Caron process. I. anodic processes, Electrochemistry in Mineral and Metal Processing VII. Electrochemical Society, pp. 197-207.

Nikoloski, A.N. and Nicol, M.J., 2010. The electrochemistry of the leaching reactions in the Caron process II. Cathodic processes. Hydrometallurgy, 105(1-2): 54-59.

Nikoloski, A.N., Nicol, M.J. and Fittock, J.E., 2003. The passivation of iron during the leaching of pre-reduced laterite ores in ammoniacal solutions, Electrochemistry in Mineral and Metal Processing VI. Electrochemical Society, pp. 205-218.

Nila, C. and González, I., 1996a. The role of pH and Cu(II) concentration in the electrodeposition of Cu(II) in NH_4Cl solutions. Journal of Electroanalytical Chemistry, 401(1-2): 171-182.

Nila, C. and González, I., 1996b. Thermodynamics of Cu-H_2SO_4-Cl^--H_2O and Cu-NH_4Cl-H_2O based on predominance-existence diagrams and Pourbaix-type diagrams. Hydrometallurgy, 42(1): 63-82.

Osseo-Asare, K., 1980. Cobalt behavior in ammonia leaching systems, Cobalt 80, 10th Annual CIM Hydrometallurgical Meeting, Edmonton, Alberta, Canada.

Osseo-Asare, K., 1981a. Application of activity-activity diagrams to ammonia hydrometallurgy. II. The copper-, nickel-, cobalt-ammonia-water systems at elevated temperatures. In: M. Kuhn (Ed.), Process and Fundamental Considerations of Selected Hydrometallurgical Systems. AIME, New York, pp. 359-69.

Osseo-Asare, K., 1981b. Application of activity-activity diagrams to ammonia hydrometallurgy: 3 - Manganese-ammonia-water, manganese-ammonia-water-carbonate, and manganese-ammonia-water-sulfate systems at 25 Deg. Transactions of the Institution of Mining and Metallurgy, Section C: Mineral Processing and Extractive Metallurgy, 90(Dec.): 152-8.

Osseo-Asare, K., 1981c. Application of activity-activity diagrams to ammonia hydrometallurgy: 4 - Iron-ammonia-water, iron-ammonia-water-carbonate, and iron-ammonia-water-sulfate systems at 25 DegC. Transactions of the Institution of Mining and Metallurgy, Section C: Mineral Processing and Extractive Metallurgy, 90(Dec.): 159-63.

Osseo-Asare, K. and Asihene, S.W., 1979. Heterogeneous equilibria in ammonia/laterite leaching systems, International Laterite Symposium. SME, New Orleans, pp. 585-609.

Osseo-Asare, K. and Fuerstenau, D.W., 1978. Application of activity-activity diagrams to ammonia hydrometallurgy: the copper-, nickel-, and cobalt-ammonia-water systems at 25 DegC. AIChE Symposium Series, 74(173): 1-13.

Osseo-Asare, K., Lee, J.W., Kim, H.S. and Pickering, H.W., 1983. Cobalt extraction in ammoniacal solution: electrochemical effect of metallic iron. Metallurgical Transactions B: Process Metallurgy, 14B(4): 571-6.

Park, K.-H., Mohapatra, D., Reddy, B.R. and Nam, C.-W., 2007. A study on the oxidative ammonia/ammonium sulphate leaching of a complex (Cu-Ni-Co-Fe) matte. Hydrometallurgy, 86(3-4): 164-171.

Perez Sanchez, M. et al., 1990. Electrochemical behaviour of copper in aqueous moderate alkaline media, containing sodium carbonate and bicarbonate, and sodium perchlorate. Electrochimica Acta, 35(9): 1337-1343.

Power, G.P., 1981. The electrochemistry of the nickel sulfides. I. Nickel(II) sulfide. Australian Journal of Chemistry, 34(11): 2287-96.

Power, G.P., 1982. The electrochemistry of the nickel sulfides. 2. Ni_3S_2. Electrochimica Acta, 27(3): 359-364.

Power, G.P. and Ritchie, I.M., 1975. Metal displacement reactions. Modern Aspects of Electrochemistry, 11: 199-250.

Prado, F.G. and Dempsey, J.P., 1986. Indigenous solid reductants in Caron type nickel plants, 25th Annual Conference of Metallurgists. CIM, Toronto, Canada.

Prado, F.L., 2004. Sixty years of Caron: current assesment, International Laterite Nickel Symposium. TMS, Charlotte, US, pp. 593-598.

Price, D.C. and Davenport, W.G., 1982. Anodic reactions of Ni_3S_2, β-NiS and nickel matte. Journal of Applied Electrochemistry, 12: 281-290.

Queneau, P.B. and Weir, D.R., 1986. Control of iron during hydrometallurgical processing of nickeliferous laterite ores, pp. 76-105.

Rábai, G. and Epstein, I.R., 1992. Equilibria and kinetics of the fast interaction between copper(II) and thiosulfate ions in aqueous solution. Inorganic chemistry, 31(15): 3239-3242.

Ramasubramanian, N., 1975. Anodic behavior of platinum electrodes in sulfide solutions and the formation of platinum sulfide. Journal of Electroanalytical Chemistry, 64(1): 21-37.

Ramos, A., Miranda-Hernandez, M. and Gonzalez, I., 2001. Influence of chloride and nitrate anions on copper electrodeposition in ammonia media. Journal of the Electrochemical Society, 148(4): C315-C321.

Real, S.G., Ribotta, S.B. and Arvia, A.J., 2008. The electrochemical dissolution of cobalt in carbonate-bicarbonate solutions from EIS and steady polarization data. Corrosion Science, 50(2): 463-472.

Reid, J.G., 1983. Some observations of roasting, leaching and washing characteristics of Greenvale lateritic ore. In: K. Osseo-Asare and J.D. Miller (Eds.), Third International Symposium on Hydrometallurgy. TMS-AIME, Warrendale, US, pp. 109-120.
Reid, J.G. and Fittock, J.E., 2004. Yabulu 25 years on, International Laterite Nickel Symposium. TMS, Charlotte, US, pp. 599-618.
Reilly, I.G. and Scott, S., 1978. Recovery of Elemental Sulfur During the Ammoniacal Leaching of Copper Sulfide. Metallurgical Transactions B, 9: 681-986.
Rhamdhani, M.A., Hayes, P.C. and Jak, E., 2009a. Nickel laterite Part 1 – microstructure and phase characterisations during reduction roasting and leaching. Mineral Processing and Extractive Metallurgy (Trans. Inst. Min Metall. C), 118(3): 129-145.
Rhamdhani, M.A., Jak, E. and Hayes, P.C., 2009b. Nickel Production through the Caron Process. High Temperature Processing Seminar 2009, Swinburne University of Technology.
Richardson, J.M., Stevens, L.G. and Kuhn, M.C., 1981. The recovery of metal values from nickel-bearing laterite ores by reductive roast/ammonia leach technology. In: M.C. Kuhn (Ed.), Process and fundamental considerations of selected hydrometallurgical systems. American Institute of Mining, Metallurgical, and Petroleum Engineers, Inc, New York, pp. 38-61.
Rickard, R.S. and Fuerstenau, M.C., 1968. An electrochemical investigation of copper cementation by iron. Transactions of the Metallurgical Society of AIME, 242(8): 1487-93.
Roach, G.I.D., 1977a. Corrosion of metals by aqueous ammonium carbonate - plant experience at Queensland Nickel. Preprinted Papers, Annual Conference - Australasian Corrosion Association, 17(Corros. Min. Ind.): Paper No M1, 9 pp.
Roach, G.I.D., 1977b. Mineralogy - it's effect on process efficieny at Queensland Nickel, Extractive Metallurgy Symposium, University of New South Wales, Australia.
Roine, A., 2009. HSC Chemistry 7.0 Database. Outotec Research Oy.
Savoye, S. et al., 2001. Experimental investigations on iron corrosion products formed in bicarbonate/carbonate-containing solutions at 90 DegC. Corrosion Science, 43(11): 2049-2064.
Senanayake, G., 2004. Analysis of reaction kinetics, speciation and mechanism of gold leaching and thiosulfate oxidation by ammoniacal copper(II) solutions. Hydrometallurgy, 75(1–4): 55-75.
Senanayake, G., 2005. Role of copper(II), carbonate and sulphite in gold leaching and thiosulfate degradation by oxygenated alkaline non-ammoniacal solutions. Minerals Engineering, 18: 409-426.
Senanayake, G., Senaputra, A. and Nicol, M.J., 2010. Effect of thiosulfate, sulfide, copper(II), cobalt(II)/(III) and iron oxides on the ammoniacal carbonate leaching of nickel and ferronickel in the Caron process. Hydrometallurgy, 105(1-2): 60-68.
Senaputra, A., 2010. Dissolution of nickel, ferronickel and nickel sulfides in ammoniacal carbonate solutions (unpublished work).
Senaputra, A., Senanayake, G., Nicol, M. and Nickoloski, A., 2008. Leaching nickel and nickel sulfides in ammonia/ammonium carbonate solutions, Hydrometallurgy VI, Phoenix, Arizona, pp. 551-560.
Sillen, L.G. and Martell, A.E., 1964. Stability constants of metal ion complexes. Chemical Society special publication number 17, London.
Simpson, L.J. and Melendres, C.A., 1996. Surface-enhanced Raman spectroelectrochemical studies of corrosion films on iron in aqueous carbonate solution. Journal of the Electrochemical Society, 143(7): 2146-2152.
Smith, R.M. and Martell, A.E., 1976. Critical stability constants 4: Inorganic complexes. Plenum Press, New York.

Smith, R.M. and Martell, A.E., 1989. Critical Stability Constants, 6. Plenum Press, New York.
Steyl, J.D.T., Pelser, M. and Smit, J.T., 2008. Atmospheric leach process for nickel laterite ores, Hydrometallurgy VI. SME, Phoenix, Arizona, pp. 541-551.
Su, L.W., 2011. Cobalt adsorption and/or co-precipitation onto ferric oxyhydroxide. Masters Thesis, University of British Columbia, Canada.
Swamy, Y.V., Kar, B.B. and Mohanty, J.K., 2003. Physicochemical characterization and sulphatization roasting of low-grade nickeliferous laterites. Hydrometallurgy, 69(1-3): 89-98.
Taylor, A., 2009. Trends in nickel-cobalt processing, ALTA Nickel/Cobalt Conference, Perth, Australia.
Tozawa, D., Umetsu, Y. and Satu, K., 1976. On Chemistry of Ammonia Leaching of Copper Concentrates. Extractive Metallurgy of Copper, 2. AIME, New York.
Tromans, D. and Sun, R.-h., 1992. Anodic behaviour of copper in weakly alkaline solutions. J. Electrochem. Soc., 139(7): 1945-1951.
Valentini, C.R., Moina, C.A., Vilche, J.R. and Arvia, A.J., 1983. The potentiodynamic behavior of polycrystalline iron in carbonate-bicarbonate solutions. Anales de la Asociacion Quimica Argentina, 71(5-6): 555-70.
Valentini, C.R., Moina, C.A., Vilche, J.R. and Arvia, A.J., 1985. The electrochemical behaviour of iron in stagnant and stirred potassium carbonate-bicarbonate solutions in the 0-75°C temperature range. Corrosion Science, 25(11): 985-993.
Vazquez-Arenas, J., Lazaro, I. and Cruz, R., 2007a. Electrochemical study of binary and ternary copper complexes in ammonia-chloride medium. Electrochimica Acta, 52(20): 6106-6117.
Vazquez-Arenas, J., Vazquez, G., Melendez, A.M. and Gonzalez, I., 2007b. The effect of the Cu^{2+}/Cu^{+} step on copper electrocrystallization in acid non-complexing electrolytes. Journal of the Electrochemical Society, 154(9): D473-D481.
Vu, C. and Han, K.N., 1977. Leaching behavior of cobalt in ammonia solutions. Transactions of the Institution of Mining and Metallurgy, Section C: Mineral Processing and Extractive Metallurgy, 86(Sept.): 119-25.
Vu, C., Han, K.N. and Lawson, F., 1980. Leaching behavior of cobaltous and cobalto-cobaltic oxides in ammonia and in acid solutions. Hydrometallurgy, 6(1-2): 75-87.
Wagner, C. and Traud, W., 1938. The interpretation of corrosion phenomena by super-imposition of electrochemical partial reactions and the formation of potentials of mixed electrodes. Zeitschrift fuer Elektrochemie und Angewandte Physikalische Chemie, 44: 391-402.
Weir, D.R. and Sefton, V.B., 1979. Development of Sherrit's commercial nickel refining process for low and high iron laterites, International Laterite Symposium. SME-AIME, New Orleans, US, pp. 325-345.
Wen, N. and Brooker, M.H., 1995. Ammonium Carbonate, Bicarbonate, and Carbamate Equilibria: A Raman Study. Journal of Physical Chemistry, 99(1): 359-68.